Effect of Concrete Composition on Splitting Cracks in Prestressed Concrete Railroad Ties: Application of Fracture Mechanics

KSU-21-8

April 2021

Dr. Aref S. Dastgerdi, Civil Engineering, KSU
Dr. Robert J. Peterman, Civil Engineering, KSU
Dr. B. Terry Beck, Mechanical & Nuclear Engineering, KSU
Dr. Kyle A. Riding, Civil and Coastal Engineering, UF

Abstract

The effect of concrete composition on end-splitting cracks in pretensioned concrete members was investigated. Specific parameters included the effect of aggregate shape and content, water-to-cementitious (w/cm) ratio, fly ash, paste and air void content. For each mixture evaluated, prisms were load tested in three-point bending at 4000, 6000 and 8000 psi to determine the effect of concrete compressive strength on crack growth potential. Corresponding splitting tensile tests were also conducted on samples at each compressive strength for all mixtures. Results show that increasing angularity, aggregate size distribution, and decreasing w/cm ratio improve fracture toughness by as much as 28% whereas changing other parameters had little effect. All improving factors were seen to be most effective at low strengths. A statistical model predicting fracture toughness was developed, and the results correlated well with observed cracking in pretensioned concrete members.

Corresponding Author: Dr. Robert J. Peterman (bob@ksu.edu)

U.S. Department of Transportation
Federal Railroad Administration

The contents of this report reflect the views of the authors, who are responsible for the facts and accuracy of the information presented herein. This document is disseminated in the interest of information exchange. The report is funded, partially or entirely, by a grant from the U.S. Department of Transportation's University Transportation Centers Program. However, the U.S. Government assumes no liability for the contents or use thereof.

METRIC/ENGLISH CONVERSION FACTORS

ENGLISH TO METRIC	METRIC TO ENGLISH
LENGTH (APPROXIMATE)	**LENGTH (APPROXIMATE)**
1 inch (in) = 2.5 centimeters (cm)	1 millimeter (mm) = 0.04 inch (in)
1 foot (ft) = 30 centimeters (cm)	1 centimeter (cm) = 0.4 inch (in)
1 yard (yd) = 0.9 meter (m)	1 meter (m) = 3.3 feet (ft)
1 mile (mi) = 1.6 kilometers (km)	1 meter (m) = 1.1 yards (yd)
	1 kilometer (km) = 0.6 mile (mi)
AREA (APPROXIMATE)	**AREA (APPROXIMATE)**
1 square inch (sq in, in^2) = 6.5 square centimeters (cm^2)	1 square centimeter (cm^2) = 0.16 square inch (sq in, in^2)
1 square foot (sq ft, ft^2) = 0.09 square meter (m^2)	1 square meter (m^2) = 1.2 square yards (sq yd, yd^2)
1 square yard (sq yd, yd^2) = 0.8 square meter (m^2)	1 square kilometer (km^2) = 0.4 square mile (sq mi, mi^2)
1 square mile (sq mi, mi^2) = 2.6 square kilometers (km^2)	10,000 square meters (m^2) = 1 hectare (ha) = 2.5 acres
1 acre = 0.4 hectare (he) = 4,000 square meters (m^2)	
MASS - WEIGHT (APPROXIMATE)	**MASS - WEIGHT (APPROXIMATE)**
1 ounce (oz) = 28 grams (gm)	1 gram (gm) = 0.036 ounce (oz)
1 pound (lb) = 0.45 kilogram (kg)	1 kilogram (kg) = 2.2 pounds (lb)
1 short ton = 2,000 pounds (lb) = 0.9 tonne (t)	1 tonne (t) = 1,000 kilograms (kg)
	= 1.1 short tons
VOLUME (APPROXIMATE)	**VOLUME (APPROXIMATE)**
1 teaspoon (tsp) = 5 milliliters (ml)	1 milliliter (ml) = 0.03 fluid ounce (fl oz)
1 tablespoon (tbsp) = 15 milliliters (ml)	1 liter (l) = 2.1 pints (pt)
1 fluid ounce (fl oz) = 30 milliliters (ml)	1 liter (l) = 1.06 quarts (qt)
1 cup (c) = 0.24 liter (l)	1 liter (l) = 0.26 gallon (gal)
1 pint (pt) = 0.47 liter (l)	
1 quart (qt) = 0.96 liter (l)	
1 gallon (gal) = 3.8 liters (l)	
1 cubic foot (cu ft, ft^3) = 0.03 cubic meter (m^3)	1 cubic meter (m^3) = 36 cubic feet (cu ft, ft^3)
1 cubic yard (cu yd, yd^3) = 0.76 cubic meter (m^3)	1 cubic meter (m^3) = 1.3 cubic yards (cu yd, yd^3)
TEMPERATURE (EXACT)	**TEMPERATURE (EXACT)**
[(x-32)(5/9)] °F = y °C	[(9/5) y + 32] °C = x °F

QUICK INCH - CENTIMETER LENGTH CONVERSION

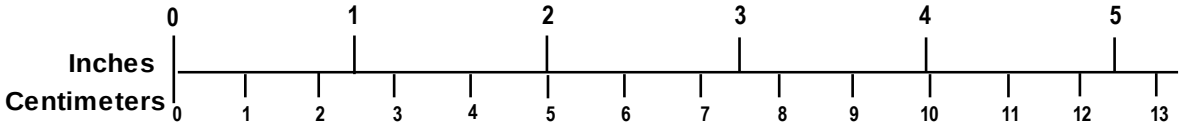

QUICK FAHRENHEIT - CELSIUS TEMPERATURE CONVERSION

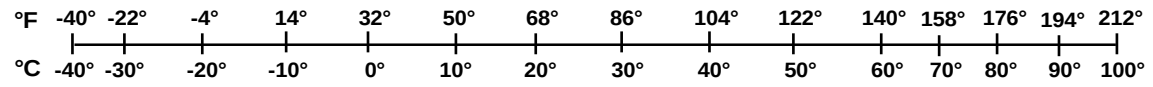

For more exact and or other conversion factors, see NIST Miscellaneous Publication 286, Units of Weights and Measures. Price $2.50 SD Catalog No. C13 10286

Updated 6/17/98

Acknowledgements

The authors would like to thank the Federal Railroad Administration (FRA) for providing the majority of funding that made this research possible. The researchers would also like to thank Dr. Hailing Yu at the John A. Volpe National Transportation Systems Center for her valuable suggestions and parallel analysis work. Finally, the authors wish to thank the Precast/Prestressed Concrete Institute (PCI) for establishing an industry advisory panel to the project and also everyone who helped during this endeavor.

Contents

Illustrations

Tables

Executive Summary

In this report, the effect of concrete composition on end-splitting cracks in prestressed concrete members was investigated. Splitting cracks sometimes occur when prestressing force is introduced at de-tensioning and high stress-concentrations form around wire within transfer length. Transfer length is the bonded length required to fully introduce the prestressing force into the prestressed concrete member. Splitting cracks have been a recurring issue in prestressed concrete railroad ties where concrete cover is typically low. To prevent these splitting failures, the prestressed cross-section, wire type and concrete material properties, should be carefully evaluated to ensure satisfactory performance. With respect to the concrete member, the concrete material needs to be resistant to crack growth at the strengths at which the pretensioned member is detensioned. In this study, the effect of different concrete parameters including aggregate shape and content, water-to-cementitious (w/cm) ratio, fly ash, paste and air void content on the crack resistance of concrete used in concrete railroad ties were investigated using the Two-Parameter Model (TPM). For each mixture evaluated, twelve plain concrete prisms were tested in three-point bending at 4000, 6000 and 8000 psi concrete compressive strengths (27.5, 41.3 and 55.1 MPa) to determine the effect of concrete compressive strength on crack growth potential. In addition, splitting tensile tests were conducted on three samples at each compressive strength for all mixtures. Finally, the results were analyzed, and the results of each utilized method was discussed. The results show that increasing angularity, aggregate size distribution, and decreasing w/cm ratio improve fracture toughness by as much as 28% whereas changing paste, fly ash and air void content negligibly influence fracture toughness. However, all improving factors were seen to be most effective at low strengths. Statistical analysis conducted on fracture parameter values and concrete parameters indicated a correlation by which a statistical model for fracture-toughness prediction was developed. Next, the most beneficial factors on fracture toughness were incorporated to make and test actual pre-tensioned concrete prisms. Mixtures including the most effective factors were designed and pre-tensioned prisms with three different reinforcement edge distances (0.750, 0.625 and 0.500 in.) were fabricated and detensioned when the concrete compressive strength reached 4500 psi. Next, splitting cracks were quantitatively assessed by direct measurement. The results indicated a strong correlation between fracture toughness and crack length measurements. Additionally, a nonlinear regression model was developed predicting splitting-crack growth in prestressed cross-sections with varied edge-distance thickness. Finally, the effect of transvers reinforcement was investigated and a novel application of polymer fiber was proposed. The results obtained from this study could lead to a significant improvement in splitting crack resistance in pre-tensioned concrete members where high amount of transverse stress is often introduced at low compressive strengths.

1. Introduction

The high-speed railroad industry is advancing at a fast pace around the world. Pre-stressed concrete railroad ties play an important role in safety and performance of this type of transportation. Concrete ties must meet demanding requirements from the time of manufacture until the end of service life.

Concrete structures such as railroad ties are exposed to high impact loads that can sometimes lead to a gradual failure without obvious warning. These failures initiate at micro-cracks in the concrete, and continue as the micro-cracks grow into visible cracks and can eventually lead to failure [1]. However, some cracks are also formed due to internal defects along with induced tensile stresses.

Splitting-cracks are commonly observed in pre-stressed concrete members with low reinforcement cover, such as railroad ties, where a high amount of stress concentration exists at the interface of wires and mortar due to the large amount of force transferred from the pre-tensioned wires to concrete members. These splitting-cracks can occur right after releasing tension or at some later point under the superimposed loading condition. In these members, splitting-crack propagation can lead to structural deterioration and significantly-reduced load-carrying capacity. Therefore, it is very important to enhance both the crack-initiation resistance and crack-propagation resistance of concrete mixtures used in pre-stressed concrete railroad ties.

It is well established that the indentation pattern of prestressing wires used in the manufacture of concrete railroad ties can significantly impact the concrete splitting propensity [2]. Moreover, for the same type of indented wire, ties made with different concrete properties exhibit different splitting-crack propensities. In order to prevent splitting-crack initiation and growth in concrete railroad ties, the best concrete materials and wires should be selected in a way that the function of their combination provides sufficient bond while minimizing the risk of splitting failures in the ties.

In this research, concrete material of concrete railroad ties was evaluated in terms of structural and durability damages. Understanding of key parameters in concrete may lead to have a better design for future design. Concrete performance in this research was categorized in two major groups: Non-destructive and destructive evaluation. Non-destructive evaluation including Ultrasonic Pulse Velocity (UPV) and Impact Echo (IE) were conducted on existing concrete railroad ties taken from track after more than 25 years. In order to evaluate concrete composition, variety of test methods were applied on aggregate, concrete mixtures and cores extracted from existing concrete tie. The materials tested in this study include the same material used by current tie producer and used in existing concrete railroad ties in track. For structural standpoint, concrete mixtures were examined by fracture toughness testing and pre-stressed prisms to investigate splitting crack performance of concrete. In terms of durability, cores from existing concrete railroad ties were taken and tested for compressive and tensile strengths, air void system, abrasion, absorption and alkali silica reaction (ASR).

Figure 1.

1.1 Objectives

Concrete railroad ties became popular in the high-speed train industry due to reduced deflections, durability, and competitive cost. It is vital to ensure these elements meet minimum requirement with respect to safety and high performance before and during service life. There are different types of damage caused by loading and environmental condition. Thus, concrete material of these ties should be design in a way that high quality and satisfactory performance of concrete ties are ensured during service life. To reach optimum design with high quality and reasonable cost, evaluation of existing concrete railroad ties can lead to a better understanding of the relation between tie's performance and its properties. There are destructive and non-destructive methods investigating the existing concrete railroad ties in the field.

The present report was conducted to answer the following questions:

- What parameters in concrete are effective regarding splitting-crack growth?
- Can a facture mechanics approach be utilized to predict splitting-crack behavior?
- Is a fracture toughness test useful as a qualification test for prestressed members?
- Is there a relation between splitting-crack initiation and concrete composition?
- What is the best way to increase splitting-crack resistance in concrete railroad tires?

1.2 Organization of the Report

This report consists of seven chapters in which relevant materials are discussed in each chapter. Following chapters are organized as explained below:

- In Chapter Two, theory and previous findings on the applied method and materials are discussed
- In Chapter Three, the first phase of this report including testing procedure and results of mechanical properties and fracture parameters of utilized material, is expressed
- In Chapter Four, testing procedure and results of prestressed prisms are presented
- In Chapter Five, the predictive models correlating splitting-cracks and concrete properties are developed and discussed
- In Chapter Six, conclusions and recommendations of first two phase of this report are summarized and presented
- In Chapter Seven, The destructive and non-destructive evaluation on concrete railroad ties are discussed
- In Chapter Eight, the references of this report are listed

2. Fracture Mechanics Testing (Phase 1)

2.1 Fracture Mechanics

In all structures when the tensile strength of material is reached, cracking is observed. Structures fail to carry loading because of either yielding or fracture. Defects impact both types of failure to some extent. In yielding-dominant failure, very small defects are typically effective such as interstitial and out-of-size substitutional atoms, grain boundaries, dislocation network and coherent precipitates. These defects are generally investigated by the mineralogy field in aggregate and rocks. Larger and clearly visible defects in structure normally caused by external agents lead to decreasing in load bearing capacity. On the other hand, significant defects affecting fracture before general yielding of the net section are necessarily in macroscopic scale. Thus, imperfections in crystal system of material indirectly influence resistance to fracture through controlling plastic flow.

Fracture mechanics has been considered as a mean to quantitatively identify the crack behavior when a minimum detectable crack initiate until maximum permissible crack length occurs. Typically, materials include defects, micro-cracks and pre-existing flaws which propagate due to factors namely fatigue, stress corrosion and creep. As defects grow, crack size increases with decreasing residual failure strength. Answering the questions concerning crack size, time to failure and resistance of material to crack growth and failure is done through fracture analysis (Janssen, Zuidema et al. 2006).

2.1.1 Linear Elastic Fracture Mechanics (LEFM)

Fracture mechanic initiated with the theory of linear elastic fracture mechanics which is well developed and includes three modes of crack surface displacement. Mode 1 is the predominant mode in many practical cases called the opening mode (mode 1) in which the crack tip in homogeneous isotropic material is under normal tensional load. Mode 2 is the sliding mode carrying shear load, and in mode 3 the crack tip is teared. In Figure 1, three mode of crack are shown [1].

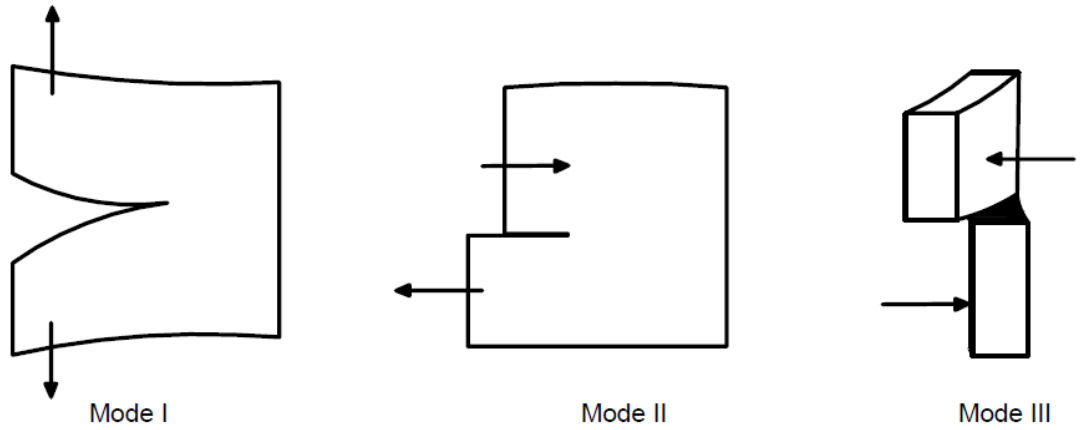

Figure 1. The three modes of crack surface displacement, Mode I: opening mode, Mode II: sliding mode, Mode III: tearing mode

The Linear Elastic Fracture Mechanics (LEFM) deals with the crack tips with very small plastic zone around the crack tip compared to the crack size which must behave elastically. Failures in fracture-dominant cases occur before yielding of the net section. According to LEFM, fracture happens when the critical stress distribution around the crack tip is reached. The material properties governing fracture may be defined as the critical stress intensity, *Kc*, critical value *Gc* in terms of energy [1].

Fracture mechanics is mostly discussed in two dimensions in which the *Z* coordinate is not involved. Plane stress and plane strain are two types of problems in which stress and strain in *Z* coordinate are considered zero, respectively.

In a plane stress situation, stress-strain equations can be considered as:

$$\varepsilon_x = \frac{1}{E}(\sigma_x - \nu\sigma_y) \quad \textbf{(1)}$$

$$\varepsilon_y = \frac{1}{E}(\sigma_y - \nu\sigma_x) \quad \textbf{(2)}$$

Strain can be derived from stress by replacing E by $E/(1-\nu^2)$ and ν by $\frac{\nu}{1-\nu}$ in plane stress equation.

In through-crack under uniaxial loading, it is known that stress component tends to infinity at crack tip. For stress filed close to the crack tip, the intensity of the stress singularity, K_I , is $\sigma\sqrt{\pi a}$.

Typically first cracks occur at surface discontinuities or corners in structures (Figure 2). There are a number of equations introduced by Irwin and Westergaard calculating intensity factor for different shapes of cracks [3, 4].

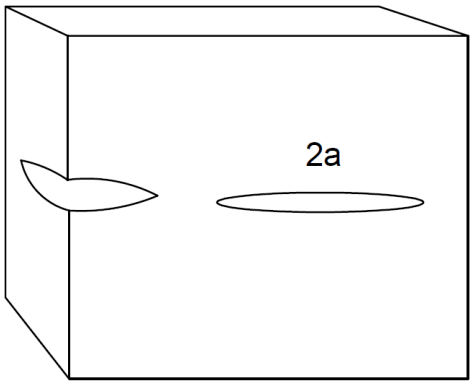

Figure 2. Center and corner crack

The intensity factor solution for different types of cracks has been developed, and also correction factors regarding geometric properties of cracked specimens have been represented.

A number of test methods are widely used to measure fracture characteristics of materials like metal and rock. The solution for some the most applicable standard test specimens are shown below.

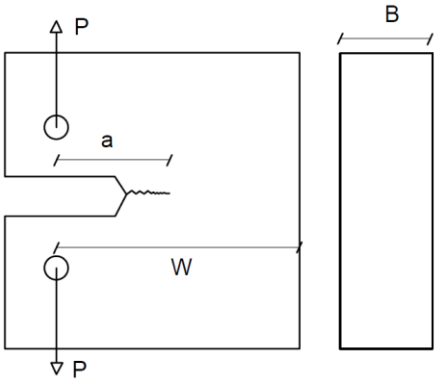

Figure 3. Compact Tension specimen (CT)

In this method, the stress intensity factor can be calculated through equations (3) and (4).

$$K_I = \frac{P}{B\,W^{0.5}} \cdot f\left(\frac{a}{W}\right) \quad \textbf{(3)}$$

$$f\left(\frac{a}{W}\right) = \frac{\left(2+\frac{a}{W}\right)\left\{0.886 + 4.64\left(\frac{a}{W}\right) - 13.32\left(\frac{a}{W}\right)^2 + 14.72\left(\frac{a}{W}\right)^3 - 5.6\left(\frac{a}{W}\right)^4\right\}}{\left(1-\frac{a}{W}\right)^{\frac{3}{2}}} \quad \textbf{(4)}$$

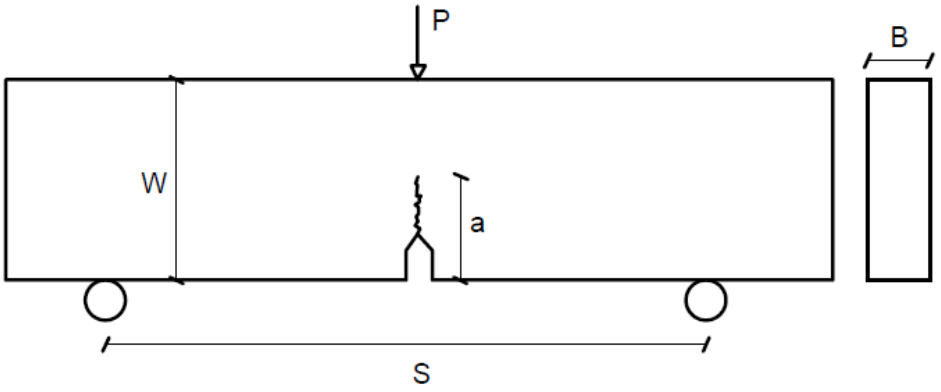

Figure 4. Single Edge Notched Bend specimen (SENB)

$$K_I = \frac{P.S}{B\,W^{\frac{3}{2}}} \cdot f\left(\frac{a}{W}\right) \quad \textbf{(5)}$$

$$f\left(\frac{a}{W}\right) = \frac{3\left(\frac{a}{W}\right)^{0.5}\left\{1.99 - \frac{a}{W}\left(1-\frac{a}{W}\right)\left[2.15 - 3.93\left(\frac{a}{W}\right) + 2.7\left(\frac{a}{W}\right)^2\right]\right\}}{2\left(1+2\frac{a}{W}\right)\left(1-\frac{a}{W}\right)^{\frac{3}{2}}} \quad \textbf{(6)}$$

In reality, very close to crack tip there is a plastic zone which can be calculated by various models. The plastic zone size according to Irwin is:

$$2r_y = \frac{1}{2\pi}\left(\frac{K_I}{\sigma_{ys}}\right)^2 \quad (7)$$

In this model, plastic zone shape is assumed a circle with radius of r_y . In other methods, shape of plastic zone is traced from a first order approximation to the size. Plastic zone shape in mode 1 can be estimated for plane stress and plane strain using the following equation:

$$r(\theta)_{\text{plane stress}} = \frac{1}{4\pi}\left(\frac{K_I}{\sigma_{ys}}\right)^2 \left(1 + \frac{3}{2}\sin^2\theta + \cos\theta\right) \quad (8)$$

In plane strain unlike plane stress, $\sigma_3 = \nu(\sigma_1 + \sigma_2)$

In order to evaluate fracture toughness, the critical stress intensity for fracture, K_C , is determined depending on specimen thickness. It is evident that beyond a certain thickness, a material will be in plane strain situation in which the critical stress intensity is prone to a constant value. However, an energy balance approach is used to enhance the precision of thickness effect on critical stress intensity which can be called fracture property of material. It is known that the plastic zone size surrounding a crack tip affects the required thickness for the plane strain condition [1].

The energy balance approach is well-utilized for materials with limited but significant plasticity [1]. The concept of crack resistance, *R*, energy balance, *G*, and slow stable crack growth are introduced in this approach which is based on an assumption that a combination of plate and loading system are considered to be isolated from its surrounding. The following equation illustrates energy content of the plate under the loading system before and after introducing a crack:

$$U = U_O + U_a + U_\gamma - F \quad (9)$$

Where:

U_o= total energy of the plate and its loading system before introducing a crack (constant),

U_a= elastic energy of the plate,

U_γ= surface energy of the plate,

F= work done by loading system = load X displacement.

Potential energy of the plate is able to perform work which is equal to:

$$U_p = U_o + U_a - F \quad (10)$$

It can be said that as long as a crack extends, potential energy of the plate decrease and the surface energy would increase. Irwin introduced energy release rate, *G*, meaning the energy available per increment of crack growth per unit thickness. And also the energy required per crack growth is called crack resistance, *R* [3].

There are practical relation in order to calculate the energy release rate and crack resistance for plane stress and plane strain cases. *G* and its relation to K_I, in a remotely loaded center cracked plate is:

$$G_{\text{Plane stress}} = \frac{\pi\sigma^2 a}{E} \quad \textbf{(11)}$$

$$G_{\text{plane stress}} = \frac{K_I^2}{E} \quad \textbf{(12)}$$

$$G_{\text{plane strain}} = \frac{K_I^2}{E}\left(1-\nu^2\right) \quad \textbf{(13)}$$

A common way to determine stress intensity factor is compliance, which is the inverse of stiffness of a body. Using following relation, stress intensity factor for certain crack shape size and specimen geometry can be calculated:

$$K_I^2 = E' = \frac{E' P^2}{2B}\frac{dC}{da} \quad \textbf{(14)}$$

For plane stress $E=E'$, and $E/(1-\nu^2)$ for plane strain.

In a plane strain condition, crack resistance of a material is independent on the crack length. For specimens with thin thickness and dominant plane stress, crack resistance is dependent on the amount of stress and initial crack length. *R* changes with increasing stress and crack size contributing to stable crack growth. This situation remains stable as far as critical combination of stress and crack length would occur. In other word, available energy release rate exceeds crack resistance, $G>R$.

In stable crack growth, the R-curve can be determined by conducting experiment either in stress control or displacement control condition. R-curve is a plot versus stable crack extension, Δa. Crack growth resistance can be described in term of energy.

$$K_R = \sqrt{E'R} \quad \textbf{(15)}$$

The resistance curve is used to calculate K_C within crack growth. For example in load control situation the load rises up gradually causing increment in crack length up to unstable crack growth situation when $K_G=K_C$.

ASTM E 561-94 is a standard test method for metals obtaining the R-curve in which three types of specimen can be fabricated and tested. In Figure 5 the relation between crack resistance and critical stress intensity factor for different initial crack length is shown schematically.

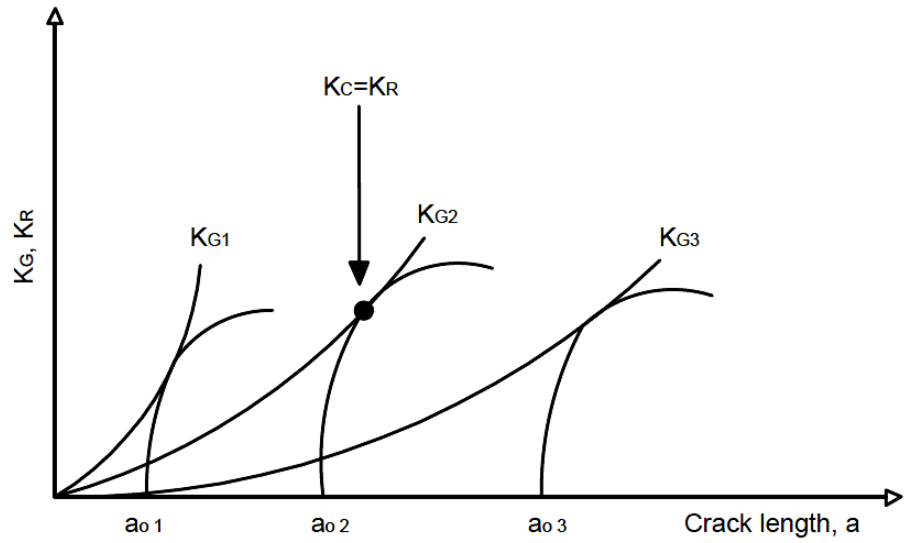

Figure 5. Obtaining K_C as function of crack initial crack length through R-curve

2.1.2 Non-Linear Elastic Fracture Mechanics

The linear Elastic Fracture Mechanics (LEFM) method has been broadly used to predict crack propagation for different materials. This method is based on the stress near the crack tip called the stress intensity factor [1]. Later Kaplan found that crack behavior in quasi-brittle materials such as concrete cannot be predicted correctly by LEFM method [5].

Fracture mechanics of concrete discusses about the condition around and front of crack throughout concrete. When a crack occurs, as the deformation increases, micro-cracks propagate throughout material leading to a true crack which is not able to transmit any load [6]. There are three levels in which fracture of concrete can be discussed. On the micro-level, mineralogical properties of concrete particles are considered. The meso-level of concrete assess the composite nature of concrete and chemical interaction between cement paste, aggregate and a bond layer between these constituents. In most studies conducted in preceding years, fracture mechanics of concrete was investigated in the macro-level in which concrete is modeled as a homogeneous isotropic material [6].

Past assessments dealt with cracks in concrete in two ways. First group investigated fracture toughness of concrete by parameters obtained from LEFM theory. Other groups mostly dealt with the recognition of cracks and fracture surface and the effect of material inhomogeneity on cracking [7].

The fracture toughness (K_{1c}) in concrete should not be considered as a material constant since the critical energy release rate changes during a unit extension of homogeneous and isotropic material, and also it is sensitive to specimen size, loading rate, etc.[8].

In concrete, breaking of the aggregate, mortar cracking and deboning of these elements separately form before global failure which is dependent on different factors such as load history, physical feature of specimen and etc. [7]. This may lead to the inability of LEFM theory in

concrete to recognize the effect of each subcritical material damage in all stages, while only in ideal brittle fracture energy is what released instantly causing local and global instability [7].

Initial cracks in concrete material occurs before loading at the aggregate-mortar interfaces attributed to mortar shrinkage. Generally speaking, initial cracks in concrete form in three phase due to inherent defects regardless of loading history. The bonding at interfaces is the weakest part, subsequent cracks form in mortar phase due where its tensile strength is relatively less than coarse aggregate [7]. It has been shown through many experiments that the tensile and compressive strength of concrete strongly depends on the distribution and orientation of these initial defects in concrete [7].

As it is shown in Figure 6, the stress-strain behaviur of concrete is not linear elastic under constant loading up to fracture, therefore, some assumptions in LEFM theory are not satisfied for concrete [7].

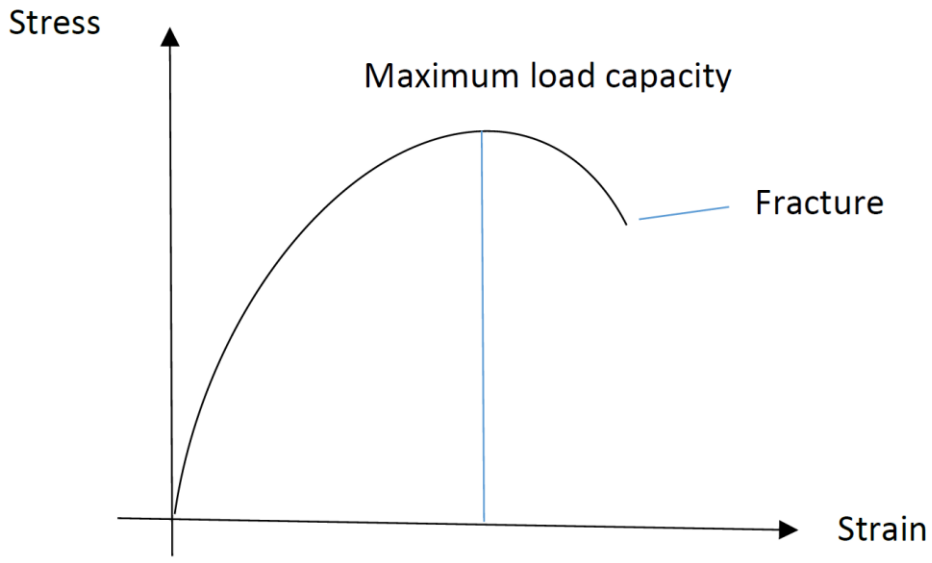

Figure 6. Typical stress-strain curve for concrete

2.1.3 Fictitious Crack Model (FCM)

In 1976, the fictitious crack model was developed by Hillerborg et al. [9]. The fictitious crack principle facilitates investigation of development of the fracture zone including initiation and propagation of the crack in quasi-brittle material like concrete. Also, it is important to note that the fictitious crack model assumes homogeneous material throughout the fracture zone. Thus, coarse aggregate as an irregular component of concrete should be a few times smaller than the size of the analyzed structure.

Hillerborg et al. proposed a well-defined model through numerical methods by which the non-linear behavior of concrete in fracture process can be determined. In this method, fracture energy is obtained by three point bend test and following equation [10]:

$$G_F = \frac{A_d + G_{mg}}{A_c} \quad \textbf{(16)}$$

Where, A_d is the area under the load-displacement curve, G_{mg} is the fracture energy by weight of the prism and A_C is the area of the ligament over the notch. The superiority of this method in representation of fracture behavior than other LEFM is asserted.

2.1.4 Cohesive Crack Model (CCM)

The cohesive crack model is known as a simple and popular method to characterize the behavior of a finite-sizer fracture process zone. This model was developed based on the fictitious crack model by Hillerborg in which a fictitious crack transmits normal stress throughout a line crack. The normal stress is a function of crack opening displacement ($\sigma = f(w)$). The more opening displacement, the less force is transmitted between two sides of a crack.

The softening curve *f(w)* described by Hillerborg in 1976 is a decaying exponential which later was simplified by Petersson [11] to a bilinear form shown in Figure 7.

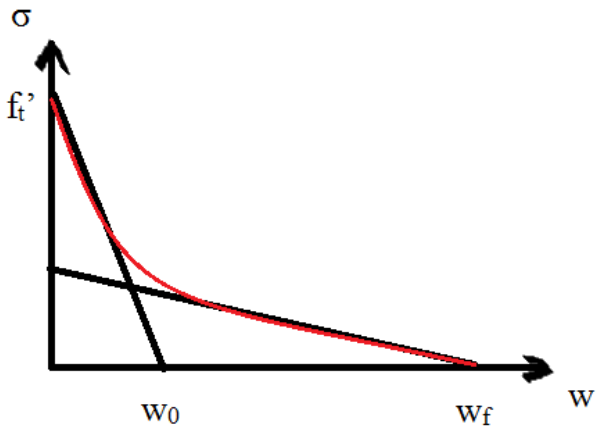

Figure 7. Bilinear softening curve (Stress vs. Crack opening)

The total dissipated energy by fracture per unit area (G_F, J/m^2) is calculated as the area under the softening curve *f(w)*. Finally, the cohesive crack model can be characterized through two parameters defined in the bilinear softening curve:

$$G_F = \int_0^{\infty} f(w)dw \quad (17)$$

$$G_f = \frac{f_t'^2}{2\sigma_0'} \quad ,(\sigma_0' = \frac{df(0)}{dw}) \quad (18)$$

As mentioned earlier, G_F is the total area under the softening curve and *Gf* corresponds to the area under the initial tangent of slope. G_f is later used to determine the maximum load of structure and the size effect consequently, remarked by Planas et al.[12].

It was noticed that fracture energy and material strength is dependent on the scaling and size effect indicating the existence of a material property, which was defined as the fracture characteristic length [3]. Regarding the use of the bilinear softening curve, fracture characteristic length of concrete can be expressed in two forms [13]:

$$l_1 = \frac{E' G_f}{f_t'^2} \quad (19)$$

$$l_{ch} = \frac{E' G_F}{f_t'^2} \quad (20)$$

It is important to note that cohesive crack model can be applied when there is uniaxial mode, or when the opening mode is the predominant mode in fracture. Also, microcracking and frictional slips adjacent to crack zone are ignored, and the crack is assumed to be an ideal straight line crack.

2.1.5 Size-Effect Model

In order to obtain fracture parameters independent of specimen size and shape, Bazant proposed the Size Effect Law determining the fracture energy of different concrete samples [14]. This method is based on the maximum load of different specimens with similar geometry of the notch. Three-point bending prisms can be fabricated with different specimen size. The span-depth ratio should be more than 2.5, and the notch depth-prism depth is considered between 0.15 and 0.4. After measurement of the maximum load for all specimens the fracture energy is determined.

2.1.6 Effective Crack Model (ECM)

Karihaloo and Nallathambi proposed an effective crack model which is independent of the size specimen. In this method the stress intensity factor is determined from a three-point bending test under quasic-static loading system [15]. A full test can take between 1 to 10 minutes as long as load reaches the peak load.

Young's modulus of concrete either can be measured by a cylindrical specimen test or an equation presented by this method. The fracture toughness of a material can be simply determined after drawing load-deflection diagram for different ratio of initial crack length/prism depth (a_0/W) as it is shown in Figure 8.

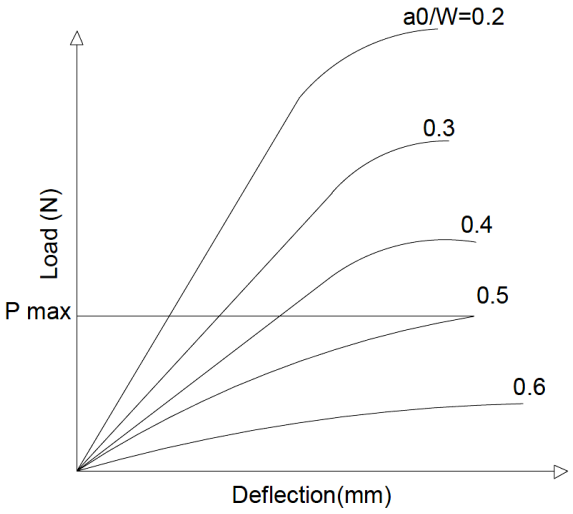

Figure 8. Typical load-deflection curve for various a_0/w

2.1.7 Two-Parameter Model (TPM)

Jeng and Shah [16] developed a model based on the fictitious crack model and previous models of metal. Since concrete is not fully compatible with a linear elastic fracture mechanics approach, two parameters (fracture toughness, $K_{Ic,}$ and critical crack tip opening displacement, $CTOD_c$) were proposed to demonstrate non-linear elastic behavior of concrete. It was assumed that when the stress intensity factor and crack tip opening displacement reach a critical point, the initial crack notch grows to an effective crack length which is the sum of the initial crack length and the effective crack growth ($a_{eff}=a_0+\Delta a$). In this model, the crack growth begins with pre-critical crack and continue till post-critical crack happens. The critical crack growth is then obtained from the difference between initial loading (C_i) and unloading compliance (C_u) immediately right after peak-load (Figure 9). when effective crack length is obtained, material properties K_{Ic} and $CTOD_c$ can be determined by maximum load, P_{max} and effective crack length, a_{eff}.

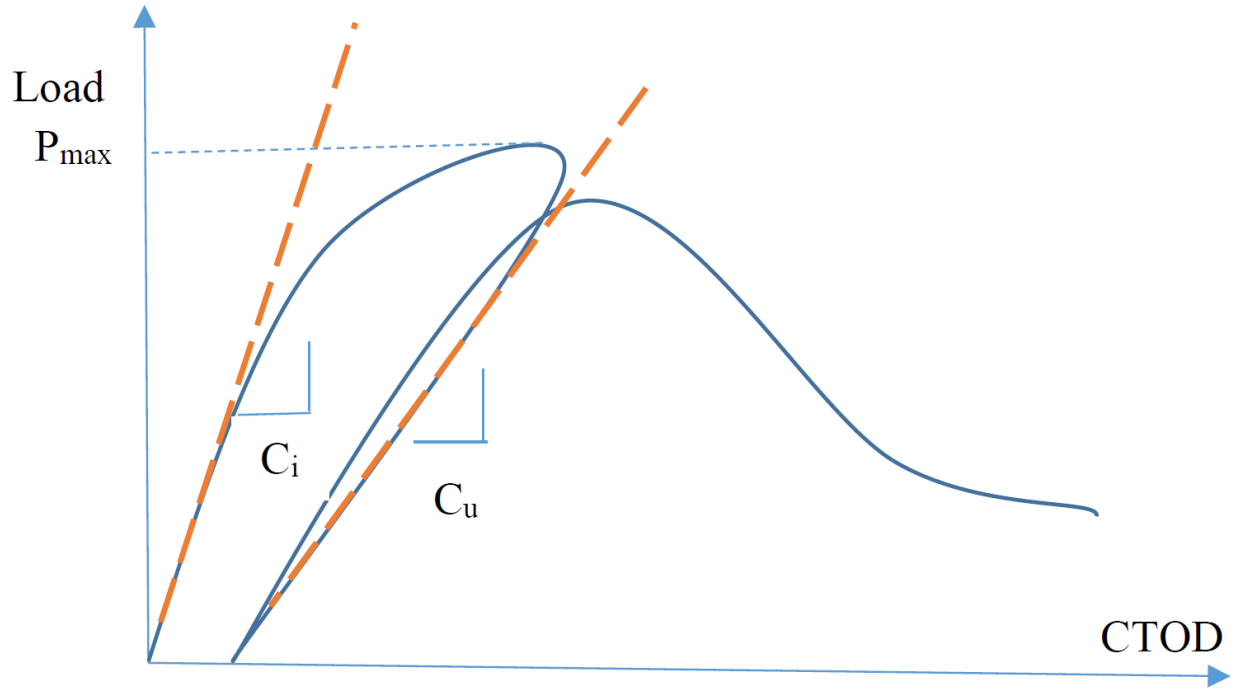

Figure 9. Stage of crack growth in Two-Parameter Model

The demonstrated figure is used to calculate three parameters including Young's modulus of elasticity (E), fracture toughness (Ks_{IC}) and critical crack tip opening displacement ($CTOD_c$). Parameter Q, was then proposed for a parametric study as it normalizes the model predictions. Q with dimension of length is expressed as:

$$Q = \left(\frac{E.\mathrm{CTODc}}{K_{IC}^{s}}\right)^{2} \qquad \textbf{(21)}$$

Also, G_R, fracture resistance can be calculated by $G_R= (K^S_{IC})^2/E$. Fracture resistance can be referred to required energy or tolerance of material to deformation prior to crack development. This concept may explain better when concrete dilation happens around prestressed wires after

de-tensioning. Apparently, fracture resistance should be taken into account when crack propagation is evaluated.

It was observed that the Two-Parameter Model and the size effect model yield very similar numerical results [17]. The values of fracture energy (G_f) in the size effect model and fracture toughness (K_{IC}) in two-parameter model are essentially the same, and their second parameters are related as [18]:

$$CTOD_C = \frac{\sqrt{32}K_{IC}\sqrt{c_f}}{\pi E} \quad \textbf{(22)}$$

Test Procedure

Different test methods have been used to calculate fracture properties of concrete. Extensive research has been conducted on the use of circular, semi-circular bend specimens for civil engineering construction materials [19-21]. Easiness and less required material for fabricating these samples have made them popular. There are other test specimens with various geometries and loading condition such as Compact tension, Wedge Splitting test [22], four point bend, Brazilian disc, edge notch disc bend, and so on, among which the closed-loop three point bend test was utilized to calculate the initial linear portion of the cohesive crack model (CCM) (Level I) and the two-parameter model parameters (Level II) [23]. It has been a continuous attempt to standardize the fracture parameters by level I and level II test procedures to obtain material properties for any concrete structure design. The notched prism in three-point bending is easy to fabricate, and also this method was recommended by the ACI 446 committee as it provides both level I and II (maximum load and post-peak control)[23]. Moreover, continuous data acquisition can be adequately done where the fracture process zone of concrete is relatively large [23]. However, to gain valid and reliable fracture toughness results from any test procedure, one should select an appropriate range for specimen dimensions. For some materials like metal with small fracture process zone, a smaller shape of specimens may lead to valid results whereas geometrical consideration should be taken into account when using mixtures with different maximum aggregate size in concrete. The rectangular prisms used in this research met the requirements, by which the adverse effect of specimen boundaries on fracture energy and fracture toughness is eliminated for all mixtures with maximum aggregate size smaller than 25mm [24].

Shah and Jeng proposed a two parameter model to evaluate fracture toughness of quasi-brittle material like concrete. In this method prism shape of the specimen has a specific dimension which is shown in Figure 10 below. It is recommended that for maximum aggregate size larger than 25.4 mm, the specimen size should be larger. Notch-depth ratio and loading-span/depth ratio are considered 1/3 and 4, respectively [25].

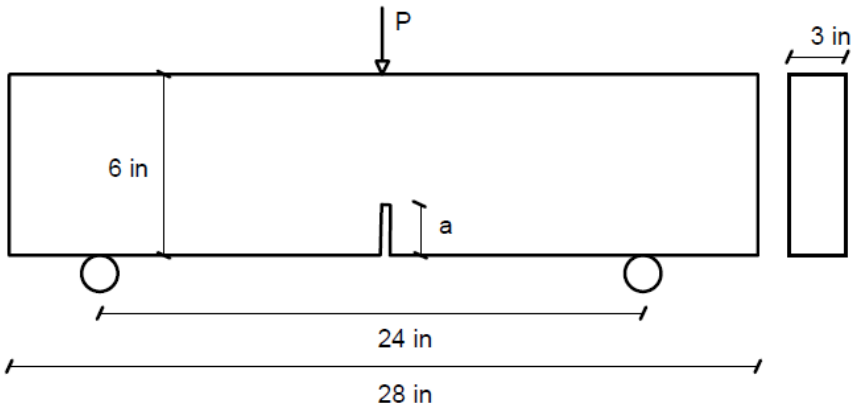

Figure 10. Geometry of specimen for three point bending prism

To measure displacement during the test, the CMOD measuring plane should be installed at the center of prism. The loading system with respect to test purpose may be changed. The rate of change of stress should be controlled particularly in quasi static tests in which peak load should be reached in less than 5 minutes within the loading part. Also, in this monotonic loading statues unloading happens when loading reaches about 95% of peak load.

There is no strict mention about the unloading condition. The unloading happens over a 10 second period [26]. This loop continues until the sample failure. It is recommended that after the first cycle the rate of loading should be increased by 10 times to finish the test in less than 30 minutes.

First aim is calculation of fracture toughness, $K_{IC,}$ which is dependent on crack length and specimen geometry. Effective crack length, a, is the sum of initial crack length and stable crack growth at peak load which can be calculated using following equations:

$$E = 6SaV_1(\alpha)/(C_u W^2 B) \quad \textbf{(23)}$$

$$V_1(\alpha) = 0.76 - 2.28\alpha + 3.87\alpha^2 - 2.04\alpha^3 + \frac{0.66}{(1-\alpha)^2} \quad \textbf{(24)}$$

$$\alpha = (a + H_0)/(W + H_0) \quad \textbf{(25)}$$

Where:

C_u= unloading compliance at peak load

H_0= clip gauge holder thickness

S = span of the prism

The stress intensity factor determined in this method can be calculated by:

$$K_{IC}^{S} = \frac{3SP_{max}}{2BW^2}\sqrt{\pi a}F(\alpha) \quad (26)$$

$$F(\alpha) = \frac{1}{\sqrt{\pi}} \frac{1.99 - \alpha(1-\alpha)(2.15 - 3.93\alpha + 2.7\alpha^2)}{(1+2\alpha)(1-\alpha)^{\frac{3}{2}}} \quad (27)$$

Where:

P_{max}= measured peak load, and $\alpha = a/W$

The specimen fails at the critical stress intensity factor corresponding to the value of $CTOD_c$.

$$CTOD_c = \frac{6P_{max}Sa}{W^2BE} V_1(\alpha)\{(1-\beta)^2 + (-1.149\alpha + 1.081)(\beta - \beta^2)\}^{\frac{1}{2}} \quad (28)$$

Where $\alpha = \frac{a}{W}$ and $= \frac{a_0}{a}$.

The two fracture parameter model is independent of specimen depth, but changes as other dimensions alter.

2.1.8 Fatigue Crack Growth (FCG)

Structures such as railroad and bridges are exposed to repeated loading leading to a gradual failure without obvious warning. It is indicated that the failure process in those structures under cyclic loading begins with crack initiation, continues with micro-cracks growth that make up macro-crack leading to final failure.

The initial crack size can be detected by non-destructive testing. This crack is made up of discontinuities which are not detectable and caused by voids, flaws, damage, and inhomogeneity.

The fatigue crack growth rate, *da/dn*, is defined as the change of crack length per each cycle which is related to various factors including, stress state, load frequency, environment, type of load cycle, temperature and load history [1].

Crack propagation rate can be divided in three parts in which micro-cracks grow slowly first, and speed up in second part and finally rapidly goes toward failure. Many studies have been conducted to describe the crack growth rate among which the Paris equation is well known and based on experimental data and it is only provided to calculate *da/dn* in the second region.

$$\frac{da}{dn} = C(\Delta K)^m \quad (29)$$

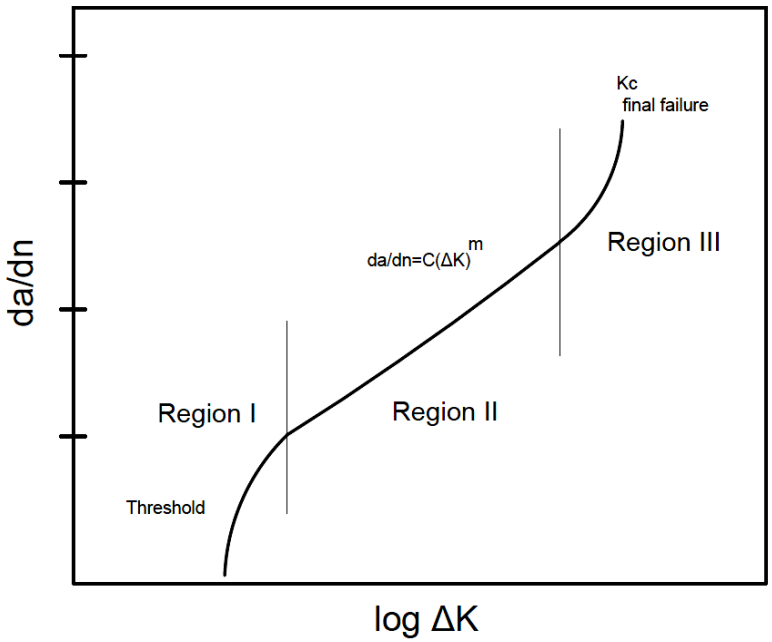

Figure 11. Schematic shape of fatigue crack growth rate curve

It has been seen that many cracks under tensile cyclic loading are closed because of plastic zone surrounding crack tip, which is a quarter of the plastic zone in monotonic loading. There are other causes for crack closure such as stress ratio, and crack front geometry.

According to some research, there is a critical crack length, l_0, below which cracks do not advance. In this situation ($a < l_0$) [27]:

$$\Delta\sigma_{th} = \Delta\sigma_e \tag{30}$$

$\Delta\sigma_e$ is the limiting stress value that makes very long fatigue lifetime. And $\Delta\sigma_{th}$ is the fatigue limit stress range when a crack is available. For longer cracks entering first part of the crack growth rate, $\Delta\sigma_{th}$ is calculated using linear elastic fracture mechanics.

$$\Delta\sigma_{th} = \frac{\Delta K_{th}}{\sqrt{\pi a}} \tag{31}$$

ΔK_{th} is the threshold stress intensity range for long cracks.

As mentioned earlier, fatigue crack growth has been well studied in metallic materials and a few standard test methods have been published. ASTM E647 – 15 has been widely used to measure fatigue behavior of metals and brittle materials. Despite all attempts at determination of fatigue crack growth in concrete, there is no standard test method measuring fracture parameters of concrete under cyclic loading.

Crack propagation under cyclic loading represents fatigue behavior of concrete in the field. Various concrete structures such as concrete bridges, concrete pavements and concrete railroad

ties are exposed to dynamic loading during service life and require fracture analysis through cyclic loading.

Various investigations have applied fracture equations for crack propagation in metals and rocks to verify validity of those formulas in fatigue crack growth testing of concrete.

Works done on fatigue behavior of plain concrete indicated that the empirical Paris' law (29) for metals may be applicable for crack growth in plain concrete [28, 29]. Also, scattered *da/dn* and *ΔK* data in log scales exhibit a straight line. Investigations show there is declaration stage of fatigue crack growth at the beginning in concrete followed by an acceleration stage continuing steadily up to failure statues [30, 31].

Models introduced by Paris and others fail to cover the entire range of *da/dn* curve versus *ΔK*. McEvily proposed a model representing the entire range of the curve based on ELFM [32]:

$$\frac{da}{dn} = C(\Delta k - \Delta k_{th})^2 (1 + \frac{\Delta k}{K_{crit} - K_{max}}) \quad (32)$$

Kolluru et al proposed a model describing declaration and acceleration stage of fatigue crack growth in a three point bend test under quasi-static and low cycle (high amplitude) loading. They also concluded that the crack length at the point of changing rate of crack growth from declaration to acceleration in constant amplitude loading can be predicted by the crack length at the peak load in quasi-static loading [31]. Also, the crack growth in acceleration stage can be accurately modeled by the Paris law expression. Later Shah et al, modified the Paris law with respect to size effect was considered to be able to accurately predict fatigue crack growth in acceleration phase [30].

Perdikaris et al. assessed fracture behavior of concrete through fatigue testing. Fracture parameters for fatigue crack growth of concrete were obtained and compared to those reached from static loading in four-point bending prism. Test results analyzed by LEFM showed that fracture toughness of concrete increases under cyclic loading, and further resistance was observed with increasing crack length and number of loading cycles [33].

However, an experimental assessment of fatigue crack growth of high-strength concrete through a wedge-splitting test indicated that when the strength of concrete increases the fatigue crack growth rate increases. In other word, the fatigue life of lower strength concrete is more than that with higher strength [34]. The same conclusion has been made by Lou et al on three point bend test with respect to the effect of mix strength on the fracture behavior of mortar. When the mix strength increases, the toughness of crack emanation from a notch increases and the resistance curve behavior increases; whereas, fatigue crack growth resistance decreases in continue. It seems there is an optimum design considering the combination of strength, fracture toughness and fatigue crack growth resistance [35].

A recent study on flexural fatigue crack growth rate under varied amplitude of loading indicated that rate of change of fatigue crack growth in concrete is not affected by specimen size in a three point bend test. Also, the stiffness of the structure progressively decreases due to a reduction in slope of post peak unloading-reloading part of load-displacement curve [30].

Cyclic Loading

Test specimens in fatigue crack growth of concrete are similar to monotonic load testing. Two widely used specimen shapes, three-point bend and wedge splitting tests, are popular due to the simple fabrication and test procedure. Cyclic loading with constant amplitude and different stress ratio can be applied while crack length is measured during each repetition. In order to address the difficulty of crack length measurement, crack length can be obtained through CMOD-compliance method for concrete [29, 33]. This technique can be also applied in the wedge-splitting test [34].

Some structures, in reality, experience variable loading amplitude during service life. The difference in maximum stress at each cycle significantly influences fracture behavior. However, variation in stress amplitude seems to be more destructive than constant loading [36].

Most of cyclic fracture testings has been conducted without rest periods. Studies have shown that due to the relaxation of concrete, rest periods between each cycle improve fatigue strength of concrete if only there are no stress reversals [37].

A recent study by Brake and Chatti on the prediction of fatigue crack growth in low cycle and high cycle testing indicated that the results of the crack resistance curve of low cycle fatigue can be used to predict the crack resistance curve under high cycle fatigue [38].

2.2 Effect of Test Condition

2.2.1 Specimen Geometry

A research on size effect of the compact tension wedge splitting test was conducted using five different approaches. For large specimens non-linear behavior of stress along crack extension was observed. However, it was concluded that the specimens' depth affects slightly on unstable fracture toughness and critical crack length increases when the depth of specimen increases [39].

Bazant and Xu investigated the size effect of a three point bend test for plain concrete. The paris' law was used and was adjusted to the different size of specimens with the same loading system. Results showed that fatigue is well explained by the stress intensity factor when specimen size is large. Moreover, smaller crack advance occurs when the size is large for the same stress intensity factor, but larger crack length happens for the same nominal stress amplitude. However, when load is cyclic the brittleness value is much smaller than for monotonic loading. However, crack length versus the number of cycles was proposed considering size effect adjusting parameters [29]:

$$N = \left(\frac{d_0}{C}\right)\left(\frac{b\sqrt{d}}{P}\right)^n \int [f(\alpha)]^{-n} d\alpha \qquad (33)$$

In which $\alpha = a/d$ is the relative crack length, d is the characteristic dimension of the specimen, b is the specimen thickness, P is the load, $f(\alpha)$ is the function on specimen geometry and C is a constant.

Tests done by Perdikaris et al. confirmed that regarding the size effect of specimens on fracture toughness and fracture energy, unlike metallic material, K_{IC} and G_{IC} are not material parameters [33].

in 2004, a study on size effect on fatigue crack growth was done proposing a new size-dependent crack growth law by which fracture energy and stress intensity factor obtained from cyclic three-point bend test can be renormalized regarding size effect [40].

$$\frac{da}{dN} = C_1(D)K_1^m \tag{34}$$

$$C_1(D) = \frac{C}{1+d}\alpha^{\beta_1}D^{\beta_1} \tag{35}$$

Where D is a characteristic structural size, m and C are material constants of the Paris-Erdogan law, d is the fractal dimensional increment with respect to the Euclidean space ($0 \leq d \leq 1$). α is relative crack depth and $b1$ is the exponent of the size-dependent fatigue crack growth law.

Through dimensional analysis of the size effect on fatigue crack growth, the most dominant parameter controlling fatigue crack propagation is the size of the structure and initial notch size [41].

2.2.2 Notch Size

Notch size sensitivity depends on the material properties. Unlike ductile material, concrete meets less stress in the net section when a notch is introduced. As the specimen size increases, the notch sensitivity increases. There are some equations taking the effect of notch size in concrete into account. The following expression proposed by Ziegeldorf assesses notch sensitivity [42].

$$\frac{\sigma_{net}}{\sigma} = \frac{K_{IC}}{\sigma}\frac{1}{\sqrt{a}\left(1-\frac{a}{b}\right)^2 F(\frac{a}{b})} \leq 1 \tag{36}$$

Where σ is the stress at the un-notched specimen, a is the crack length, and b is the prism depth.

Carpinteri proposed a parameter to evaluate brittleness of mortars and concrete by which the notch sensitivity can be determined [43].

$$S = \frac{K_c}{\sigma_u b^{0.5}} \tag{37}$$

Where S is the test brittleness number, σ_u is the maximum tensile strength and b is the prism depth. In accordance with euqation (*37*) it can be implied that the concrete specimen with 650 mm depth or higher and cement paste with 100 mm depth or higher are notch sensitive.

Selection of notch size depends on the specimen size, aggregate size and supports distance. There is constraint dictating proper notch depth. Small notch depth may cause unstable cracking during testing and large notch depth may lead to quick failure and inadequate data points. Baluch et al. chose a notch to prism depth ratio of 0.5 meeting limitation [28]. It has been seen that as span and notch depth in the three-point bend specimen increases, the fracture toughness of concrete decreases due to the reduction in net fracture zone area [44].

2.2.3 Loading

The stress-strain curve of concrete is affected by the rate of loading. The bigger the rate of loading the more slope in the stress-strain behavior will be observed leading to higher young

modulus and compressive strength. Whereas, a slow rate of loading causes lower fracture load. This may be attributed to forming of subcritical cracks and bigger flaws before fracture, also creep behavior in slow loading increases total strain in a specific load [7].

An investigation on loading rate shows the fracture energy is sensitive to the loading rate and its sensitivity depends on the loading rate in a three point bend test. Loading rates below 0.007 mm/s have a small effect. However, as the loading rate increases, an increase in fracture energy and peak load occurs [45].

It has been reported that in dynamic loading with large number of cycles, decreasing maximum stress level and stress range values leads to an increase of reparations to failure [46].

Loading frequency affects fracture strength particularly in high stress level. As frequency of loading increases, fatigue strength increases for higher stress level [46, 47]. Other investigation showed effect of rate of loading is insignificant for frequencis between 70-440 cycles per minute [48]. Furthermore, some results illustrated that in saturated and surface-dry prism fatigue testing, there is negligible difference between fatigue strength obtained in the range of 4 to 20 Hz loading [49].

The effect of various factors on fatigue crack growth in an overload condition has been assessed through sensitivity analysis, and the results express that the fracture toughness is the most dominant factor making acceleration of fatigue crack length under overloading [50].

2.2.4 Temperature

It has been observed by some studies that temperature influences fracture properties of concrete in different ways. Unlike plain concrete, the fracture parameter of steel fiber reinforced concrete is considerably affected by higher temperature, such that as the temperature increases the fracture energy decreases [51].

The same results were observed by an investigation in which 80 notched prisms were tested under cyclic heating and cooling. The temperature range was between 50 -300 ^{o}C. It was concluded that as temperature increases the residual fracture toughness of concrete decreases. Also, increasing in the number of heating and cooling cycles caused a further decrease in fracture toughness of concrete [52].

Other investigations of effect of heating temperature, exposure time and curing age on residual fracture toughness of normal and high-strength gravel concrete indicated that heating concrete over 200 ^{o}C decreased fracture toughness whereas below 200 ^{o}C some inverse effects were observed. The same trend occurred for longer exposure time in which early exposure stage, under 12 hour, showed significant effect [53]. Another experimental study on fracture toughness of a three-point bend specimen at different temperatures from 20 to 1300oC was conducted, illustrating that increasing the testing temperature leads to the reduction in the stress intensity factor for ordinary and refractory concrete [54].

An assessment of the simultaneous effect of temperature and humidity on fracture energy of concrete showed a slight effect of saturate situation in room temperature but a significant impact at temperatures close to 100 ^{o}C [55].

Prism tests performed in the temperature range of 20 to -35°C showed a higher fracture energy for lower temperature. There was a 50% increase in fracture energy with declining temperature from 20 to -35 °C [56].

Bazant and Prat proposed an equation relating the temperature and facture energy of a bending prism [55]:

$$G_F = G_{F0}.exp\left[\gamma\left(\frac{1}{T} - 1/T_0\right)\right] \quad (38)$$

Where T_0 is the reference temperature in *K*, T is the actual temperature, G_{F0} is the fracture energy at reference temperature and Y is the material constant.

2.2.5 Curing

Curing condition may influence fracture toughness of concrete in terms of time, humidity level, and temperature. Well cured concrete has higher fatigue strength at a given time of loading. An investigation indicated that fatigue strength of concrete specimens after about 3 months of casting increases whereas beyond that time no significant changes are observed [57]. In other work, specimen exposed to heating temperature, showed a slight difference in toughness of concrete in the first 28 days of curing. For a longer curing age, very little influence on toughness in high temperature was observed [53].

Fracture toughness of concrete with different coarse aggregate at early ages from 1-28 days was assessed by Zollinger et al. The results express that as age increases, the brittleness concrete decreases [58].

Experiments done on prism fatigue test by Galloway et al. indicate that different curing conditions cause changes slightly from each other. However, specimens cured in air with high humidity showed the weakest fatigue and flexural strength [59].

2.3 Effect of Concrete Mixture

2.3.1 Aggregate Type

It is hypothesized that the type of aggregate influences the fracture behavior of concrete. Since most failures initiate at the interface of aggregate and mortar, chemical and physical properties of aggregates affect bonding between aggregate and cement past. Some of preceding studies have shown that the type of aggregate slightly affects the fatigue strength of concrete [60]. However, according to an investigation of the effect of coarse aggregate type on fatigue properties of plain concrete in flexure, plain concrete with gravel has higher fatigue strength compared to concrete with limestone. Moreover, different fine aggregates slightly change the fatigue strength of concrete [61].

Recent investigations on the effect of using new materials as aggregate replacement exhibited that they might have an improving effect on the fracture properties of concrete. Using a varied replacement ratio of recycled waste fiber aggregate in concrete can increase ductility and fracture toughness of concrete [62].

Steel fiber reinforced concrete with rubber as partial replacement of fine aggregate has been recently assessed through three point bend test. The results indicated that increasing rubber

content to a certain amount enhance fracture toughness and fracture energy of concrete but with further increment of rubber those parameters decrease [63].

2.3.2 Aggregate Shape and Texture

Initial defects (cracks) in concrete materials may exist prior to any super-imposed loading being applied. It has been proposed that most of the crack propagation happens along interface of mortar and aggregate in concrete where the bonding is weak. Thus, crack tips, which already initiated because of interfacial flaws and voids between aggregate and mortar, tend to advance along the interface of these materials, in which less energy is required to overcome crack resistance around the crack tip [64].

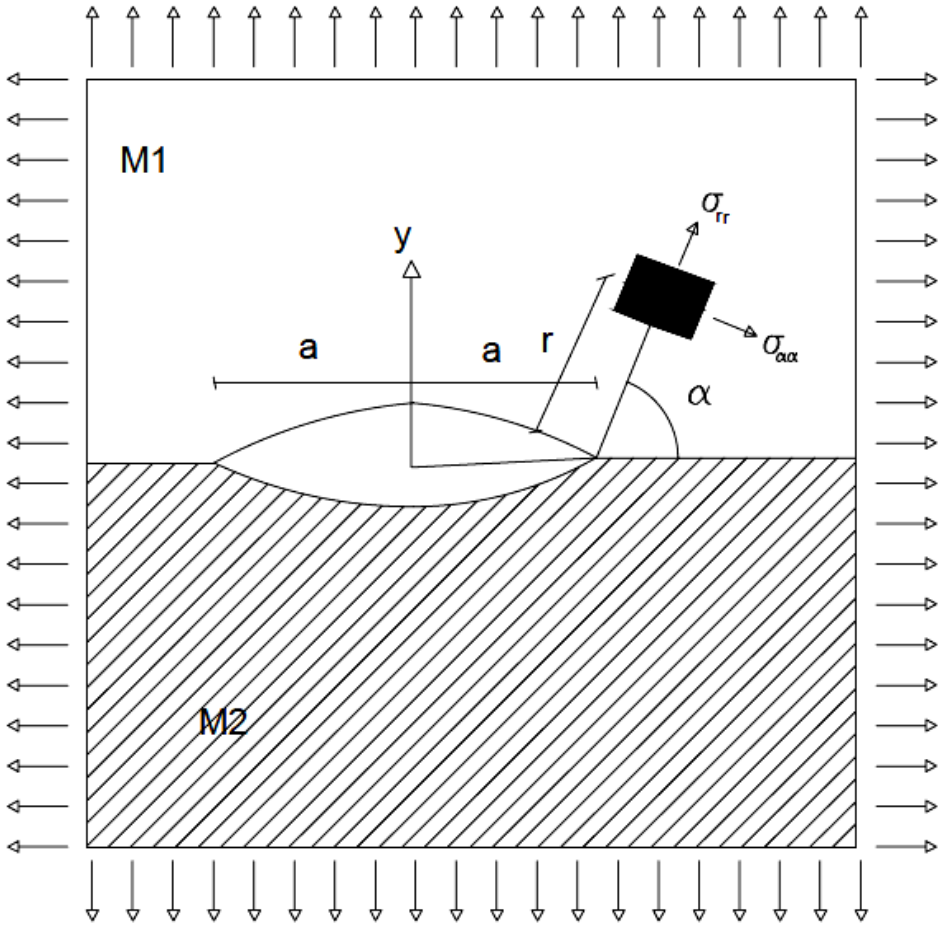

Figure 12. Notation for interfacial crack

Crack extension will take place when one of the following condition is reached:

$$\sqrt{2\pi r_0}\,\sigma_{\alpha\alpha}{}^{1}(\alpha_0^1, r_0) = K_{IC}^1 \qquad 0 < \alpha_0^1 \leq \pi \tag{39}$$

$$\sqrt{2\pi r_0}\,\sigma_{\alpha\alpha}{}^{2}(\alpha_0^2, r_0) = K_{IC}^2 \qquad -\pi < \alpha_0^2 \leq 0 \tag{40}$$

$$\sqrt{2\pi r_0}\,[\sigma_{\alpha\alpha}^2(0, r_0) + \sigma_{r\alpha}^2(0, r_0)]^{1/2} = K_b \qquad \sigma_{\alpha\alpha} > 0 \tag{41}$$

Where $K_{Ic,}$ is the critical stress intensity factor of adjacent materials to crack tip, and K_b is considered as the critical parameter related to adhesive of the bond together with the coplanar crack propagation r_0 is related to the material properties, and is the maximum length of the stress intensity factor zone.

An investigation illustrated by testing four point bending prism of a constitutive model of concrete and paste cement mortar, that the interface between concrete and paste cement mortar is quite weak. Also, fracture energy for phase angle between 0^o-60^o varies between 2-16 J/m^2, while for phase angles higher than 70^o is higher than 20 J/m^2 [65].

Although it has been hypothesized that the aggregate shape influences the fracture behavior of concrete in different ways, the impact of aggregate type at different concrete compressive strengths has not been fully addressed. According to a study done by Nallathambi, the fracture zone around a crack is affected by micro-cracks and bond-cracks formed around aggregates which are highly affected by texture and angularity of the coarse aggregate (Figure 13). Crushed aggregate in concrete mixes contributes to a higher crack initiation stress than rounded aggregate because of enhanced surface area and angularity of the aggregate [44]. On the other hand, some investigation showed an adverse effect of polygonal shape and higher volume fraction of aggregate on tensile strength [66].

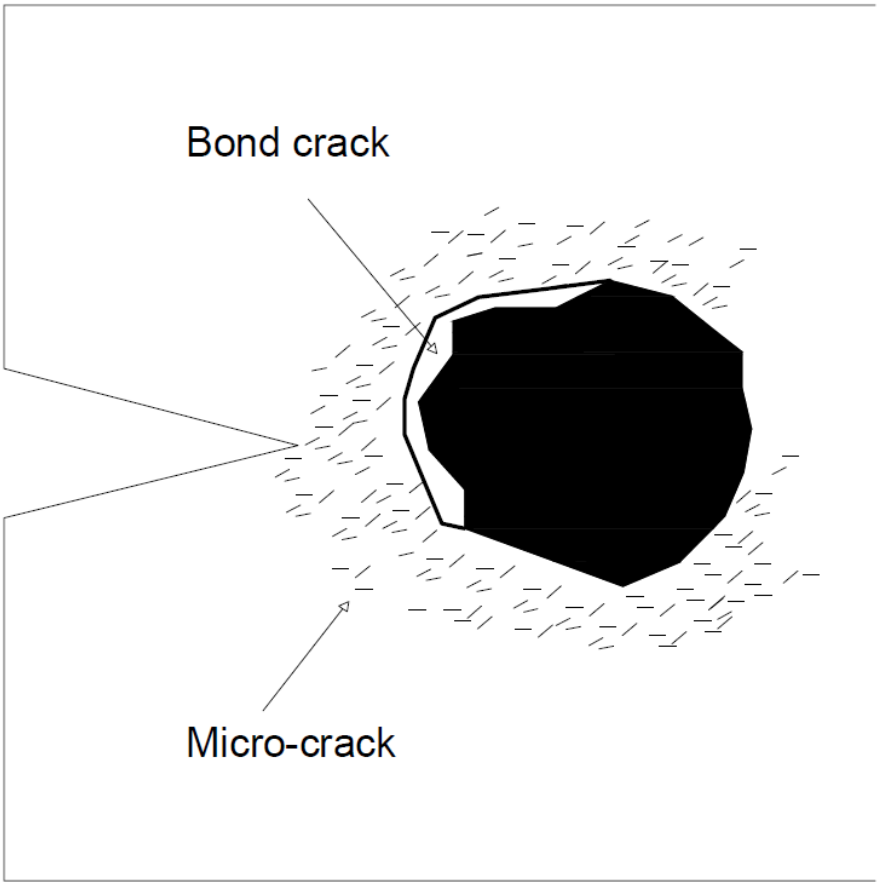

Figure 13. Bond crack and micro-cracks around an aggregate

2.3.3 Aggregate Size and Distribution

Generally, there is no direct relation between the size of the aggregate particles and toughness even though the results of some experiments imply less toughness for coarse aggregate than finer materials [67]. It has been observed that as the coarseness of aggregate increases, the fracture parameters enhance [44, 68, 69]. Le et al. showed that the maximum size of aggregate profoundly affects the fracture energy, peak strain and crack width of concrete in uniaxial tension [70]. Moreover, as the maximum size of aggregate increases, the fracture toughness and fracture energy calculated by the Size-Effect method increases [71].

2.3.4 Coarse Aggregate Volume

It has been seen by some studies that the volume of coarse aggregate is very effective in altering fracture parameters such as fracture energy (G_F), fracture process zone length and the brittleness number [5, 5, 69, 69, 72, 73]. However, some research has shown that although the size distribution of the aggregate significantly impacts the fracture energy value of high strength concrete, there is no significant change in fracture toughness value [74, 75]. Nikbin et al showed that an increase in coarse-aggregate volume causes a significant increase in fracture energy of self-compacting concrete although its effect was not determined at the same strength for all specimens [72]

2.3.5 Water/Cementitious Material Ratio

Generally, low water/cementitious material ratio contributes to higher strength in the matrix. It has been observed that brittleness of concrete as function of characteristic length l_{ch} increases when the strength of concrete rises. In other word, the fracture toughness of concrete increase as the *w/cm* decreases [76]. In cement paste the same behavior is observed, but the decrease in porosity does not lead to higher toughness [67]. The same results were observed by Nallatambi, indicating the adverse effect of higher w/cm ratio effect on fracture toughness. Moreover, despite of higher surface energy for mixes containing crushed aggregate, those with higher water/cement ratio exhibited less fracture toughness than mixes containing rounded aggregate [44].

Studies showed that as the water/cement ratio increases, crack propagation rate increase because of porosity around the aggregate –cement fracture zone. This trend has been observed despite of presence of various admixtures [77].

2.3.6 Fly Ash

Bharatkumar et al.[78] reported that slag and fly-ash decrease the fracture toughness and fracture energy of concrete mixtures with the same w/cm ratio, likely due to the presence of large un-hydrated particles. Also, the presence of fly ash increases workability and air content of concrete [79] which can lower fracture resistance of concrete at low strengths. On the other hand, some investigations reported an improving effect of fly ash on fracture parameters, with fracture toughness and fracture energy enhanced for mixes containing 10-20 percent fly ash. These values decreased when fly ash content exceeded 20% [80, 81].

2.3.7 Paste Content

Brown showed that the mortar has a higher fracture toughness than cement paste [82]. Additionally, increasing the volume of paste decreases the fracture resistance of concrete mixtures [83]. According to an investigation of the effect of aggregate on fracture behavior of high-strength concrete, for high-strength concrete, fracture toughness (K_{IC}) and fracture energy (G_F) reach maximum values at an aggregate volume of 60% [84]. Therefore, it has been hypothesized that increased aggregate content in concrete mixtures may increase fracture resistance.

2.3.8 Air Void Content

One of the factors resisting freeze-thaw cracking in concrete is air-void content due to space accommodation [85]. On the other hand, increasing air void can negatively impact other aspect of durability like shrinkage cracking [86]. However, at the time of this study, the effect of increased air content on fracture toughness and cracking was largely unknown. Aliha et al. found that by increasing air void content form 3% to 7%, the fracture toughness of asphalt mixtures remarkably decreased for pure and mixed modes of fractures [87]. It was hypothesized that presence of air voids could ease crack propagation around the crack tip and transition zone in concrete.

2.3.9 Admixture

It is said that presence of admixture causes a stronger paste-aggregate transition zone which can affect fracture behavior of concrete. Varied materials have been used to improve concrete performance in different ways. The effect of various admixtures on fracture parameters have been assessed through many studies.

An Investigation showed that slag and Fly ash as a widely used material decrease fracture toughness and fracture energy of concrete for same water/cementitious material ratio samples likely due to the presence of large unhydrated particles [78]. On the other hand, some investigations exhibited an improving effect of fly ash on fracture parameters of high-performance concrete in which fracture parameters such as fracture toughness and fracture energy enhanced for the mixes containing 10-20 percent fly ash. These values decreased with fly ash content exceeding 20% [80].

Various studies have been done on use of different materials in concrete influencing the mechanical properties of concrete. Using fine-ground ceramics as supplementary cementitious material has a slight effect on fracture parameters of concrete [88]. It has been seen that concrete containing polymer has higher fracture energy due to the polymer phase [89].

2.3.10 Reinforcement

Reinforcement evidently affects fracture properties of concrete regarding type, composition and tensile strength of the material used. Research on the effect of steel fibers and concrete strength on the fracture energy showed that the concrete with higher strength- higher water/cement ratio- is well compatible with steel fiber with higher tensile strength. On the other hand, the lower tensile strength of steel fiber showed good performance when water/cement ratio increased [76].

Fracture parameters determined by other studies have shown that the presence of different amounts of micro fibers contributes to an improvement in facture energy and toughness of concrete [90]. Experiments on the effect of steel fiber in concrete on fatigue life exhibited an improving effect of reinforcement within fatigue crack growth. It has been observed that crack length in a bending specimen progresses slowly and in large scale compared to plain concrete. In fact, the presence of steel fiber causes a larger declaration stage but wider at the beginning. However, the crack bridging zone significantly affects fracture behavior and fatigue life of concrete. Crack bridging degradation can happen in different ways. For steel fibers, interfacial bond degradation is the main reason, while fiber fatigue rupture is the most effective factor for polymeric fibers [91].

2.4 Fracture and Mechanical Properties (Phase 1)

2.4.1 Material Preparation

In order to investigate the effect of different properties of concrete on crack growth, fracture toughness tests were conducted on nine (9) different mixtures including different proportions and aggregate types. For this purpose, 12 concrete prisms (3in.×6in.×21in.) and 25-30 concrete cylinders (4in. diameter×8in. length) were made for each mix according to ASTM C192 to obtain fracture toughness, compressive strength and splitting-tensile strength parameters at 4000, 6000 and 8000 psi (27.5, 41.3 and 55.1 MPa).

To make sure that the samples were tested at the targeted compressive strengths, the compressive strength of 10-15 4-in.x 8-in.cylinders were tested at appropriate intervals. After reaching each targeted strength, three splitting-tensile tests on cylinders and four fracture toughness tests on prisms were conducted. All specimens were cured in a moist room (RH>98%, 75^{o} F) until 30 – 60 minutes before testing. This procedure was repeated for the nine different concrete mixtures.

Aggregate Type

To evaluate the effect of coarse aggregate type on concrete crack propagation, five different types of coarse aggregate (CA) were used. Four of these (CA2-CA5) were representative of sources used by concrete tie producers in the United States, while one (CA1) was a source local to the researchers in Manhattan, KS. Also, a locally-available natural silica sand was used as the fine aggregate (FA) for all mixtures in this research. Table 1 tabulates the aggregate particle size distribution for materials used in this study.

CA1 (Pea gravel)

CA2

CA3

CA4

CA5

FA

Figure 14. Coarse aggregates and fine aggregate

Table 1. Grain size distribution of aggregate

Sieve	Opening (mm)	CA1	CA2	CA3	CA4	CA5	FA
		Passing %					
1 in	25.4	-	100	-	100	100	-
3/4 in	19.0	100	78.1	-	92.3	98.0	-
1/2 in	12.7	85.4	31.3	-	52.9	85.4	-
3/8 in	9.51	65.1	9.2	100	30.5	62.6	-
#4	4.76	5.1	-	25.6	5.2	5.4	95
#8	2.38	0.7	-	0.5	2.2	0.7	80
#16	1.19	0.3	-	-	1.4	0.4	50
#30	0.595	-	-	-	-	-	25
#50	0.297	-	-	-	-	-	12
#100	0.149	-	-	-	-	-	2

Cement Type

Cement type might affect fracture resistance of concrete material at a given strength. Although it is well understood that durability is affected by cement type, there is limited research has addressed the impact of cement type on the fracture behavior at a certain strength. In the present research, ASTM C150 [92] Type III cement, which is commonly used by tie manufacturers to reach early strength in concrete, was used for all mixtures. Table 2 lists the properties of the Type III cement used in this study.

Table 2. Material properties of Type III cement

Component/ Property	Value
Silicon dioxide (%)	21.8
Ferric oxide (%)	3.4
Aluminum oxide (%)	4.27
Calcium oxide (%)	63.2
Magnesium oxide (%)	1.95
Sulphur trioxide (%)	3.18
Loss on ignition (%)	2.64
Free lime (%)	0.99
Sodium oxide (%)	0.21
Potassium oxide (%)	0.52
Sodium-equivalent alkalies (%)	0.55
Blaine Surface Area (m^2/kg)	559
Tricalcium silicate (%)	49.2
Dicalcium silicate (%)	25.3
Tricalcium aluminate (%)	5.6
Tetracalcium aluminoferrite (%)	10.3

Admixture Types

An ASTM C494 Type A and Type F high range water-reducing (HRWR) admixture was used to enhance the workability of the mixtures, particularly with low w/cm ratios. This admixture was a polycarboxylate-based superplasticizer. Air-entraining admixture was also used based on ASTM C260 only for the mix designed with 6% air void content.

2.4.2 Mechanical Properties

Sample preparation

In order to maintain consistency throughout the lab phase, all aggregates were oven-dried and cooled before mixing. Mix#1 (control mix) and Mix#2 were similar in design to mixtures used by concrete tie manufacturers. Mix proportion of mixtures used in the present research is tabulated in

Table 3.

To assess the effect of different factors, Mix#1 was designated as the Control Mix, and other mixtures were created by varying one or more parameters from the control mix. Variables for each batch made in this study are summarized in

Table 3. A slump of 5-6 in. was measured for Control Mix and HRWR admixture dosage was adjusted to keep the slump nearly constant for all mixes. Also, the Control Mix contained 1.7% air content while 5.6% air content was measured for the 6% air-entrained design.

Table 3. Concrete mix proportion designs

Mix	Aggregate (lb per yd^3)						Cement (lb per yd^3)	w/cm Ratio	HRWR Admixture (fl oz per yd^3)	Target Air Entrainment	Fly ash Class F	Crushed aggregate (%)	λ	Variable
	CA1	CA2	CA3	CA4	CA5	FA								
Mix#1	1445.0	-	-	-	-	1445.0	813.8	0.38	40	0%	-	23	0.5	Control mix
Mix#2	-	897.6	538.7	-	-	1436.5	813.8	0.38	40	0%	-	47	0.37	Aggregate Size Distribution
Mix#3	-	-	-	1457.0	-	1457.0	813.8	0.38	40	0%	-	99	0.35	Aggregate Type and Shape
Mix#4	-	-	-	-	1457.9	1457.9	813.8	0.38	40	0%	-	10	0.48	Aggregate Type and Shape
Mix#5	1305.2	-	-	-	-	1305.2	813.8	0.38	31	6%	-	23	0.5	Air Content
Mix#6	1550.2	-	-	-	-	1550.2	813.8	0.28	84	0%	-	23	0.5	W/CM ratio
Mix#7	1730.3	-	-	-	-	1153.5	813.8	0.38	40	0%	-	23	0.62	Coarse Aggregate Volume
Mix#8	1357.9	-	-	-	-	1357.9	900.0	0.38	40	0%	-	23	0.5	Paste Content
Mix#9	1506.1	-	-	-	-	1506.1	610.4	0.38	50	0%	25%	23	0.5	Fly Ash

Compressive and Splitting-Tensile Strength

It is hypothesized that the splitting tensile strength of concrete may be a good indicator of the likeliness of crack formation, whereas fracture-toughness is a better indicator of the likeliness of crack propagation.

4-in. x 8-in. Cylindrical specimens were made from the same batch and several compressive tests were conducted throughout the curing period of each mix. All cylinder specimens were tested according to ASTM C39/C39M and ASTM C496/C496M to obtain compressive and splitting tensile strength respectively (Figure 15).

(a) (b)

Figure 15. a) Compressive strength test setup. b) Splitting tensile strength test setup

Three replicates were tested for each of compressive and splitting tensile test at target strengths. To calculate splitting tensile strength the peak load was measured and following equation was used:

$$T = 2P/\pi ld \quad (42)$$

Where, *P* is the maximum applied load, l is the length of specimen (8 in.), and d is diameter (4 in.).

Fracture Toughness Test

Fracture toughness tests were conducted on 3 in. x 6 in. x 21 in. (76.2 mm. x 152.4 mm x 533.4 mm) prisms (Figure 16) based on the Two-Parameter method proposed by Shah et al. [25]. Also, the fracture toughness values obtained by this method are in good relation with other methods such as the size-effect law and effective crack model [25]. After making a 1.5 in.-deep (38.1 mm) notch at the middle of specimens by 0.0084 in. (1.7 mm) width saw-cut, a clip gauge measuring crack mouth opening displacement (CMOD) was mounted across the notch and a load was applied at a rate that produced a constant crack-opening displacement (CMOD) of 0.0038 mm (0.00015 inch) per minute. The rate was selected so that the peak load was reached in approximately 5 minutes, and the loading rate provided a stable crack growth rate both before and after peak load. In this method, crack mouth opening displacement (CMOD) was measured within the loading and unloading phases by the clip gauge that was mounted at the bottom of

specimen. In order to cause the crack to close during the un-loading phase and compensate weight of specimen, cantilevered counterweights were used at the end of the specimens as shown in Figure 18. The length and weight of cantilevered counterweights were calculated so that a negative moment equal or larger than specimen weight was created at the notch location. The moment by specimen's weight at the middle of prism is 2.625w-4.5w. For specimens with the average weight of w=33lb, the moment is -61.875 lb.in.. In order to ease the counterweight installation, the cantilever length (distance from weigh to the hinge support) was chosen 14.5 in.. The required weight at each side then needs to be at least 4.5 lb. To ensure specimen self-weight is compensated, 15 lb steel cylinder was placed on the cantilever and secured by a screw and a plate at the end.

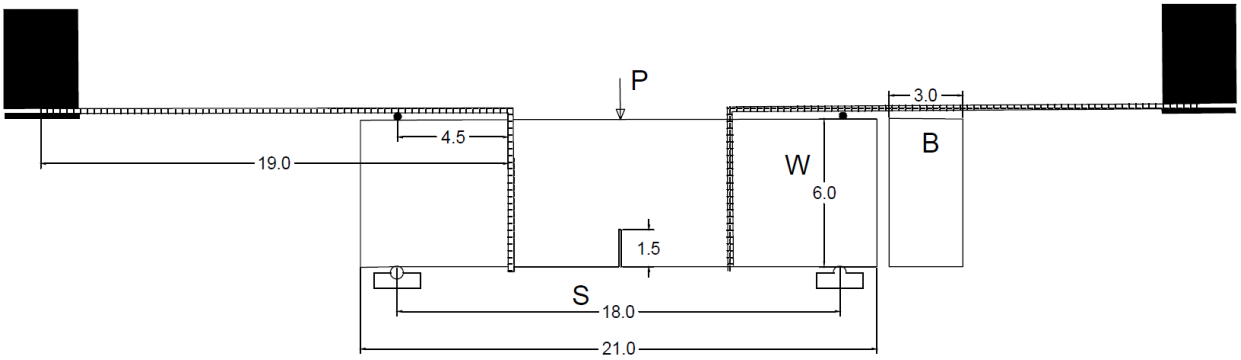

Figure 16. Specimen geometry for the fracture toughness test

Figure 17. Clip Gauge utilized in this study

Figure 18. Fracture toughness test setup

Figure 19. Mounted clip gauge on and installed weigh compensator

In order to calculate the fracture toughness (K_{IC}), the first step was to calculate the modulus of elasticity (E) by equation (43) through (45) developed by Shah et al. for the two-parameter model [25]:

$$E = \frac{6Sa_0 V_1(\alpha)}{C_i W^2 B} \tag{43}$$

$$V_1(\alpha) = 0.7 - 2.28\alpha + 3.87\alpha^2 - 2.04\alpha^3 + \frac{0.66}{(1-\alpha)^2} \tag{44}$$

$$\alpha = (a_0 + H_0)/(W + H_0) \tag{45}$$

Where C_i is loading compliance calculated in the range of 10% to 50% of peak load where the crack tip opening is still in the elastic range, and a_0, S, W, B and H_0 are the specimen dimensions shown in Figure 16. The effective crack length (a_e) at peak load is obtained using equation (43) by replacing C_i and a_0 with unloading compliance (C_u), which is calculated in the range of 10 % to 80% of the maximum load at unloading phase, and a_e respectively. Ultimately, K_{IC} value was calculated using equation (46) [25] as follow:

$$K_{IC} = \frac{3SP_{max}}{2BW^2}\sqrt{\pi a_e}F(\alpha) \tag{46}$$

$$F(\alpha) = \frac{1}{\sqrt{\pi}}\frac{1.99 - \alpha(1-\alpha)(2.15 - 3.93\alpha + 2.7\alpha^2)}{(1+2\alpha)(1-\alpha)^{\frac{3}{2}}} \tag{47}$$

$$\alpha = \frac{a_e}{W} \tag{48}$$

Where P_{max} is the measured peak load and a_e is the effective crack length.

Fatigue Crack Growth Test

In order to assess the effect of cyclic loading and fatigue on crack growth, prims in three point-bending were tested in a servo-controlled MTS test frame. The prism dimensions were similar to those made for the fracture toughness test (3 in. x 6 in. x 21 in./76.2 mm x 152.4 mm x 533.4 mm).

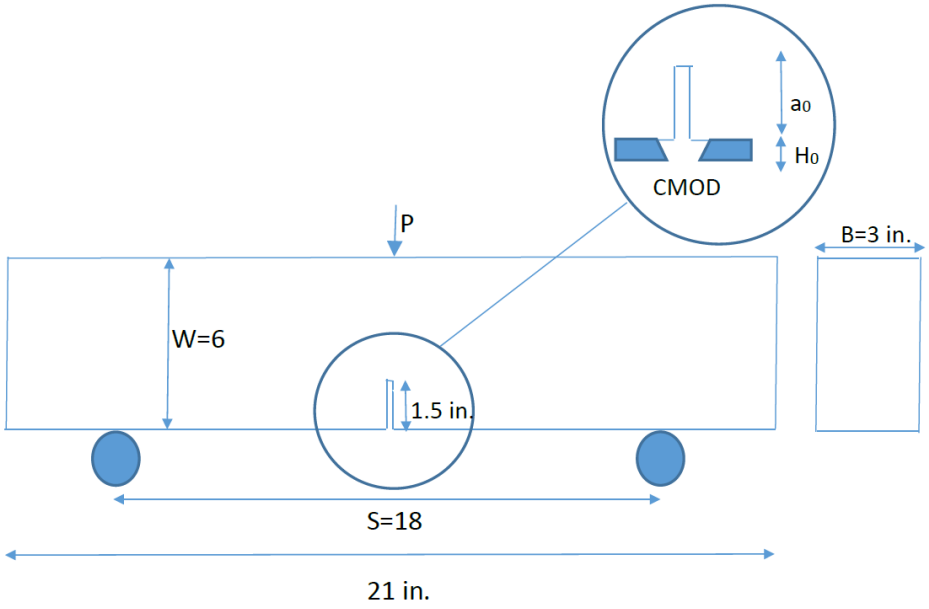

Figure 20. Schematic figure of specimen geometry for the fatigue test

Figure 21. Fatigue crack growth test set up.

Also, the same setup was used except for the loading condition and weight compensator shown in Figure 21. The clip gauge was mounted across the 1.5 in.-deep (38.1 mm) crack notch made by a saw-cut to record the crack opening displacement during each cycle.

The cyclic loading was based on a constant loading amplitude and frequency (1 Hz). The maximum load was calculated by setting the maximum tensile strength at the top of the notch equal to six time the square-root of the concrete compressive strength as illustrated below.

$$M = \frac{PL}{4} = \frac{P(18\ in)}{4} = 4.5P$$

$$S = \frac{(3\ in)(4.5\ \text{in})^2}{6} = 10.125\ in^3$$

$$\frac{M}{S} = \frac{4.5P}{10.125\ \text{in}^3} = 0.44\text{P} = 6\left(\sqrt{8000\ \text{lb}}\right) \rightarrow \text{P} \approx 1208\ lb$$

Where, P is the maximum load, L is the load span. All fatigue tests were conducted at the compressive strength of 8000 psi. The load ratio of 0.2 (P_{min}/P_{max}) was selected providing a stable crack growth and a large enough number of cycles. Hence, the applied lower and upper load levels were 240 lb and 1200 lb. Ultimately, minimum and maximum load along with crack mouth opening displacement (CMOD) were recorded every 5 cycles.

2.5 Results and Discussion

Depicted data in a load-Crack Mouth Opening Displacement (CMOD) graph was analyzed by calculating fracture toughness values for each loop, as explained in Appendix A. Figure 22 demonstrates an example of fracture toughness test results obtained in this research.

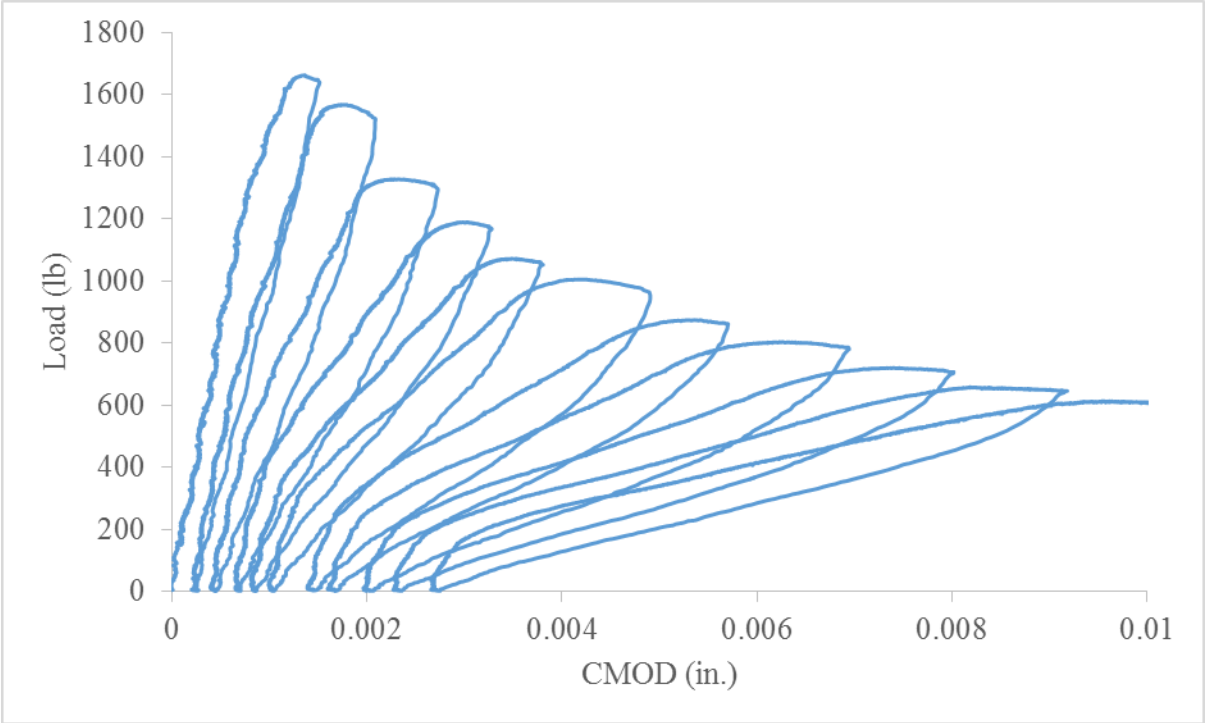

Figure 22. Load versus crack mouth opening displacement obtained from fracture toughness test

As shown in Figure 23, analyzed data on four replicates of a mixture at 4000 psi indicates a negligible alteration in fracture toughness results at various crack length. The changes in values due to crack tip shape and heterogeneity of concrete material are less than the variance of fracture toughness results at identical crack lengths, which means that fracture toughness results might be independent of crack length as suggested in previous studies. Moreover, this parameter can therefore be considered as a material property of concrete as discussed by Shah et al [25].

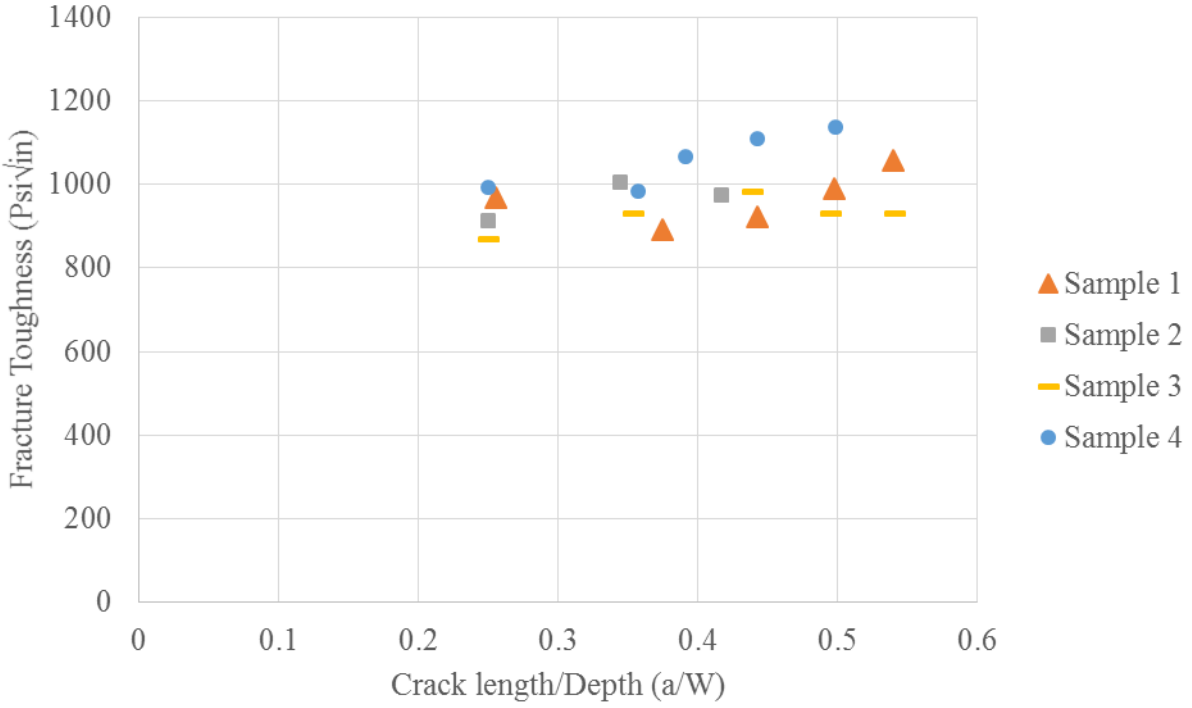

Figure 23. Fracture toughness results of four replicates at different crack length/ depth

2.5.1 Effect of Angularity

Three types of coarse aggregate with different textures were used in this study. Mix#1 (control mix) contained pea gravel, Mix#3 contained a highly-angular crushed granite, and Mix#4 contained a well-rounded natural river gravel. Angularity of each coarse aggregate type was evaluated using AASHTO TP 61 and these results are tabulated in Table 4. Figure 24 shows that the resulting failure surfaces of fracture-toughness specimens for Mix#1 and Mix#4 after testing at 4000 and 8000 psi. To have a better perspective of crack path and fracture surface regarding the effect of angularity of aggregate, the number of split coarse aggregate at the fractured surface of the sample was counted after complete failure of specimens.

Table 4. Percentage of fracture in coarse aggregate by AASHTO TP61

	CA1	CA2	CA3	CA4	CA5
Aggregate type	Pea Gravel	Crushed Gravel	Gravel	Granite	Natural River Gravel
% Fracture in agg.	23%	31%	74%	99%	10%

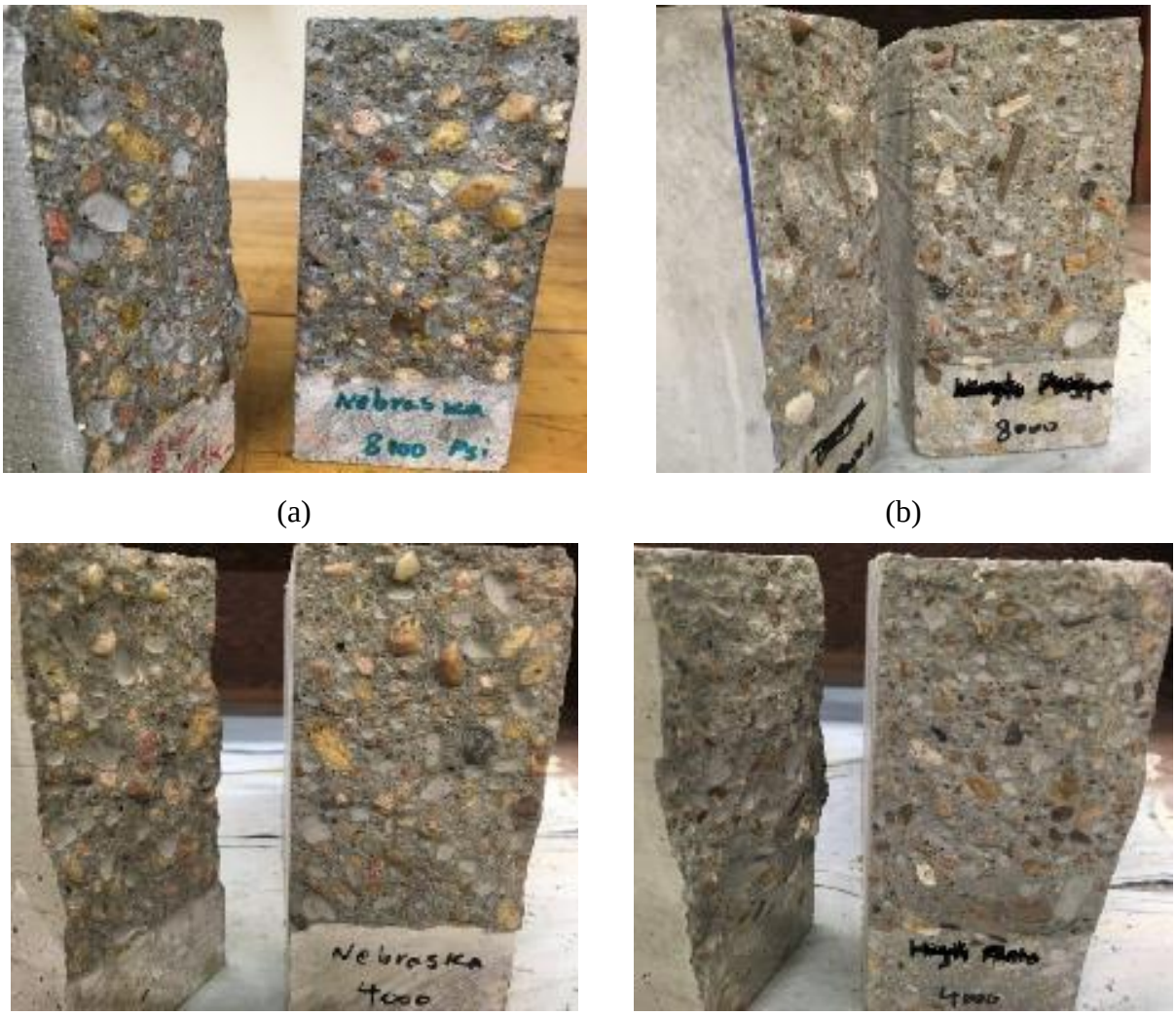

Figure 24. Fracture surface of specimen in fracture toughness. a) Natural round gravel at 8000 psi. b) Crushed gravel at 8000 psi. c) Natural round gravel at 4000 psi. d) Crushed gravel at 4000 psi.

Figure 25, Figure 26, and Figure 28 present the results from splitting tensile tests, fracture toughness, and fracture resistance, respectively. These bar charts show the average of at least

three test results along with error bars showing one standard deviation above and below the average.

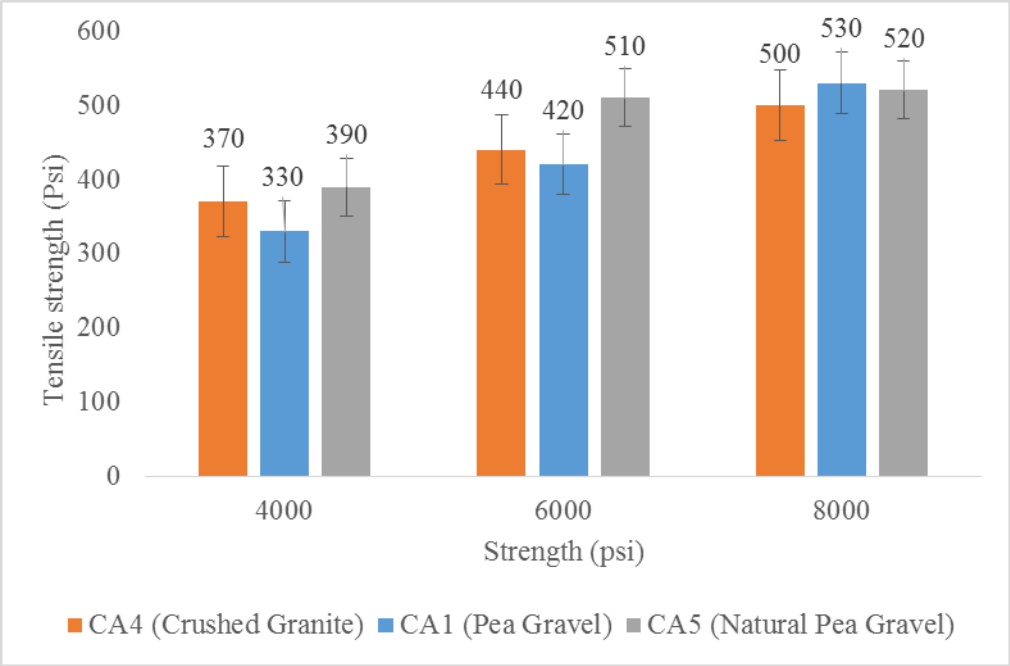

Figure 25. Splitting tensile strength at three strengths for specimen with different coarse aggregate shape

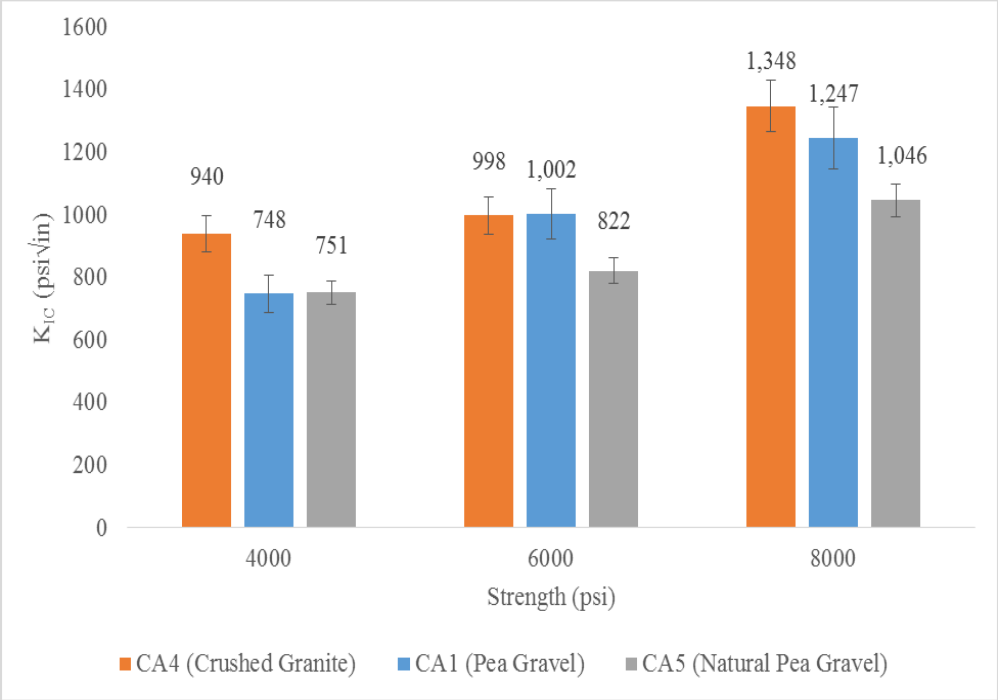

Figure 26. Fracture toughness results at three strengths for specimen with different coarse aggregate shape

The results presented in Figure 25 and Figure 26 show that as the compressive strength increases, both the splitting tensile strength and fracture toughness increase as expected. From Figure 26, there is a 25% increase in fracture toughness at 27.5 MPa (4000 psi) when angular (crushed granite) aggregate is used compared with rounded (river gravel) aggregate (KIC = 940 Psi√in = 1.033 MPa√m) compared to 751 Psi√in = 0.825MPa√m). However, this same effect is not found with splitting tensile strength (Figure 25). The average splitting tensile strength of Mix #4 (natural gravel) is higher than the mix with crushed granite (Mix#3) at both 4000 psi and 6000 psi compressive strengths. Additionally, from Figure 26, there is a 28.5% increase in fracture toughness at 8000 psi for Mix#3 (granite) compared with Mix#4 (natural gravel). In fact, there are no overlapping data points between the fracture toughness of natural gravel and crushed granite specimens. However, the splitting tensile strength of these specimens at 8000 psi compressive strength is essentially the same.

The results shown in Figure 26 demonstrate an increase of fracture toughness when coarse aggregate is highly angular. This may be attributed to the effect of interfacial bond between aggregate and mortar. As shown in Figure 24 the number of aggregate particles separated from mortar for specimens made with natural gravel is more than ones with pea gravel. As expected, at lower strengths where the bond between mortar and aggregate is weak, cracks tend to propagate along the interface of mortar and aggregate. Thus, the more surface area and angularity of the aggregate, the more energy is required for a crack to pass through the tortuous and longer path along the interface.

The results of fracture toughness at 4000 psi for mixtures with different angularity demonstrated a high correlation between percentage of crushed aggregate and fracture toughness values, as shown in Figure 27. 4 different mixes were plotted in this graph including Mix#1, Mix#2, Mix#3 and Mix#4. The percentage of crushed aggregate was tabulated in Table 4.

On the other hand, fracture resistance appeared to be less influenced by angularity at low strength. This could mean that angularity is not effective in increasing deformation tolerance of concrete prior to fracture at low strength when there is still a weak aggregate-mortar interlock.

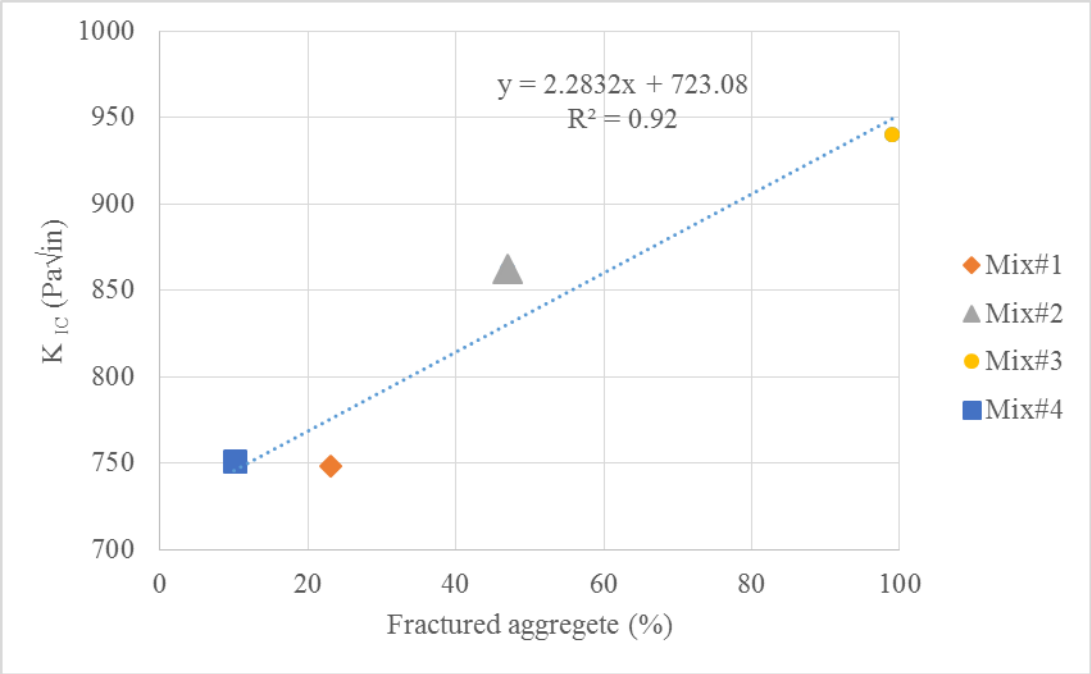

Figure 27. Fracture toughness versus percentage of crushed aggregate at 4000 psi

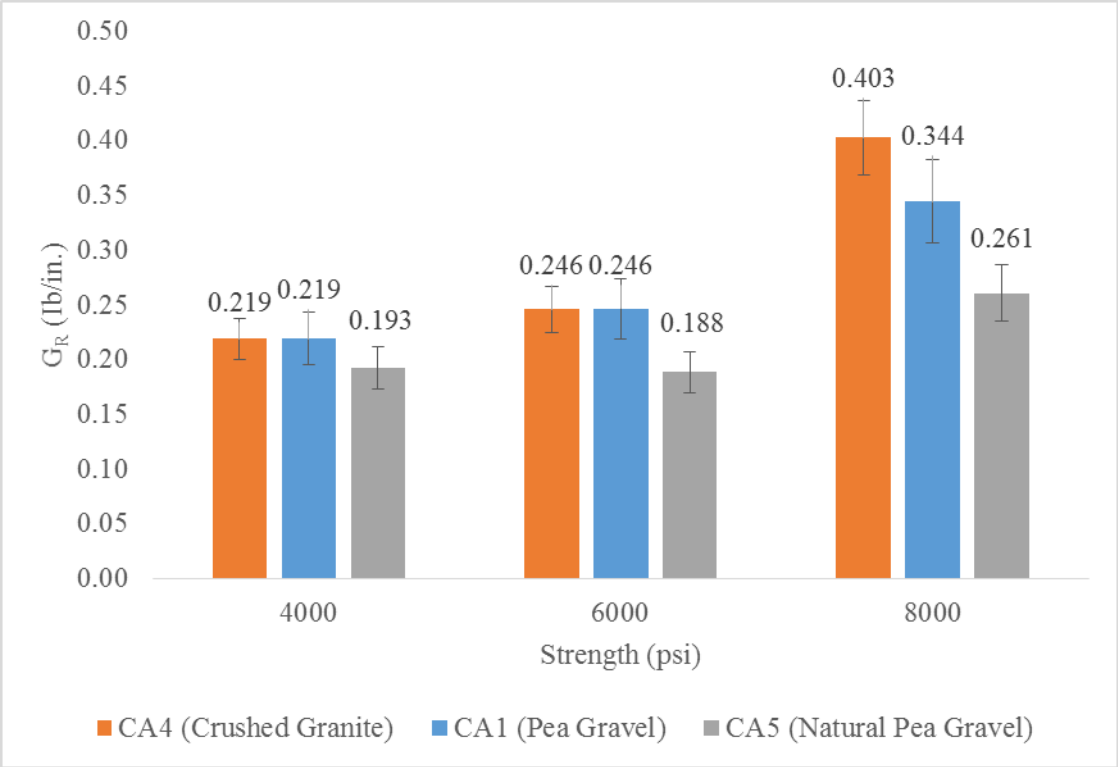

Figure 28. Fracture resistance at three strengths for specimen with different coarse aggregate shape

To further investigate mixture behavior, modulus of elasticity of the mixes determined from fracture toughness test was plotted in Figure 29. This showed that there is a negligible difference in modulus of elasticity at 6000 and 8000 psi whereas 57% increment was observed when crushed granite was used. It might be attributed to a better aggregate-paste interlock caused by texture and fractured surface in crushed granite. Also, there is no essentially a significant change in values as strength increases for Mix#3 (CA4). Which may explain why modulus of elasticity solely is not indictor of fracture resistance of mixture.

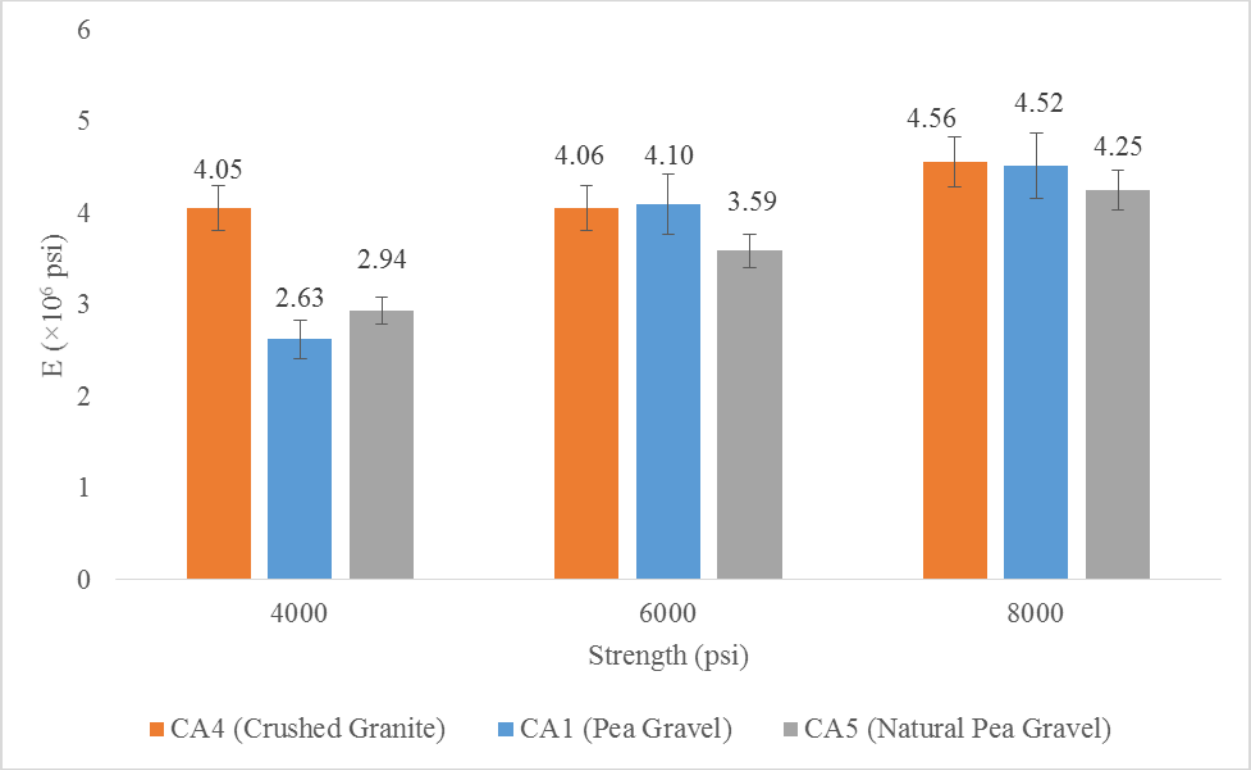

Figure 29. Modulus of elasticity at three strengths for specimen with different coarse aggregate shape

2.5.2 Effect of Aggregate Size and Distribution

Mix#2 contained a combined crushed gravel (mixture of CA2 and CA3) that had a larger aggregate size distribution than the control mix (Mix#1). To determine the coarseness of the internal random grain structure of concrete (λ), equation (49) was suggested by Amparano et al [93]:

$$\lambda = \frac{1}{D_{ave}\,(1 - V_a)} \tag{49}$$

where D_{ave}, is the average diameter of the aggregate particles, and V_a is volume fraction of the coarse aggregate.

Thus, for mixes with a fixed volume fraction, a smaller size of aggregates leads to a higher λ and consequently a finer grain structure. It has been shown by Zollinger et. al. that as the average

aggregate size increases, the fracture process zone of the concrete increases [58]. The calculated λ values for Mix#1 and Mix#2 are 0.50 and 0.37, respectively. This indicates that Mix#1 has a larger fracture process zone thereby resulting in lower fracture toughness of concrete. Although it has been shown by preceding studies [58, 74] that, as the λ increases the fracture energy and fracture toughness decreases, its sensitivity at different compressive strengths was unknown.

From Figure 31. the splitting tensile strength of the mixture with larger aggregates (Mix#2) is consistently higher than the splitting tensile strength of the control mix when tested at the same concrete compressive strength.

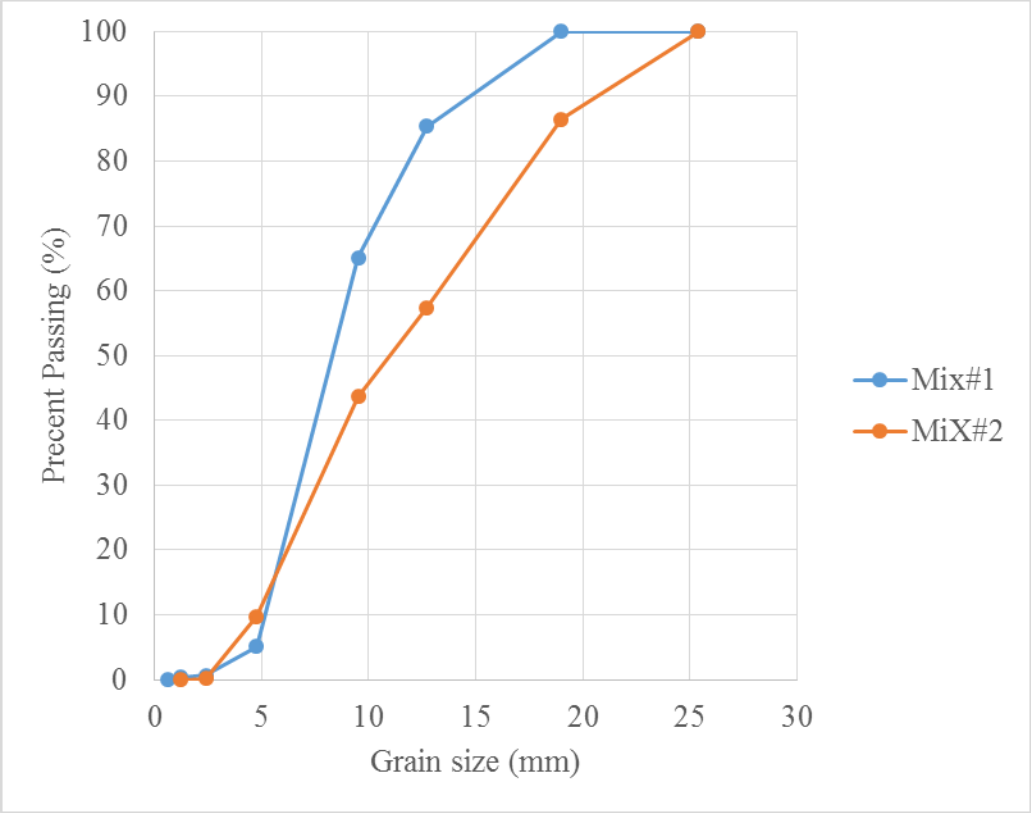

Figure 30. Grain size distribution curve

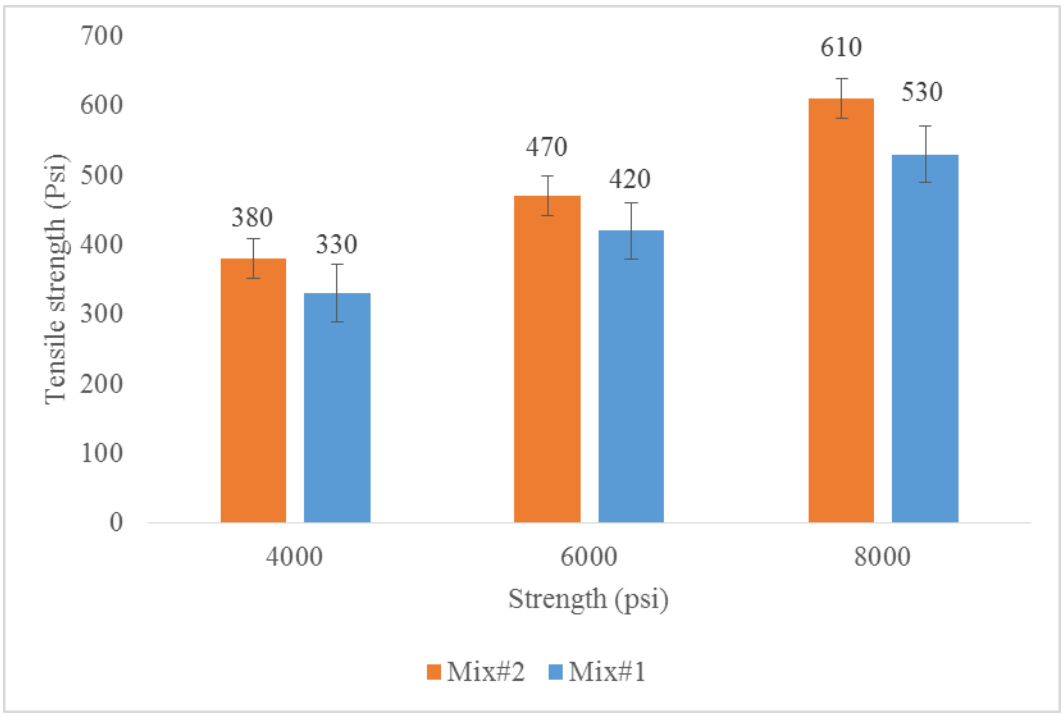

Figure 31. Splitting tensile strength results at three strengths for specimen with different aggregate size distribution

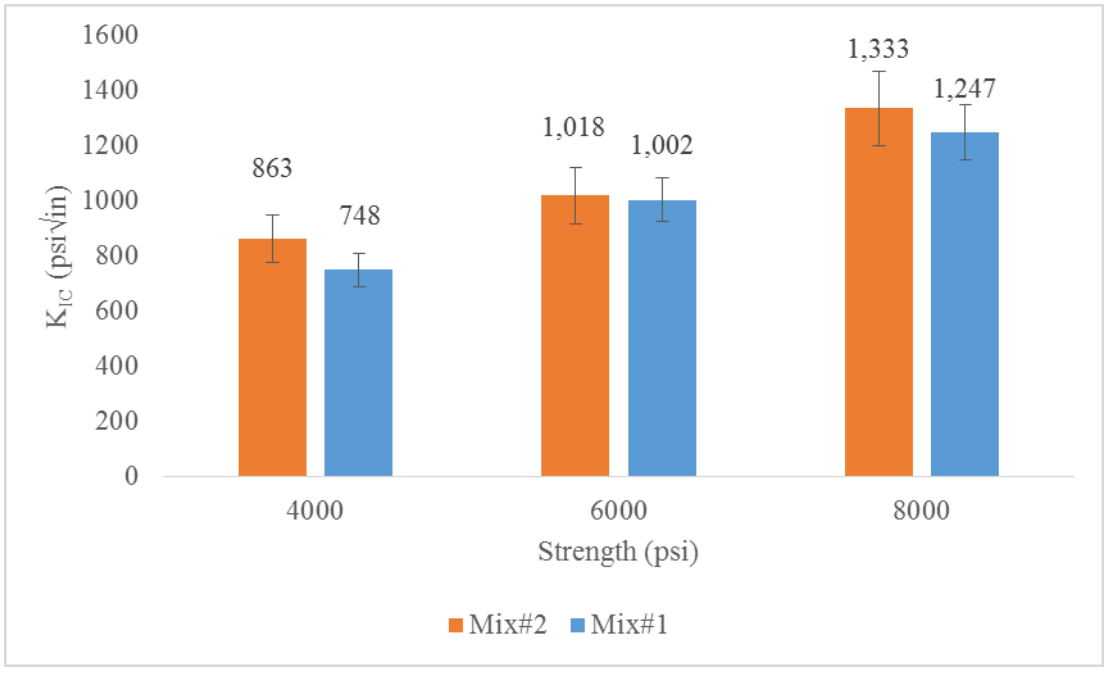

Figure 32. Fracture toughness at three strengths for specimen with different aggregate size distribution

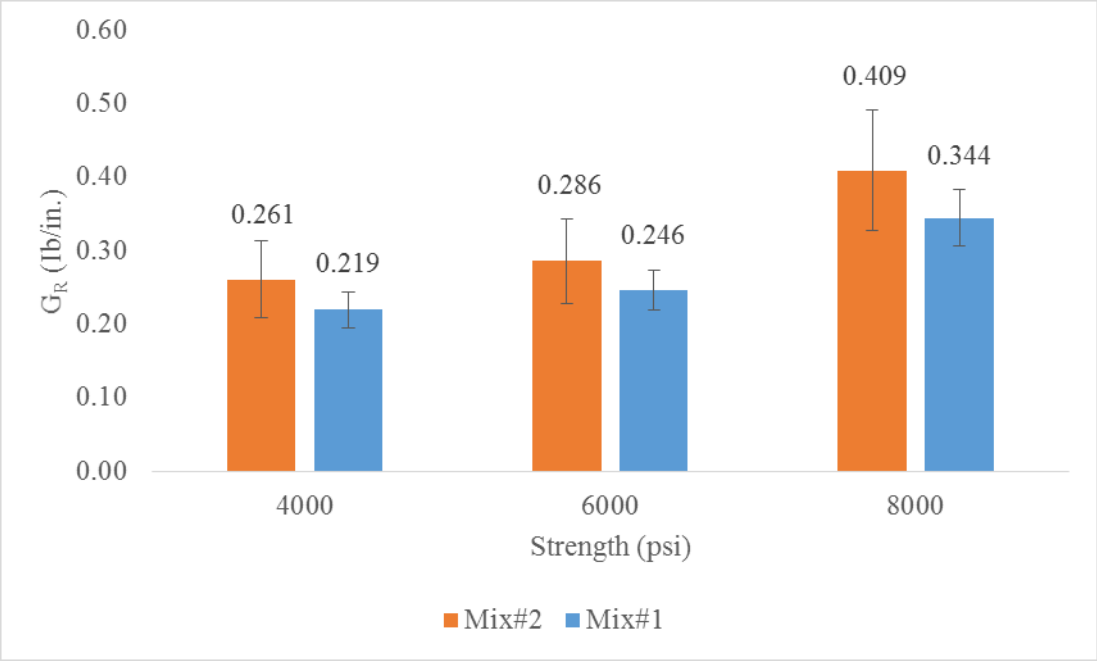

Figure 33. Fracture resistance results at three strengths for specimen with different aggregate size distribution

From Figure 32, size distribution of coarse aggregate also affects the fracture toughness. When both the maximum and average size of aggregate was increased the fracture toughness increased by 15% at 4000 psi. However, as the strength of concrete increases the values of fracture toughness for both mixes tend to converge. A denser coarse aggregate distribution seemingly causes both a better crack initiation and propagation resistance as the crack path becomes more tortuous. This difference would likely be more profound at lower strength when the aggregate-mortar bond is still weaker than the aggregate. Furthermore, the denser mixture demonstrates a better aggregate interlock which helps reduce the crack width and allows the transfer of more tensile force from one side of crack tip to the other side through contact between the particles of aggregate. The same trend was also seen on fracture resistance with larger difference between two mixes. It is believed that, in general, mix#2 should have a superior performance in terms of cracking. Further investigation of this effect was achieved by fabrication of prestressed prisms with similar mixes.

However, fracture toughness of mixtures including different coarse aggregate distribution like Mix#1, Mix#2, Mix#3 and Mix#4 were plotted against their lambda value (λ). As shown in Figure 34, there is strong correlation between λ and fracture toughness values at 4000 psi. It may mean that the denser graded the aggregate, the better fracture performance at low strengths.

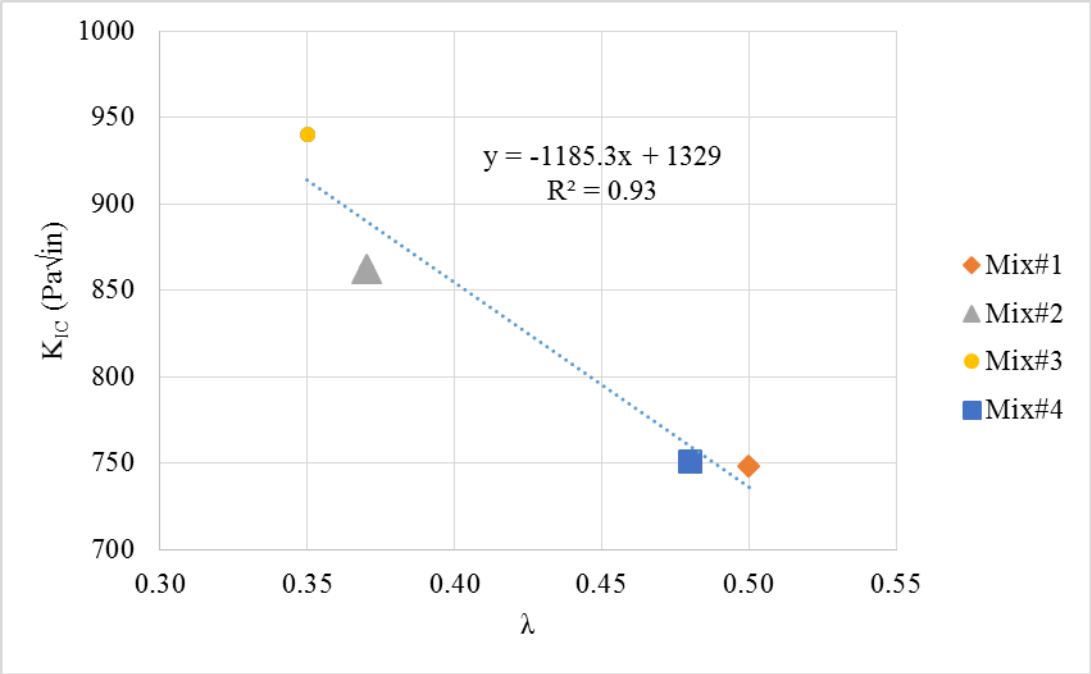

Figure 34. Fracture toughness versus aggregate distribution parameter at 4000 psi

2.5.3 Effect of Coarse Aggregate Volume

As discussed in section 2.3.4, the volume of coarse aggregate or ratio of coarse/fine aggregate might influence the fracture behavior regardless of coarse aggregate size and distribution. Hence, two mixtures with the same aggregate material and w/cm ratio were designed so that only the ratio of coarse/fine aggregate was different. While the ratio of coarse/fine aggregate was 1.0 for control samples (Mix#1), a companion mix (Mix#7) with ratio of 1.5 was investigated.

It can be seen in Figure 36 and Figure 37 that a 17 % and 9% increase in average fracture toughness and fracture resistance respectively, occurs at 4000 psi while there is a diminishing difference at higher strengths. The same trend was observed as the coarse aggregate size distribution was altered which might be attributed to the bigger surface when the crack has to pass through more coarse aggregate. It has been observed that, fracture process zone of concrete increases as the amount of coarse aggregate increases [58]. Besides, the smaller the fracture process zone, the more brittle the failure pattern [93]. This means that increasing coarse aggregate can lead to enhanced fracture resistance of concrete at lower strengths.

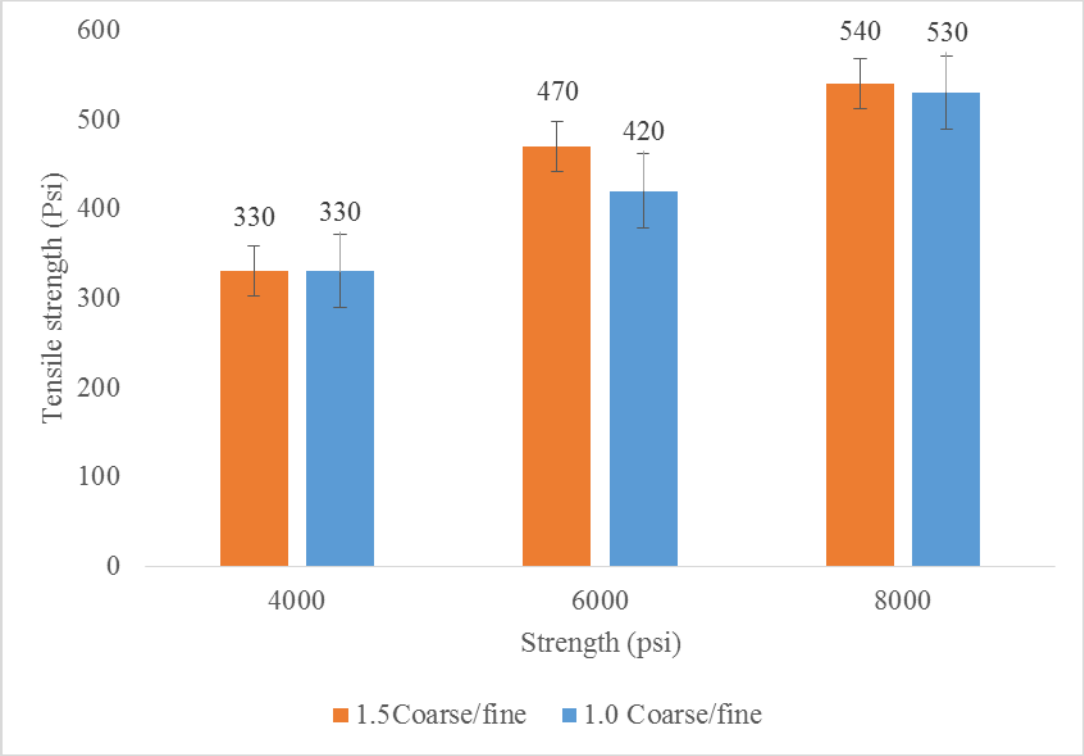

Figure 35. Splitting tensile strength results at three strengths for specimen with different coarse aggregate volume

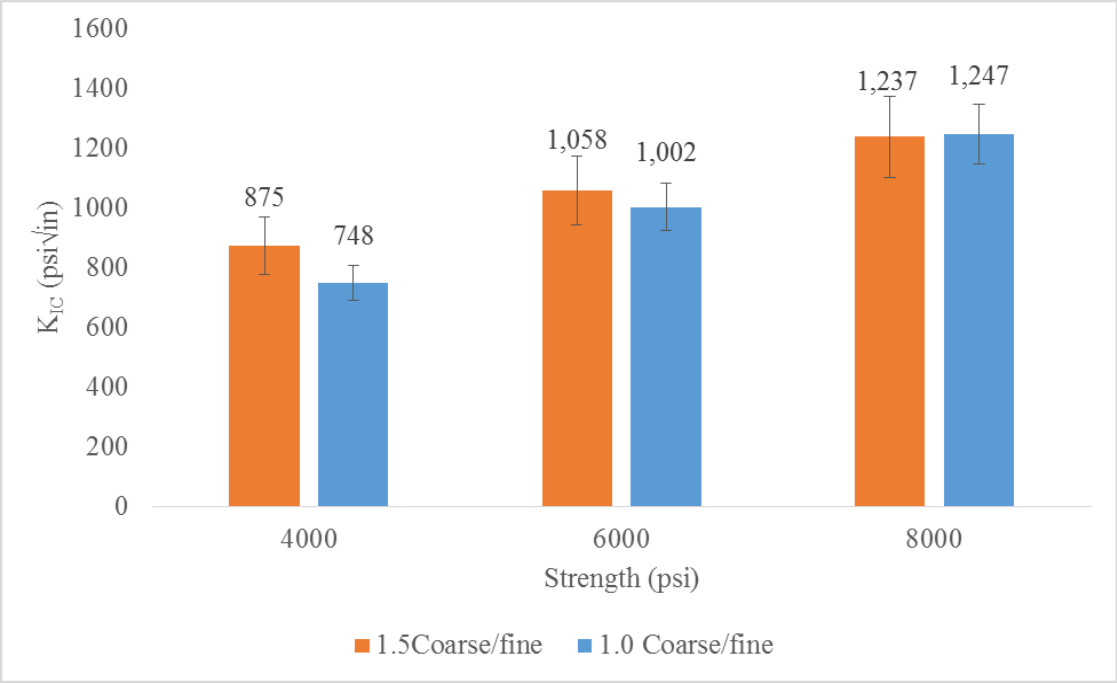

Figure 36. Fracture toughness results at three strengths for specimen with different coarse aggregate volume

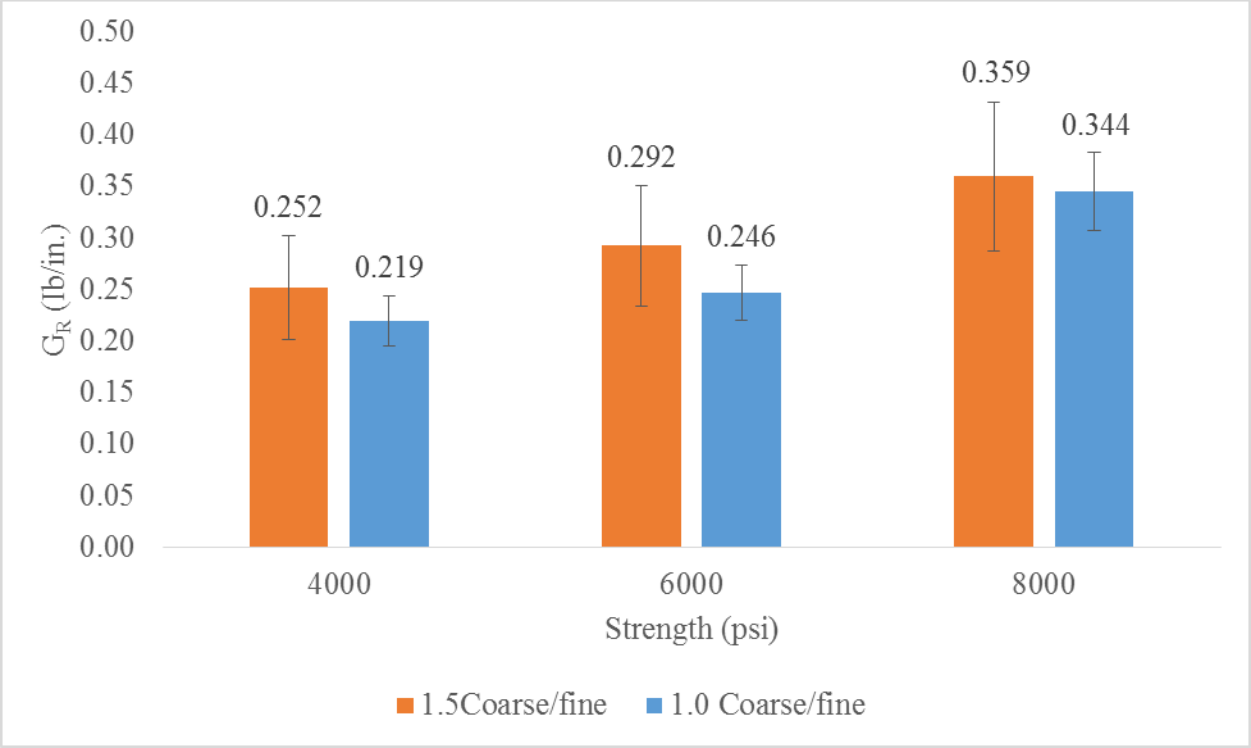

Figure 37. Fracture resistance results at three strengths for specimen with different coarse aggregate volume

2.5.4 Effect of Water-To-Cementitious (W/CM) Ratio

As noted previously, lowering the w/cm results in targeted strengths being achieved at an earlier time period. Moreover, as the strength increases the fracture parameters also consequently increase. In order to eliminate the impact of strength on fracture toughness and to see the exclusive effect of w/cm ratio, specimens with 0.38 and 0.28 w/cm ratio were made and tested at 4000, 6000 and 8000 psi. The results shown in Figure 38 through Figure 40 indicate that, lowering w/cm ratio from 0.38 to 0.28 increases the average splitting tensile strength by 17% and the average fracture toughness and fracture resistance by 30% and 19% respectively, at a compressive strength of 4000 psi. At 6000 psi, the lower w/cm concrete had a 21% increase in average splitting tensile strength and an increased fracture toughness of 4%. However, at 8000 psi the trend is not the same, with the higher w/cm concrete having a significantly-higher splitting tensile strength and very close fracture toughness. It must be noted that the time to reach 8000 psi for the concrete with 0.38 w/cm was nearly 3 weeks, while the mixture with 0.28 w/cm ratio achieved 8000 psi within the first 24 hours. It is hypothesized that the interfacial bond between aggregates and paste may be enhanced by the significantly-longer curing period although the tensile strength at 8000 and 6000 psi do not exhibit the same trend which might be due to variability in the test results.

At lower compressive strengths, lowering w/cm ratio might lead to formation of finer spherical and cylindrical particles of the hydration products causing better homogeneity of the pore structures [94]. Also, Scanning Electron Microscope (SEM) micrographs have previously shown

a denser cement matrix and strong interfacial transition zone in concrete when lower w/cm is used leading to stronger interfacial bonds [95]. This improvement is likely to be more effective at the interface of mortar and aggregate where the crack incline to grow at early stage of concrete. However, as the strength of concrete increases, less cracks propagate through interfacial zone meaning change in paste properties by w/cm ratio slightly alters the fracture behavior of concrete.

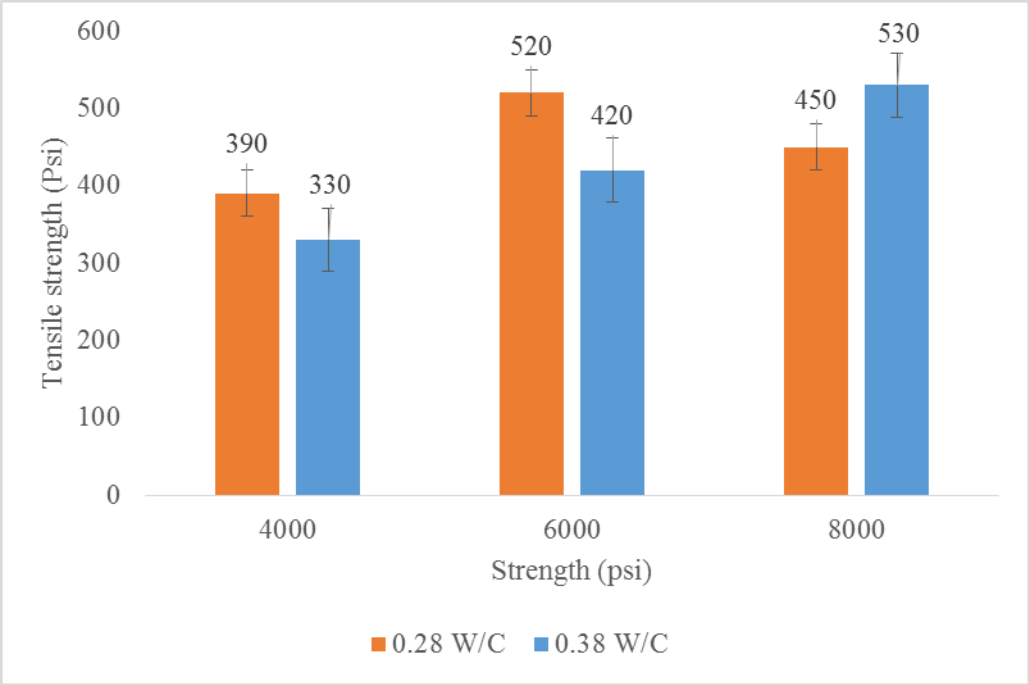

Figure 38. Splitting tensile strength results at three strengths for specimen with different water/cement ratio

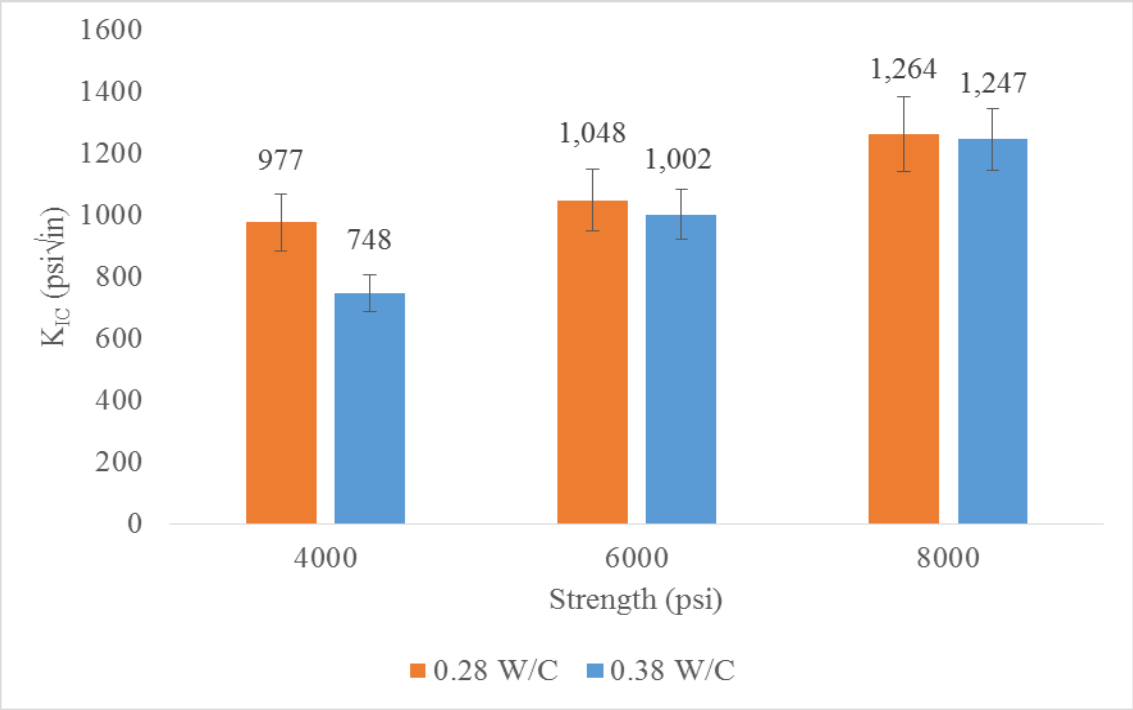

Figure 39. Fracture toughness results at three strengths for specimen with different water/cement ratio

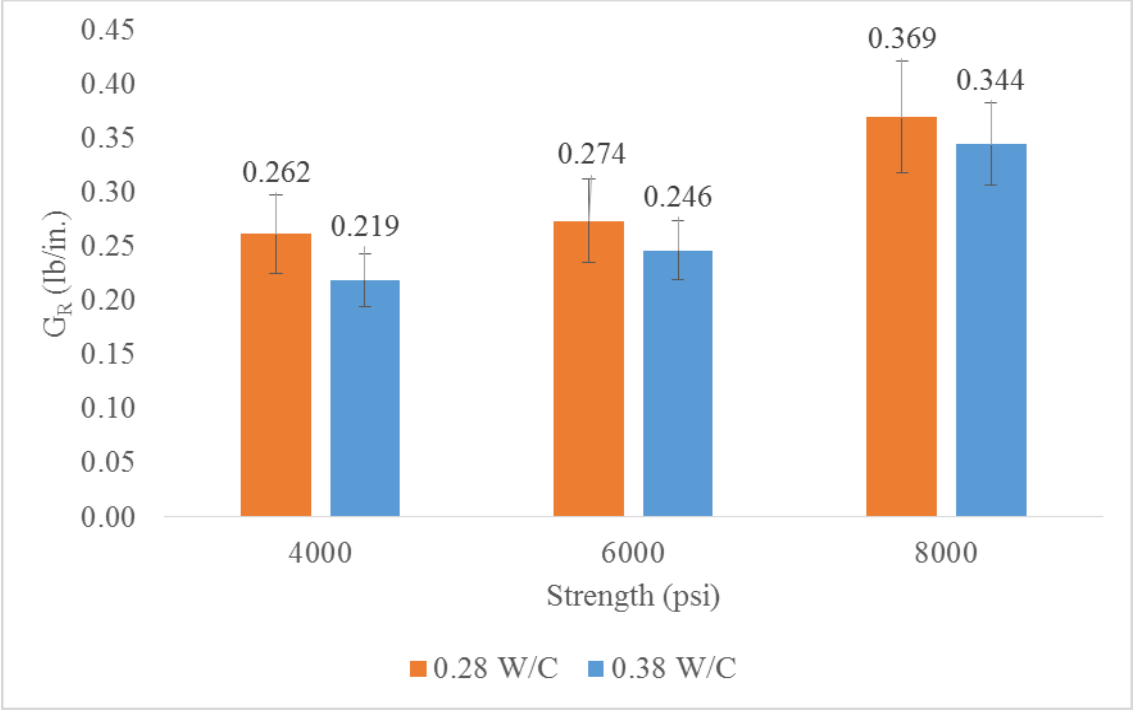

Figure 40. Fracture resistance results at three strengths for specimen with different water/cement ratio

2.5.5 *Effect of Fly Ash*

Class F fly ash is often used in concrete mixtures to reduce concrete cost and to improve workability and durability aspects [96, 97]. To evaluate the effect of fly ash on splitting and fracture toughness, one mixture (Mix#9) included a 25% cement replacement with a Class F fly ash. The results from this mixture were then compared with the corresponding 0% fly ash mixture (Mix#1). It is shown in Figure 42 that fly ash slightly improves fracture toughness at 4000 and 6000 psi as expected according to previous studies [96]. However, at 8000 psi there was not an appreciable change to fracture toughness. In addition, the results at 4000 psi have considerable overlap while at 6000 and 8000 psi the splitting tensile strength of the fly ash mix is significantly larger.

From Figure 42, class F fly ash increases fracture toughness by 13% at 4000 psi whereas there is no improvement in splitting tensile strength and fracture resistance at the same strength. It has been observed that mechanical properties of concrete containing fly ash display better results in long term due to pozzolanic reaction of fly ash [98] confirming the present result of splitting tensile strength. On the other hand, the enhancement in fracture toughness declines as the strength of concrete increases. This reverse trend in fracture toughness might be attributed to a better and uniform coating of coarse aggregate by cementitious material resisting crack growth through interface of aggregate-paste at lower strengths or issues with the aggregates-fracture through aggregates. Surprisingly, crack resistance of Mix#9 including fly ash increases at 6000 psi. Although slight enhancement is expected to be observed at 6000 psi, authors believe that this noticeable change is attributed to variability of test results. Seemingly, fly ash is less likely to improve crack propagation of concrete both in low and high strengths.

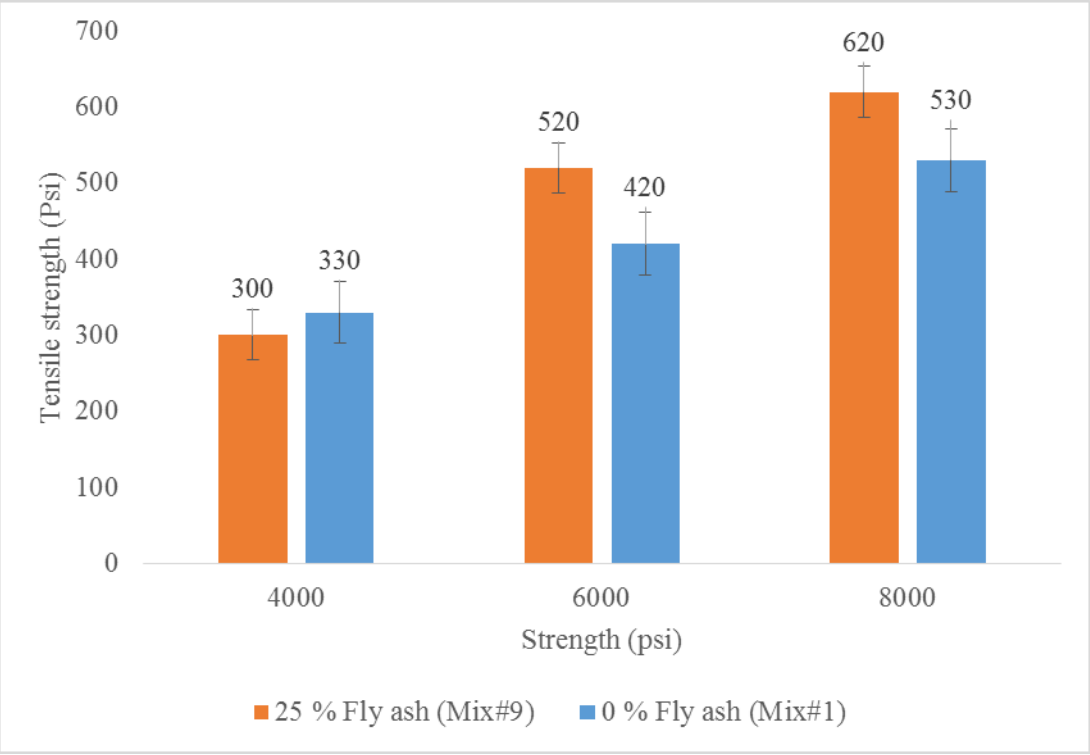

Figure 41. Splitting tensile strength results at three strengths for specimen with different fly ash content

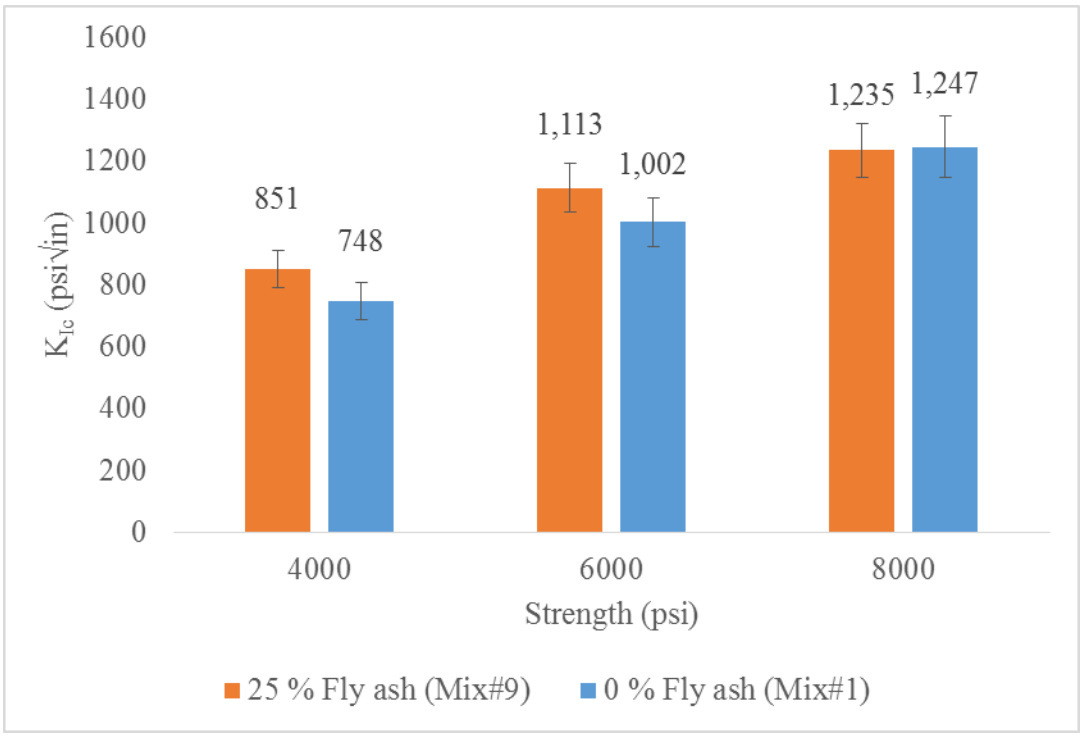

Figure 42. Fracture toughness results at three strengths for specimen with different fly ash content

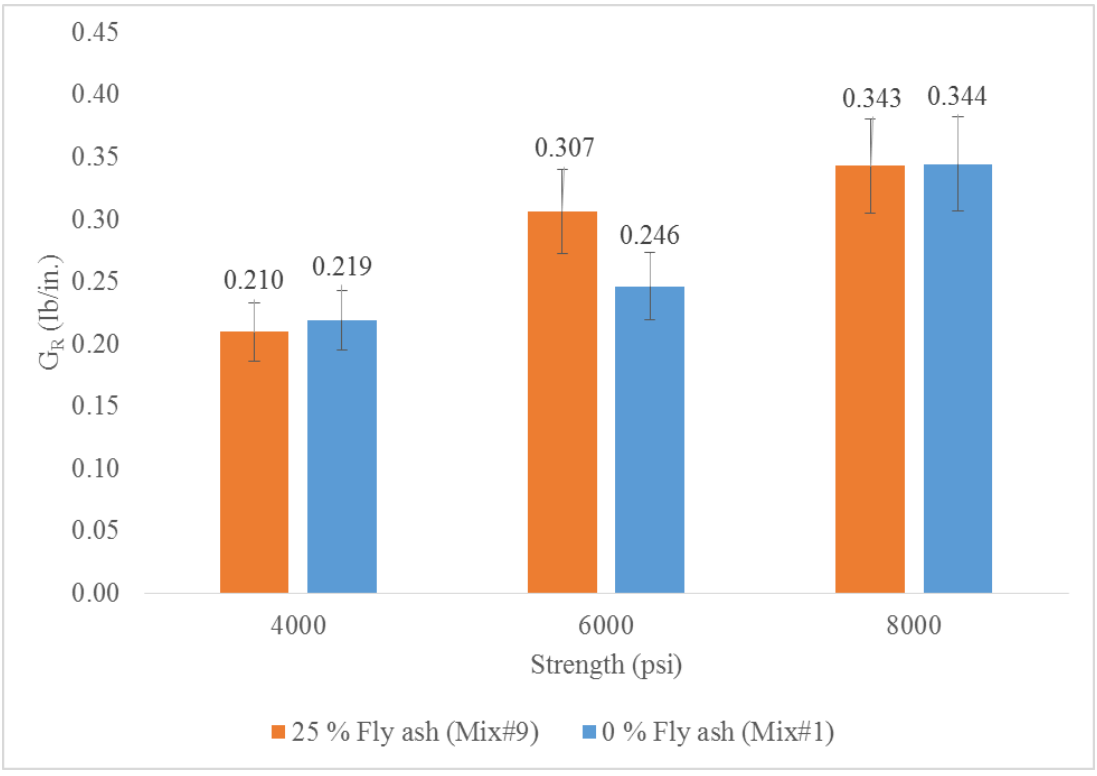

Figure 43. Fracture resistance results at three strengths for specimen with different fly ash content

2.5.6 *Effect of Paste Content*

In order to investigate the effect of paste content, the amount of cement was increased from 813 lb/yd^3 (482.8 kg/m^3) (Mix#1) to 900 lb/yd^3 (533.9 kg/m^3) (Mix#8). The results in Figure 45and Figure 46 do not show significant change in fracture toughness and fracture resistance when the paste content is increased, with the exception of a 12% increase indicated at 4000 psi. However, there is considerable overlap in the fracture toughness data at this strength.

Similar behavior has been observed by preceding studies [82, 83]. It has been seen that as distance from the aggregate decreases the roughness of the paste increases by 50%. Also, at distances greater than 100 µm from the aggregate, the effect of aggregate-paste interfacial transition zone fades suggesting that the transition zone is about 100 µm thick [5]. Increasing the ratio of cement/aggregate from 0.28 (813 lb) to 0.33 (900 lb) may not have improving effect due to negligible effect of roughness of the paste on interfacial transition zone.

Interestingly, the splitting tensile strength at 4000 psi was increased by 26% with increased paste content. However, there was essentially no effect at 6000 psi.

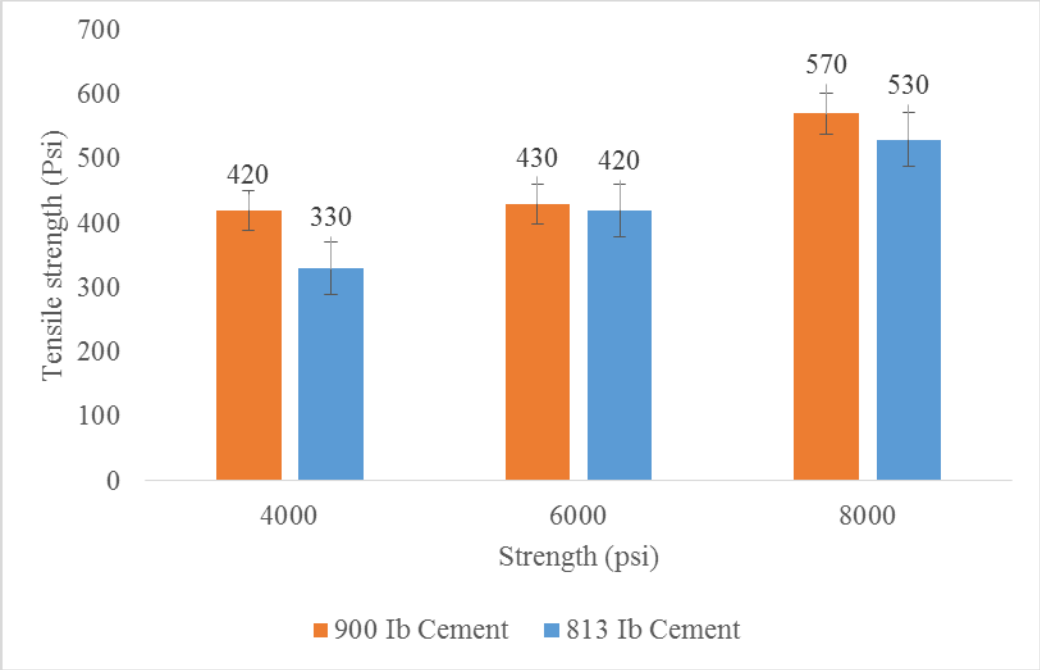

Figure 44. Splitting tensile strength results at three strengths for specimen with different paste content

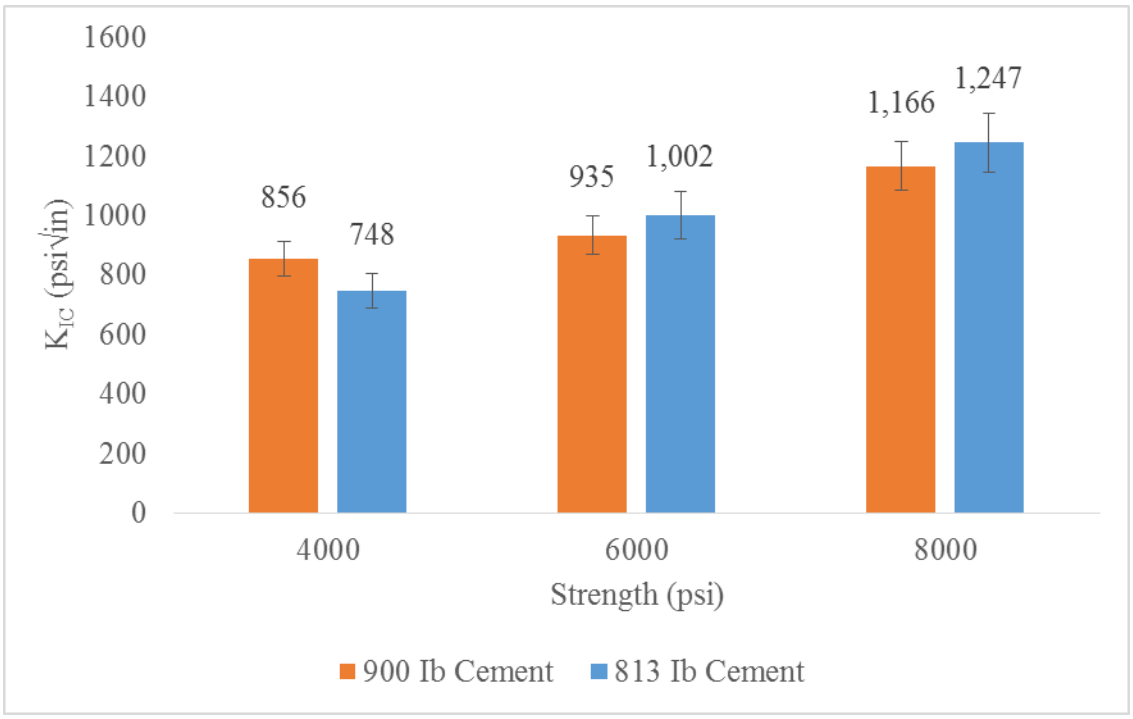

Figure 45. Fracture toughness results at three strengths for specimen with different paste content

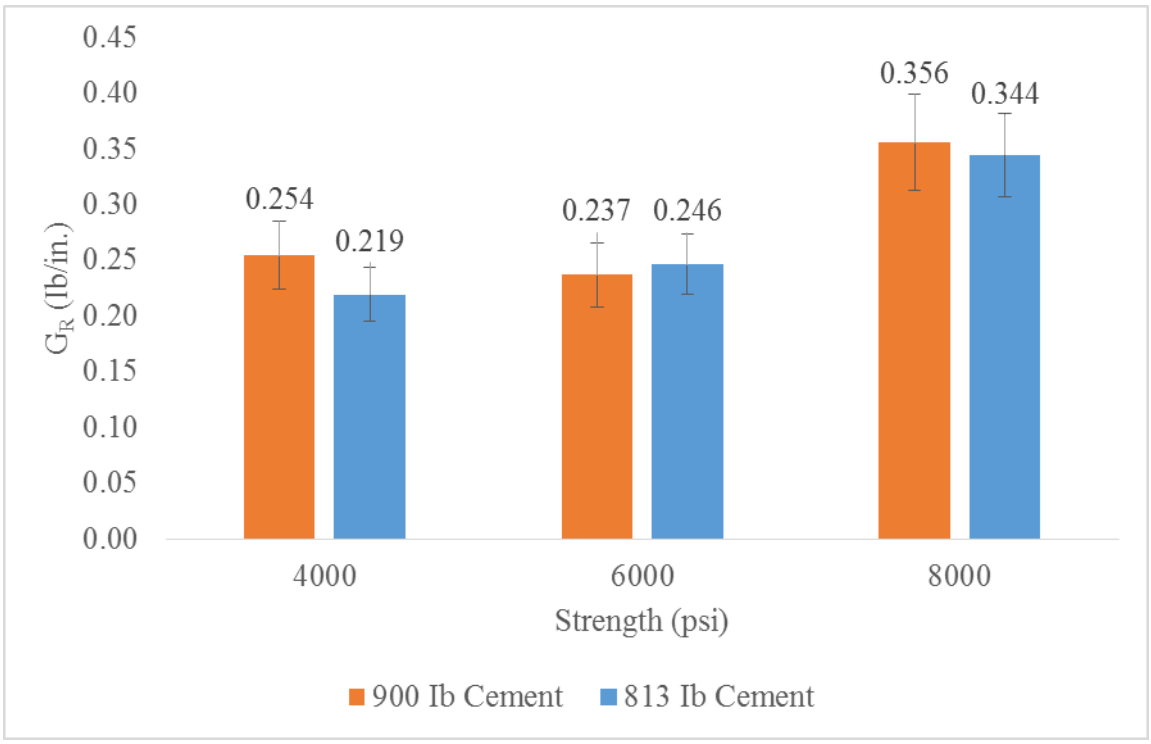

Figure 46. Fracture resistance results at three strengths for specimen with different paste content

2.5.7 Effect of Air Entrainment

A mixture designed with 6% targeted air content was made using an air-entraining admixture to evaluate its effect on the splitting tensile strength and fracture parameters. For this purpose, samples with 6% targeted air void (Mix#5) were fabricated and compared to control samples with 0% air void (Mix#1). The actual hardened air content was measured at 5.6%. Figure 48 and Figure 49 show that raising air void percentage has negligible influences on both fracture toughness and fracture resistance values. Evidently, increasing air void content decreases compressive and splitting tensile strength of concrete [99-102] while splitting tensile is negligibly impacted by air content at the same low strengths.

It should be noted that air bubbles size and distribution may lead to a meaningful alteration in fracture behavior of concrete. It seems entraining air voids might ease crack transition at top of the notch tip zone otherwise increasing air content, solely may not have meaningful impact on fracture toughness since the chance of having distributed air bubbles at crack tip zone is low. It is important to note that unnecessarily increasing air void content in a mix design might yield an unstable mix resulting in segregation which might cause increased variation in test results. Since water reducer is normally used to facilitate workability of the mix, the range should be selected so that the slump measurements remain the same.

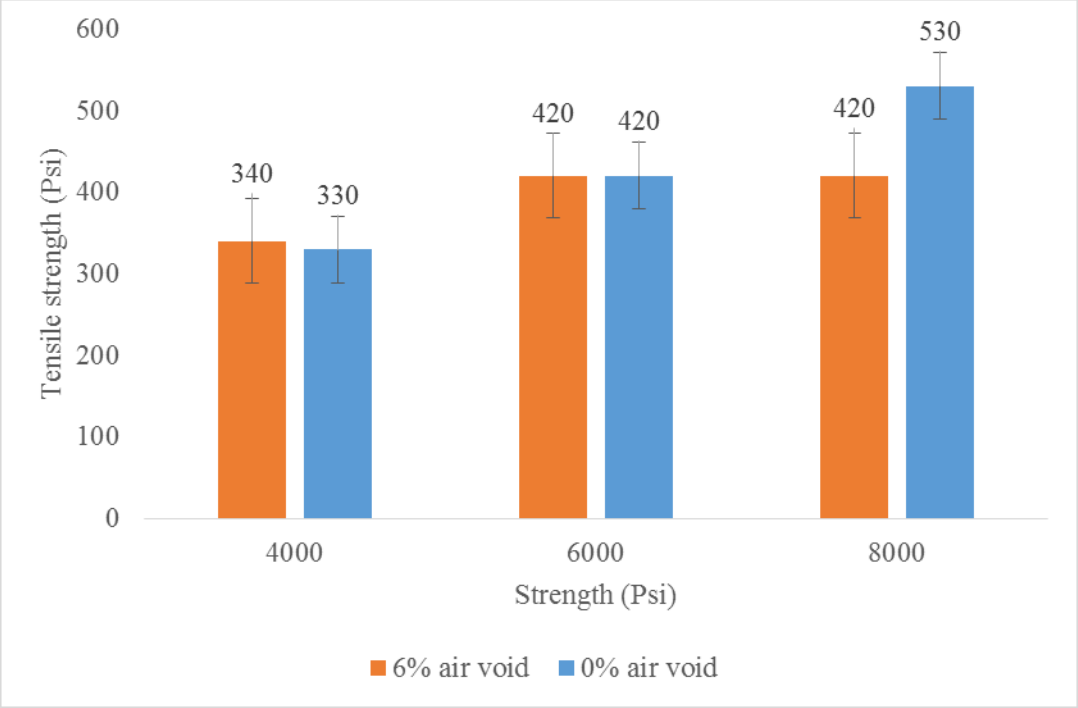

Figure 47. Splitting tensile strength results at three strengths for specimen with different percentage of air void

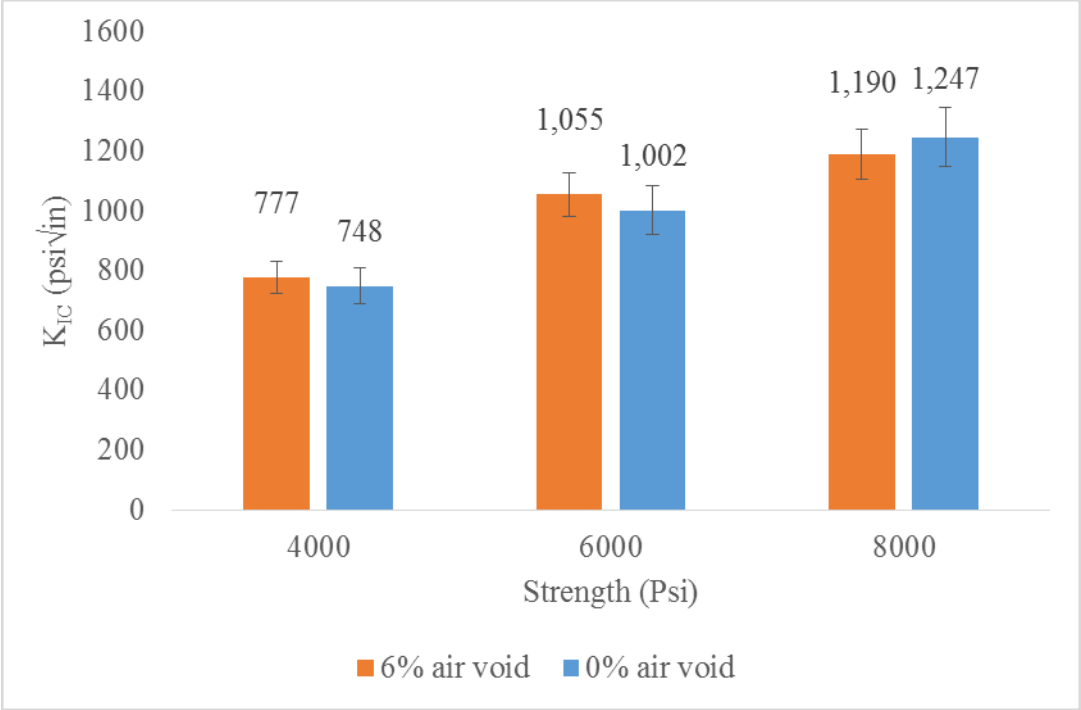

Figure 48. Fracture toughness results at three strengths for specimen with different percentage of air void

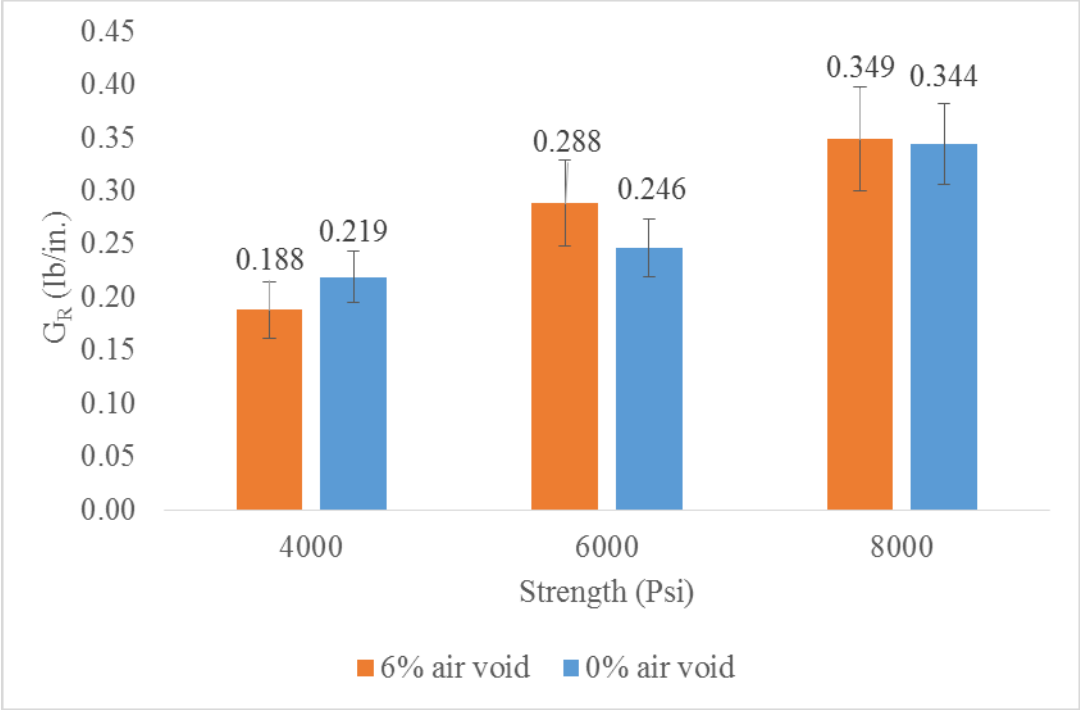

Figure 49. Fracture resistance results at three strengths for specimen with different percentage of air void

2.5.8 Fatigue Crack Growth

Three prisms from two mixes (Mix#1 and Mix#2) were made to evaluate the effect of cyclic loading on crack propagation. The specimens were tested at compressive strength of 8000 psi. As noted previously, Mix#1 and Mix#2 were made of pea gravel (CA1) and Tucson coarse aggregate (CA2 and CA3), respectively. As seen in Figure 50 and Figure 51, the results of crack mouth opening displacement (CMOD) versus number of cycles up to failure are highly variable. It seems that the quality of the notch highly affects the fatigue crack growth in concrete where the material is not consistent. The presence of a coarse aggregate directly at the top of the cut notch may significantly alter the number of cycles to failure. Also, for inhomogeneous material like concrete, high variability of fatigue results was also noted in previous studies. [31, 103-105]. Because of the large variability of the fatigue tests, this test series was discontinued after evaluation of the first two mixes.

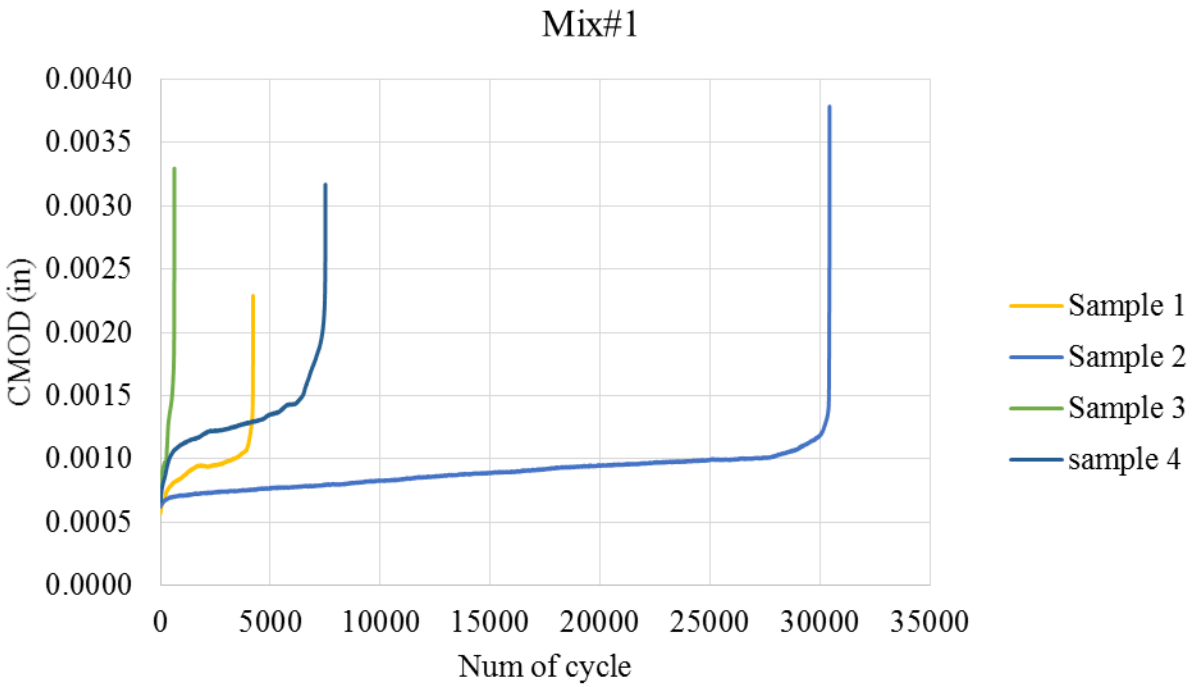

Figure 50. Result of fatigue test for Mix#1 at 8000 psi

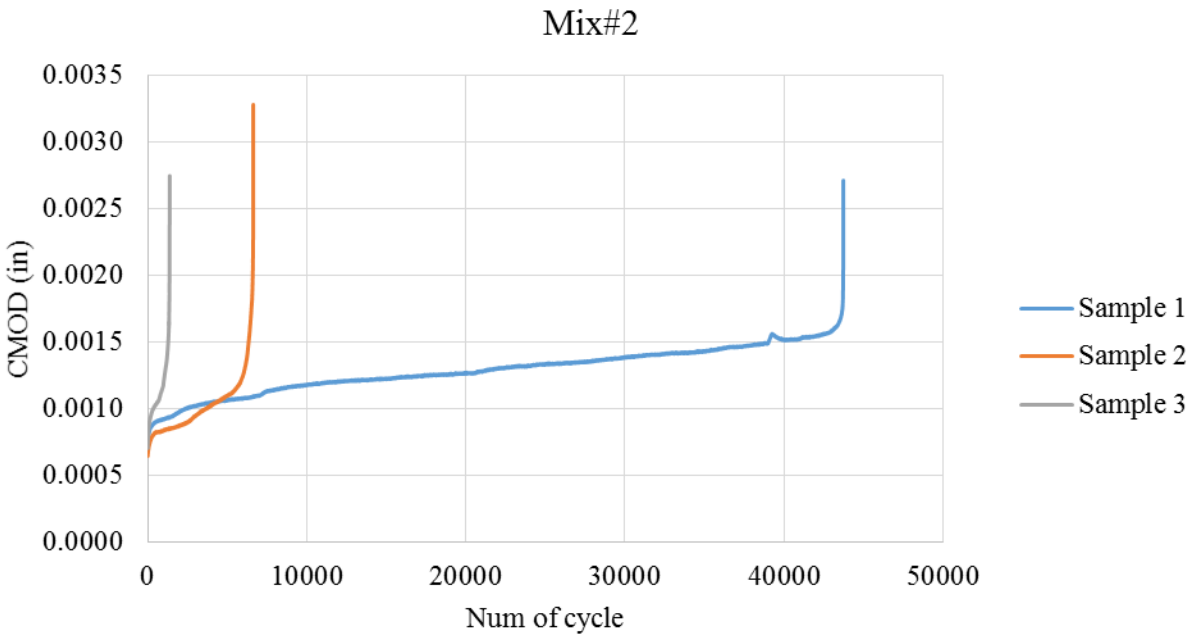

Figure 51. Result of fatigue test for Mix#2 at 8000 psi

2.5.9 Applicability and Variability

In order to develop a qualification test for prestressed concrete members to predict splitting-crack growth, it is important that a practical test with high reliability is chosen. In addition, parametric analysis of fracture toughness test results from the effect of each factor should be conclusive. Parameters obtained by TPM method at 4000 psi are tabulated in Table 5.

The results acquired from fracture toughness test were compared regarding overlapping and variability. As shown, the change in concrete constituents does not necessarily lead to a significant change in fracture parameter values. Although this improvement indicates higher crack growth resistance, actual prestressed members should be tested with the identical material to evaluate the effect of this improvement on actual cracking performance. Unlike proposed models, no meaningful agreement between proposed parameters (like l_{ch} and Q) and splitting tensile strength is observed although the result of l_{ch} representing brittleness for different mixes, confirm previous findings [44, 58, 93]. Also, the maximum difference between fracture toughness results for all mixes evaluated was only 30%, which indicates there is a large data overlap. It is believed that high variability of fracture results at low strengths is attributed to coarse aggregate cut right at the notch tip which contributes to higher crack growth energy than those with notch tip thoroughly in paste. Bond and splitting tensile of paste are considerably less than rock at low strengths. Hence, it is suggested that to avoid variation of results at low strengths (<5000 psi) a pre-notch should be made while casting concrete.

Moreover, the highest coefficient of variation is observed for $CTOD_c$ which may be attributed to the difficulty of measurement of unloading compliance. As noted previously, unloading occurs at 95% of peak load. Due to the brittle behavior and abrupt post-peak crack growth, unloading at

exactly 95% maximum load is undoubtedly problematic resulting in high variation of unloading slop and fracture parameters consequently. Based on the results of this research, it seems that TPM may not be a sufficient mean for qualification test evaluating splitting-cracks of prestressed members.

Table 5. Summary of obtained results at 4000 psi

Mix num.	$CTOD_c$ (×10-3 in.)		KIC (psi √in)		MOE (×10-6 psi)		f't (psi)		Q (in.)	G_R (Ib/in)	l_{ch} (in.)
	Avg.	CV %	Avg.	CV %	Avg.	CV %	Avg.	CV %			
Mix#1 (control mix)	0.50	35	748	9	2.62	17	329	10	3	0.21	5.17
Mix#2	0.90	35	863	15	2.90	3	377	6	9	0.26	5.25
Mix#3	0.80	20	940	10	4.05	14	367	11	12	0.22	6.57
Mix#4	0.72	17	751	5	2.93	6	388	5	8	0.19	3.74
Mix#5	0.50	18	777	5	3.27	10	341	14	4	0.18	5.19
Mix#6	0.78	31	977	10	3.68	11	386	9	9	0.26	6.40
Mix#7	0.62	58	874	11	3.11	9	333	2	5	0.25	6.88
Mix#8	0.80	4	856	2	2.88	2	416	5	7	0.25	4.23
Mix#9	0.72	10	851	8	3.53	15	301	4	9	0.21	8.00

2.6 Summary and Conclusion

Nine different concrete mixes were developed and evaluated for fracture toughness and splitting tensile strength tests at 4000, 6000 and 8000 psi. These mixtures were used to evaluate the effect of coarse aggregate shape, aggregate size distribution, w/cm ratio, fly ash, paste content and air void content on fracture toughness. The following conclusions are drawn from the present research.

- Angularity and type of aggregate has been shown to increase fracture toughness by up to 25% when tested at the same concrete compressive strength.
- When aggregate coarseness (λ) decreases from 0.5 to 0.37, the fracture toughness increases by 15%. This effect was most pronounced at 4000 psi for fracture toughness and becomes less significant at higher compressive strengths.
- Increasing volume of coarse aggregate from 50% to 60% of total aggregate, enhances fracture toughness and fracture resistance up to 16% and 10% at 4000 psi, respectively.
- When w/cm ratio was lowered from 0.38 to 0.28 the fracture toughness improved by 30% at 4000 psi and by 5% at 6000 psi compressive strength. At 8000 psi, the mixture with higher w/cm ratio actually had a higher splitting tensile strength, perhaps due to the significantly-longer curing period required to achieve the higher strength.
- The addition of 25% Class F fly ash as a cement replacement had a slight positive effect on fracture toughness when tested at both 4000 psi and 6000 psi. At 8000 psi, however, both mixes had a similar fracture toughness.
- There was no appreciable difference in fracture toughness caused by changing paste and air void content of concrete within the ranges evaluated.
- The results of this study indicate that alteration in aggregate and paste of concrete is more effective at lower strengths (4000 - 6000 psi) than at higher strength (8000 psi). This finding is particularly notable for prestressed concrete railroad ties where the prestress force is typically applied when the concrete is in the same 4000 – 6000 psi range.
- According to results of this research, the maximum enhancement of fracture toughness was up to 30%. It can be concluded that the utilized method may not be applicable as a qualification test to assess the splitting-crack resistance of concrete regarding variability and overlapping of the results.
- The fracture toughness test obtained by loading and un-loading the specimen and fatigue crack growth test, create more variation due to high sensitivity of results to the notch tip, un-loading compliance value and the difficulty of crack growth control within un-loading phase.
- The use of fatigue tests as a qualification test for splitting was also eliminated due to the high variability of results.

3. Splitting-Crack Evaluation (Phase 2)

To further evaluate the effect of concrete mixtures on splitting-cracking and the relation between fracture indices and splitting-cracking, prestressed prims were made using mixtures having improved fracture toughness. This test was developed at Kansas State University under the same research project sponsored by Federal Railroad Administration (FRA) [106-109]. This test method was used to quantitatively evaluate performance of prestressed concrete prims, in terms of splitting-cracks, after detensioning.

Moreover, although the factors affecting fracture toughness were determined in Phase 1 of this research, the effect of these factors was still unclear on actual prestressed prisms and splitting-crack growth. Since the concrete parameters affecting fracture toughness were found to be most significant at lower concrete strengths like 4000 psi, prestressed prisms with identical materials were fabricated and tested at 4500 psi.

3.1 Prestressed Concrete Member

The idea of prestressed concrete was initially developed to increase tensile capacity of concrete. Prestressed concrete ties like all prestressed concrete members are designed to increase the loading capacity under high impact load. To fabricate prestressed concrete members, wires/strands are prestressed prior to casting and then de-tensioned at desired concrete strength. The required length to fully introduce the pre-tensioning force from wires to concrete member is called “Transfer Length”. There are various factors affecting the transfer length such as diameter of restressing reinforcement [110], reinforcement’s surface [111], release strength [112], and concrete composition [113]. It also was evident that as the transfer length reduces, the bond stress around pretensioned wires increases. This increased stress around wires causes high amount of tensile stress in concrete perpendicular to wire leading to splitting-cracks around wire.

3.1.1 Splitting-Cracks

Splitting-cracks initiate at the end of a prestressed member. For members such as concrete railroad ties that typically do not contain any transverse reinforcement, splitting-cracks can propagate longitudinally and lead to structural failure of the tie itself, endangering safety. These splitting-cracks can occur right after releasing tension or at some later point under the superimposed loading condition. In these members, splitting-crack propagation can lead to structural deterioration and significantly-reduced load-carrying capacity. Therefore, it is very important to enhance both the crack-initiation and crack-propagation resistance of concrete mixtures used in prestressed concrete railroad ties. It is believed that there are different factors causing formation and aggravation of splitting-cracks, including environmental condition, concrete cover, wire indentation type, and concrete material around wire [2, 114-117]. It is hypothesized that concrete properties and its strength can significantly impact splitting-cracks propagation in concrete railroad ties.

There are three different modes when it comes to modeling of crack growth behavior [1]. Opening, sliding and tearing modes are considered as mode I, mode II and mode III, respectively. In prestressed concrete members, splitting-cracks happen mostly after de-tensioning when tensile stress normal to the plane of crack reaches the maximum tensile stress of concrete.

Since the stress in these members is dominantly influenced by tensioning force of wires, the opening mode is predominant and shear stress near the crack tip can be neglected.

3.2 Test Set up

A structural steel prestressing bed having a motorized mechanical gear jack was used to fabricate the prestressed concrete prisms at the Kansas State University laboratory [108]. This bed was long enough to allow fabrication of three 59.5 in. prisms with approximately a 10 in. gap between each prism. Three prisms with different cross-section dimension were fabricated end-to-end. More details on dimension of prisms are presented in the following section. This frame allowed the simultaneous tensioning of prestressing of wires up to 7000 lb per wire which is the allowable limit of 75% of specified minimum tensile strength of the wire. Load cells with a precision of 0.25% of full scale were used to accurately measure prestressing force in each wire at the "Dead End" of the prestressing frame as shown in Figure 52. This end is considered the "Dead End" since it remains fixed during the tensioning and gradual de-tensioning of wires. At the "Live End", wires were tensioned using the mechanical gear Jack. Initially, all 4 wires were manually tensioned to 300 lb per each wire by adjusting hollow bolts as shown in Figure 53. Next, steel tendons were pulled simultaneously using the motorized mechanical gear jack to reach 7000 lb for each wire (28,000 lb total).

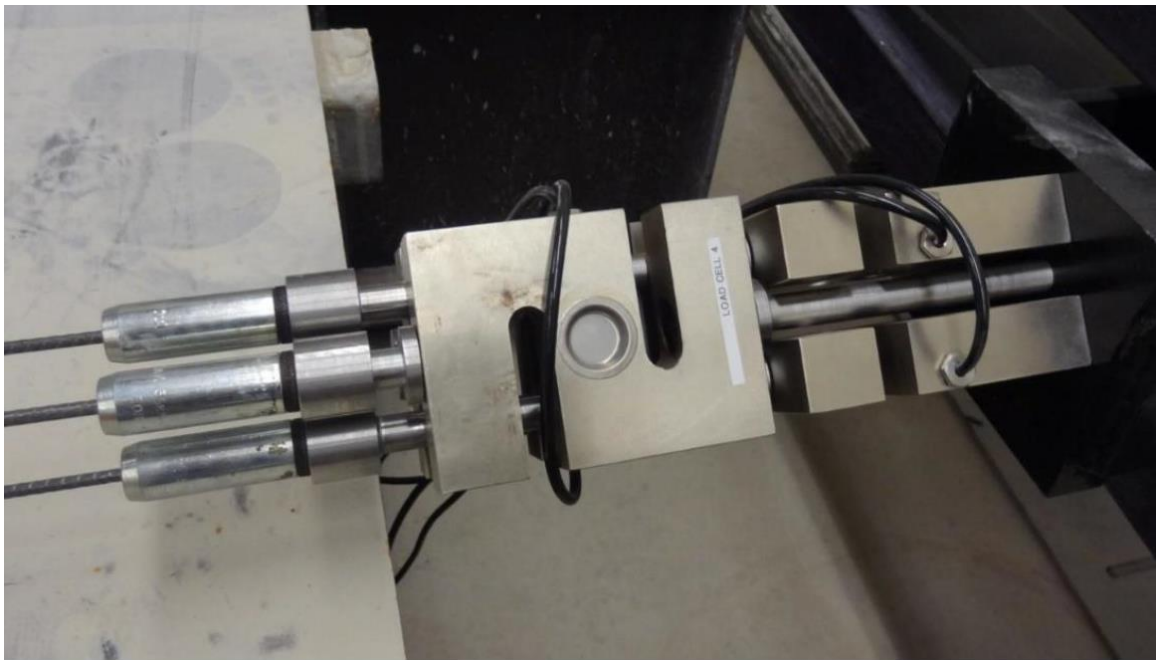

Figure 52. Load cells attached to individual prestressing wires at the "Dead End"

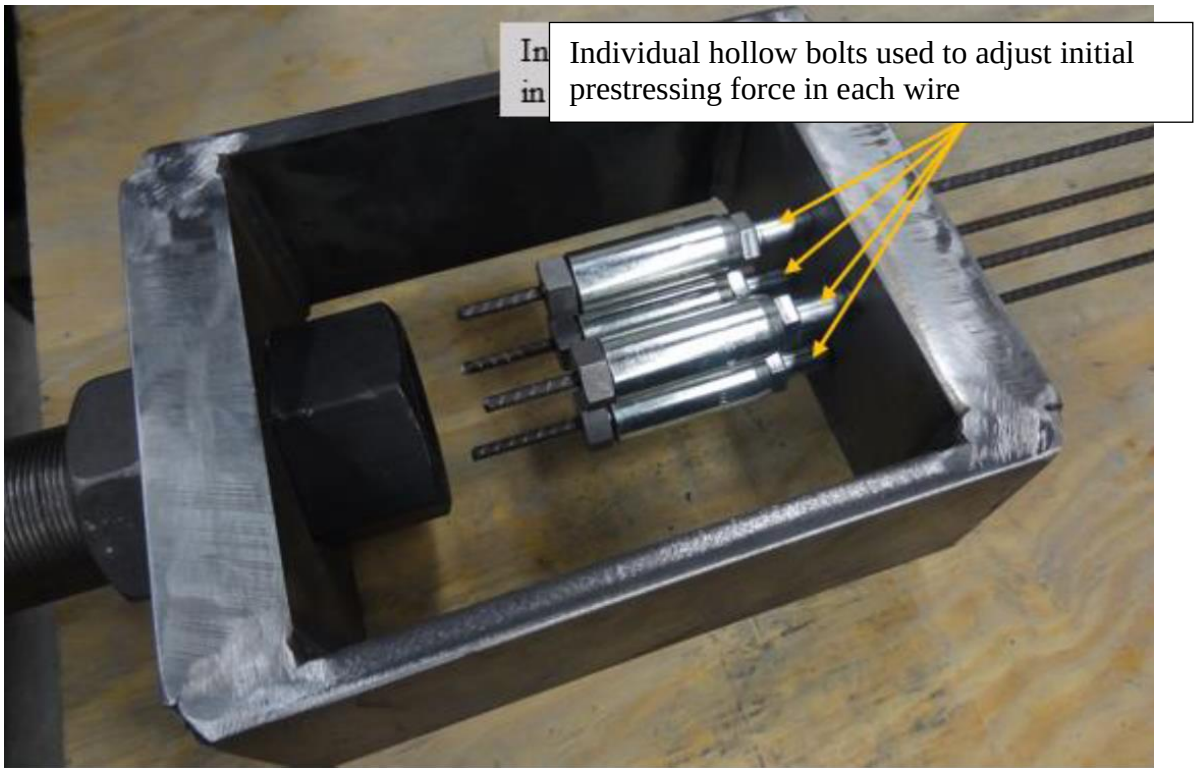

Figure 53. Hollow bolts adjacent to anchor chuck were used to manually adjust the initial prestressing initial force in each wire to 300 lb

3.3 Sample Preparation

Each test included three prisms, each with different edge distances to the prestressed wires (0.500, 0.625, and 0.750 in.) as shown in Figure 54. The edge distance is defined as distance from tendon center to edge of prism. Also, the distance between center of adjacent wires in all prisms was 2 in.

A wire generically labeled WP (in the overall FRA-funded study) was used for all prisms to eliminate the effect of wire type and indentation. Geometric properties of wire WP in this research are tabulated in

Table 6 [106, 107]. The geometric characteristics of wires were determined by a high-resolution automated prestressing wire indent profiling system developed at Kansas State University [107, 118-120].

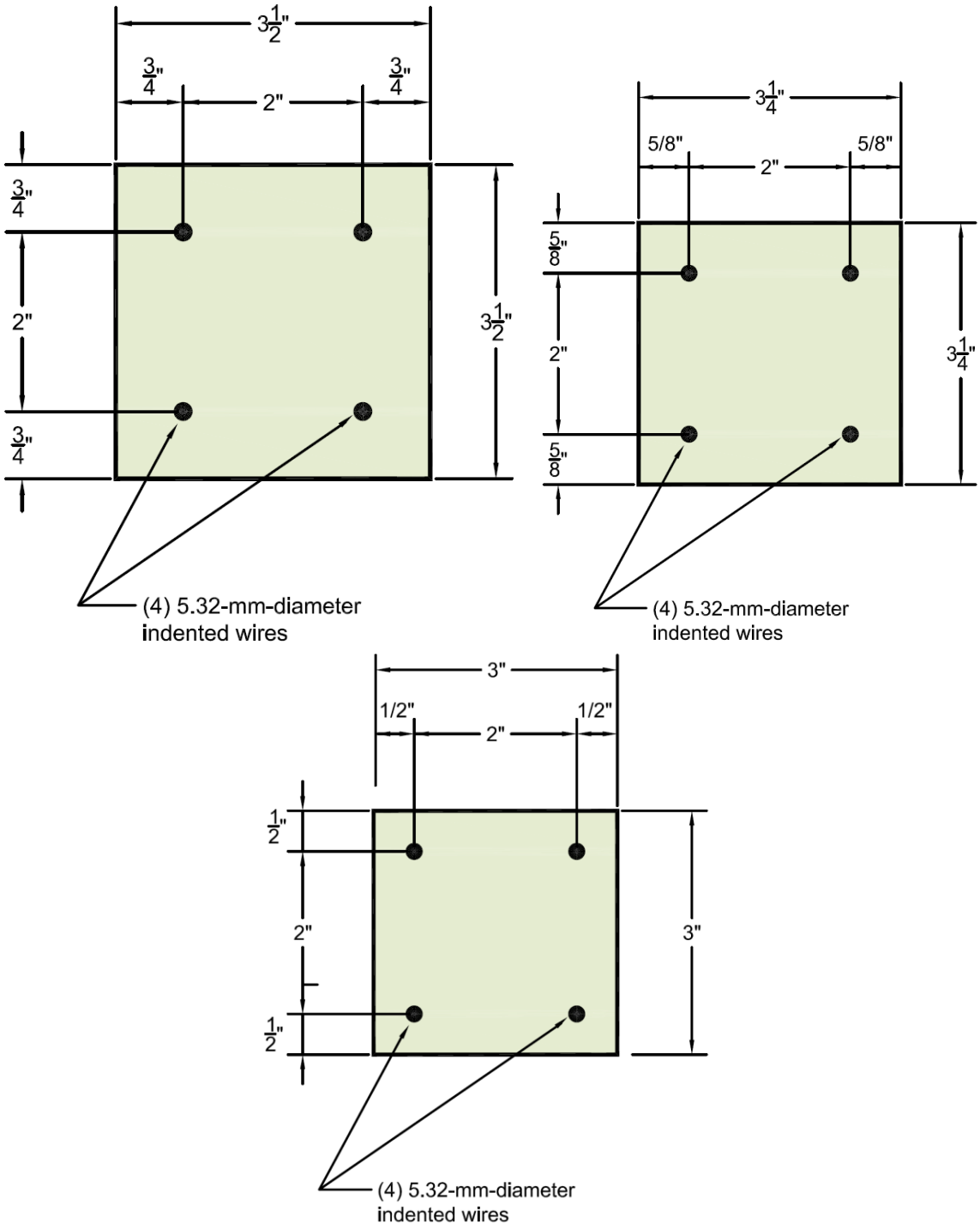

Figure 54. Cross section of three prisms for each set of prism [108]

Table 6. Geometric parameters for WP wires

Wire Label	Indentation type	Diameter (in)	Depth of indentation (in)	Volume of indentation (in^3)	Average Edge wall angle (deg)
WP	Chevron	0.209 (5.32mm)	0.0046 (0.117 mm)	0.002705 (1.745 mm^3)	29.0

Figure 55. Close-up view of indentation pattern of WP wire

Before casting specimens, all 4 wires in prisms were tensioned up to 7000 lb per wire shown in Figure 57. For each mix, nine 4" x 8" temperature-match cured cylinders (Figure 58) were made along with the three prims. These were then tested during the curing process to ensure that de-

tensioning occurred at the desired compressive strength of 4500 psi ± 200 psi.

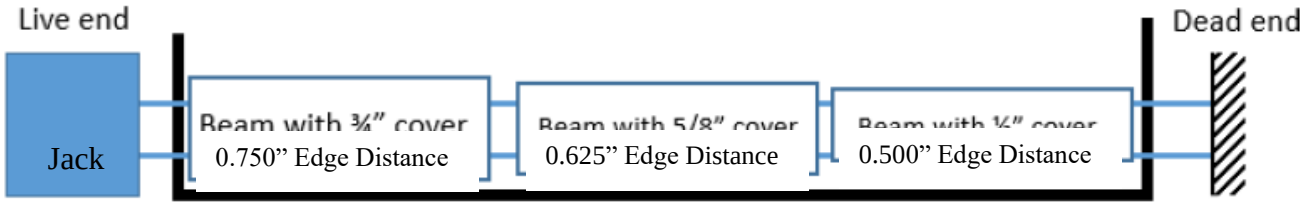

Figure 56. Schematic figure of prestressed prims set up [108]

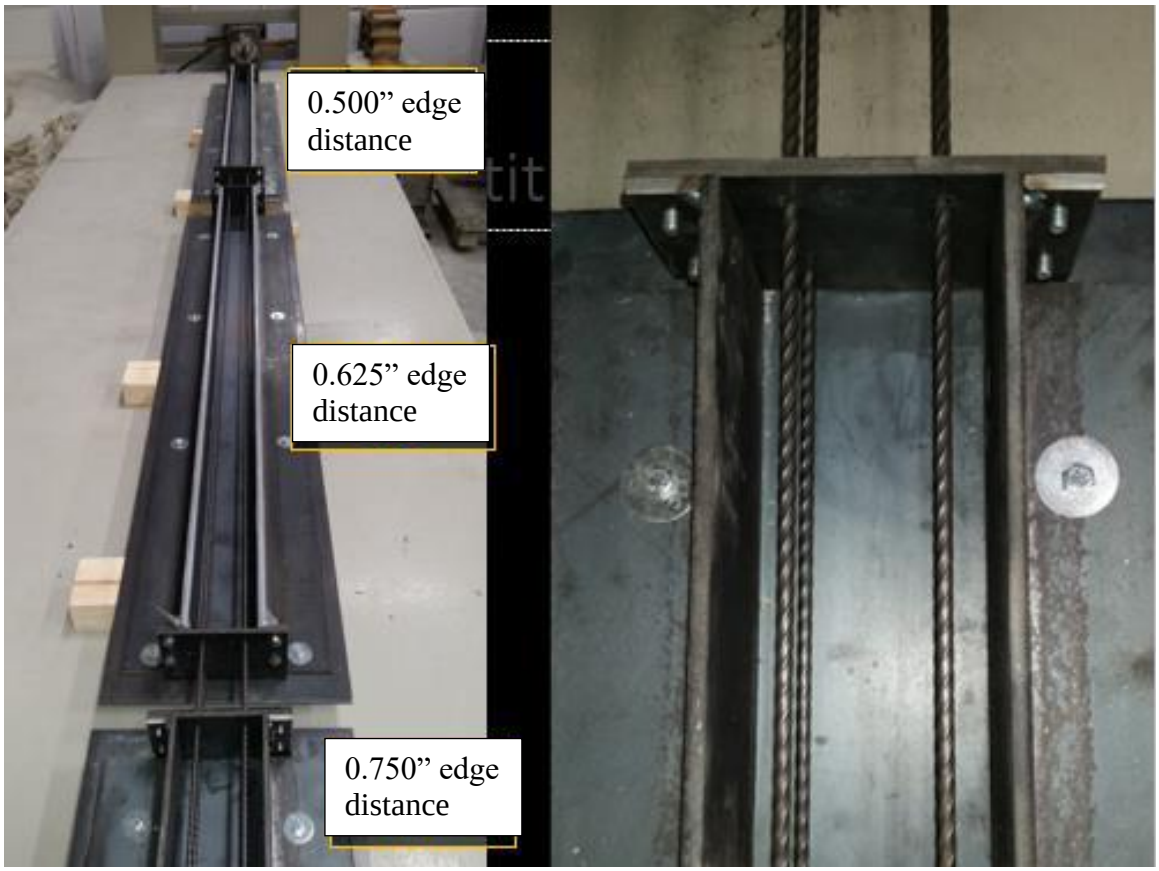

Figure 57. Prestressed prisms forms [108]

Figure 58. A commercial "Sure-Cure" system was used to temperature-match cure the test cylinders

3.4 Mix Designs

The mixtures were designed so that the most effective factors (contributing to fracture toughness) from the previous section were included. These factors are angularity, coarseness, volume of coarse aggregate, class F fly ash, and w/cm ratio. In addition, 5 mixes were designed to assess the effect of transverse reinforcement on splitting-cracks.

Therefore, the following additional mixtures were designed as summarized in Table 7. Each mixture had 813 lb/yd^3 (482.8 kg/m^3) cementitious material. Control Mix (B101) was similar to the mixture used by a tie manufacturer at the time of this study. Mixture codes in Table 7 are used to identify the batch ID. For example, mixture B101 stands for (B-10-1), where "B"= Batch, "10" is the mixture number, and "1" is the trial number.

Table 7. Mix proportions and variable of prestressed concrete prisms

Mixture	Aggregate (Kg/m^3)					Cement Type III (Kg/m^3)	w/cm	Fly ash Class F(lb/yd^3)	Polycarboxylate water-reducing Admixture (fl oz per yd^3)	Wire Type	Variable
	CA2	CA3	CA4	CA5	FA						
B101	562	337	0	0	889.2	488.2	0.32	0	40	WP	Control Mix
B114	661	396	0	0	705	366.2	0.32	203.4	40	WP	Fly ash+coarse agg. volume
B121	674	404	0	0	719.2	488.2	0.32	0	40	WP	Coarse agg. volume
B131	511	306	0	0	817.6	488.2	0.45	0	20	WP	W/CM ratio
B141	551	330	0	0	882.2	366.2	0.32	203.4	40	WP	Fly ash
B151	0	0	0	874.7	874.7	488.2	0.32	0	40	WP	Angularity
B161	562	337	0	0	899.2	488.2	0.32	0	> 160	WP	Segregation
B171	0	0	904.5	0	904.5	488.2	0.32	0	40	WP	Angularity
B181	562	337	0	0	889.2	488.2	0.32	0	40	WB	5% polymer fiber+Wire type
B191	0	0	0	874.7	874.7	488.2	0.32	0	40	WP	Angularity + 5% polymer fiber only at ends
B201	0	0	1088	0	725	488.2	0.32	0	57	WP	Angularity+ Coarse agg. volume
B211	0	0	0	874.7	874.7	488.2	0.32	0	40	WP	Angularity+ Stirrups
B221	0	0	0	874.7	874.7	488.2	0.32	0	40	WP	Angularity + 5% polymer fiber

3.5 Test Procedure

After casting specimens, temperature-match cured cylinders were tested at periodic intervals to determin the compressive strength. As soon as the cylinders reached 4500 psi, the prisms were gradually detensioned. The length and width of cracks were measured using a ruler and concrete crack comparator (Figure 59), respectively, after 90 days. This time delay was used to evaluate long term creep behavior of splitting-cracks.

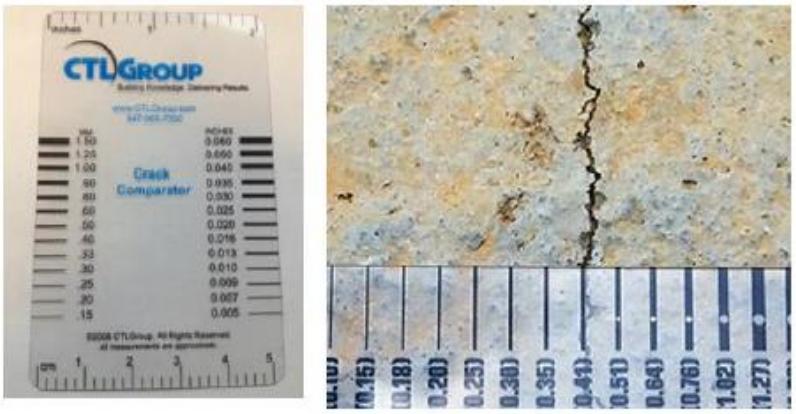

Figure 59. Crack measurement through crack comparator

To quantify formation of splitting-cracks after detensioning, the number of occurrence of splitting-cracks around the wires was counted. As explained in Section 4.2, each of three prestressed prisms with different edge distance (0.75, 0.625, and 0.5 in.) had two ends (live end and dead end) including 4 wires coming out of concrete which were subsequently cut after complete gradual detensioning. For instance, each prism could have from 0 to 8 cracks around the wires. This "digital" evaluation helps provide a better perspective of the severity of low-quality concrete. For example, one cracked corner might be attributed to variability of the experiment condition, whereas 8 cracked corners is attributed to a severe conditions.

To have more accurate evaluation of splitting-cracks for each prism, an analog assessment of cracks (length and width) was also carried out on all samples. Prisms with less total crack lengths are considered to be more resistant to crack propagation.

3.6 Results and Discussion

To evaluate the findings of previous section and its implementation in splitting-crack performance of pretensioned prisms, twelve sets of prestressed prisms were fabricated and tested. The results from these prisms are discussed in the following sections.

3.6.1 Effect of Angularity and Aggregate Distribution

In Chapter 3 it was determined that angularity considerably affects the fracture toughness. Furthermore, when crushed aggregate increased from 10% to 99%, fracture toughness increased

more than 25%. Therefore, three sets of prisms were made and compared in terms of total crack length and number of cracks in each prism.

From Figure 60, mix B171 with 99% crushed material had less cracking than mix B151 with 10% and B101 with 47% crushed material for both 0.750 and 0.625 edge distance. The results demonstrate that angularity and texture have a profound effect on splitting-crack formation and propagation. Angularity can contribute to a better aggregate-mortar interlock as well as larger crack surface around aggregate.

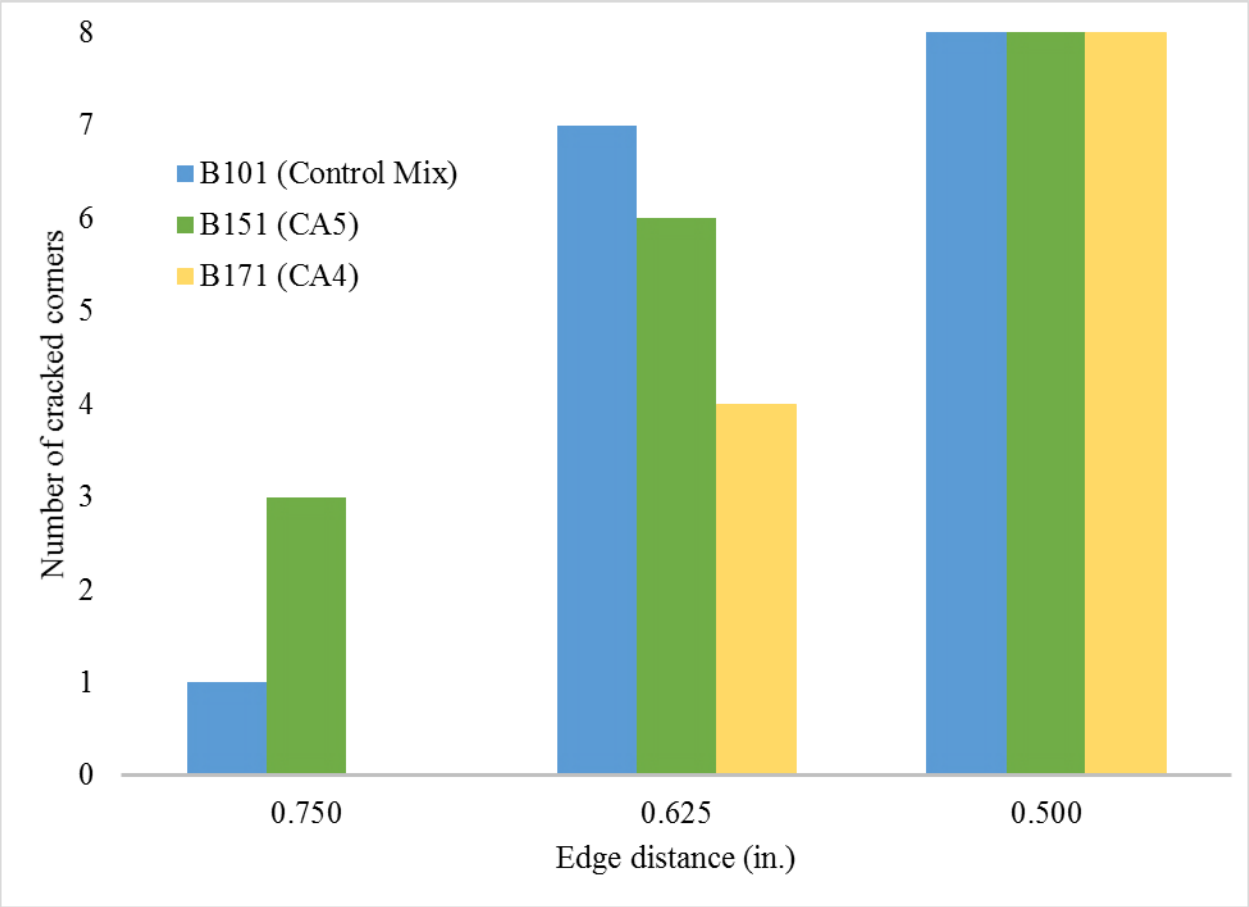

Figure 60. Number of cracked corners for prisms made with different angularity of coarse aggregate

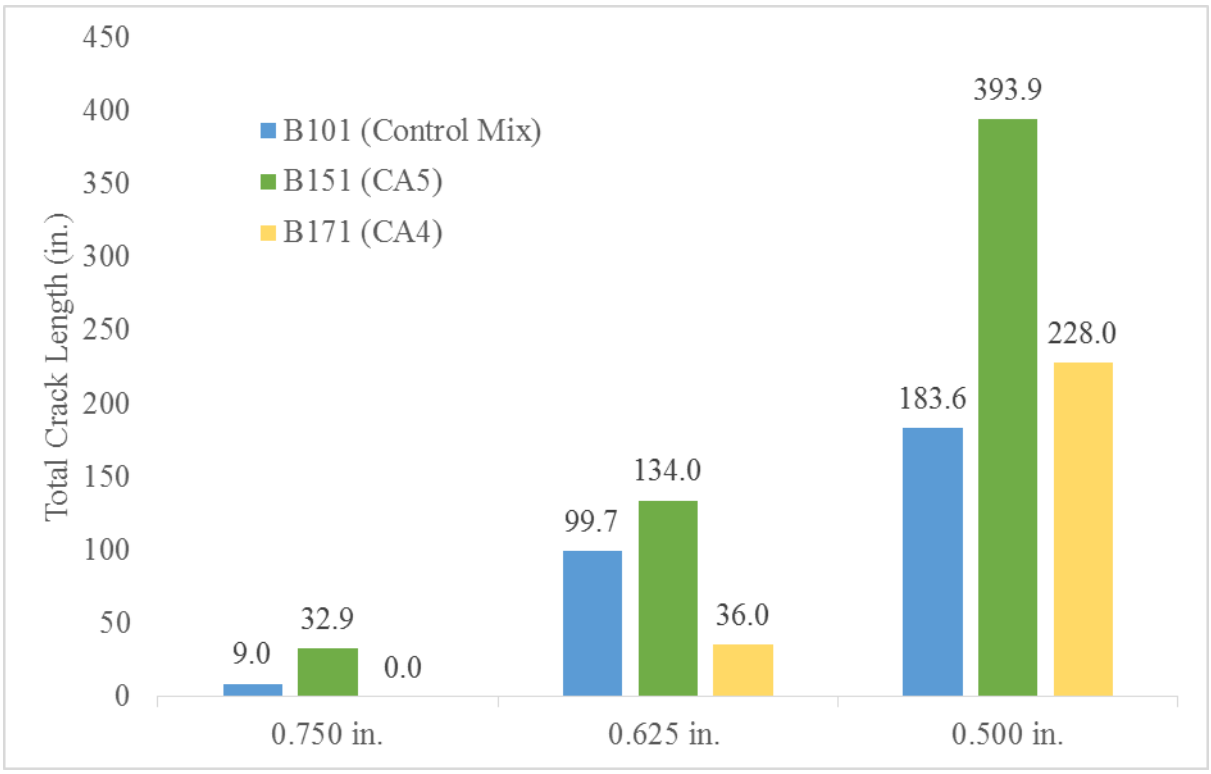

Figure 61. Total crack length for prisms made with different angularity of coarse aggregate

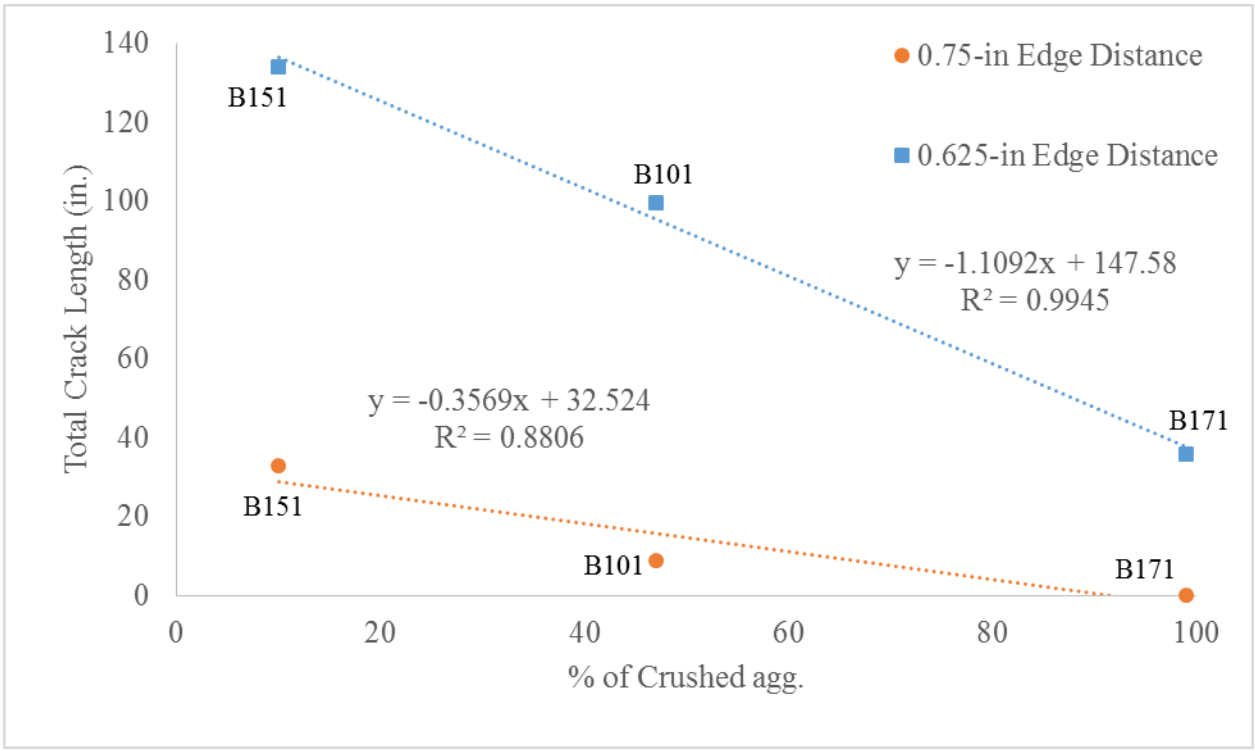

Figure 62. Percentage of fractured aggregate vs. total crack length for prisms made with different angularity of coarse aggregate

As shown in Figure 60-Figure 62, for mixes B101 and B151 the mixtures with less crushed material showed higher amounts of cracking around wires. However, the figures show that as the wire edge distances decreases, the amount of splitting-cracks increases significantly. This indicates the importance of minimum required cover for prestressed members regardless of concrete material. 0.75-in. edge distance prisms made with mix B171 which possess the highest fracture toughness showed the best cracking performance. It means, that as angularity of aggregates increases the likelihood of splitting-cracks profoundly decreases. This improving factor even positively impacts splitting-cracks for prisms with low edge distance like 0.625 in.

The results demonstrated a meaningful relation between angularity, fracture toughness and the likeliness of splitting-cracks. Even with the variability of test results, one could conclude that fracture toughness test can be used to rank the crack-resistance of different concrete mixes [121].

Figure 62 illustrates that as the percentage of fractured aggregate increases, the total length of cracks or tendency of crack growth significantly reduces. It is believed that, there is a meaningful relation between fracture toughness values and total crack length. Also, the variably of prestressed prisms test at 0.500-in. edge distance can be misleading as the cracks are mapped and assessed by human which is impacted by operational errors.

The same trend was observed when edge distance is decreased to 0.625. Although there are more cracked corners in prisms with mix B101 than B151, its total crack length is still remarkably less than B151 with lower fracture toughness natural round aggregate and about three time of B171 containing well-angular coarse aggregate.

Splitting-cracks happened for all prisms with 0.500 in. edge distance [106, 108]. Although the same trend is seen for prisms with 0.500 in. `edge distance, this illustrates the importance of minimum cover in prestressed concrete member regardless of the mixture used.

3.6.2 Effect of Coarse Aggregate Volume and Segregation

In Phase 1, it was determined that fracture toughness increases up to 20% when coarse/fine aggregate ratio increases from 1 to 1.5. With B101 utilized as the control mix, the ratio of coarse/fine aggregate was increased from 1.0 to 1.5 in mix B121 to assess the effect of coarse aggregate volume on splitting-cracks. Additionally, an intentionally segregated mixture was designed to further evaluate the effect of coarse aggregate volume in a mixture.

It was hypothesized that prisms made with segregated mix (B161) would display severe cracking at the top of the prisms. B161 was essentially the same mixture as B101 except for a high dosage of polycarboxylate causing segregation in prisms. Figure 64 and Figure 65 show the casting and mixing procedure of segregated mixture.

Figure 63. Slump-flow (spread) of segregated mix (B161)

Figure 64. Segregation of Mix B161 during casting

Figure 65. Prims made of segregated mix after placement and consolidation (B161)

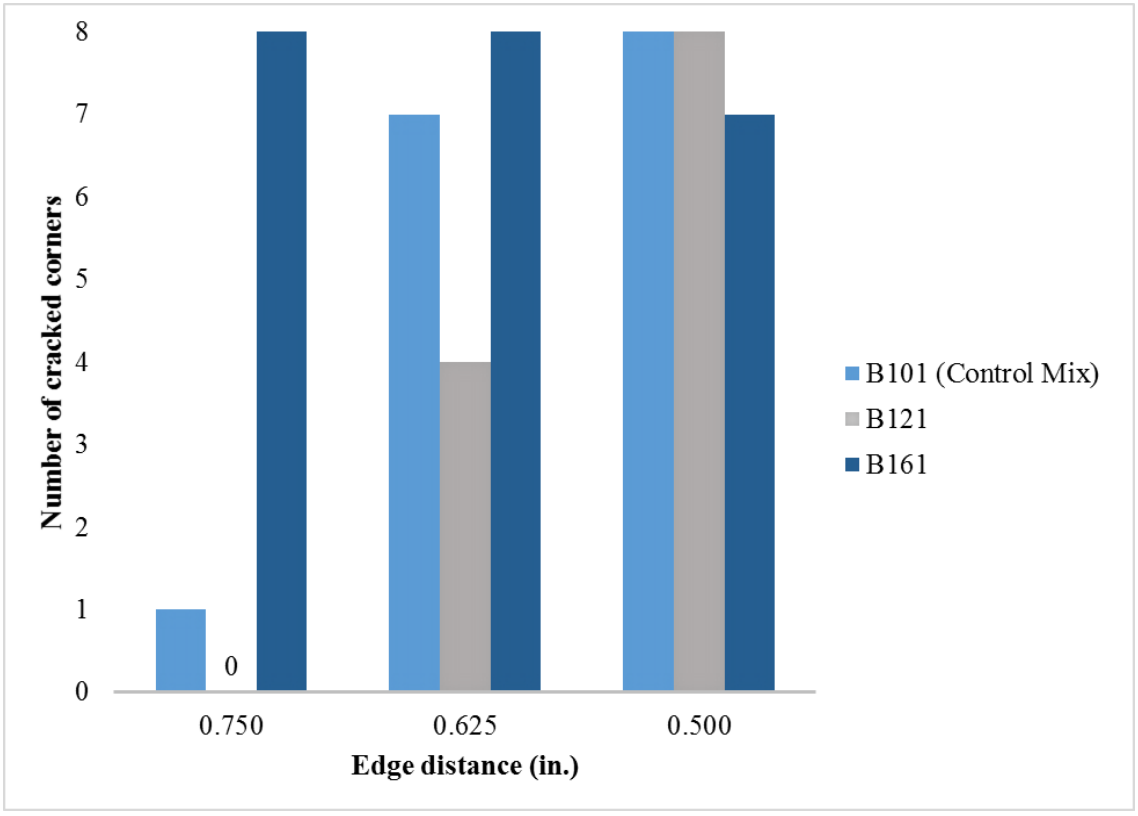

Figure 66. Number of cracked corners for prisms made with different volume of coarse aggregate

Live End (0.750 edge distance)

Dead End (0.750 edge distance)

Live End (0.625 edge distance)

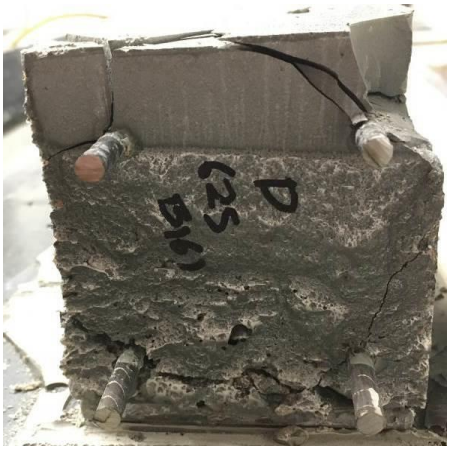

Dead End (0.625 edge distance)

Live End (0.500 edge distance)

Dead End (0.500 edge distance)

Figure 67. Splitting-cracks of segregated mix (B161)

It was observed when volume of coarse aggregate was increased from 1 to 1.5 coarse/fine aggregate, the number of cracks decreased by 12.5% and 40% in 0.750 in.-edge distance and 0.625 in.-edge distance prisms respectively. Again, the effect of edge distance is dominant and

prisms split at all corners in the prisms with 0.500 in.-edge distance. However, as shown in Figure 67, segregation led to splitting-cracks at all corners although a higher amount of coarse aggregate was present around wires at bottom of prims.

This demonstrates that lack of uniformity may negatively affect the cracking at all locations. It also suggests that there is an optimum amount of coarse aggregate in mixture by which crack growth in concrete is improved. The measurements for Mix B121 indicate that increased coarse aggregate volume in concrete leads to shorter and thinner.

Total crack length measured in Figure 68 demonstrates increasing 50% volume of coarse aggregate led to no splitting-crack in 0.750in.-edge distance prisms and 56% improvement in 0.626in.-edge distance prisms. Obviously, lowering the edge distance to 0.5" significantly increases the likelihood of cracking and crack growth. Nevertheless, increasing volume of coarse aggregate significantly improve crack resistance in concrete at larger edge distances.

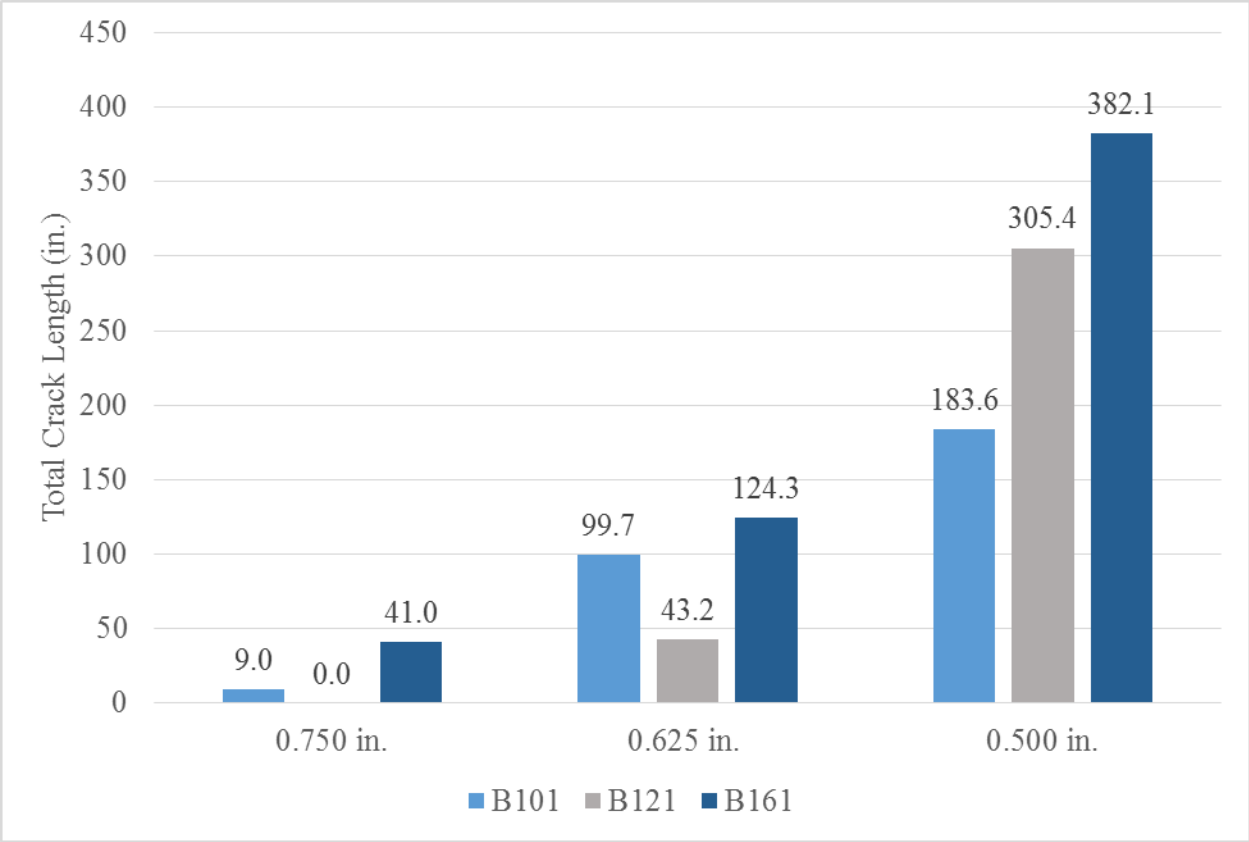

Figure 68. Crack length measurements for prisms with different volume of coarse aggregate

3.6.3 Effect of Fly Ash Class F

The result of fracture toughness showed a slight improvement when 25% fly ash used in mixture. On the other hand, fly ash caused a reduction in fracture resistance. To have a better evaluation of fly ash in mixture, prisms (B141) with 25% fly ash were made. This mix is essentially the same as B101 except for 25% fly ash replacement. According to results shown in Figure 69 and Figure 70, adding fly ash into mixture has a slight effect on 0.750in.-edge distance prisms. In overall, substitution of fly ash negatively affects prisms in terms of splitting-cracks. Like fracture toughness test results, the variability of trend in result may be attributed to the random presence of pozzolanic particles around the wire.

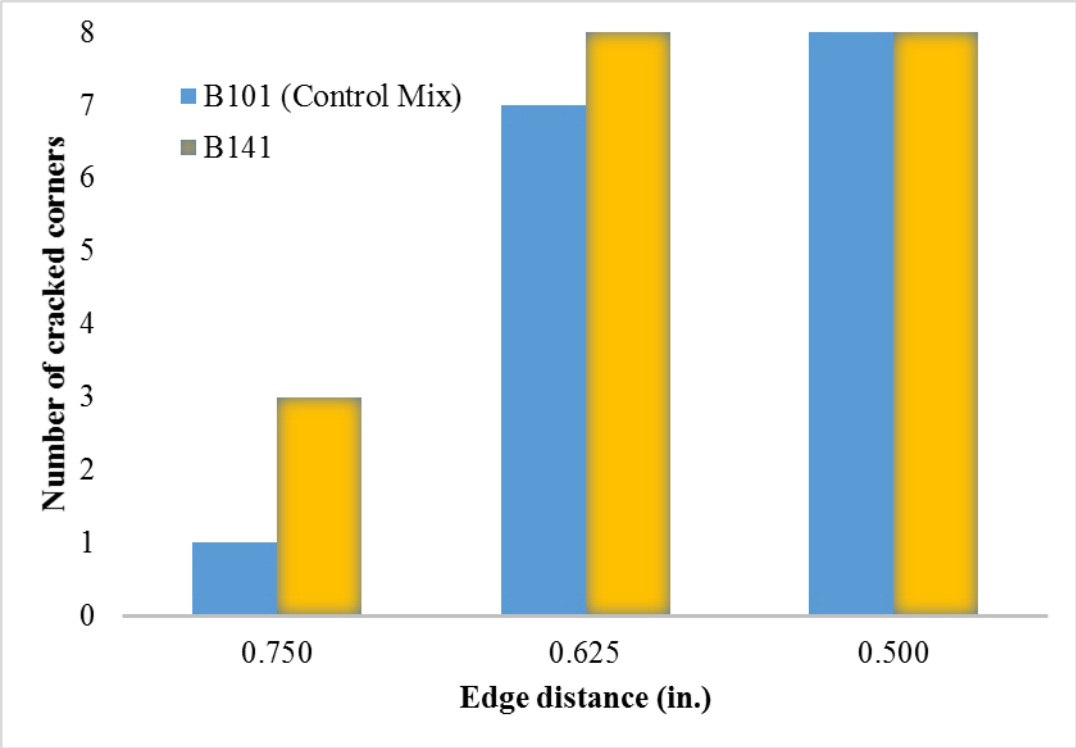

Figure 69. Number of cracked corners for prisms made with 0 and 25% Fly ash when edge distance is 0.750 in.

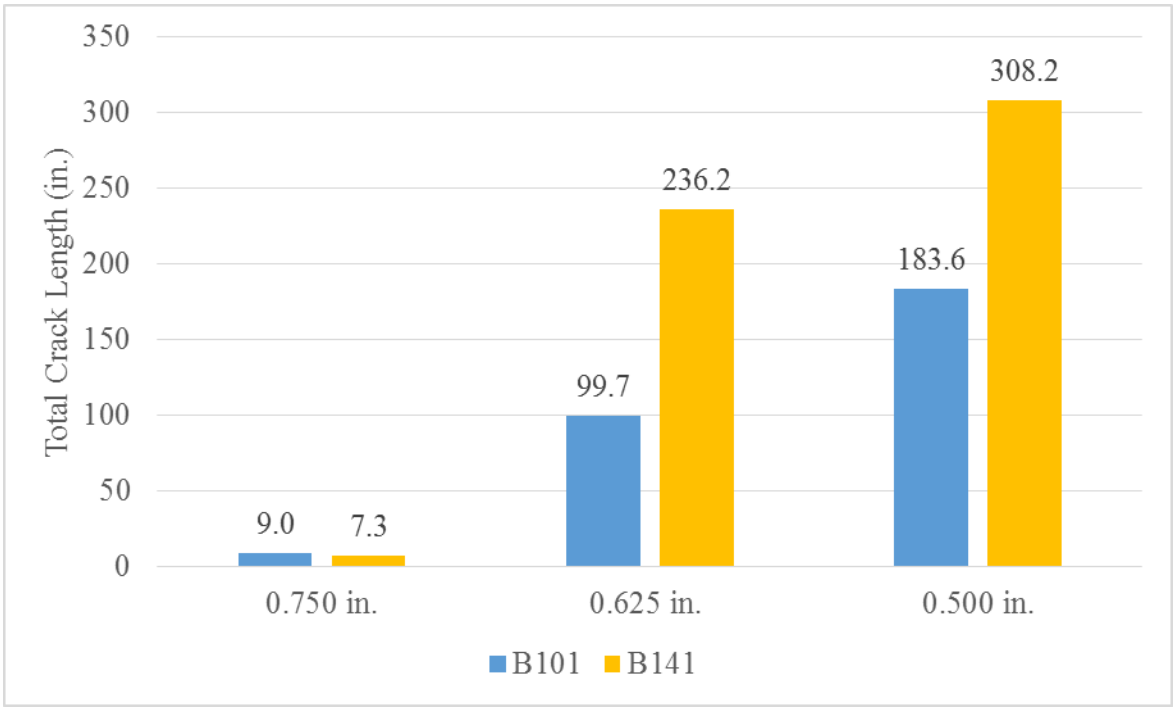

Figure 70. Crack length measurements for prisms with 0 and 25% Fly ash

3.6.4 Effect of Water-Cementitious Ratio

According to fracture toughness test results, lowering w/cm ratio by 25%, fracture parameters increased by 30%. It was hypothesized that increasing w/cm from 0.32 (used for control mix) to 0.45 may cause progressive splitting-crack growth. Prisms B131 were made using B101 except with higher w/cm ratio of 0.45.

As exhibited in Figure 71, increasing w/cm from 0.32 to 0.45 resulted in an increase in the number of splitting-cracks by 40% for 0.750in.edge-distance prisms. Also, total crack length for all prisms remarkably increased when the higher w/cm ratio was used (Figure 72). Although the same trend was observed for different edge-distance, cracking was dominantly influenced by edge-distance rather than mix properties.

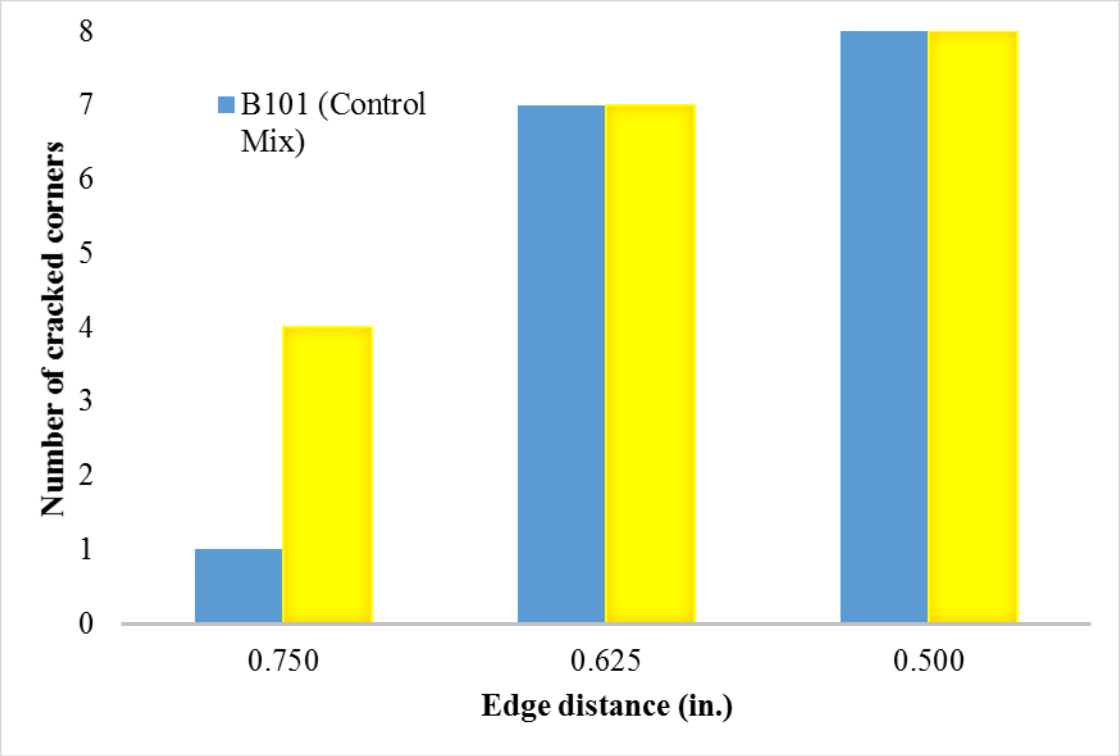

Figure 71. Number of cracked corners for prisms made with 0.32 and 0.45 W/CM ratio

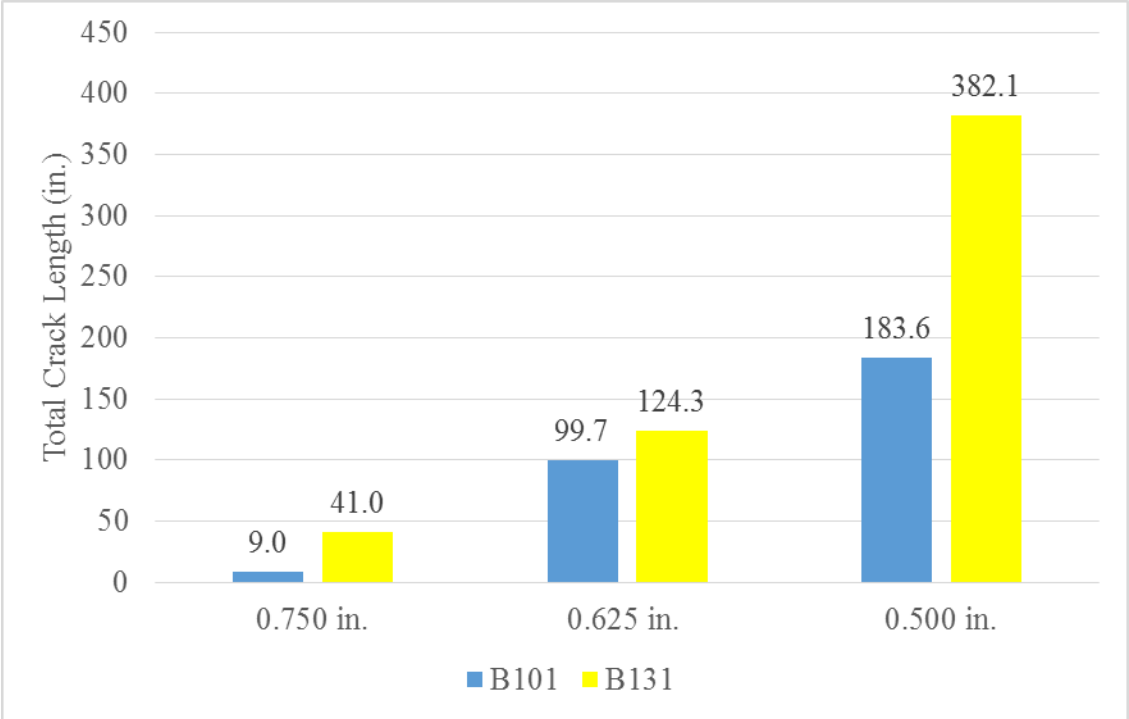

Figure 72. Crack length measurements for prisms with 0.32 and 0.45 W/CM ratio

3.7 Effect of Reinforcement on Splitting-Cracks

3.7.1 Effect of Fiber Reinforcement

It is well-stablished that reinforcing concrete in various ways can lead to a greater crack resistance (Banthia and Sheng 1996) (Matsumoto and Li 1999), (Rossi et al. 1986) . To improve the mechanical properties of concrete material, polymer fibers have been widely used with different percentages.

A monofilament polypropylene micro-fiber was also added to the concrete of a select number prestressed prisms. This fiber complied with ASTM C 1116, Standard Specification for Fiber Reinforced Concrete and Shotcrete. Table 8 tabulates the engineering properties of this fiber.

Table 8. Engineering properties of polymer fiber

Material	100% virgin monofilament polypropylene
Specific Gravity	0.91
Fiber Length	0.750 in.
Fiber Diameter	150 micron
Typical dosage rate	0.67 - 1.0 lb/yd3 (0.4 - 0.6 kg/m3)
Melt point	320^{o}F (160^{o}C)
Electrical and Thermal Conductivity	low
Water Absorption	negligible
Acid and Alkali Resistance	excellent

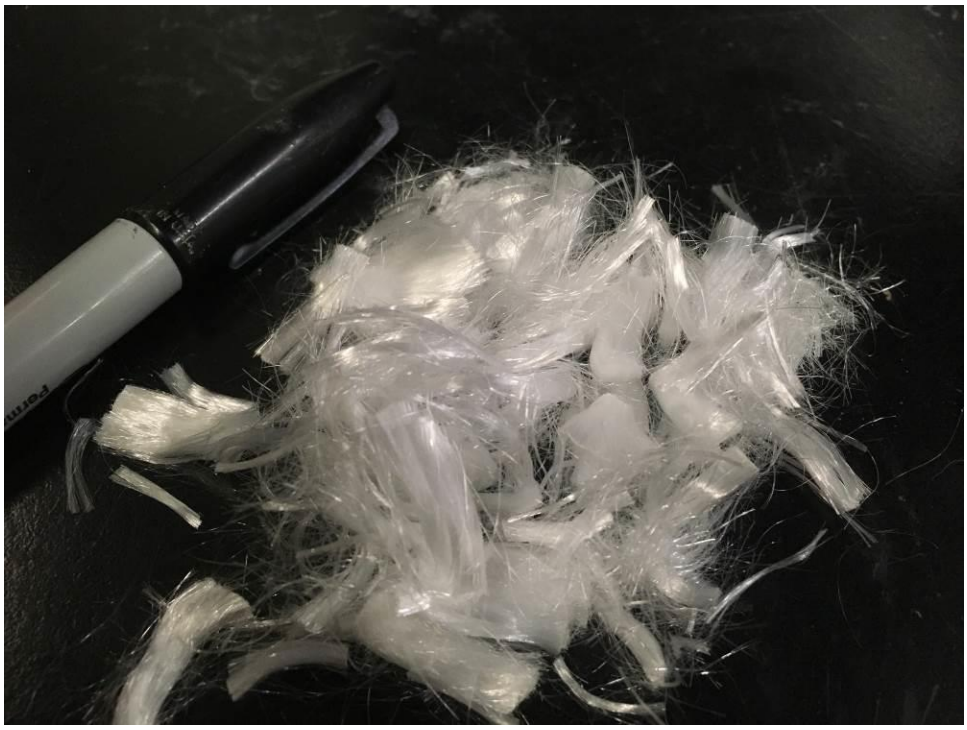

Figure 73. Polymer Fiber

In this research, 5% polymer fiber (based on concrete mass) was added to the mixes with low quality aggregate (natural gravel CA5). Prisms B151 made of low-quality coarse aggregate were seen to be less resistant to crack growth. 5% polymer fiber added to mix B151 to investigate its effect on splitting-crack propagation in prestressed prisms (B221).

The result from pretensioned prism test with fibers (Figure 74 and Figure 75) resulted in a noticeable improvement when 5% polymer fiber added to mixture made with a round natural gravel. The number of detectable cracks declined by more than 30% when polymer fiber was used. However, the number of splitting-cracks was reduced at 0.500-in. edge distance (Figure 74). Hence, there is a significant enhancement in crack propagation resistance when polymer fiber is used (Figure 75).

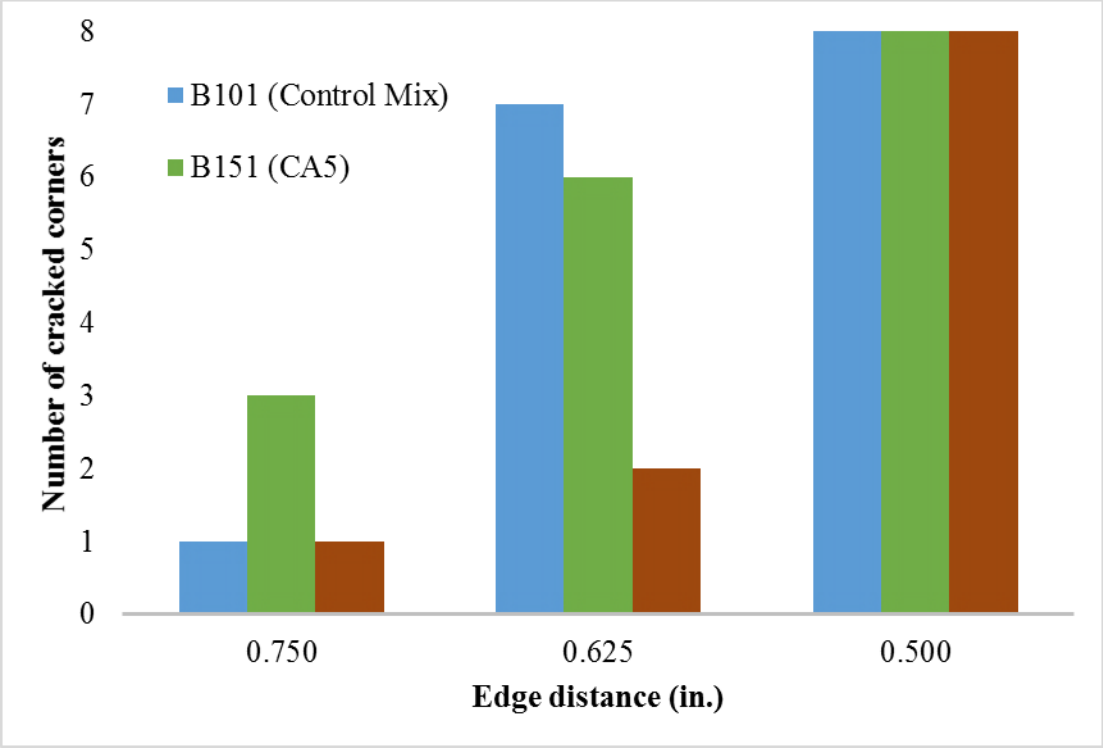

Figure 74. Number of cracked corners for prisms made with 0% and 5% polymer fiber

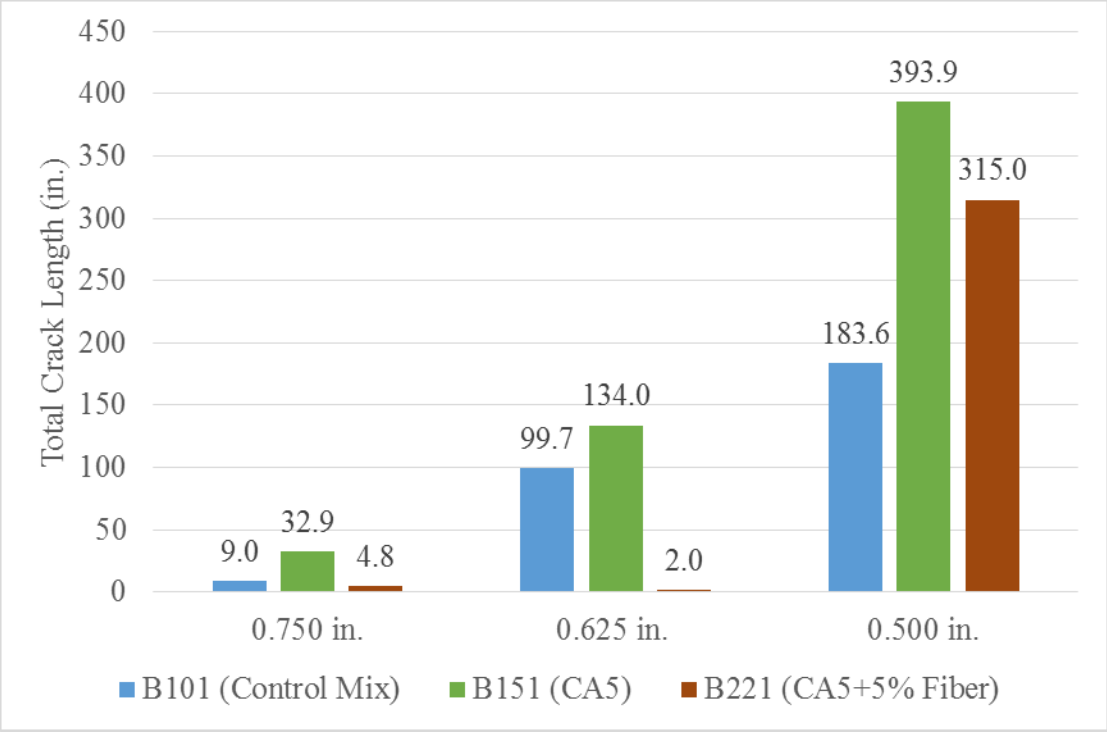

Figure 75. Crack length measurements for prisms with 0% and 5% polymer fiber

Considering the improving effect of polymer fiber on low-quality coarse aggregate, adding polymer fiber in mixture with high-quality and crushed coarse aggregate might also be beneficial in order to reach zero number of splitting-cracks in concrete.

There are other factors contributing to splitting-cracks in prestressed prisms such as wire type and indentation and concrete strength (Savic et al. 2018)[106] . It was questioned whether reinforcing current concrete material of concrete ties with polymer fiber can enhance splitting-crack resistance when wires changes. To address this issue, wire WB which showed the worst performance in terms of splitting-cracks in research by Savic et al. (Savic et al. 2018), was used to fabricate 3 additional prisms. Geometric characteristics of WB are listed in Table 9 and Figure 76 [107, 109, 122].

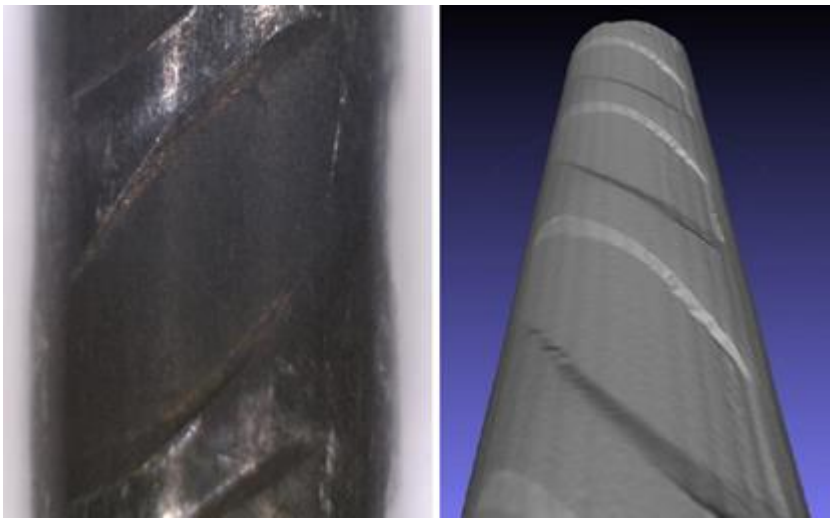

Figure 76. WB wire

Table 9. Geometric parameters for WB wires

Wire Label	Indentation type	Diameter (in)	Depth of indentation (in)	Volume of indentation (in^3)	Average Edge wall angle (deg)
WB	Chevron	0.21 (5.32 mm)	0.0046 (0.119 mm)	0.0001035 (1.696 mm^3)	16.4

The results of prestressed prisms (B181) demonstrated that adding 5% polymer fiber to B101 did not prevent splitting-crack growth in prisms when wire WB was used. It appears that wire type and indentation is much more influential than concrete composition. Therefore, polymer fiber reinforcement can increase the resistance of crack growth if only the wire type meets minimum requirements for splitting-crack performance.

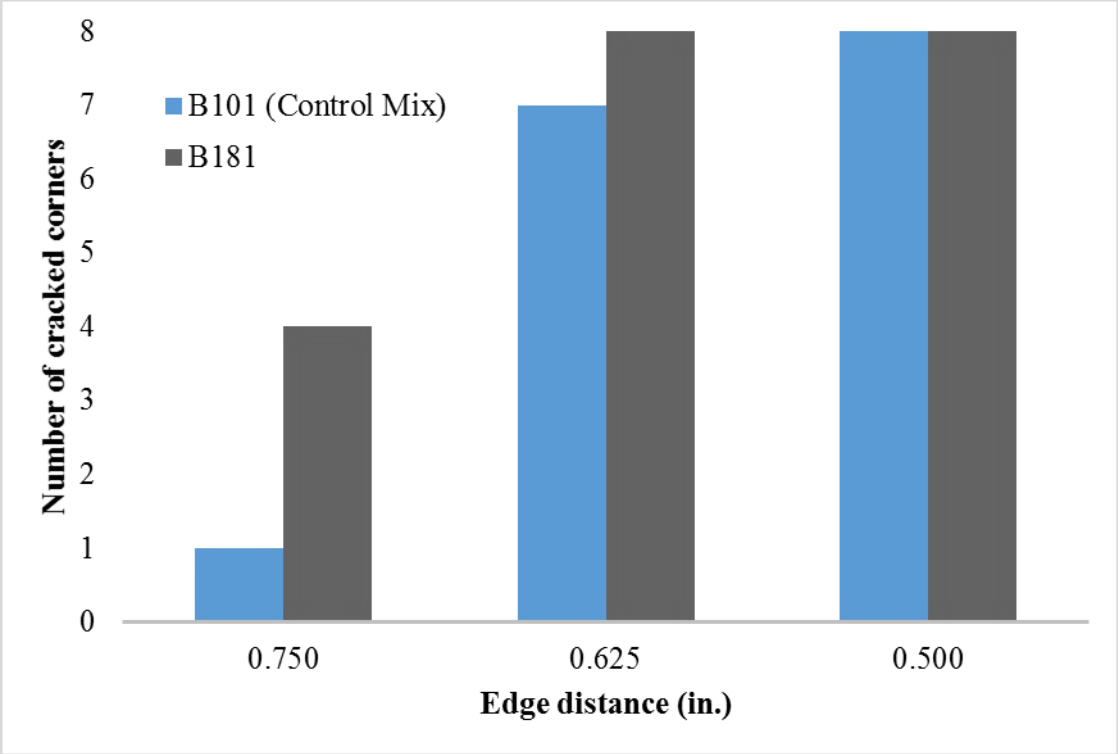

Figure 77. Number of cracked corners for prisms made with different type of wire

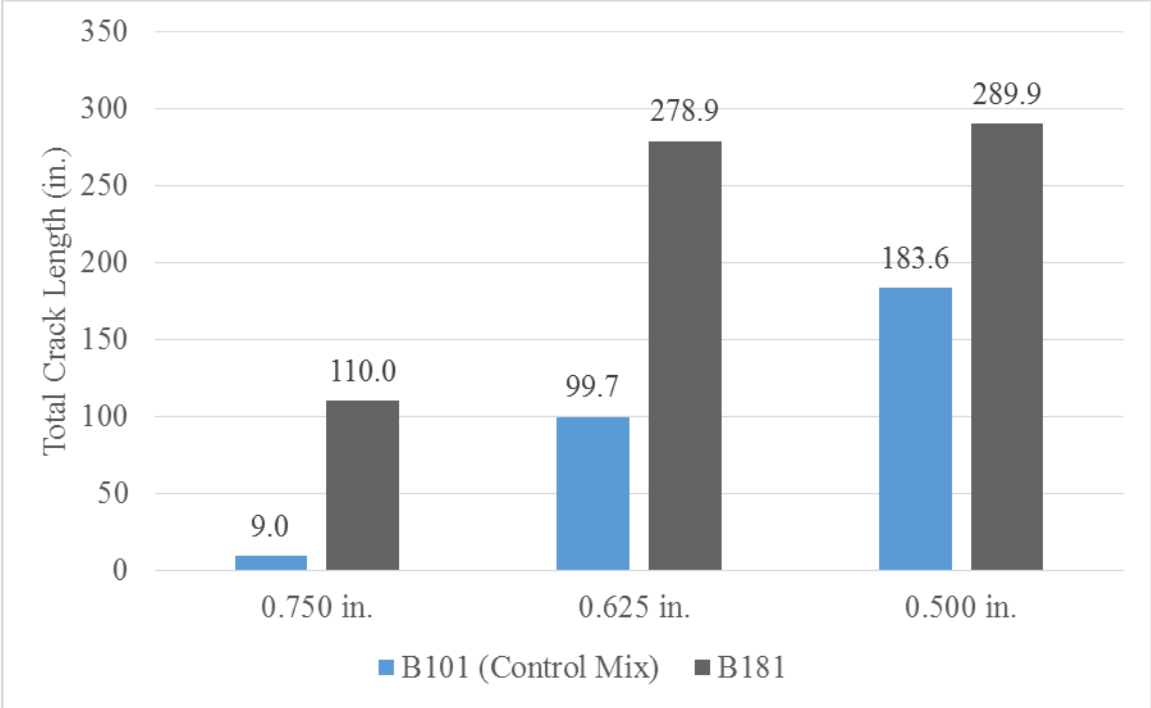

Figure 78. Crack length measurements for prisms with different type of wire

3.7.2 Effect of Partial Fiber Reinforcement

Application of polymer fiber reinforcement may not be an interest of manufacturers due to the initial fabrication cost. It is hypothesized that, since splitting-cracks initiate at the end of prisms, crack resistance should be focused in the area where cracks tend to form and grow. It was further hypothesized that partial reinforcement of concrete may lead to the same performance as polymer fiber added to the entire prism. Needless to say, the material costs decline significantly in this case. In a special prism test series, end 6-inches of prisms was reinforced with 5% polymer fiber while plain concrete (without fiber) was used for the rest of prisms. In such, wood dividers were made and placed before casting (Figure 79). First, fiber reinforced concrete was placed in the end sections and then, plain concrete was placed for the middle section of prisms. Finally, dividers were taken off and surface was finished. Prestressed prisms were manufactured with natural round aggregate (CA5) and were de-tensioned when the strength of cylinders made of plain concrete mixture reached 4500 psi.

The result of splitting-cracks on these prisms are shown in Figure 80 and Figure 81. As seen, partial fiber reinforcement, performed like fully reinforced concrete prisms indicating the importance of end sections of prestressed prisms in splitting-crack performance. The likelihood of splitting for both sets of prisms (B221 and B191) are the same. Also, crack length measurements do not show superiority of B221 rather than B191 (Figure 81). It also is apparent, that when cracks grow to more than 4 in. in a partial reinforced prism, the cracks are most likely to propagate through the plain concrete.

a) Framwork ready for concrete

b) Concrete with fiber placed

c) All concrete placed

d) Consolidated together

Figure 79. Partial fiber reinforcement

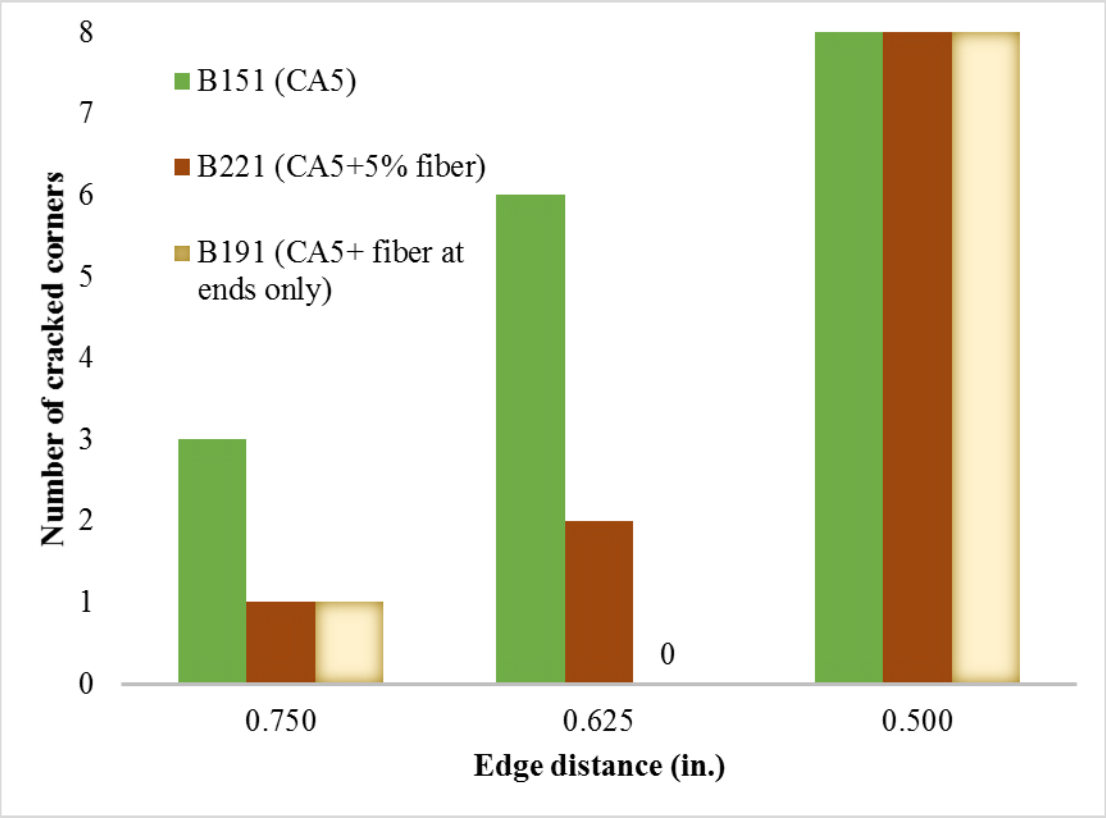

Figure 80. Number of cracked corners for prisms made with 0%, 5% polymer fiber and partial polymer fiber when edge distance is 0.750 in.

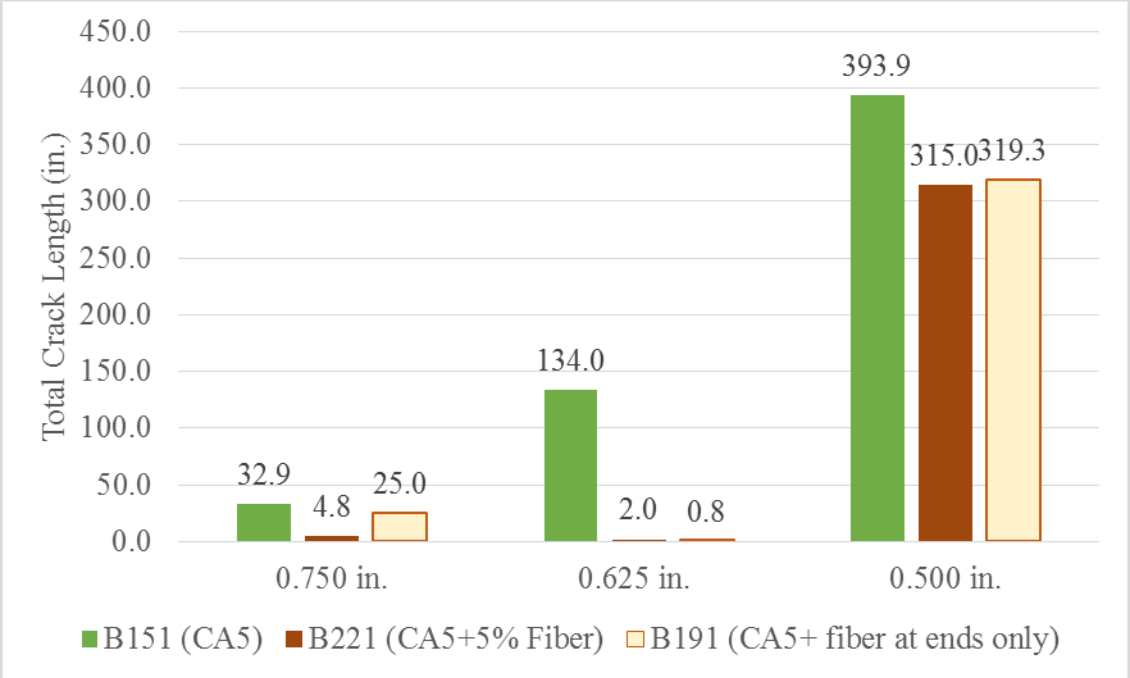

Figure 81. Crack length measurements for prisms with 0%, 5% polymer fiber and partial polymer fiber

3.7.3 Effect of Stirrups

Another way to arrest crack growth that is utilized by some tie producers in concrete to use transvers stirrups to reinforce the concrete. In this study, a set of prisms were made using end stirrups to evaluate the effect of this reinforcement on splitting-crack propagation (Figure 83). The stirrups were made from steel wire that had a diameter of 5 mm. They were formed at the KSU lab prior to the fabrication of the prims.

As discussed earlier, spitting cracks initiate and grow from the end part of prestressed prisms. Hence, ASTM A1064 W4 (diameter = 5 mm) wires were placed around prestressed wires at 2 in. from the end of prisms. For each prism, one stirrup for each end was employed. The concrete mixture was chosen to include poor-quality (well-round) coarse aggregate (CA5). B151 was used to cast the prisms and the results of splitting-cracks of prisms with and without stirrups were compared.

Figure 84 and Figure 85 show that stirrup can significantly reduce crack propagation. Application of stirrup is seen to be beneficial for low covers. The number of splitting-cracks was decreased by more than 50% in 0.625in.-edge distance prisms. Cracks measurements also confirmed the arresting effect of stirrups in prestressed prisms. Although stirrup performance are seen to be advantageous, they were not nearly as effective in prism with low edge distance of 0.500 in. Despite of arrested splitting-cracks in prims with 0.750 in. and 0.625 in. edge distance, existence of splitting-cracks maybe attributed to very small edge-distance over stirrups.

Figure 82. Stirrups with 5 bends made at KSU lab

Figure 83. Stirrups preparation and set up

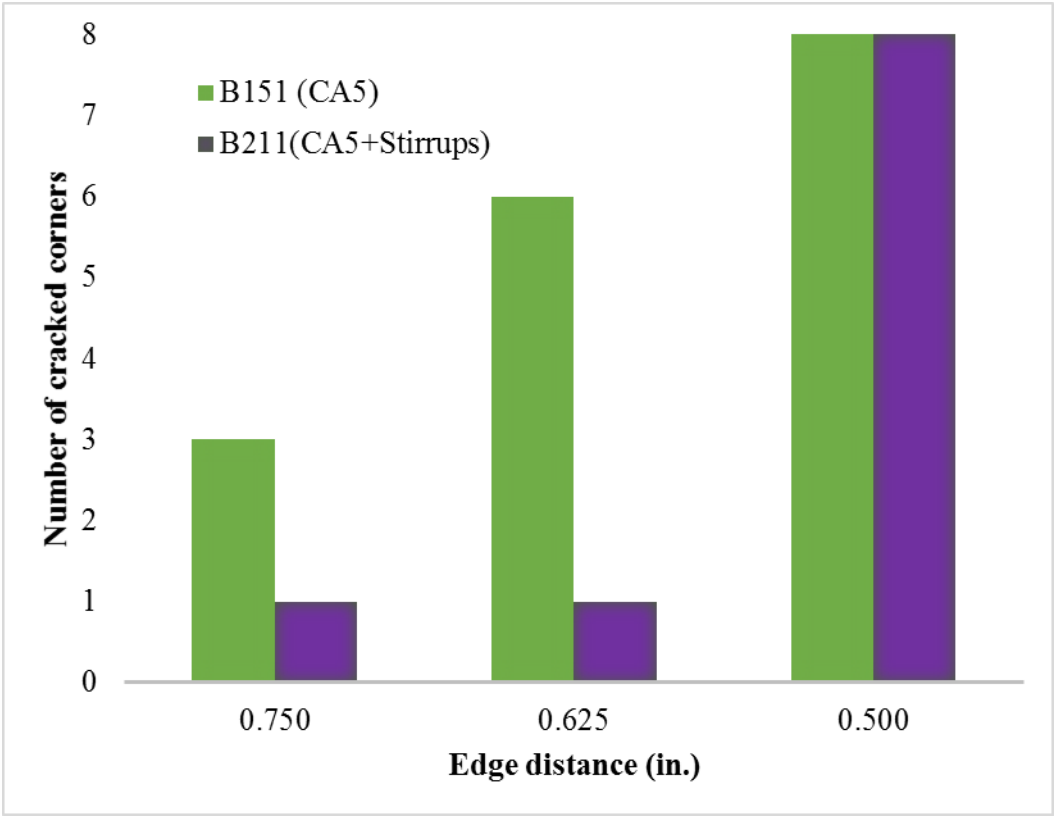

Figure 84. Number of cracked corners for prisms made with and without stirrups

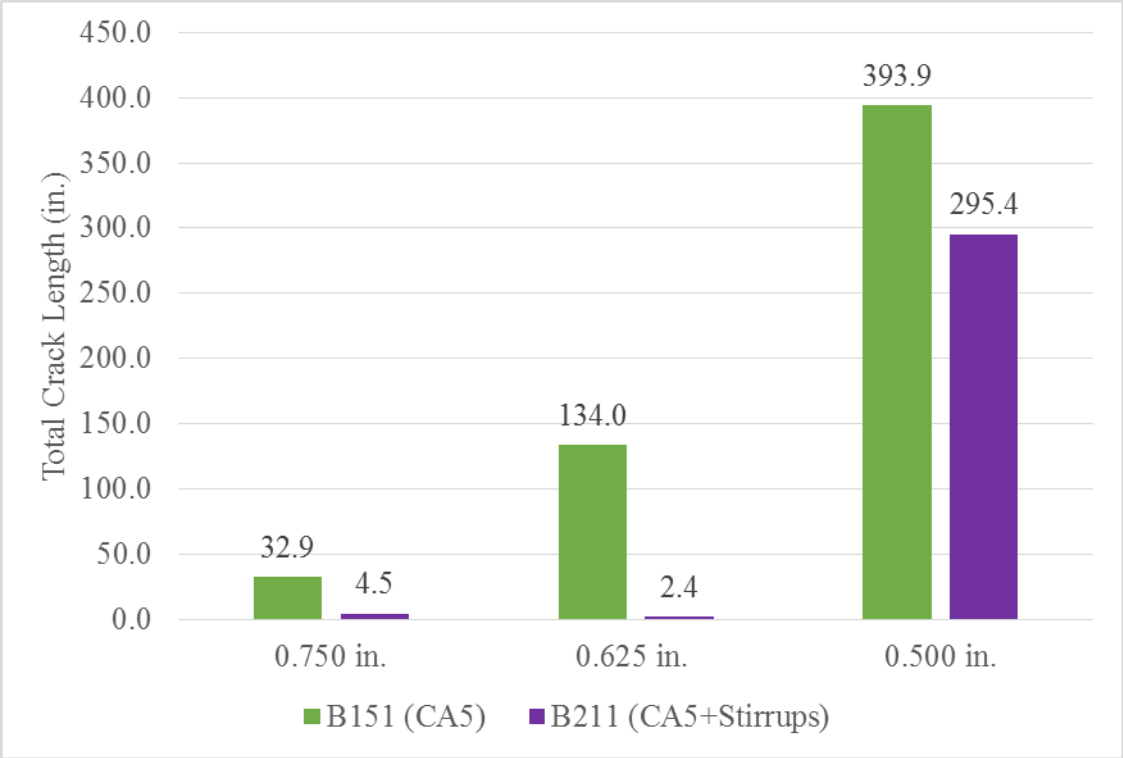

Figure 85. Crack length measurements for prisms with and without stirrups

3.8 Promising Concrete Design

After quantitative and qualitative evaluation of different concrete mixtures, it was observed that some factors seem to be remarkably effective in preventing splitting-crack propagation in prestressed prisms [121]. These effective factors, as discussed earlier, include angularity, volume of coarse aggregate, and water/cementitious ratio. Therefore, hypothetically, prisms including these elements are expected to perform the best in terms of splitting-cracks. Thus, the most promising mixture was designed based on observations and results were compared with current concrete ties mixtures. Prisms B201 containing 99% crushed coarse aggregate (CA4) with 1.5 ratio of coarse/fine aggregate and 0.32 ratio of w/cm were fabricated and tested. Table 10 shows mix design for proposed "super mix".

Table 10. "Super Mix" Design Information

Mixture	Aggregate (Kg per m3)		Type III Cement (Kg per m^3)	W/CM	Admixture (fl oz per m^3)
	CA4	FA			
B201 Super Mix	1088	725	488.2	0.32	73

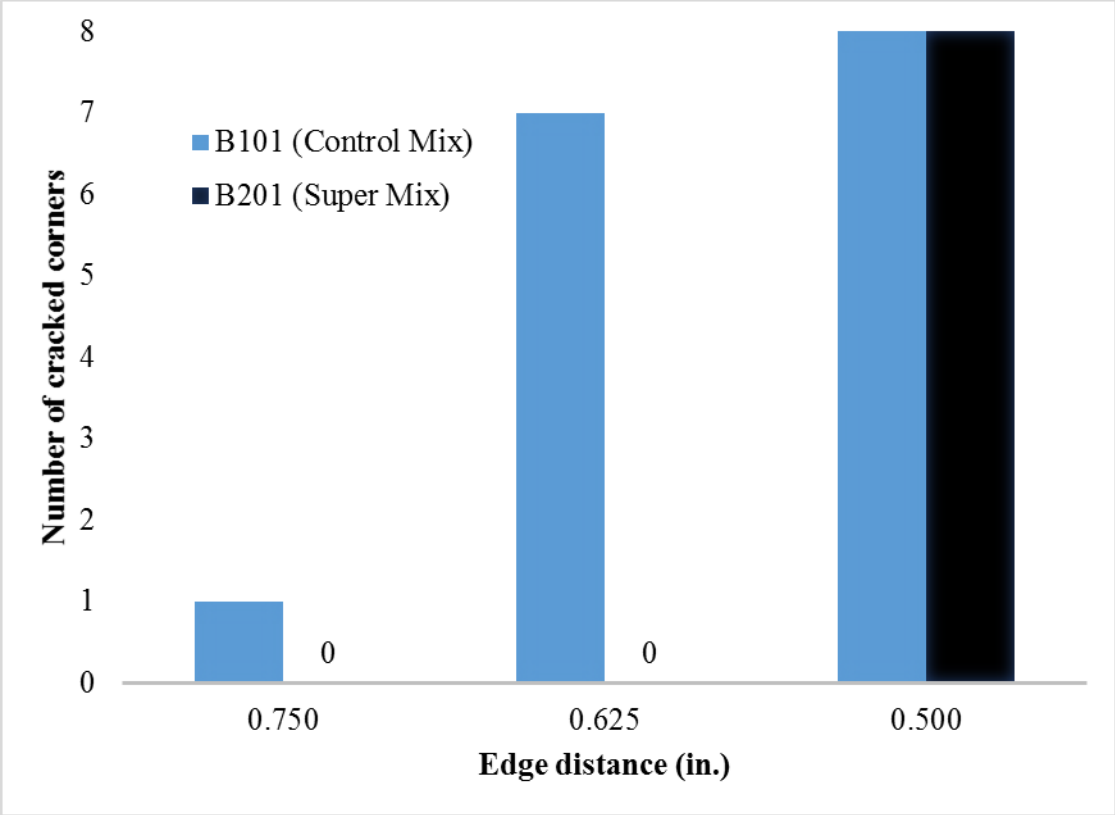

Figure 86. Number of cracked corners for prisms made with promising and usual mix

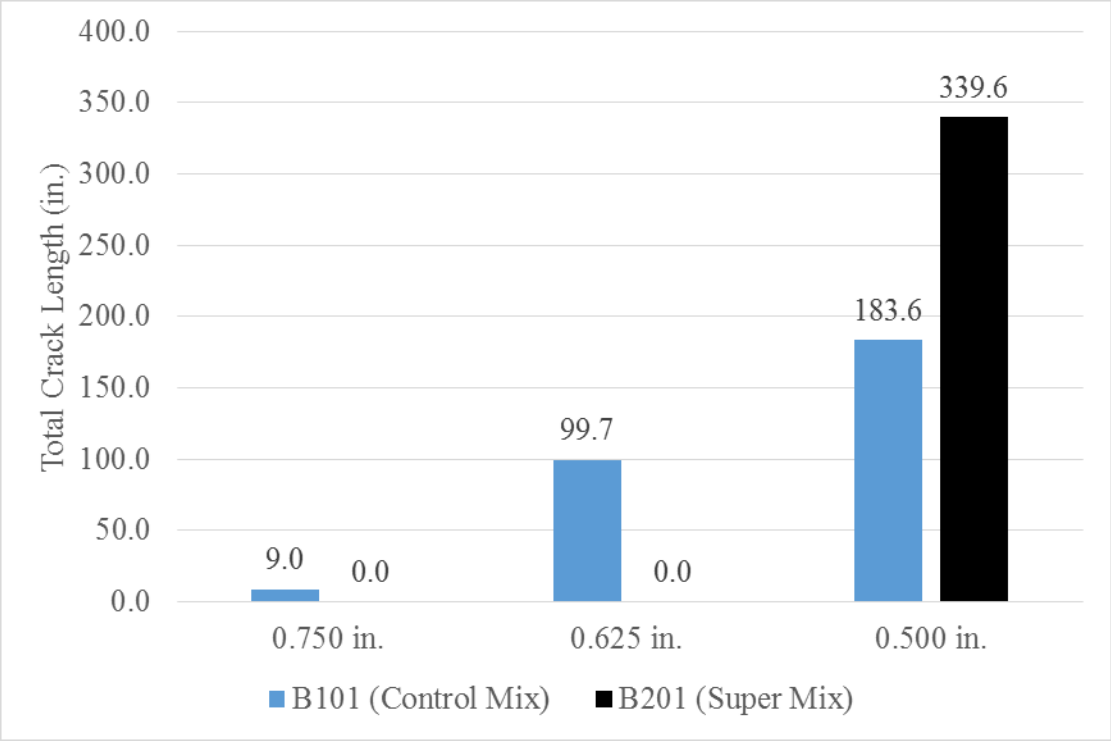

Figure 87. Crack length measurements for prisms with promising and usual mix

The results of prestressed prisms display a significant improvement in terms of splitting-crack propagation where no splitting-crack formed in 0.625 and 0.750in.-edge distance prisms. However, at 0.500 in edge-distance full splitting along all wires occurred and crack lengths for B201 mix were actually longer than for B101 mix.

3.9 Summary and Conclusions

Eleven sets of prisms consisting of three prisms with different edge distances to prestressed wires were tested to evaluate splitting-crack behavior in each mixture. The wire type (except for B181), and pre-stress forcing were kept consistent in all prisms. Figure 88. shows a comparison of the possible solutions investigated in this study to reduce splitting-crack length of mixtures containing round coarse aggregate (B151).

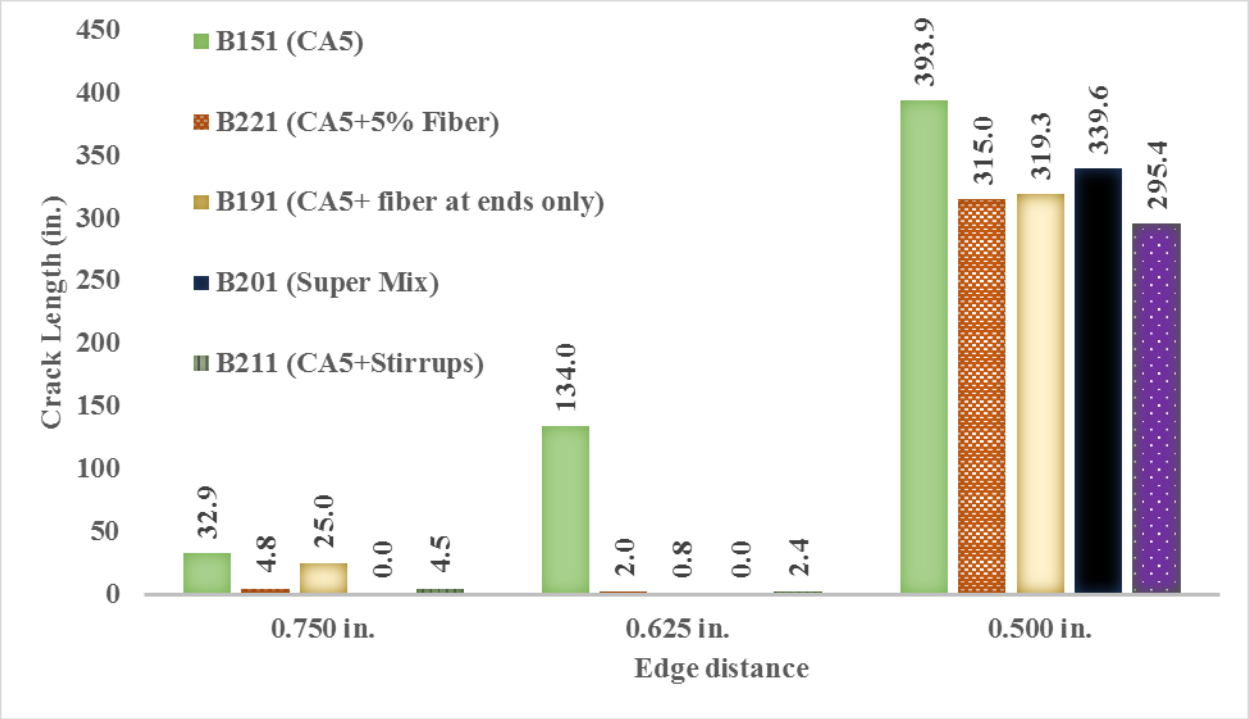

Figure 88. Comparison of total crack length of prisms with round aggregate, a super mix, and reinforcement at different edge distances

Following conclusions can be drawn from obtained results:

- Edge distance is the most important factor affecting splitting cracks in pretensioned concrete prisms, as perveiously noted by Savic et al. (Savic et al. 2018).
- The effective concrete factors on splitting-crack behavior include Angularity, Volume of coarse aggregate and water-to-cementitious ratio.
- Fly ash has a negative effect on splitting-crack formation and growth which might be due to higher water-to-cementitious ratio in concrete

- Reinforcement by 5% polymer fiber and stirrups significantly improved splitting-crack propagation of mixtures containing low quality aggregate.
- Partially reinforced prisms with 5% polymer fiber performed as well as fully reinforced prisms with polymer fiber. This novel method decreases significantly the likeliness of splitting-cracks while reducing the cost of fiber reinforcement.
- Wire type predominantly controls the likeliness of cracking despite of reinforcing concrete mixture.
- Promising mixture containing effective parameters performed very well in terms of spitting cracks even in 0.625in.-edge distance prisms.

4. Statistical Model for Crack Prediction

4.1 Prediction of Fracture Toughness

Estimation of fracture parameters requires time and effort along with high testing expenses. Numerical and statistical models have been employed to predict the fracture parameters without running actual fracture tests. The outcome is influenced by the number of samples and concrete parameters. Due to the high variation in fracture behavior of concrete material, questions typically arise about the accuracy and reliability of these models. Moreover, selecting the most effective factors such as coarse aggregate type and distribution and water-to- cementitious ratio have a great impact on fracture toughness test results. Considering the results from fracture toughness tests in this study, a few factors appeared to be the most effective on fracture toughness. Furthermore, the effect of concrete parameters such as aggregate and proportioning is notable in low strength in the range of 4000 to 5000 psi.

As stated in literature, concrete strength is directly related to fracture toughness and fracture energy [58, 123]. The result of this research also showed that as the strength increases, the fracture values increase (refer to Figure 89)

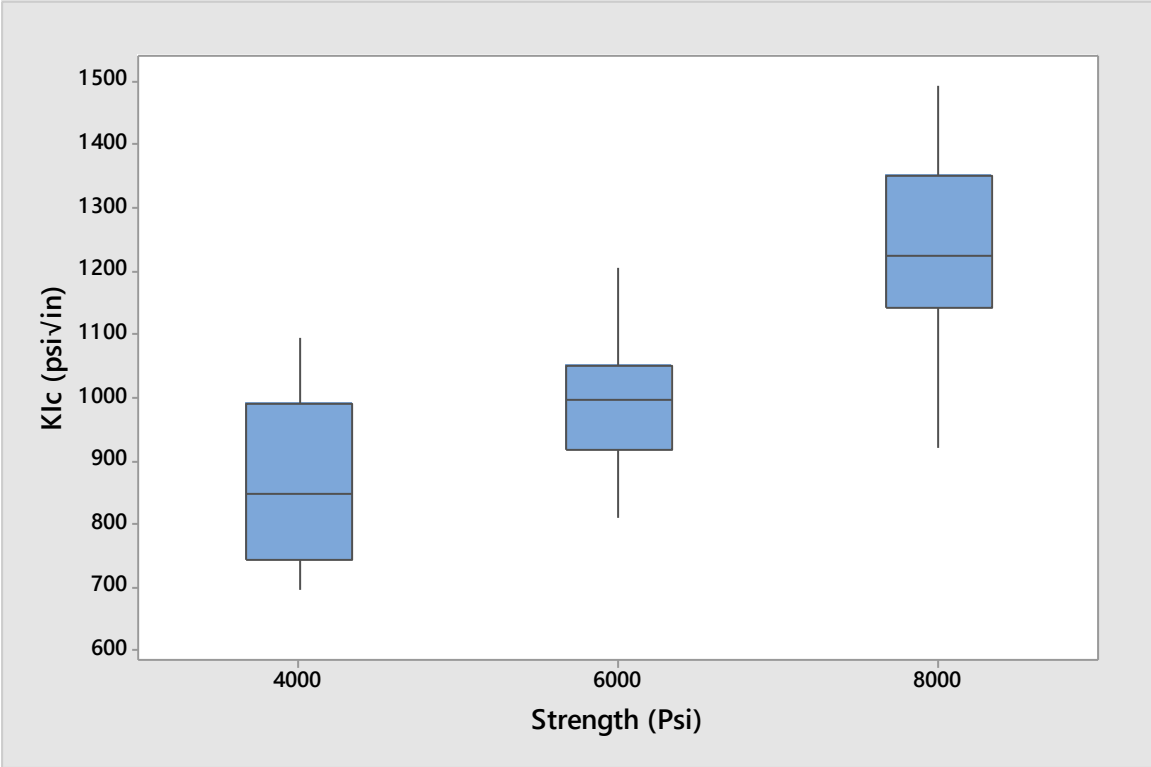

Figure 89. Distribution of fracture toughness test results at three different strengths

A linear regression model was developed incorporating the concrete strength and the other factors that were found to affect the fracture parameters in concrete. As discussed in Chapter 3, coarse aggregate volume, angularity and water-to-cementitious ratio were determined to be the most effective parameters and these were incorporated into linear regression model. The best fit model obtained had a coefficient of determination, R^2, 0.71. In this model, 70 data points from fracture toughness test results for 8 different mixes at three strengths (4000, 6000 and 8000 psi) were used. The resulting best-fit equation is shown below.

$$FT = 0.092f_c + 120CF - 1023.2WC + 648Ang - 294.3D_{ave} + 1342.8 \quad (50)$$

Where:

FT= fracture toughness (Psi√in)

f_c= compressive strength of concrete (Psi)

CF= ratio of coarse/fine aggregate

WC= water-to-cementitious ratio

Ang= fraction of crushed aggregate

D_{ave} = average of coarse aggregate dimeter (in.)

When the average of fracture toughness test results in section 3.3, were plotted versus predicted fracture toughness values from equation (51) for each mix at given strengths, a strong correlation (R-squared = 0.90) was observed (Figure 91.). Twenty one (21) facture toughness values (7 mixtures x 3 strengths) were used in this correlation in which the actual fracture toughness values are the average of three to four replicates for each mix at certain strength. The data used for model development in equations (50) and (52) are tabulated in Table 11.

Table 11. Data used for model development

#	MIX	Ang.	WC	CF	D_{ave} (in)	Strength (Psi)	Sample 1 (Psi√in)	Sample 2 (Psi√in)	Sample 3 (Psi√in)	Sample 4 (Psi√in)	Avg. Actual (Psi√in)	Predicted Equ. 50	Predicted Equ. 51
1	Mix#1	0.23	0.38	1	2.65	4000	708	694	843		748	811	851
2	Mix#1	0.23	0.38	1	2.65	6000	1050	1052	906		1002	995	1035
3	Mix#1	0.23	0.38	1	2.65	8000	1143	1350	1242		1247	1179	1219
4	Mix#2	0.47	0.38	1	3.07	4000	1042	804	743		863	843	864
5	Mix#2	0.47	0.38	1	3.07	6000	1014	1088	995	976	1018	1027	1048
6	Mix#2	0.47	0.38	1	3.07	8000	1173	1493	1331		1333	1211	1232
7	Mix#3	0.99	0.38	1	3.89	4000	1034	1017	804	906	940	939	934
8	Mix#3	0.99	0.38	1	3.89	6000	1013	983	990		998	1123	1118
9	Mix#3	0.99	0.38	1	3.89	8000	1284	1468	1355	1287	1348	1307	1301
10	Mix#4	0.1	0.38	1	2.75	4000	733	807	714		751	697	697
11	Mix#4	0.1	0.38	1	2.75	6000	809	834	820		822	881	881
12	Mix#4	0.1	0.38	1	2.75	8000	921	1070	1148		1046	1065	1065
13	Mix#6	0.23	0.28	1	2.65	4000	847	989	1094		977	913	851
14	Mix#6	0.23	0.28	1	2.65	6000	948	1207	990		1048	1097	1035
15	Mix#6	0.23	0.28	1	2.65	8000	1364	1165	1261		1264	1281	1219
16	Mix#7	0.23	0.28	1.5	2.65	4000	994	722	912	871	875	871	851
17	Mix#7	0.23	0.28	1.5	2.65	6000	1115	1205	905	1006	1058	1055	1035
18	Mix#7	0.23	0.28	1.5	2.65	8000	1333	1145	1062	1456	1237	1239	1219
19	Mix#8	0.23	0.38	1	2.65	4000	879	857	832		856	811	851
20	Mix#8	0.23	0.38	1	2.65	6000	926	867	1012		935	995	1035
21	Mix#8	0.23	0.38	1	2.65	8000	945	1135	1330	1255	1166	1179	1219

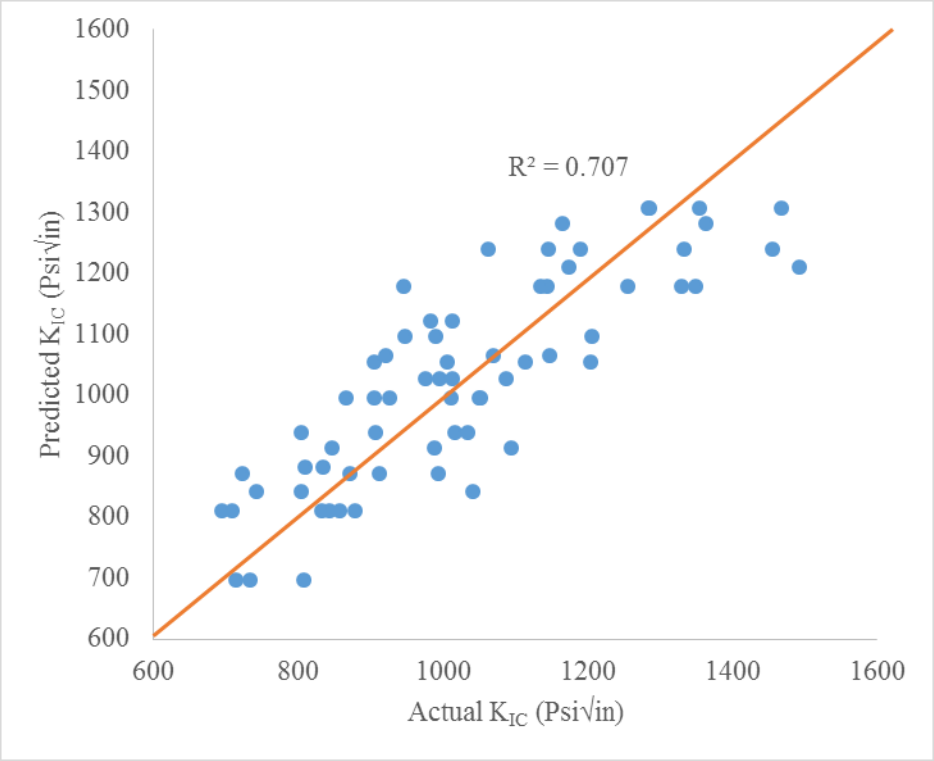

Figure 90. Actual data vs. predicted data from equation (50)

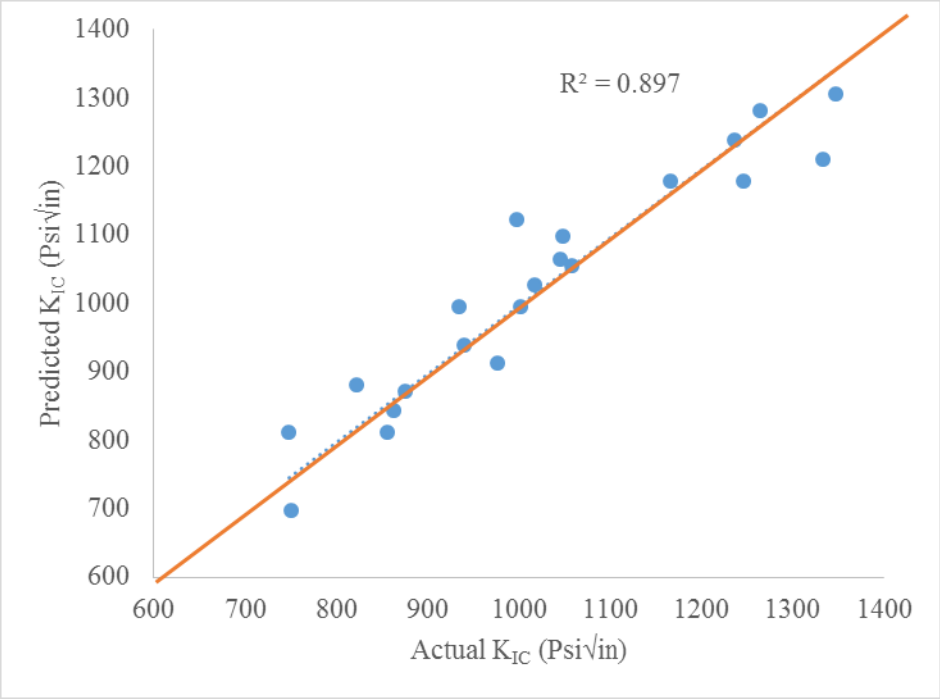

Figure 91. Predicted fracture toughness values versus average of actual test results

It should be noted that the effect of superplasticizer was eliminated in this model. Also, although change in paste content negligibly influenced the fracture toughness results, application of this model to low paste content concrete should be further investigated.

However, to simplify the equation (50), a three parameter model with the R-squared of 0.68 was obtained from the same data set.

$$FT = 0.092f_c + 840Ang - 448D_{ave} + 1477 \quad (51)$$

where FT, Ang, and D_{ave} are the same parameters used in equation 50.

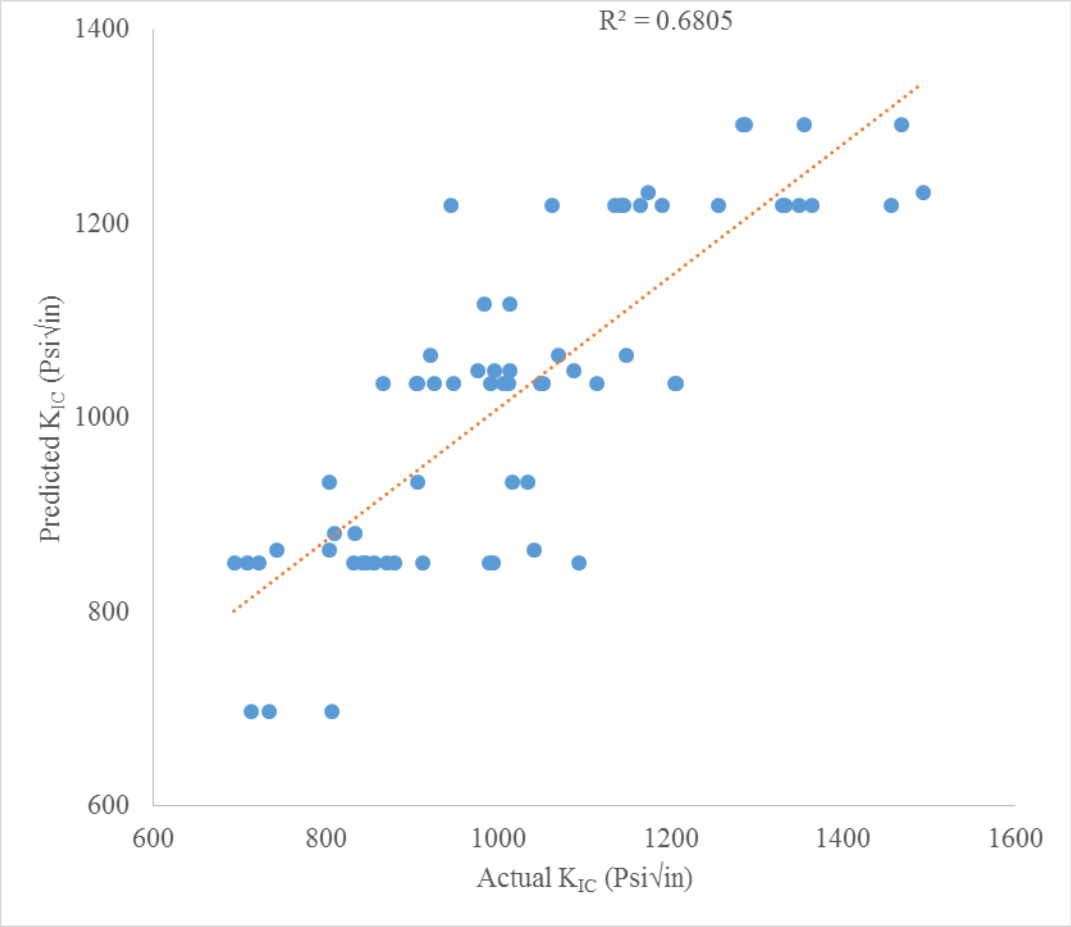

Figure 92. Actual data vs. predicted data in equation (52)

4.2 Prediction of Splitting Cracks

As discussed in the Chapter 4, concrete composition considerably influences splitting-crack formation and growth for wire type WP. This trend is in correlation with concrete edge distance. At very low edge distance range, concrete properties were not as effective on crack growth resistance. This indicates that there is interrelation between edge distance and concrete properties. The best combination of cover and concrete parameters may lead to a reliable and economic solution. As discussed earlier, it was found that fracture toughness is correlated with

concrete proportioning and properties while other parameters calculated from fracture toughness test were not seen to be highly correlated with concrete properties.

To evaluate the tendency of splitting-crack for a given concrete material, fracture toughness of concrete was calculated using equation (50).

In Figure 93. to Figure 96. , the results of prisms made with mixes B101, B114, B121, B131, B141, B151, and B201 are plotted versus facture toughness of the mixes at 0.750" and 0.625" edge distance. From these figures, fracture toughness is highly correlated to crack length and probability of cracking. As shown in Figure 93. to Figure 96. , as edge distance decreases, the variability of results increases, indicating the dominant effect of edge distance in splitting-crack length. One may conclude that the most reliable relationship may be obtained by using results of prisms with larger edge distance. The result of prisms with 0.500" edge distance were ignored due to a high variation in crack measurements.

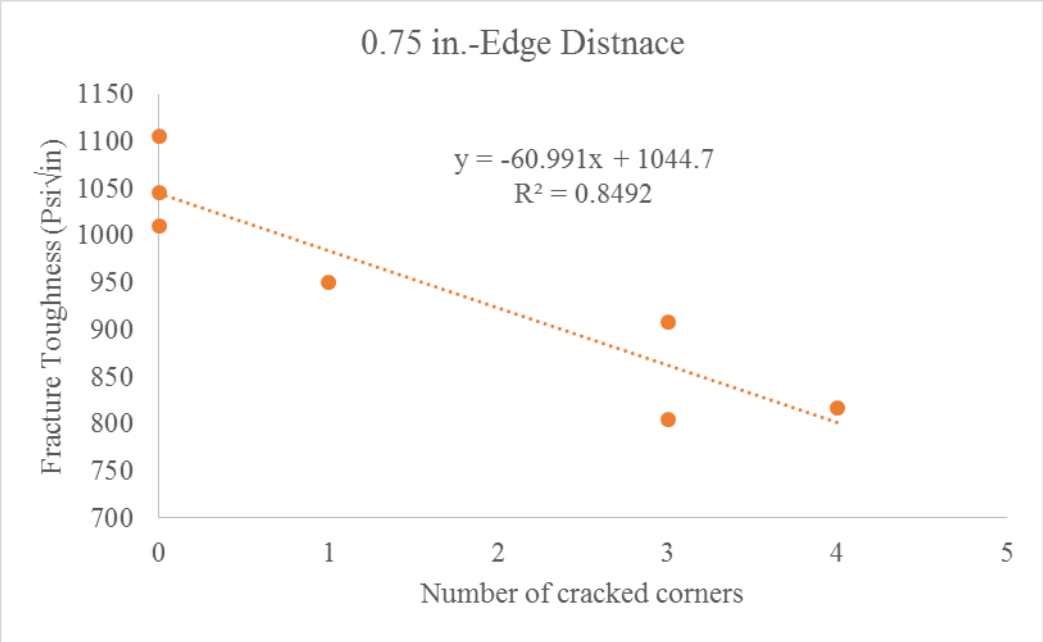

Figure 93. Number of cracked corners of 0.750 in.-edge distance versus fracture toughness of concrete

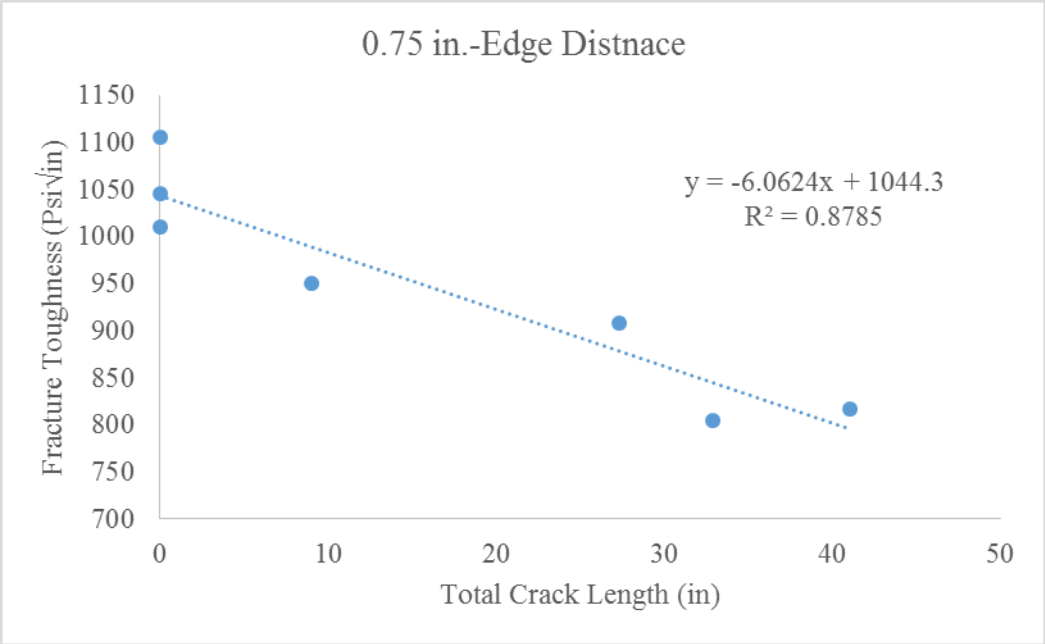

Figure 94. Total crack length of 0.750 in.-edge distance versus fracture toughness of concrete

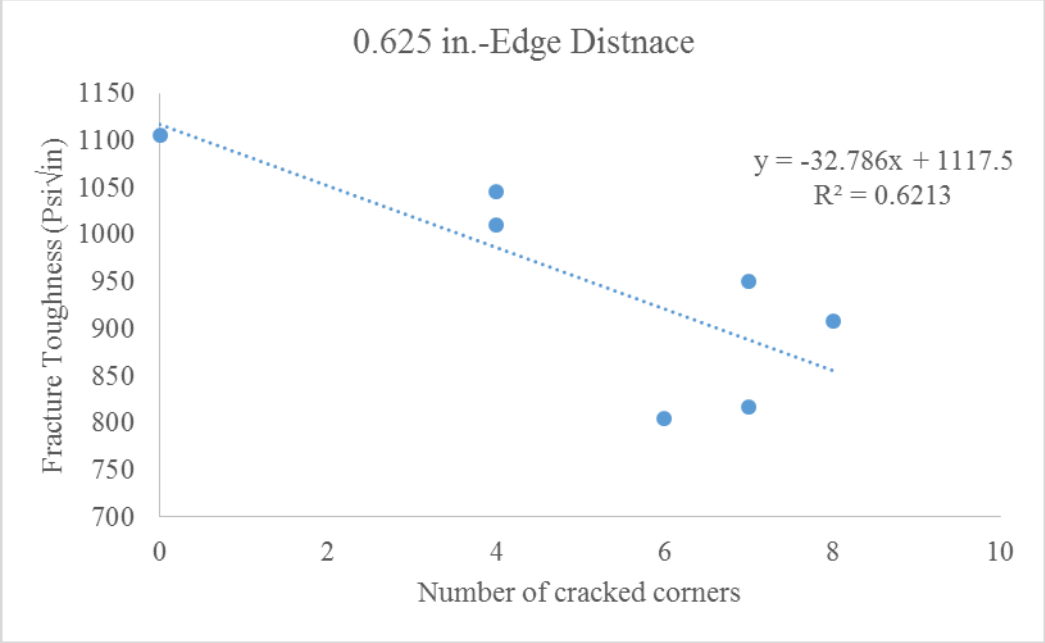

Figure 95. Number of cracked corners of 0.625 in.-edge distance versus fracture toughness of concrete

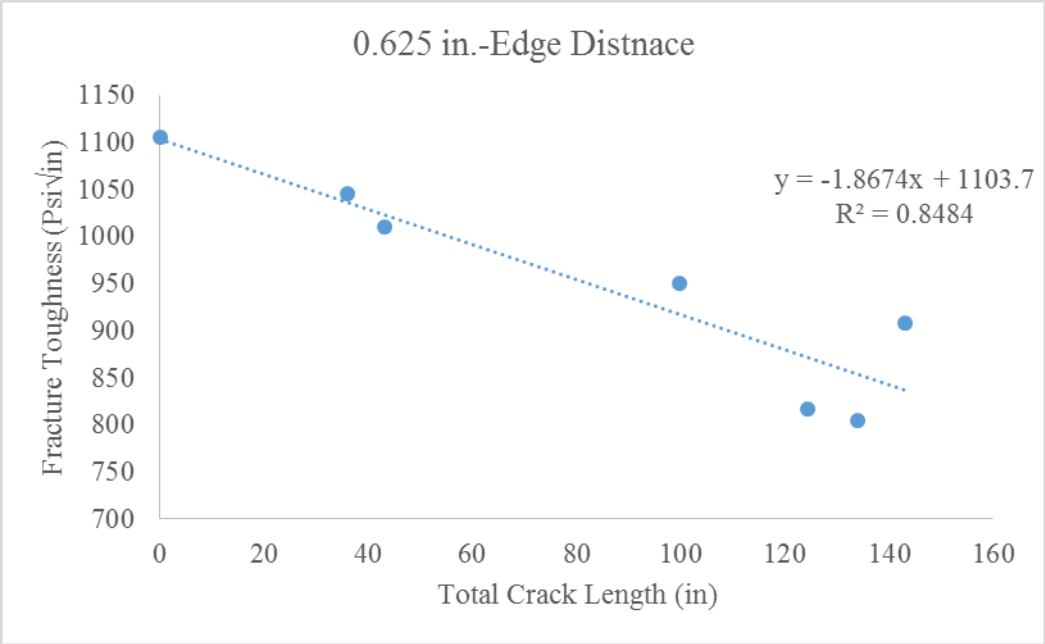

Figure 96. Total crack length of 0.625 in.-edge distance versus fracture toughness of concrete

A regression model predicting the number and length of splitting-cracks, was developed. Two variables including fracture toughness and edge distance were employed to evaluate and predict the splitting-crack behavior. As tabulated in Table 12, 7 sets of prestressed prisms containing 3 prisms (21 in total) were used to train the model.

The equations indicate that splitting-crack length and numbers are in a good agreement with fracture toughness and edge distance.

$$CL = -1213.8Cover - 0.3FT + 1182.8 \quad R^2 = 0.85 \tag{52}$$

$$CN = -24Cover - 0.011FT + 30.8 \quad R^2 = 0.80 \tag{53}$$

Where, *CL*, *CN*, Cover and *FT* are total crack length (in.), number of cracked corners, distance from tendon center to edge (in.), and fracture toughness of concrete material (Psi√in), respectively. In this case, it is assumed when *CL* is equal or less than zero, there is no crack in prestressed prisms.

Table 12. Results from Prestressed prisms

#	Mix	Total Crack length (in.)	Crack number	Edge distance	Strength (Psi)	KIC (Psi√in)
1	B101	9.0	1	0.75	4500	950
2	B101	99.7	7	0.625	4500	950
3	B101	183.6	8	0.5	4500	950
4	B114	27.3	3	0.75	4500	908
5	B114	143.1	8	0.625	4500	908
6	B114	328.9	8	0.5	4500	908
7	B121	0.0	0	0.75	4500	1010
8	B121	43.2	4	0.625	4500	1010
9	B121	305.4	8	0.5	4500	1010
10	B131	41.0	4	0.75	4500	817
11	B131	124.3	7	0.625	4500	817
12	B131	382.1	8	0.5	4500	817
13	B141	7.3	3	0.75	4500	848
14	B141	236.2	8	0.625	4500	848
15	B141	308.2	8	0.5	4500	848
16	B151	32.9	3	0.75	4500	805
17	B151	134.0	6	0.625	4500	805
18	B151	393.9	8	0.5	4500	805
19	B201	0.0	0	0.75	4500	1106
20	B201	0.0	0	0.625	4500	1106
21	B201	339.6	8	0.5	4500	1106

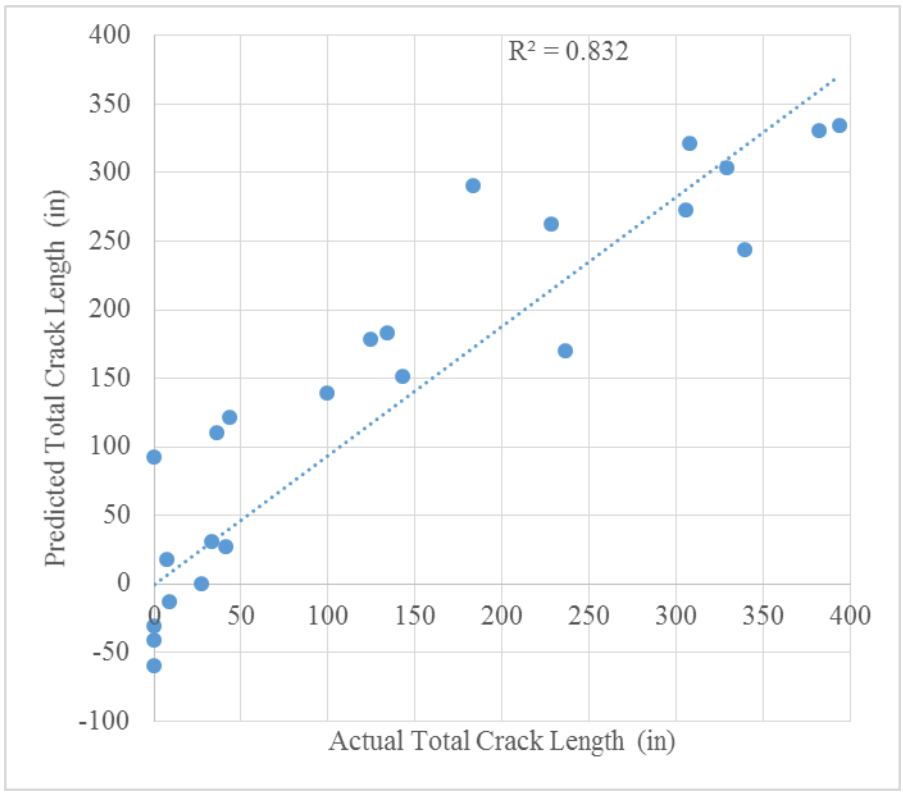

Figure 97. Predicted crack length vs. actual crack length

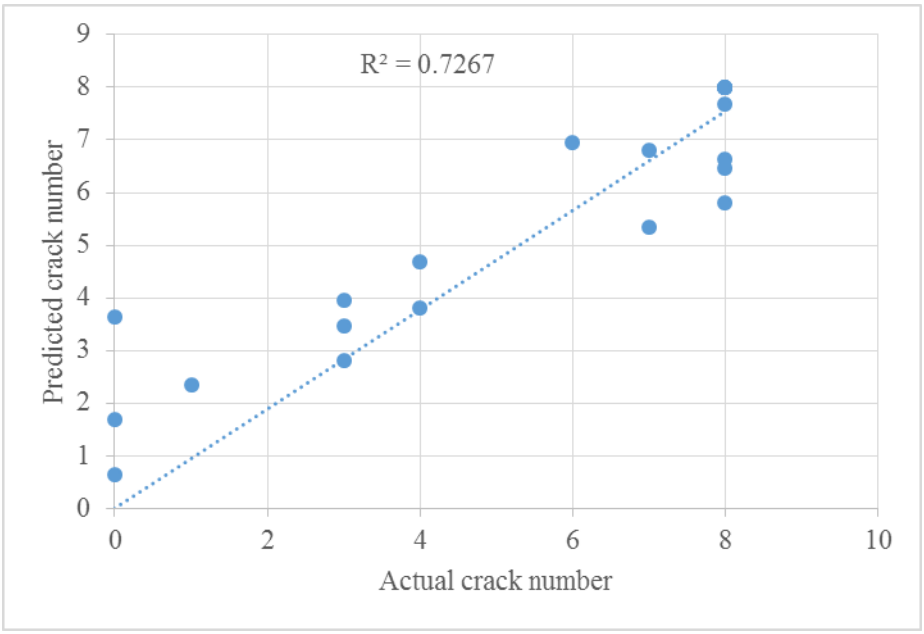

Figure 98. Predicted crack number vs. actual crack number

As shown in Figure 99. , number of cracks and total crack length are highly correlated when data of 0.625 and 0.750 in.-edge distance prisms are plotted. Cover effect is vividly dominant on cracking of prisms. Also, as the edge-distance decreases, the variability of crack length data

significantly increases. Generally speaking, a requirement of having zero cracking in the field is most likely not possible as cracks sometimes are not visible and/or can occur due to some other factors such as environmental condition, creep and shrinkage. While possibility of crack propagation can be estimated by counting small crack length in prisms. For example, one may use correlation between crack length and number of cracks to identify what the allowable crack length could be if the number of splitting-crack is less than 1. According to Figure 99. , for having number of crack less than 1, one may expect total crack length less than 2.1 in.

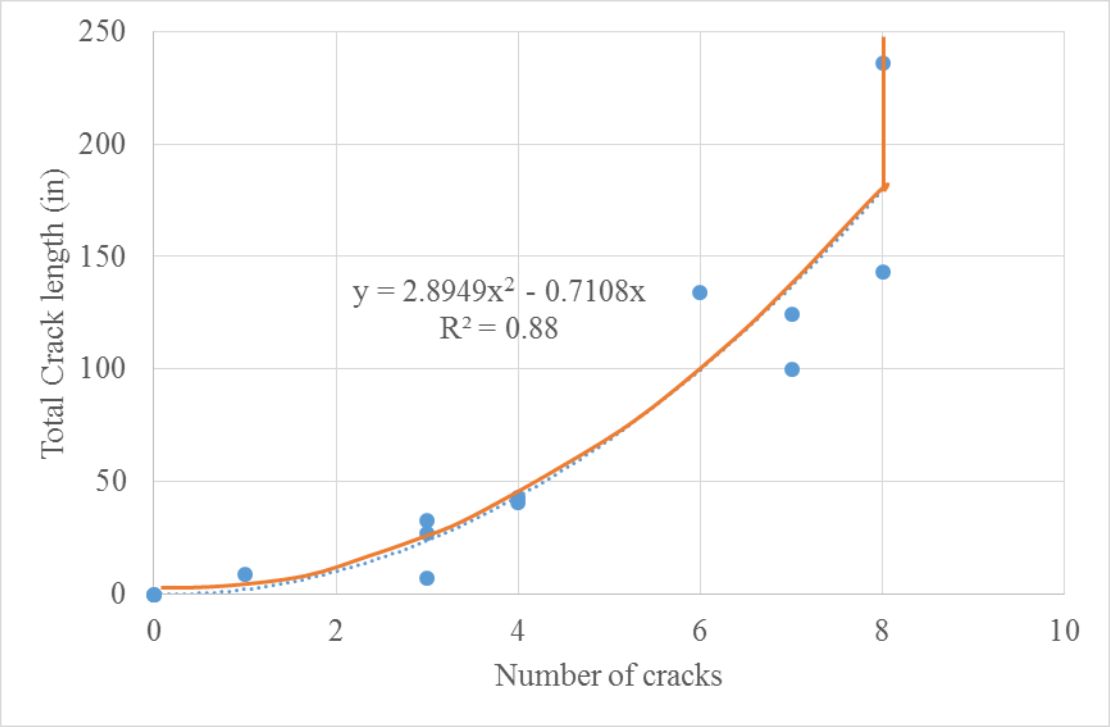

Figure 99. Total crack length versus number of cracks for 0.625 and 0.750 in.-edge distance prisms

Furthermore, for *CN* smaller than 1, probability of spitting crack formation is considered zero. It should be noted that more samples are needed to make a robust predictive model. In addition, in order to develop an extended model for all prestressed prisms, it is suggested that a variable representing the type of wire is incorporated into the model. The final equation indicates a good correlation between splitting-crack characteristics and fracture toughness. Hence, more data and additional effective factors like wire type may result in a robust model containing all effective factors on splitting-cracking in prestressed prisms.

5. Destructive Evaluation of Existing Concrete ties

In order to have a precise evaluation of material characteristics of existing concrete ties, 12 different types of concrete ties, as shown in Figure 100 were taken from track and shipped into civil engineering lab in Kansas State University, then destructive testing was conducted on concrete samples extracted from concrete ties. The destructive evaluation included compressive and tensile strength, air void system, abrasion, absorption, alkali-silica- reaction (ASR), and unit weight. These tests are essentially in compliance with ASTM standards. Cylindrical 2-in. cores were taken by 2-in. diameter drill to obtain compressive and splitting tensile strength and unit weight of concrete. 3-in.X 4-in. slices were also extracted to carry out air void system, abrasion, absorption and ASR tests. For each test, three slices from each type of tie, were cut with at least 12-in.^{2} surface area. All slices from 12 type of ties were marked and categorized for each test as shown in Figure 100.

Figure 100. Sliced samples from 12 different types of ties

5.1 Compressive and Splitting Tensile Strength

According to previous studies, compressive strength and splitting tensile test are correlated in concrete materials [124, 125]. There are many factors affecting splitting tensile and compressive strength. Splitting tensile could be predicted using compressive strength, w/c ratio, and age of concrete [126]. Paste and aggregate properties have great impact on these parameters [127]. One of the efficient ways to find the strength of existing concrete structures is to take some cylindrical cores from concrete elements and determine compressive and splitting tensile strength based on available ASTM standards. Although coring concrete structures may bring some difficulties in practice, it is still one of the most promising method to obtain the strength of concrete. In this study 12 different type of concrete ties were shipped into Kansas State University lab and cored to determine the mechanical properties of concrete in existing concrete ties. As mentioned earlier, these ties have been in track for more than 25 years. For each type of ties, a minimum of 6 cores were taken for compressive and tensile strength testing.

In order to obtain the compressive strength of the concrete of the ties, three 2 in. cores were taken according to ASTM C42. Due to the difficulty of acquiring cores without wires, a 2 in. core was chosen, which is equal to or larger than 4 times the nominal size of aggregate meeting ASTM C42 standard requirements. It has been observed that the compressive strength of nominal 2 in. diameter cores is somewhat lower and more variable than cores with 4 in. diameter

[128]. The average should be used with caution as a large variability of some data is caused by the large variability of the in situ concrete strength within small cores [128]. Also, final cores were tested based on ASTM C39 after cutting and capping the top and bottom of the cores accordance with ASTM C617 (Figure 101). It is very important to provide a very smooth and even pressure at the top and bottom surface of the cores.

Figure 101. Capped cores extracted from the ties

Figure 102.Compressive strength test setup for 2 in. diameter cores

Figure 103. Prepared cores for splitting tensile test

Figure 104. Splitting tensile test setup for 2 in. diameter cores

Splitting tensile test was done on the 2 in. cores extracted from the ties based on ASTM C496 (Figure 103). Three samples from each tie were cored so that no wire is in cores, as having wires throughout the fracture plane affects splitting tensile strength results. In some ties, extracting cores without wire was not possible due to very short spacing between the wires. It should be noted that wires must not cross the fracture plane of the splitting tensile test samples.

Figure 105 and Figure 106 illustrate the results of compressive and splitting tensile strength of the cores. The compressive strength values of 2 in. cores are lower than what was expected. Although obtained results may not be a good indicator of existing ties strength, this is the best attempt to characterize these samples. Also, the results exhibit the superiority of ties F and D in

compressive strength which might be attributed to mix properties of concrete. Also, as expected, the same trend was observed in splitting tensile strength results.

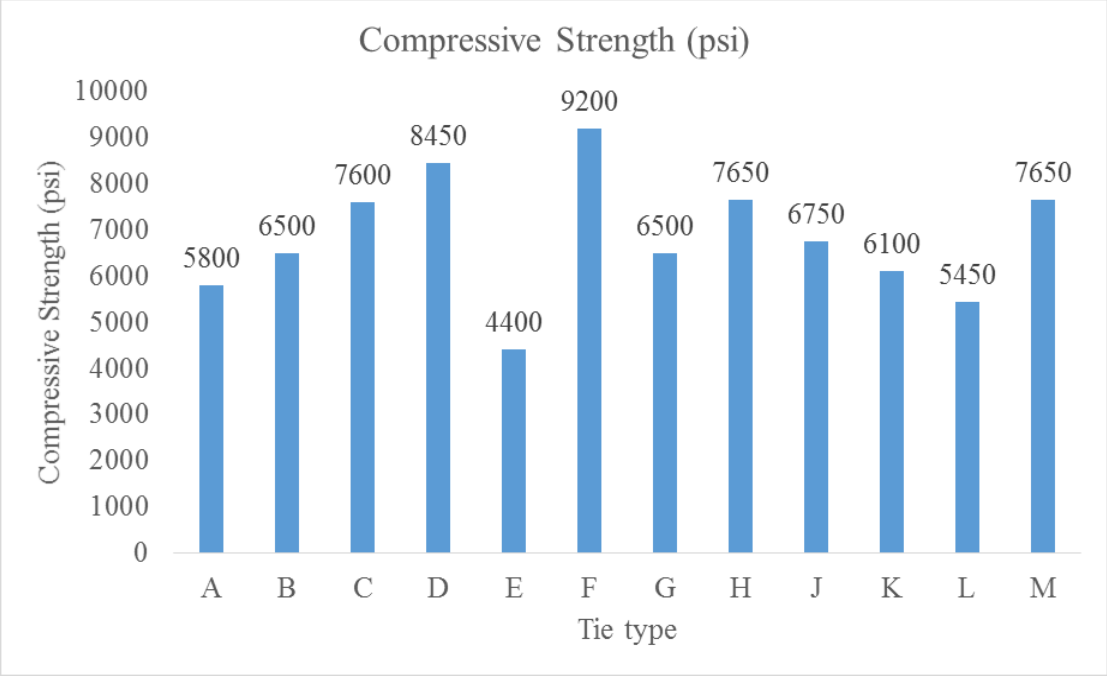

Figure 105. Compressive strength test results

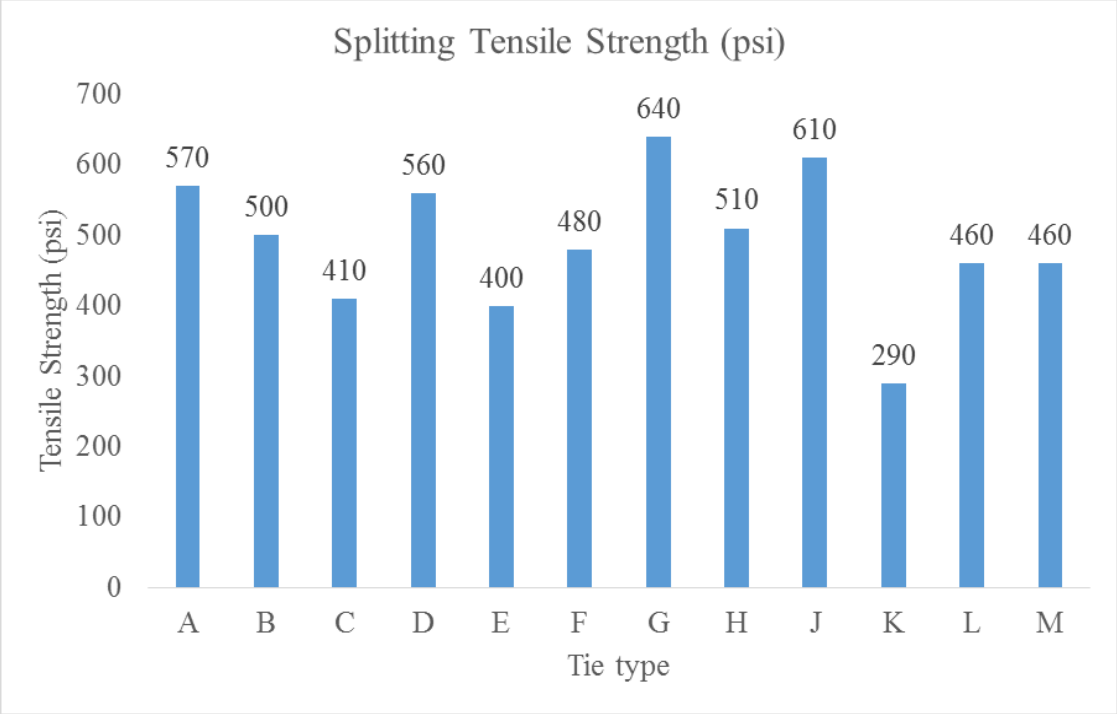

Figure 106. Splitting tensile test results

Table 13 indicates that the ratio of splitting tensile/ compressive strength tends to vary for different samples. Although previous studies have indicated a correlation between f_t/f_c and concrete strength [125, 129], this relation does not seem to be consistent with all cores, which might be due to negative impact of sample size and coring procedure

Table 13. Average of strength results from cores

Tie Type	Compressive strength		Splitting tensile strength		
	Average	St.Dev	Average	St.Dev	f_t/f_c
A	5800	590	570	80	0.10
B	6500	351	500	134	0.08
C	7600	528	410	133	0.05
D	8450	956	560	68	0.07
E	4400	1365	400	100	0.09
F	9200	1251	480	134	0.05
G	6500	467	640	68	0.10
H	7650	1859	510	60	0.07
J	6750	1379	610	133	0.09
K	6100	1043	290	6	0.05
L	5450	149	460	16	0.08
M	7650	1859	460	121	0.06

5.2 Air Void System

It is evident that freeze-thaw damage is one potential cause of concrete railroad tie deterioration in locations with cold climates, especially in the northern region of the U.S. [130]. To prevent freeze-thaw damage, concrete materials should be designed with adequate entrained air voids. Air voids in concrete could also ease crack propagation in pre-stressed concrete railroad ties.

Air void content is affected by many factors that stem from the constituent materials used, mixing condition, or placement. For instance, increasing cement alkali level, cement content, water reducer, and sand content may increase air content in concrete. However, mixture capacity, vibration, and placement influence the air content [131]. Fractures, capillary voids, and aggregate voids are voids and can erroneously be counted as air voids in an analysis, but do not contribute to freeze-thaw durability [132]. Entrained air has been used in concrete for many decades, when addressing freeze-thaw damage became a necessity. The air void system includes the total air content, average spacing factor between air voids, and specific surface, which can be obtained using ASTM C457. The ideal air system for freeze-thaw damage has fine bubbles that are well dispersed, giving a low spacing factor and high specific surface. The average spacing factor is recommended to not exceed 0.008 in. for frost protection [133]. It has been observed that increasing air content negatively impacts the strength of concrete [99-101]. Moreover, inclusion of air voids affects compressive strength more than modulus of elasticity [102].

To obtain air void system of the concrete material of the ties, the ties were cut by a 36 in diameter, 0.5 in thick sawblade so that the final surface was parallel to the wires, as shown in Figure 107

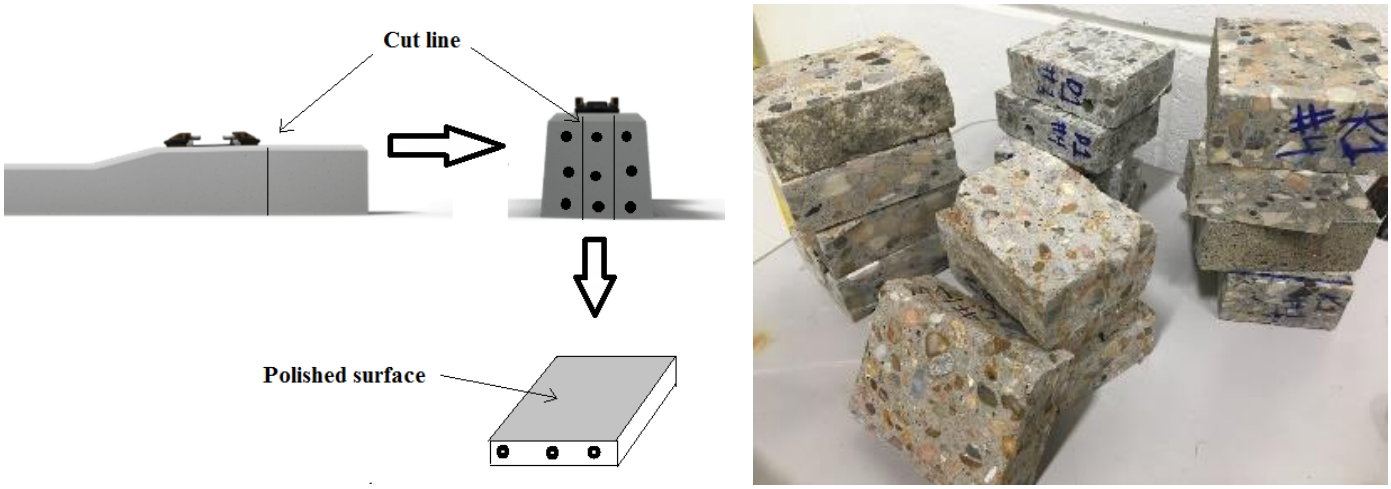

(a) (b)

Figure 107. a) Schematic steps of saw-cutting slices extracted from concrete railroad ties. b) Final slices for polishing procedure

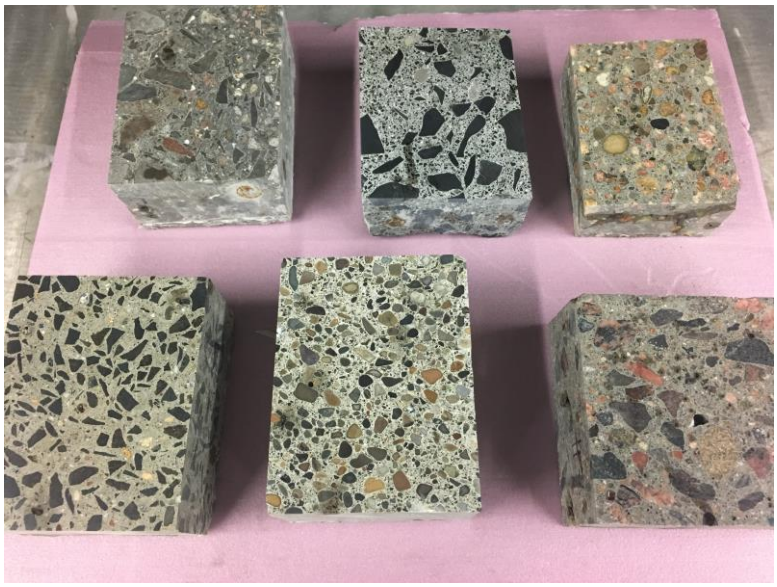

Figure 108. Polished samples from 12 types of ties

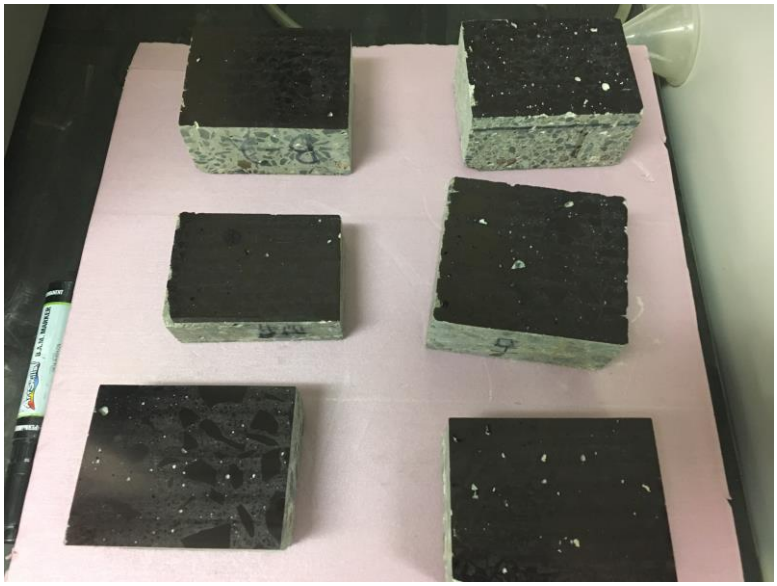

Figure 109. Painted samples for air void system analysis

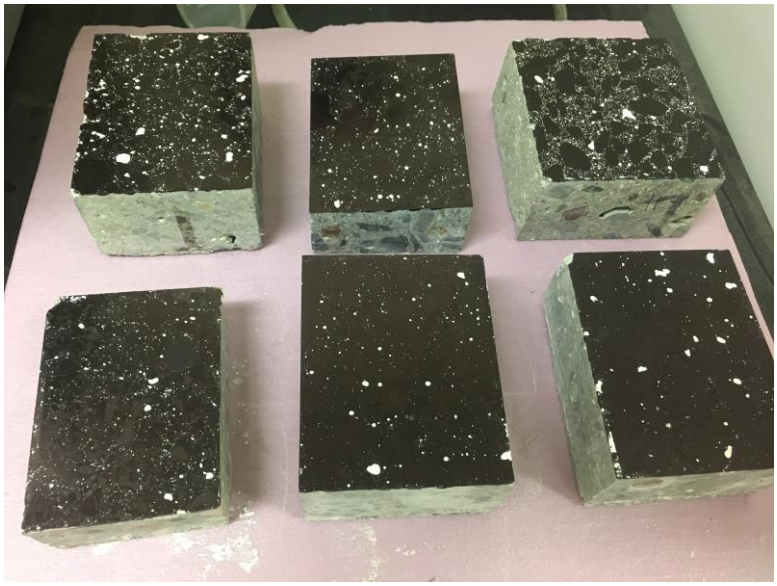

Figure 110. Painted samples filled with Barium Sulfate

As shown in Figure 107, first a cubic section was extracted, then slices were cut parallel to wires direction so that the final slice could be polished for air void system measurement. The final pieces were 3 × 4 in., meeting ASTM C457 requirements (Figure 108). Samples were polished by polishing Machin with #50, #80, #100, #180, #360, #600, #1200, and #1500 abrasive disc to obtain the best polished surface. Samples were later tested and analyzed according to ASTM C457, calculating total air content, average spacing factors, and specific area of the air bubbles. Figure 109 shows polished samples before multiple painting samples with black sharpie and

filling the air voids with Barium Sulfate ($BaSO_4$)(Figure 110). Final samples were scanned and analyzed using KSU lab program.

Air void analysis was done on the samples taken from the ties. As shown in Table 14, air void content sporadically changes between different ties. Ties K and H have the highest air void content which might have been designed for freeze-thaw damage. According to ACI 201.2R and ACI 211.1, for air-entrained concrete designed, air content is usually more than 4 % and the specific surface is in range of 25 to 45 mm^{-1}also the spacing factor should not exceed 0.2 mm. Table 14 summarizes the air void system results for all ties in which ties K and J seem to be designed for freeze-thaw damage meeting air content, spacing factor and specific surface criteria. To calculate the amount of air voids, paste content of concrete samples needs to be determined. Not having adequate information of mix design of existing concrete railroad ties, 30 % paste content was assumed. This value normally varies between 20 to 30 % in concrete. Altering paste content assumption slightly impacts the spacing factor of air bubbles.

Table 14. Results of air void system analysis from 12 different types of ties

Tie type	A	B	C	D	E	F	G	H	J	K	L	M
Air Void Content, %	0.7	1.4	3.5	1.6	2.3	3.7	2.3	6.4	5.9	10.2	4.4	4
Spacing Factor, mm	0.57	0.56	0.25	0.29	0.28	0.18	0.4	0.24	0.17	0.09	0.36	0.39
Specific Surface, 1/mm	21.5	15.6	22.1	26.6	25.1	29.2	17.9	18.5	24.5	26	14.7	13.3
Entrapped Air Void Content, %	0.3	0.6	1	0.5	0.5	0.2	0.7	1.4	0.6	0.9	1.8	1.4
Entrained Air Void Content, %	0.4	0.8	2.5	1.1	1.8	3.5	1.6	5	5.4	9.3	2.6	2.6
Air Voids Smaller than 50 microns, % by area	4.6	2.1	2	4.1	3.8	2.9	1.9	0.9	0.9	1.8	1.2	0.7
Air Voids Smaller than 10 microns, % by area	0.04	0.02	0.01	0.01	0.04	0.02	0.01	0.01	0	0.01	0.01	0

5.3 Absorption

One of the factors that indicates durability of concrete material is water absorption in which cementitious system takes in water through capillary suction. To measure absorption, specimen is dried to a constant mass and then immersed in water. The increase in mass is measured and calculated as a percentage of dry mass. There are different methods measuring water absorption among which ASTM C1585 is widely used to determine the rate of absorption of water in unsaturated hydraulic cement concrete. Water absorption of concrete can significantly influence freeze-thaw durability for cementitious structures in the field. [134] demonstrated that when the initial absorption is greater than 0.5 ml/m^2 per second within first 10 minutes, it is considered as high absorption while smaller than 0.25 ml/m^2 per second is considered low absorption. The amount of water absorbed by concrete during the test is dependent on existing moisture already

in concrete samples. Hence, it is important to ensure all samples are preconditioned in a same way and have the same amount of moisture before testing. Samples should be conditioned for 18 days before testing. Finally, the absorbed water volumes at different time intervals are plotted versus the square root of time.

In this report, ASTM C1585 entitled as “Measurement of Rate of Absorption of Water by Hydraulic Concrete” was followed to measure water absorption of extracted samples from concrete ties. The purpose of this test is to obtain the sorptivity of water in two low permeability recipes and normal air mixture. 3-in. x 4-in. x 2-in. slices from ties were cut as explained in section 5.2 and pre-conditioned to deliver all samples to the same level of humidity. First, slices were placed in an environmental chamber at 80±3% RH and 50°C oven for three days. The RH is controlled in the desiccator with a saturated solution of potassium chloride. The solubility of potassium chloride is 70 g/100 ml of water. Next, specimens were placed in sealed container, and container is not larger than five times the specimens’ volume. Then containers were placed in 23°C environment for another 15 days, which allows all specimen to reach equilibrium RH through its thickness. After reaching steady internal RH after 15 days, specimen dimensions were measured in multiple directions. Specimen side was sealed by duct tape, and a plastic sheet covered/sealed on top surface. The weight of specimens was recorded before and after sealing the surface. A pan containing water and support for specimens were placed in shrinkage room which has a constant temperature of 23°C with constant humidity. The water level was 0.118 inch (3 mm) above support device.

Figure 111. Pre-conditioned samples for absorption test

Figure 112. Covered samples placed on water surface

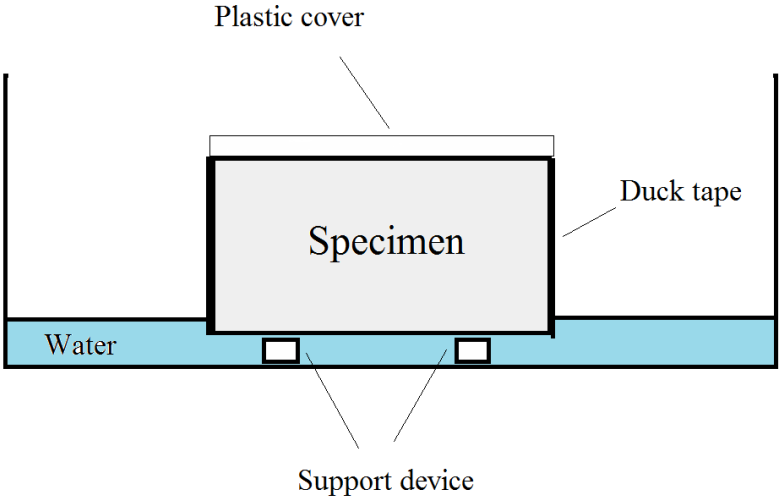

Figure 113. Schematic figure of absorption samples in water

The experiment was conducted in 23°C room where two stage of measurements were taken: initial absorption and secondary absorption. In initial absorption, the weight of specimens was measured at 0, 1, 5, 10, 20, 30, 60 minutes followed by 2, 3, 4, 5, and 6 hours. The secondary stage includes measurement in 1, 2, 3, 5, 7, and 9 or 11 days. Before putting samples on scale with a precision of ±0.01 gr, the samples were damped to remove extra water. Caution should be taken within measurement phase according to ASTM C1585.

To calculate absorption rate (I), mass change is divided by exposed area and water density by following equation:

$I = m_t/ad$

Where, I is absorption (mm), m_t is mass change at time t (gr), a is area of exposed surface (mm^2), d is water density (gr/mm^3).

Figure 114 shows water absorption rate for different type of tie in which tie L and B have the highest sorptivity indicating high capacity to absorb water. Figure 115- Figure 126 show the initial and secondary absorption of 3 specimens for each tie.

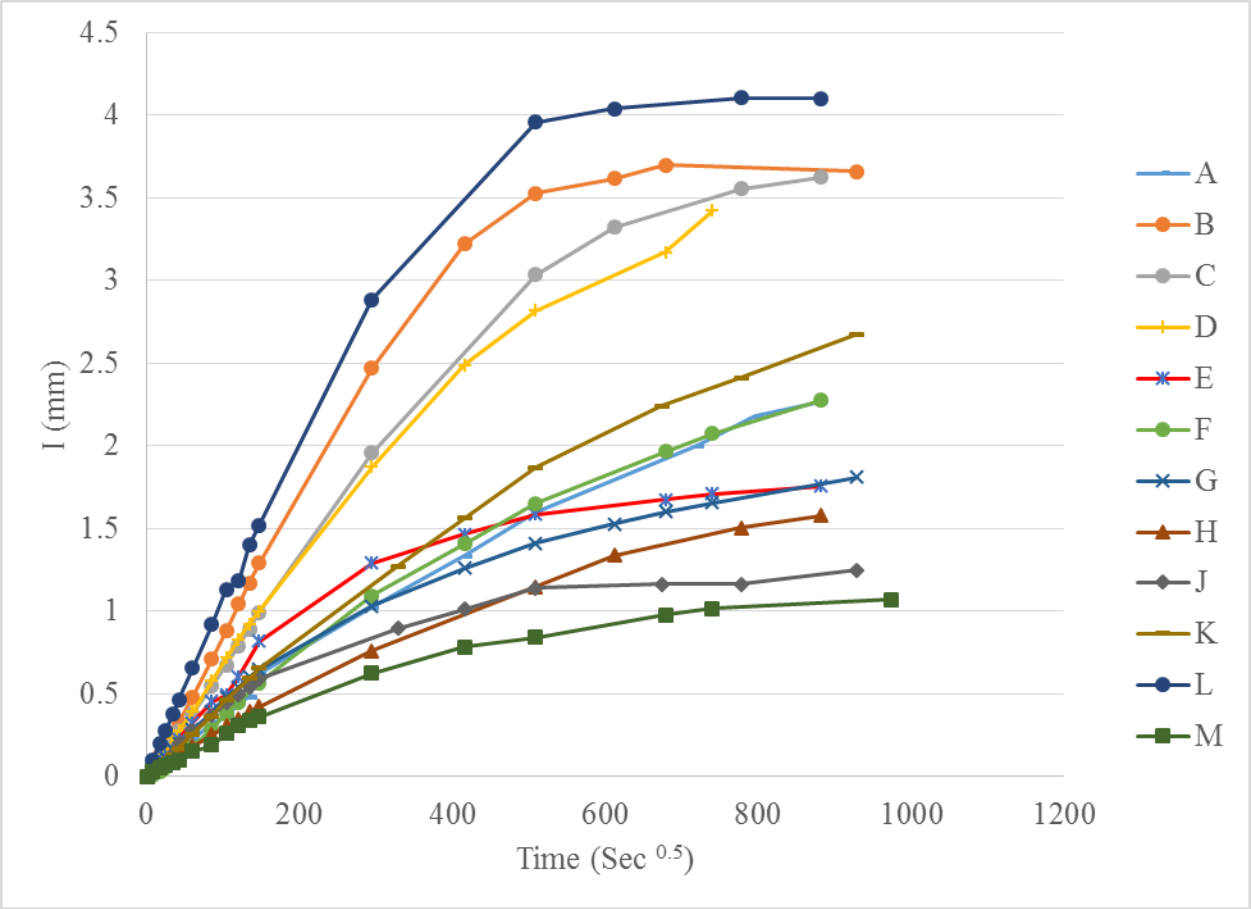

Figure 114. Water absorption rate for different types of ties

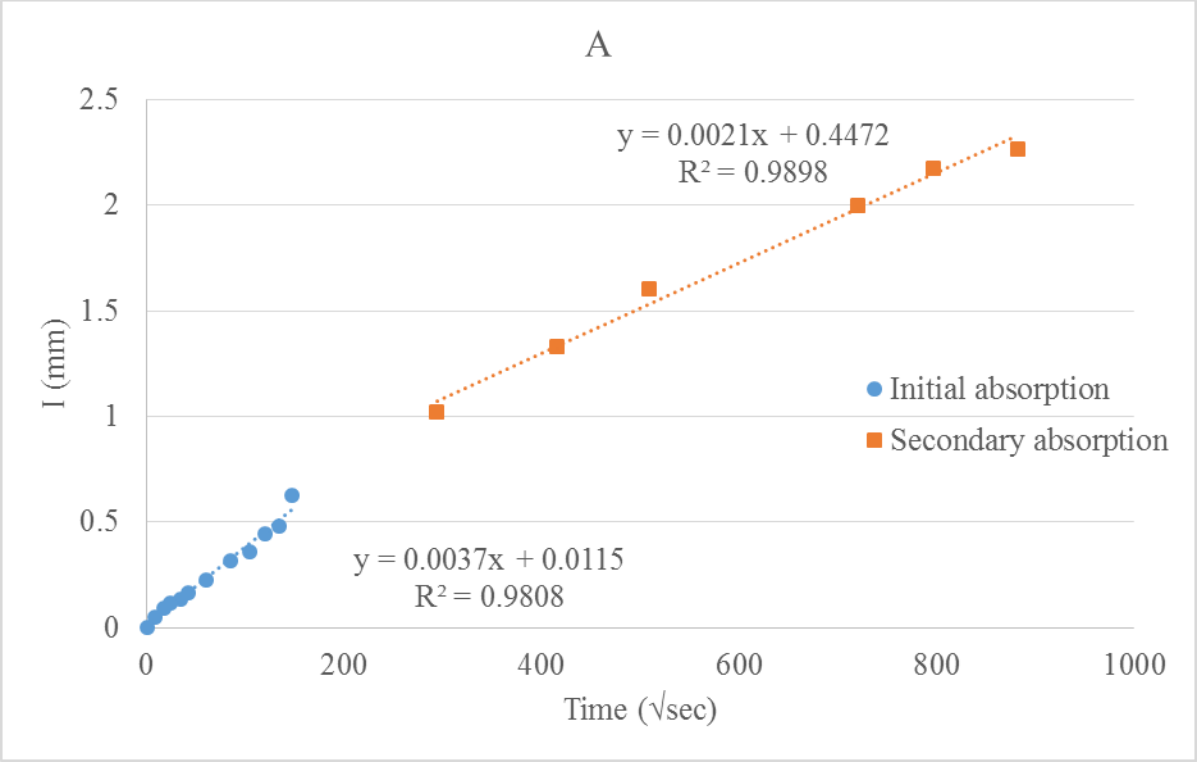

Figure 115. Initial and secondary absorption rate for tie type A

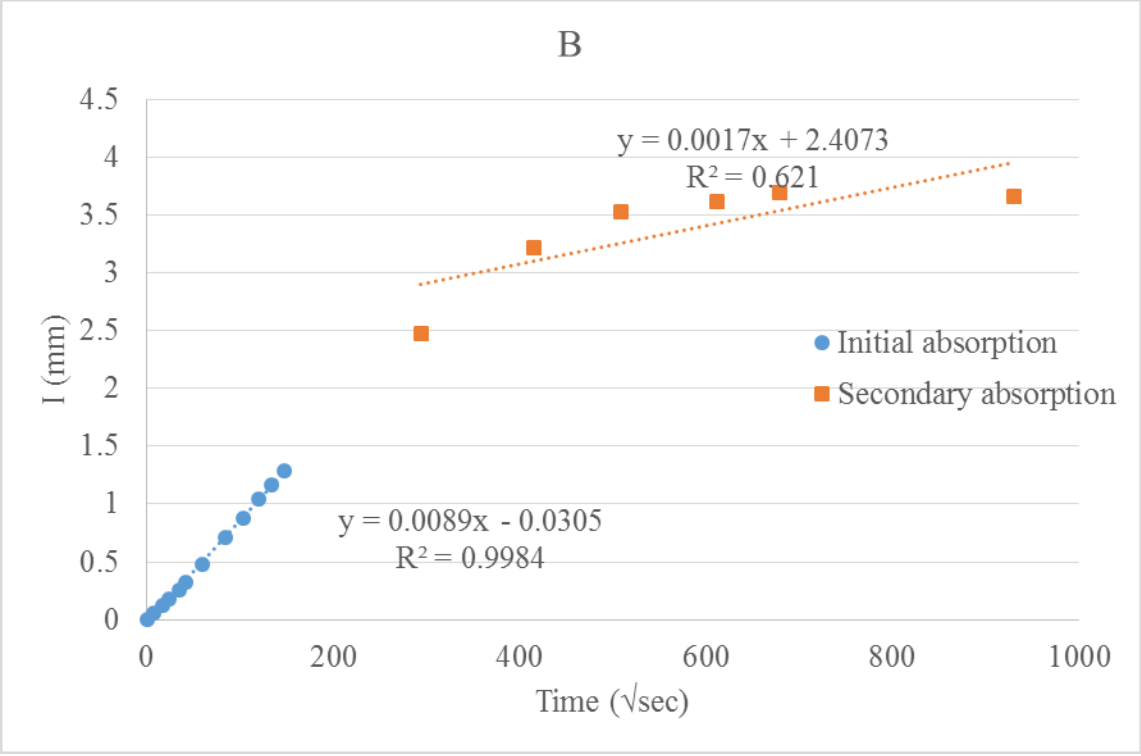

Figure 116. Initial and secondary absorption rate for tie type B

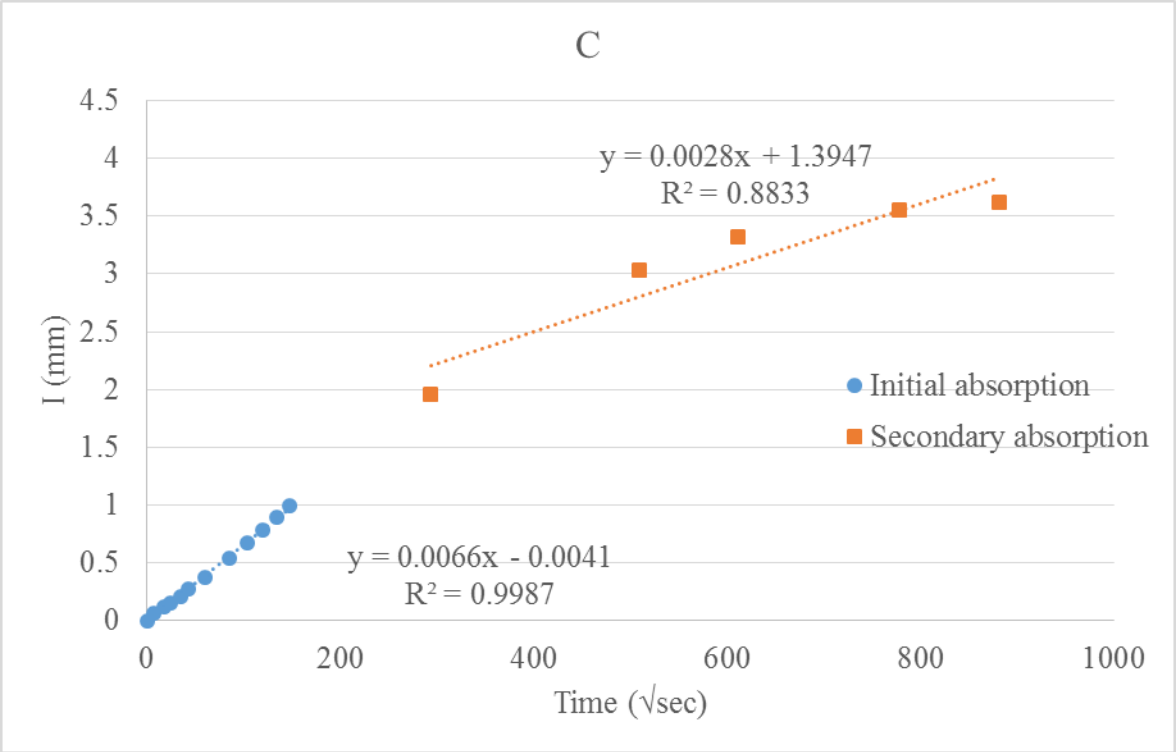

Figure 117. Initial and secondary absorption rate for tie type C

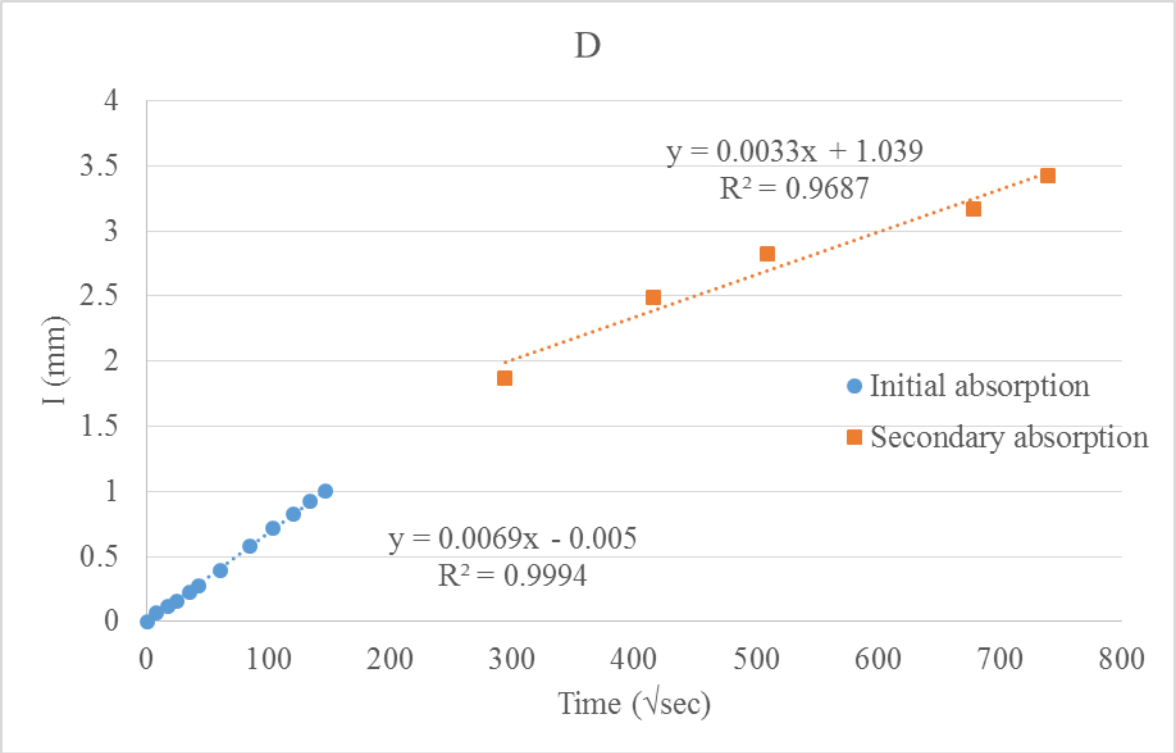

Figure 118. Initial and secondary absorption rate for tie type D

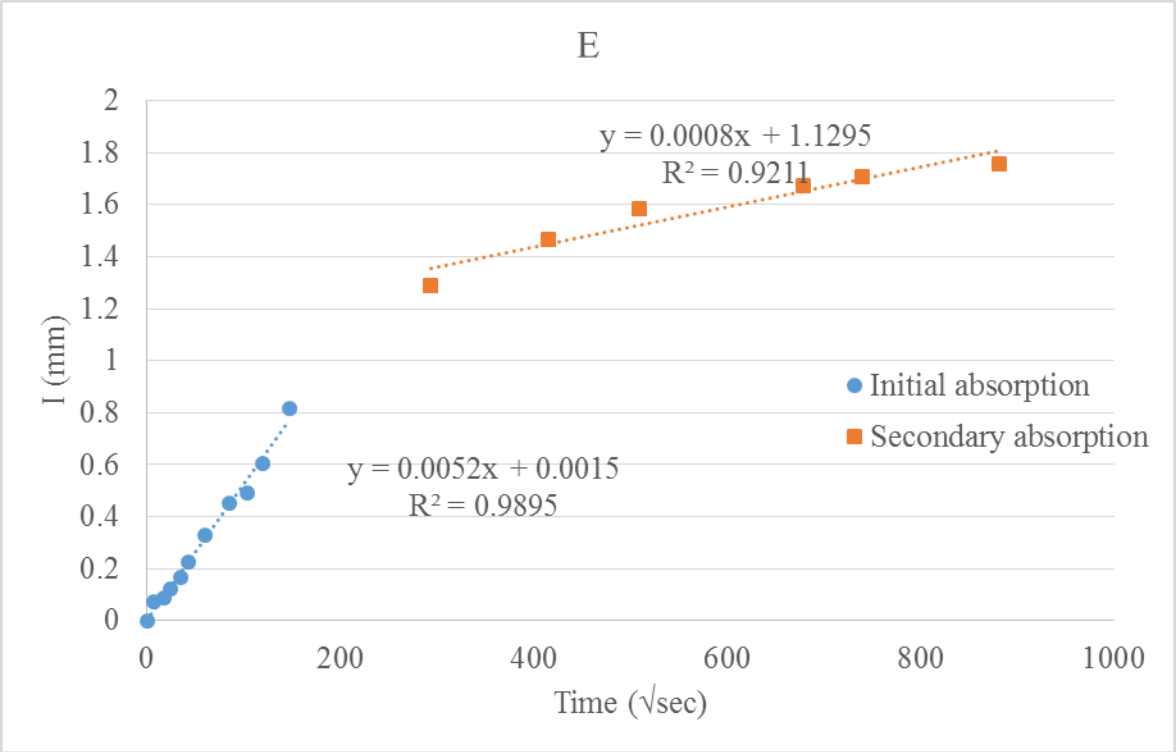

Figure 119. Initial and secondary absorption rate for tie type E

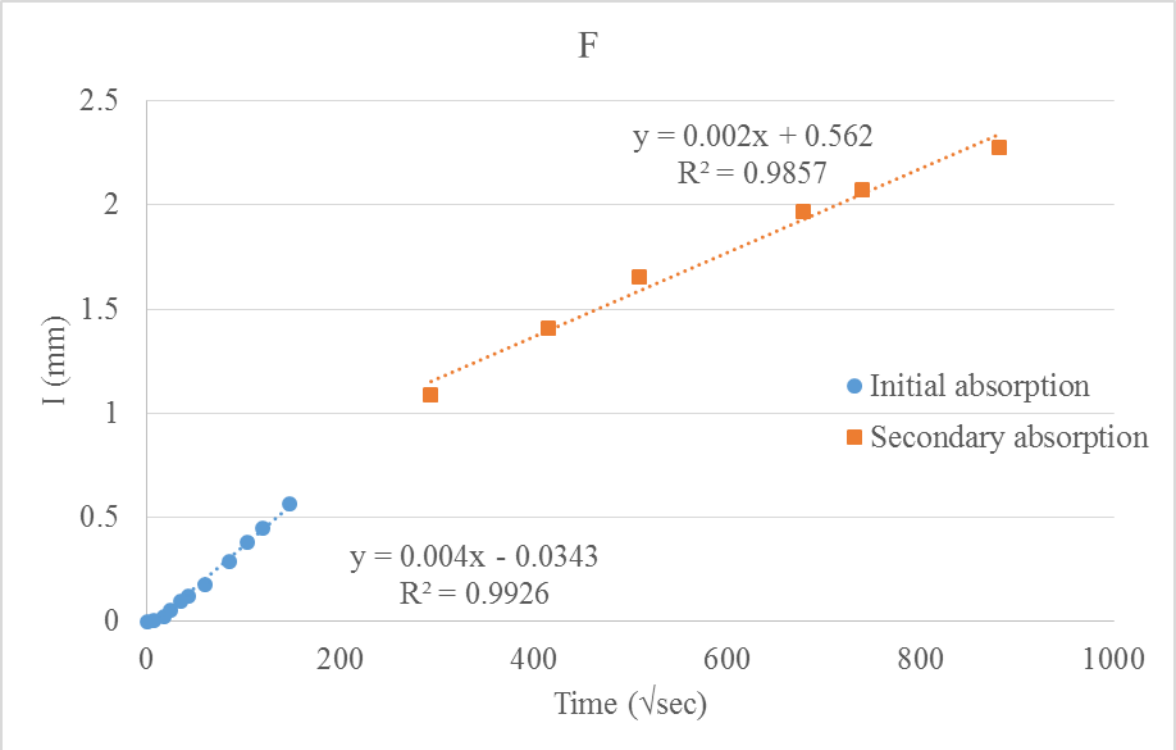

Figure 120. Initial and secondary absorption rate for tie type F

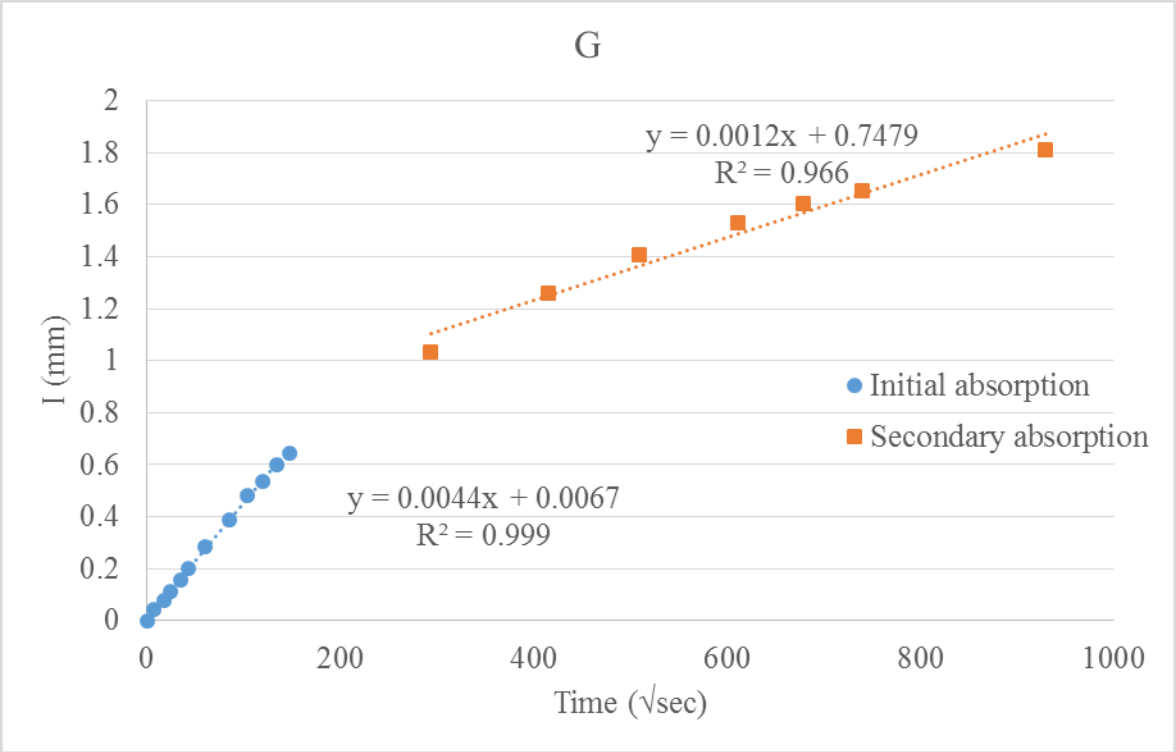

Figure 121. Initial and secondary absorption rate for tie type G

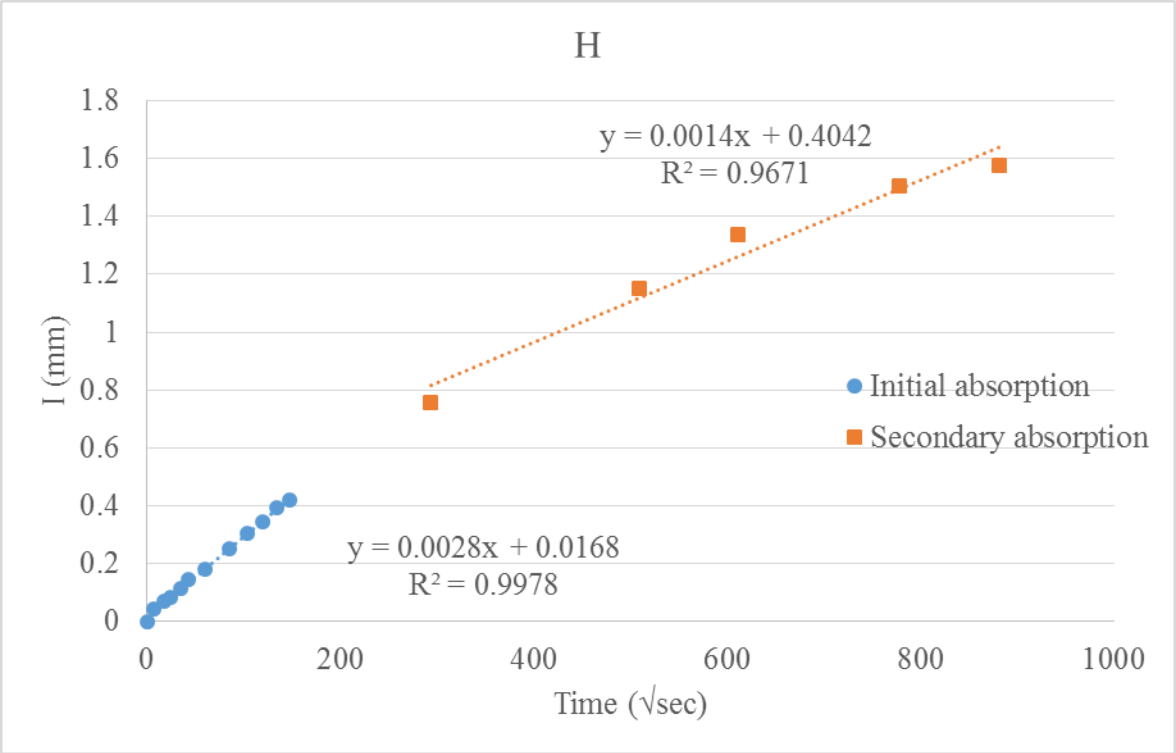

Figure 122. Initial and secondary absorption rate for tie type H

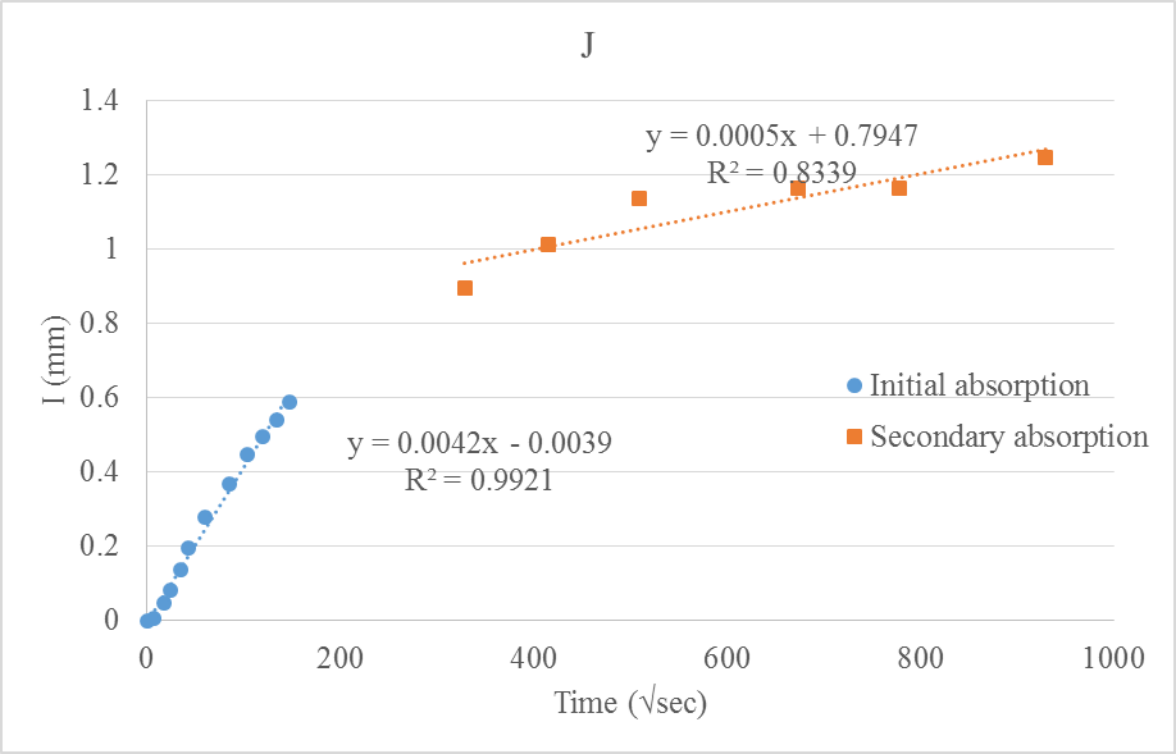

Figure 123. Initial and secondary absorption rate for tie type J

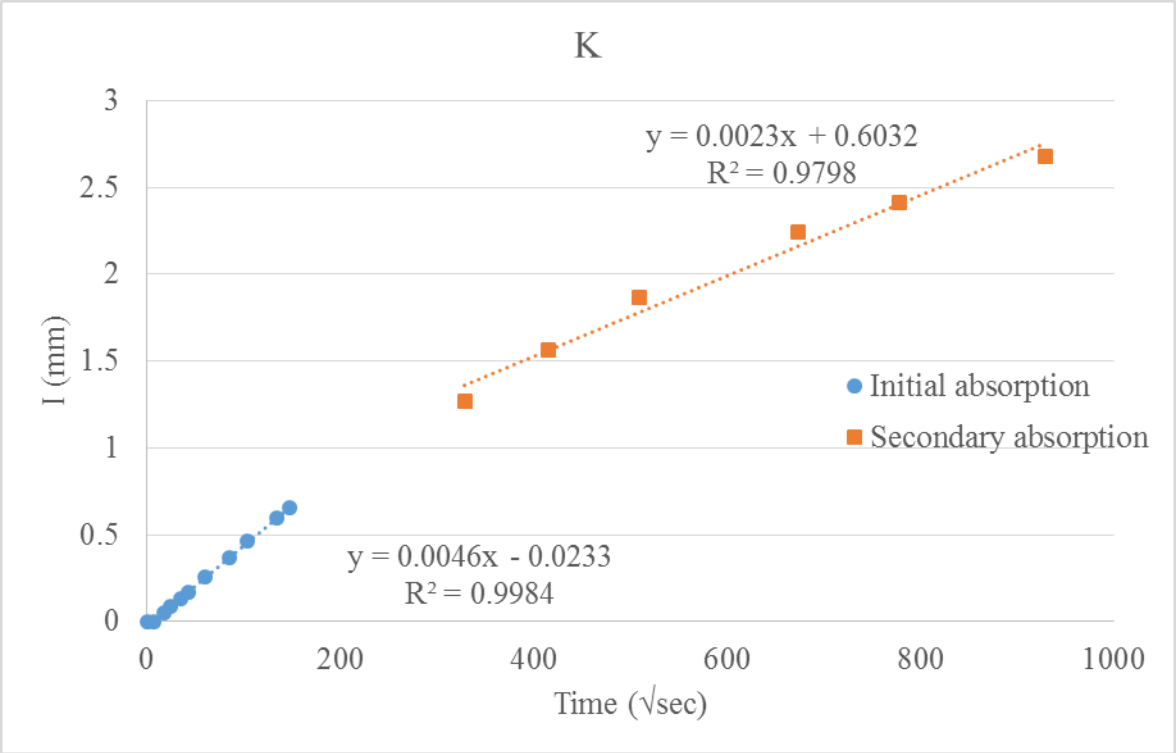

Figure 124. Initial and secondary absorption rate for tie type K

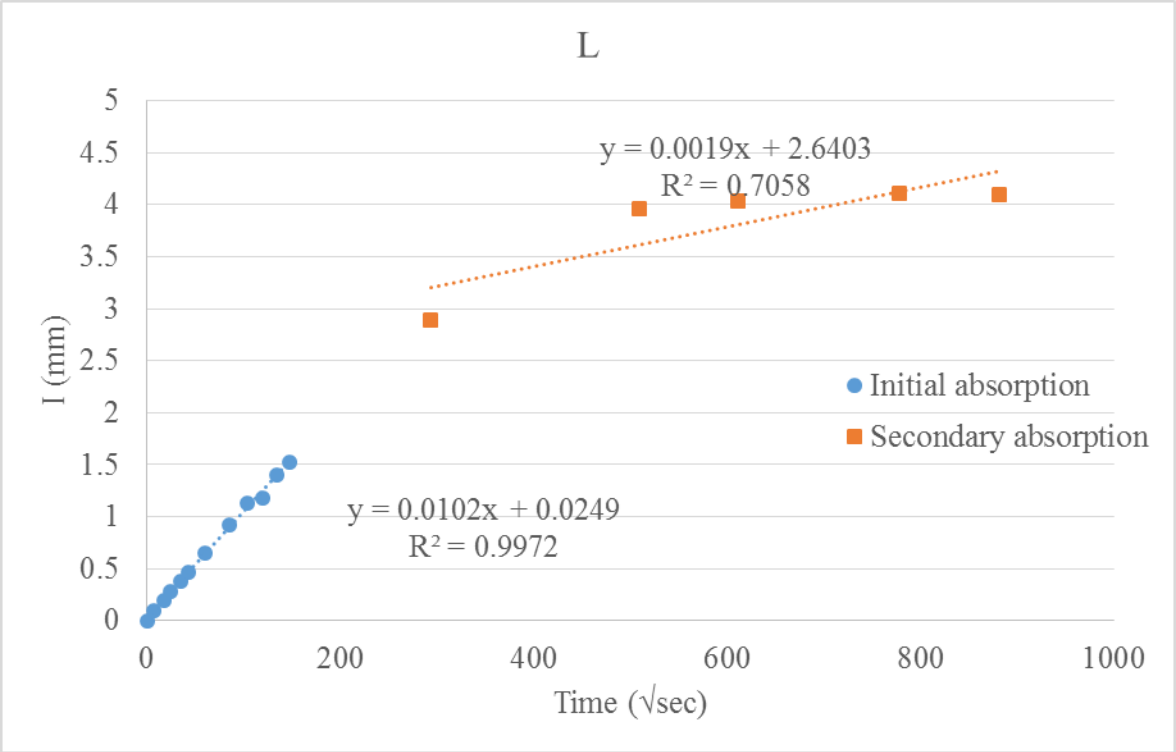

Figure 125. Initial and secondary absorption rate for tie type L

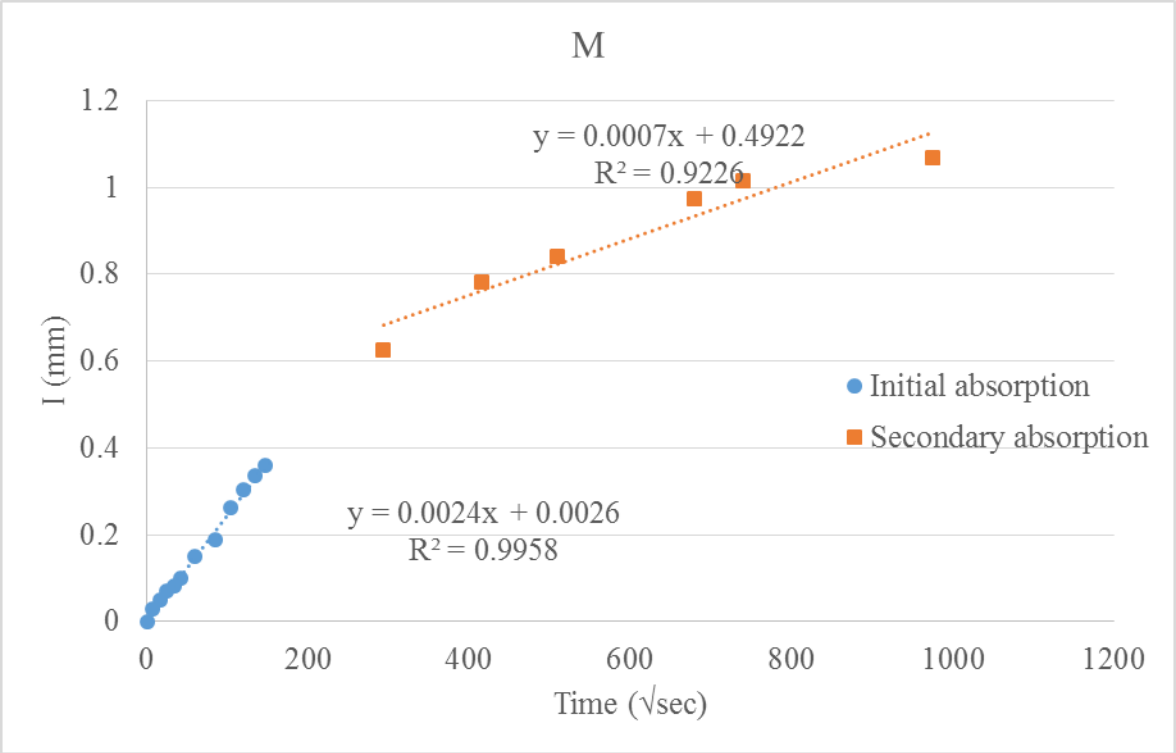

Figure 126. Initial and secondary absorption rate for tie type M

5.4 Abrasion

Rail seat deterioration has been considered as the most critical problem with concrete tie in North America. This damage is primarily caused by abrasion [135].There are different test methods quantifying abrasion resistance of concrete in which abrasion is simulated by means of rolling wheel, impact, or hydro abrasion, while concrete ties are abraded from grinding abrasion. It is known that some factors in the field including moisture, abrasive fines and impact contribute to fast deterioration or early abrasion. It has been seen that abrasion is in relation with compressive strength. The more compressive strength, the more abrasion resistance is observed [136]. Moreover, aggregate mineralogy was observed to be effective on abrasion resistance. Concrete made with high-stiffness aggregate shows an improved abrasion resistance like trap rock, quartzite, granite or hematite [136]. In addition, fiber reinforced concrete performs better than plain concrete in terms of abrasion. Steel fiber and polypropylene fiber were used and improved the abrasion resistance of concrete [137].

However, there is a correlation between surface properties and abrasion resistance. It has been found that surface finishing methods highly affects the abrasion resistance so that concrete surface with high-quality finishing and microstructure leads to resistant surface [138].

Different methods have attempted to assess the resistance of concrete to abrasion, and no one can include all effective factors in abrasion damage. ASTM C415-05 proposes measuring the loss of volume of concrete after sandblasting the concrete surface. ASTM C779-05 determine three test procedures by which concrete surface of concrete can be tested for laboratory or field use. One uses revolving disc test to abrade the surface in which silicon carbide is fed as an abrasive material. In the dressing wheel test a drill pressed is used to force while rotating for 30 minutes at 0.92 Hz. in all methods the depth of wear is measured as final result.

Van Dam developed a new method for concrete railroad ties in which the most effective environmental factors were included [139]. Concrete railroad ties are exposed to aggressive environmental condition where moisture, impact load exist while abrasive fine is grinding the surface. In this method, concrete samples are saw-cut and then placed on an abrasive revolving surface while moisture and load are incorporated into the test. This test was developed based on prescription of ASTM C779, British (BS 812-113) and Turkish (TS 699) standards.

In this report, abrasion test was developed following previous findings and methods [139]. to simulate the actual abrasion condition of concrete ties in the field, abrasive fine along with moisture and impact load were applied to slices extracted from the ties. The slices were prepared as explained in section 5.2. To carry out this experiment a pottery wheel, as shown in Figure 127, was modified in civil engineering lab at Kansas State University. The modified pottery wheel is capable of adjustable revolution speed. A water hose was installed at the top of revolving disc. A 17-in. diameter disc covered with #36 silica sand was mounted on the revolving wheel. Next, protecting lid holding specimen was set by a wooden frame. 3-in.x4-in. slices with 1.5 in. thickness were mounted on polymeric cylinders by hot glue gun to provide a degree of freedom for specimens to spin while being abraded. To incorporate the effect of impact load on samples, 4 lb mass was placed at the top of polymeric cylinders as shown in Figure 130.

To prepare the specimens for the experiment, the specimens were immersed in water for 24 hours before the test. Also, the exposed surface was polished with polishing machine and #80 abrasive disc for more than 15 min to make an even surface for the experiment. 3 samples for each tie were weighted and the dimension of the specimens were measured. Moreover, thickness

of each sample at 12 different locations was measured by digital caliper. After mounting the specimen to the cylinder, it was placed on the lapping plate with the rate of 1 revolution per second. Also, the 4 lb mass was put on the cylinder and water was added to the abrasive disc with a rate of 180 ml/min.

The wear depth of the samples was measured at 0, 10, 30 and 60 min of abrasion. According to ASTM C779, the long term abrasion resistance can be evaluated by values from 60 min of abrasion in the test. The average wear depth of three samples for each tie was compared with other ties in Figure 131, which shows low abrasion resistance of samples from ties A and G. This might be attributed to the hardness of concrete and aggregate used in these ties. Tie M showed a drastic change in wear depth after 60 min. This remarkable increase may be due to the splitting of aggregate or paste particles from the surface causing significant change in values. The rest of the ties showed the same performance in terms of abrasion resistance.

Figure 127. Pottery wheel used for abrasion test

Figure 128. Mounting samples on polymeric cylinder

Figure 129. Prepared samples for abrasion test

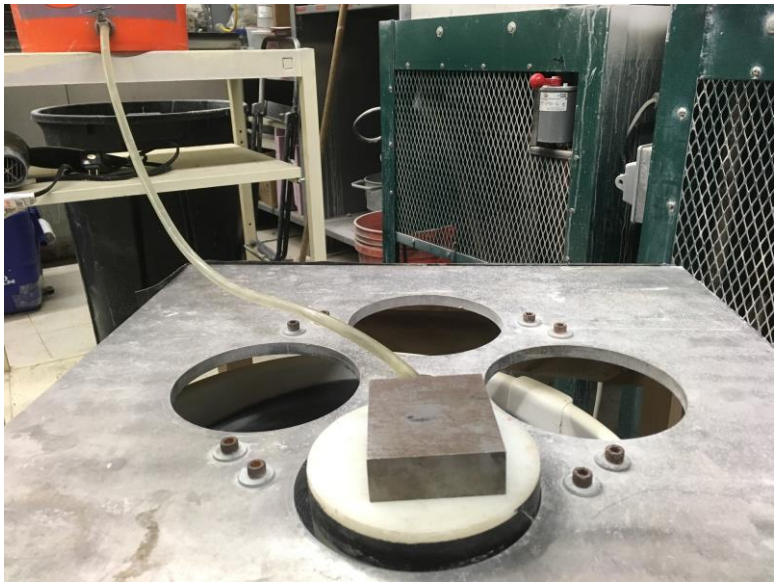

Figure 130. Abrasion test setup

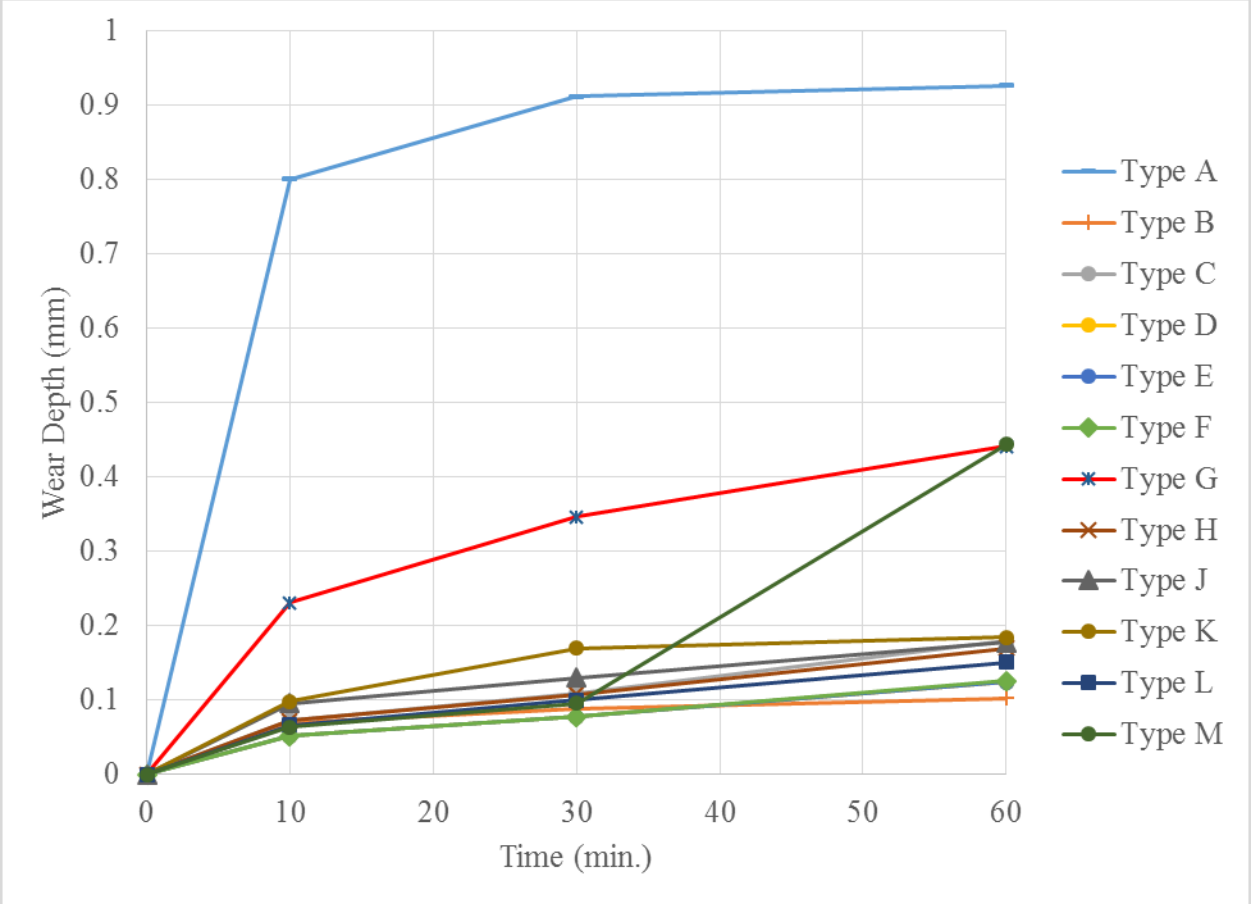

Figure 131. Abrasion test results for different types of ties

5.5 Alkali-Silica-Reaction (ASR)

When a chemical reaction between alkaline of the concrete pore solution and certain siliceous mineral phases of the aggregate happens, a deteriorative process influencing durability of concrete begins which leads to cracking of concrete structures. There are different signs indicating that ASR occurs and progress like production of silica gel which swells in the presence of moisture and further expansion and cracking.

Studies have been done to detect the intensity level of this harmful reaction in concrete. Different tools and procedures have been developed to assess the concrete condition and the potential for further distress of concrete due to ASR. It is still recommended that the result of these methods should be confirmed by traditional petrographic methods [140]. Petrographic is considered as a powerful tool for evaluation of the concrete structure and predicting future durability.

Damage Rating Index (DRI) has been observed to be the most effective procedure quantifying the ASR related damage and expansion. DRI methods can be done on laboratory samples of cores taken from the field. First of all, the samples are saw-cut and polished to produce a smooth and clean surface. Then, petrographic examination of a well-lapped section of concrete is utilized. There are specific features associated with ASR shown in Table 15. Different studies have proposed various weight factor for each feature as believed specific features contribute distinctively to ASR distress. In fact, the damage rating index of a sample is the sum of the number of occurrence of each features which is multiplied by the given weight factor for each feature. The final results is usually normalized to a 100 cm^2 area. It is Ideal to evaluate the nature and degree of damage features and find a correlation between the DRI and either the expansion of damaged concrete or losses in mechanical properties. Previous investigation on cores from ASR-affected bridges showed that DRI is well-correlated with the result of mechanical testing of the cores [141].

To obtain DRI, slices were cut from the ties as explained in section 5.2. First, slices were prepared before microscopic inspection. The surface of samples was polished with abrasive diamond-coated discs (#80, #100, #260, and #360). Polishing process lasted till reaching smooth and even surface. A minimal water was used while polishing to prevent alkali-aggregate reaction gel elimination. 1cm-square grids were drawn on samples by soft pencil. Next, at least 120 cm2 surface area was utilized for petrographic examination by a digital microscope capable of 15x magnification.

DRI was then calculated by counting specific features associated with ASR at each square. Each feature is weighted to represent its impact on ASR deterioration. The DRI of the concrete is then the sum of the number of occurrence of each feature times the weight factor for each particular feature. Finally, the DRI is normalized to a 100-cm^2 for all samples.

$DRI = (DRI_{tabulated} \times 100)/\text{Area in } cm^2$

Different weight factors were suggested by previous studies. In Table 15, different weight factors for specific feature were tabulated.

The calculated DRI for all ties is shown in Figure 136. The results illustrate that ties with DRI number less than 50 are less likely to be affected by ASR damage. On the other hand, ties M and E showed DRI more than 100 which may be attributed to ASR damage. Typically, DRI of 400 indicates that the concrete has a significant level of ASR damage [140].

Table 15. Weight factor used for DRI method [142]

Petrographic features	Weight Factor	
	original values	latest study
Cracks in coarse aggregate	0.5	0.5
Opened cracks in coarse aggregates	0	2
Crack with reaction product in coarse aggregate	2	2
Coarse aggregate debonded	3	3
Cracks in cement paste	2	3
Cracks with reaction product in cement paste	4	3
Air void lined with gel (AV)	0.5	0
Reaction rim around aggregate (R)	0.5	0
Disaggregate/corroded aggregate particle	0	2

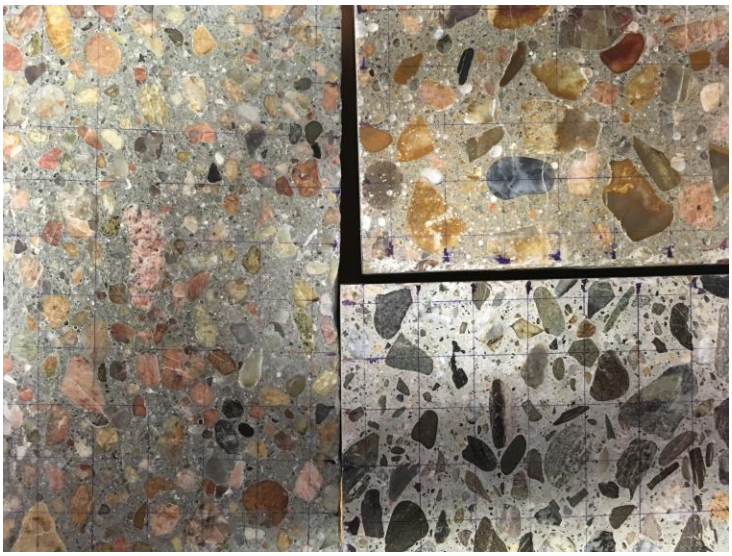

Figure 132. Polished samples for DRI method

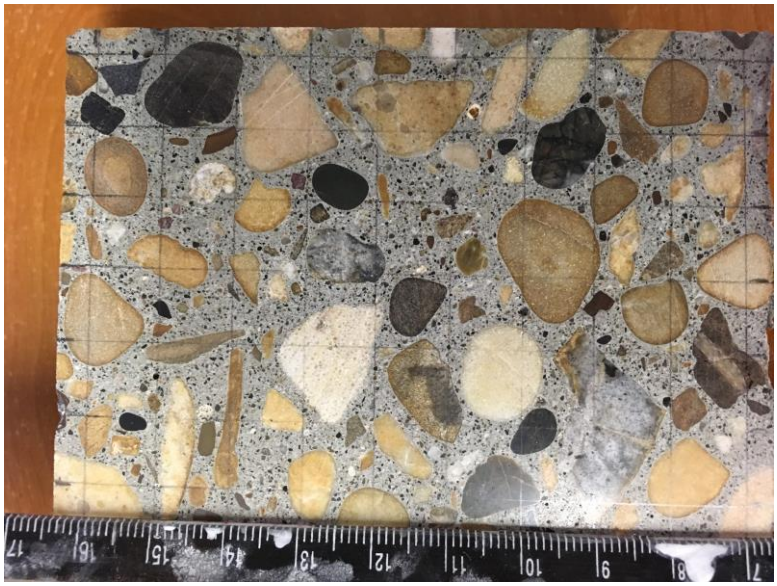

Figure 133. Polished samples with 1 cm^2 grids for DRI method

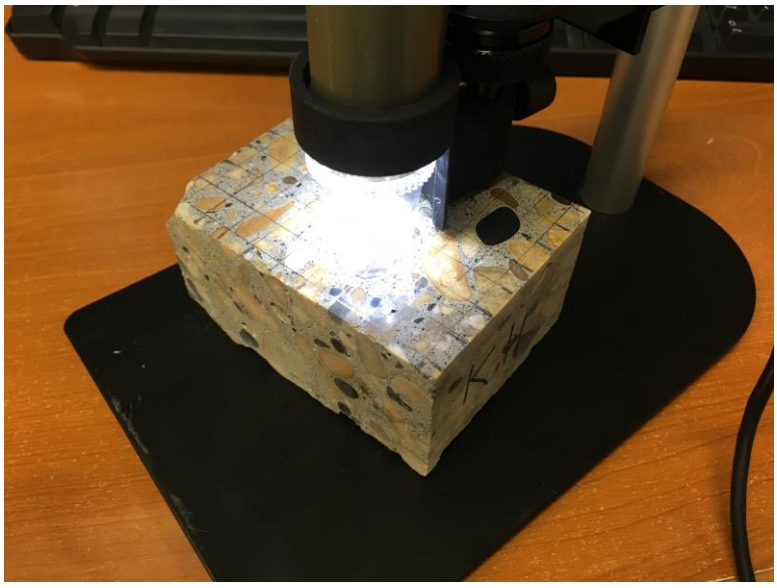

Figure 134. Evaluation of samples by digital microscope in DRI method

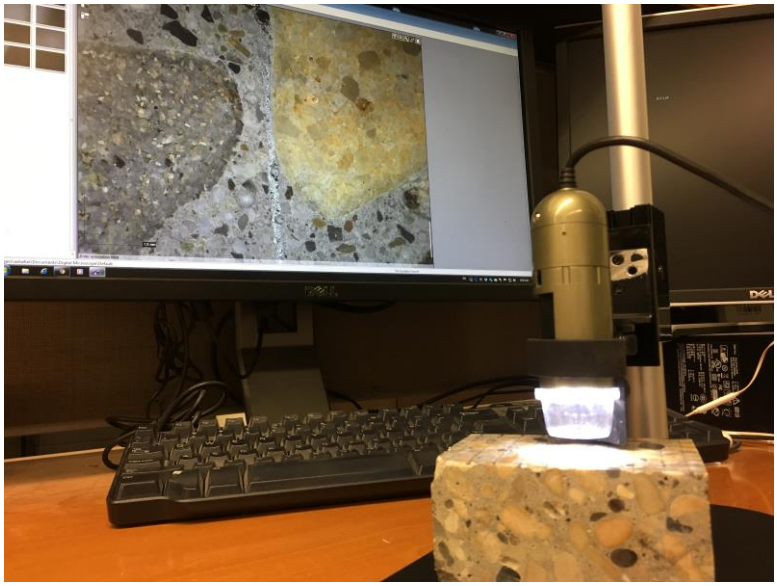

Figure 135. Picture of zoomed in 1 cm^2 area of samples

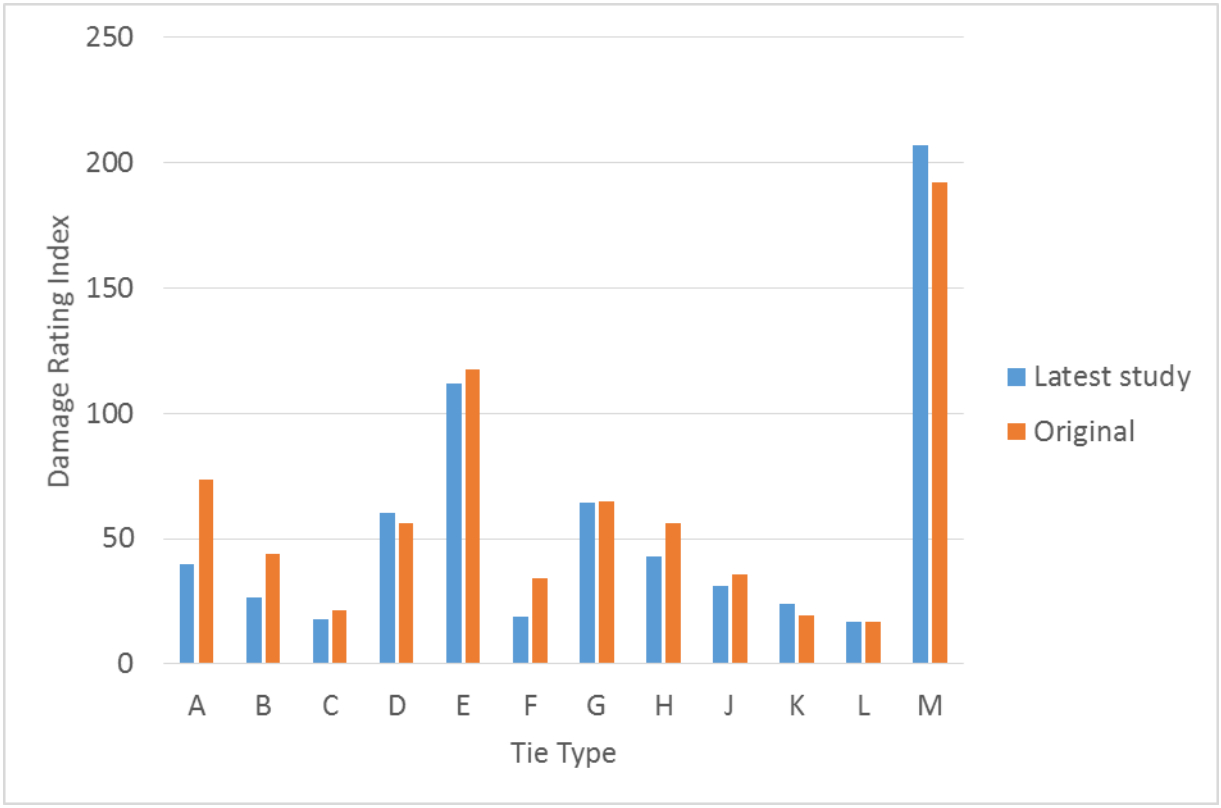

Figure 136. DRI results for different types of ties

5.6 Unit Weight

Unit with of material is considered as fundamental property of concrete. The unit weight of hardened concrete is determined by saturating samples in water for 24 hours and measuring saturated weight, dry weight, and saturated-surface dry weight. Cylindrical 2-in. cores with approximate length of 4 in. were used to determine the unit Wight of concrete. It is important to note that to achieve accurate results, caution should be taken to avoid any wire in cores.

Table 16. Results from unit weight test on cores form ties

#	Tie Type	Dry Weight (gr)	Suspended Saturated (gr)	SSD (gr)	SG
1	A	492	294.0	502.3	2.36
2	B	496	307.1	509.7	2.45
3	C	450	271.9	464.2	2.34
4	D	456	273.0	465.7	2.37
5	E	487	287.7	493.4	2.37
6	F	461	268.4	471.2	2.27
7	G	490	288.0	492.7	2.39
8	H	478	281.9	483.5	2.37
9	J	499	298.8	503.7	2.44
10	K	480	284.5	494.0	2.29
11	L	464	267.4	475.7	2.23
12	M	490	286.8	492.0	2.39

6. Non-destructive Evaluation of Existing Concrete ties

Use of concrete railroad ties as essential part of high-speed railroad has grown in US requiring high maintenance. One of the most common challenge is in-situ investigation of concrete railroad ties due to covered surface of railroad ties through tie pads, rail or ballast. Concert ties are exposed to weathering and high loading leading to cracking, abrasion, deterioration or other type of defects. In addition, internal damages and defects caused within construction and within service period are not easily visible. Railroad ties are systematically inspected for external and internal damage and defects before and during service.

One of extensively used way to investigate concrete railroad tie integrity is non-destructive methods which are categorized into those investigate characteristics of concrete ties, such as voids, flaws, cracks, and deterioration and those that assess strength of concrete. Ultrasonic pulse velocity (UPV) and Impact-echo (IE) tests are known as promising techniques for investigation of uniformity and defect of concrete.

From 1980 to 1997, The Impact-echo method was developed in the United States as an acoustic method for nondestructive evaluation of concrete and masonry [143]. Ultrasonic pulse velocity is based on pulse velocity method which is sensitive indicator of microstructural features. Also, there are some patterns by which the quality of concrete construction may be measured [144]. Preceding works show an inherent uncertainty of various standards used for ultrasonic pule velocity test [145]. However, non-destructive tests are affected by a number of factors such as aggregate, air voids, temperature and etc. which may not influence mechanical properties of concrete like concrete strength [146]. Generally speaking, results of non-destructive tests should be interpreted using engineering judgment as the tests rarely present data which can be unambiguously defined [147]. Thus, this matters how UPV and IE tests result are reliable particularly for concrete railroad ties in different testing condition.

In this report, the variability of ultrasonic pulse velocity and impact echo tests results on concrete railroad ties was assessed in which two concrete railroad ties with the same manufacture and load history condition were tested using both methods. Two additional concrete ties with the same manufacture and load history as each other with visible longitudinal cracks were also examined to see how the damage affected the variability measured. Table 17 shows ties condition in which ties 1 and 2 are in good condition after service with the same loading history and manufacturer whereas ties 3 and 4, also taken from track have a different design and manufacture than ties 1 and 2, but the same as each other.

Table 17. Ties condition

Tie #	Uncracked	Cracked
Tie 1	✓	-
Tie 2	✓	-
Tie 3	-	✓
Tie 4	-	✓

6.1 Ultrasonic Pulse Velocity (UPV)

Ultrasonic scanning is a well-known non-destructive assessment test to qualitatively evaluate the homogeneity and integrity of concrete. This test is based on measuring travel time, T of ultrasonic pulse of waves with different frequency, generated by an electro-acoustical transducer. Ultrasonic pulse velocity depends on the density and elastic properties of material. Qualitatively, higher wave velocity is reached when concrete quality is in good condition in terms of density, uniformity, homogeneity etc. Transducers are placed in contact with the concrete during the test and receiving waves are sent by a similar transducer in contact with the surface at the other end. The test is done according to ASTM C 597-09 and BS EN 12504-4. It is shown that wave velocity, V, of longitudinal stress waves in a concrete mass is related to its elastic properties and density following the relation [148]:

$$V^2 = \frac{E_d(1-\mu)}{\rho(1+\mu)(1-2\mu)}$$

where ρ is density, and μ is Poisson's ratio.

Moisture condition affects pulse speed as it changes while passing through water filled voids. Changing modules of elasticity will affect pulse velocity. Cracks and other defects in the concrete will slow the wave speed through the concrete. Moreover, generally Poisson's ratio value is approximately considered which is not precise. However, it is indicated a change in value of Poisson's ratio from 0.16 to 0.25 reduces the modulus approximately by 11 percent [147]. When ultrasonic pulse passing through concrete meets a concrete-air interface, direct beam of ultrasonic will be obstructed due to negligible transmission of energy across this interface. Large delamination in the concrete that are not visible should significantly decrease the measured wave velocity.

Generally speaking, for a given material and the same location of transducers, higher velocity will be obtained for specimen with less defects and cavities. Also, based on UPV mechanism, before testing the precise distance between centers of transducers is required to calculate velocity more accurately, $V=L/t$ [148].

According to UPV standard test method (ASTM C597-09), this method can be applied to evaluate the uniformity and relative quality of concrete. Hence, in order to estimate the cracks and voids in concrete, the UPV results may be compared if only the test condition and material properties are constant

UPV test was performed according to ASTM C597-09 in which the UPV testing device was setup and the bottom of the two shear wave transducers were coated with lubricant and placed firmly on both side of testing location to make full contact between transducers and concrete ties. Spacing between shear wave transducers was measured and input into the UPV program. This procedure was repeated for a total of 30 tests at the same location on each concrete tie. In order to evaluate the different distances and location of transducers on concrete ties, all abovementioned steps were performed for the following locations in the given order (Figure 137):

- Shoulder to Shoulder on the concrete tie (Black)
- Shoulder to middle of the concrete tie (Red)

- Sides of the first rail-seat (Green)
- Sides at the middle of the tie (Blue)
- Sides at the second rail-seat (Purple)
- End to end of the concrete tie (Yellow)

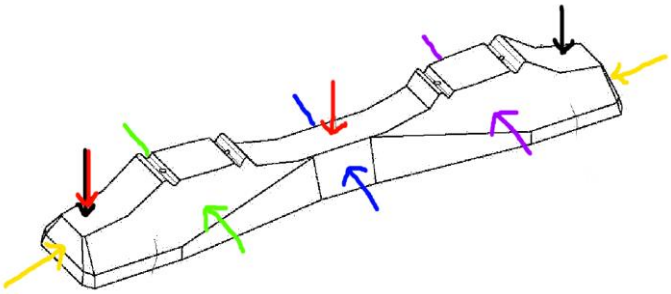

Figure 137. Location of shear wave transducers on concrete ties

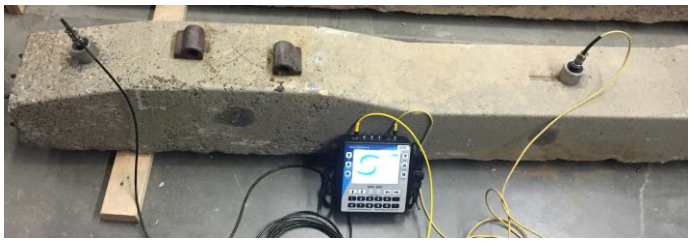

Figure 138. UPV transducers on good tie in mid to shoulder position

UPV test results were acquired from six locations for each ties. As it can be seen from Figure 139 to Figure 144, values from longer distances like shoulder to shoulder have less consistency while transverse records such as sides' measurement shows less dispersion through 30 samples.

In Figure 139, velocity values for four ties regardless of tie condition vary significantly in each test when the UPV was measured from the shoulder-to-shoulder positions. As expected, average pulse velocity of uncracked ties 1 and 2 is more than average UPV result of tie 3 since the pulse velocity is dependent on density and dynamic modulus of elasticity. Unlike tie 3, average UPV values of tie 4 are considerably higher than good ties which may be attributed to different physical and mixture characteristics. Also, test results are dependent on concrete properties like aggregate size, grading, type and content. Although there are many elements affecting concrete properties, some influence negligibly on pulse velocity outcomes. Among those factors, aggregate size, water-cement ratio, admixtures and age of concrete have considerable effect on pulse velocity test [149].

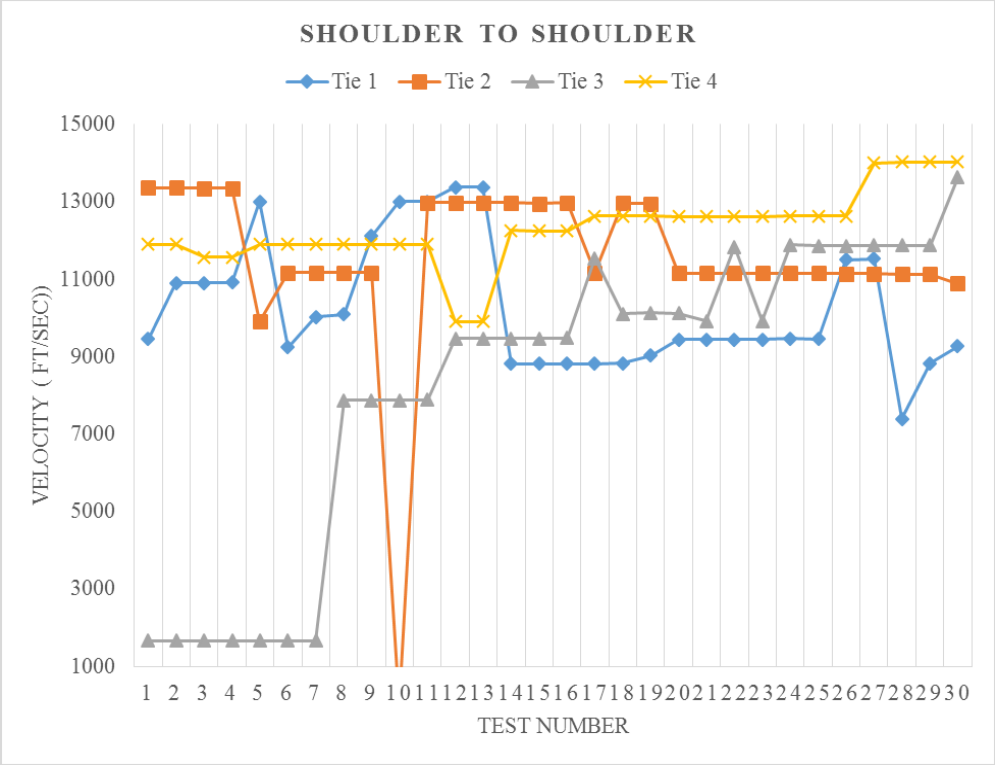

Figure 139. UPV result for shoulder-to-shoulder position of transcoders on tie

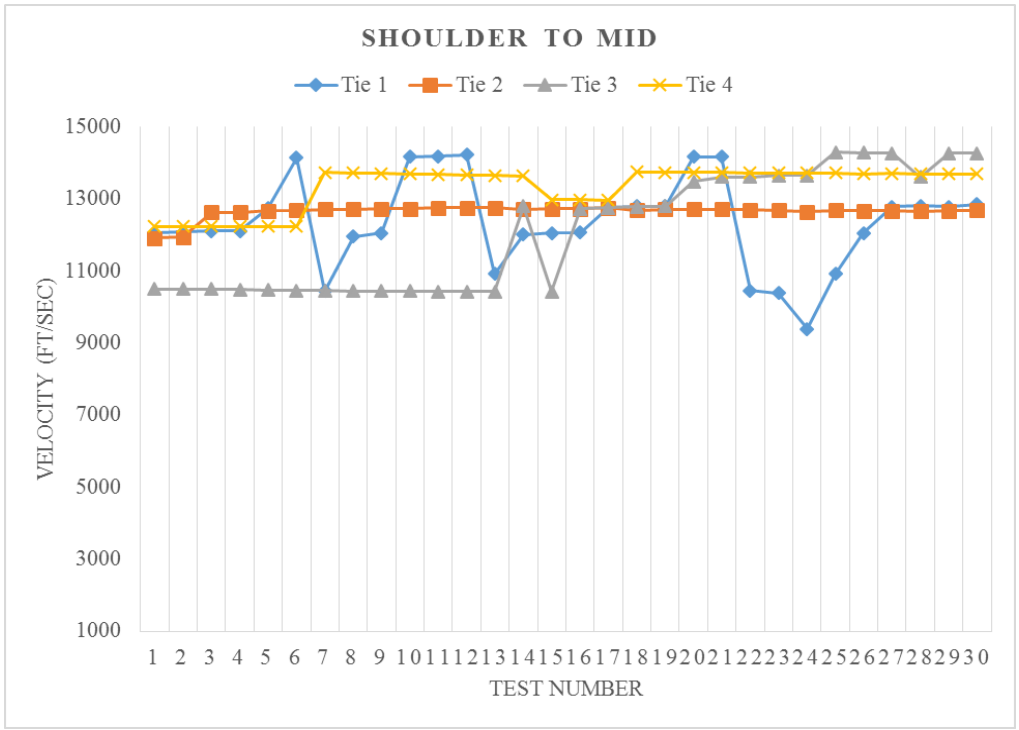

Figure 140. UPV result for shoulder to mid position of transducers on tie

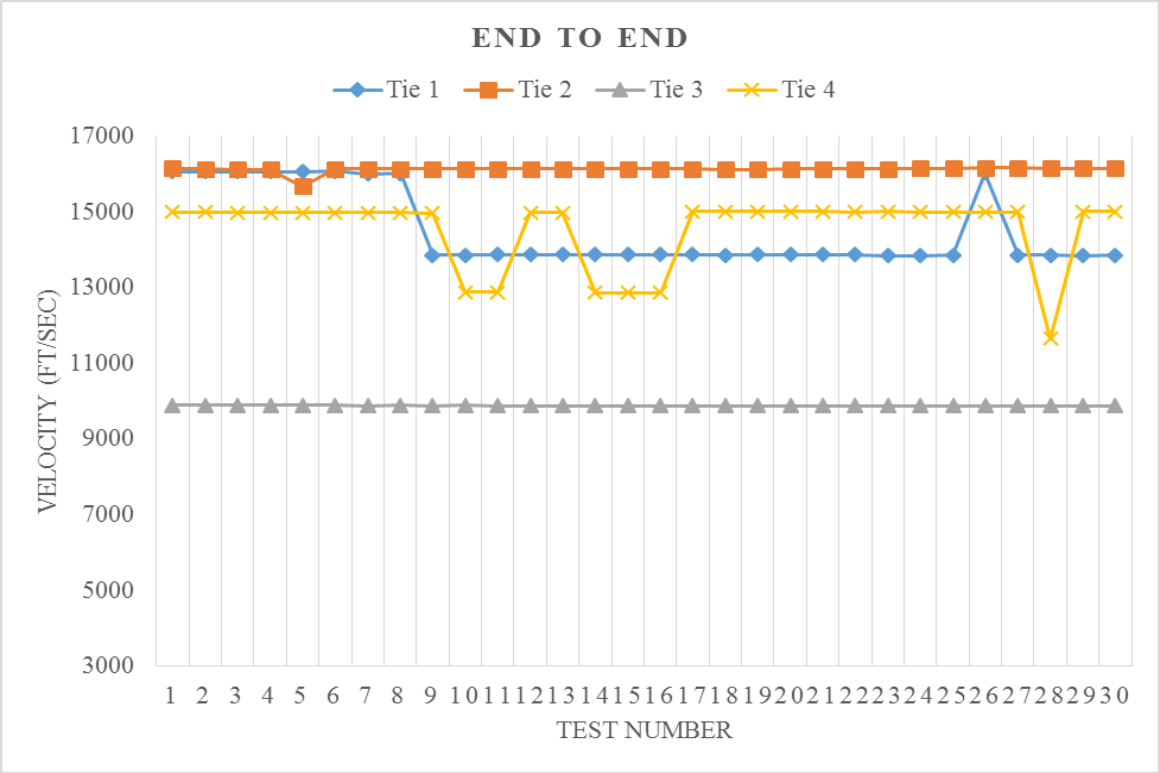

Figure 141. UPV result for end to end position of transducers on tie

Based on results in Figure 140, variability of UPV results in shoulder-to-tie middle location was lower when compared to shoulder-to-shoulder position even though same trend is observed for all ties. This is likely to be explained by less distance traveled by waves through concrete.

Velocity values in end to end position shows less variability. Furthermore, although pulses propagate longitudinally through the concrete tie similarly in the shoulder-to-shoulder and shoulder-to-tie middle configurations, UPV in the end-to-end condition are significantly higher than those testing configurations. There are possibly some reasons contributing alteration in pulse velocity in concrete ties. One can be attributed to the wave movement direction of transducers which travel horizontally and vertically when transducers are on top of tie while move in one direction in end to end location.

Generally, the best results will be given when the transducers are located directly opposite each other [148]. There are other factors influencing the test results like transducer contact, temperature of concrete, path length, size and shape of a specimen, and presence of reinforcing steel. It is more likely that pulse speed in the longitudinal direction of concrete ties are influenced by prestressing steel which is the most significant factors affecting pulse velocity of concrete. It is said that pulse speed in reinforced concrete is 1.4 to 1.7 times the pulse speed in plain concrete [150], [151].

Figure 142 through Figure 144 illustrate the least variability in UPV results in which transducers are located on the sides of concrete ties to measure pulse speed traveling in transverse direction. This is likely because the concrete ties did not contain reinforcing steel in the transverse direction, forcing the waves to travel the entire distance between sensors through the concrete. Average values in three testing condition varies in same order representing more reliability.

Pulse velocity measured from damaged ties did not exhibit more variability compared to uncracked ties. In other words, variability of UPV results is likely to be independent of the condition.

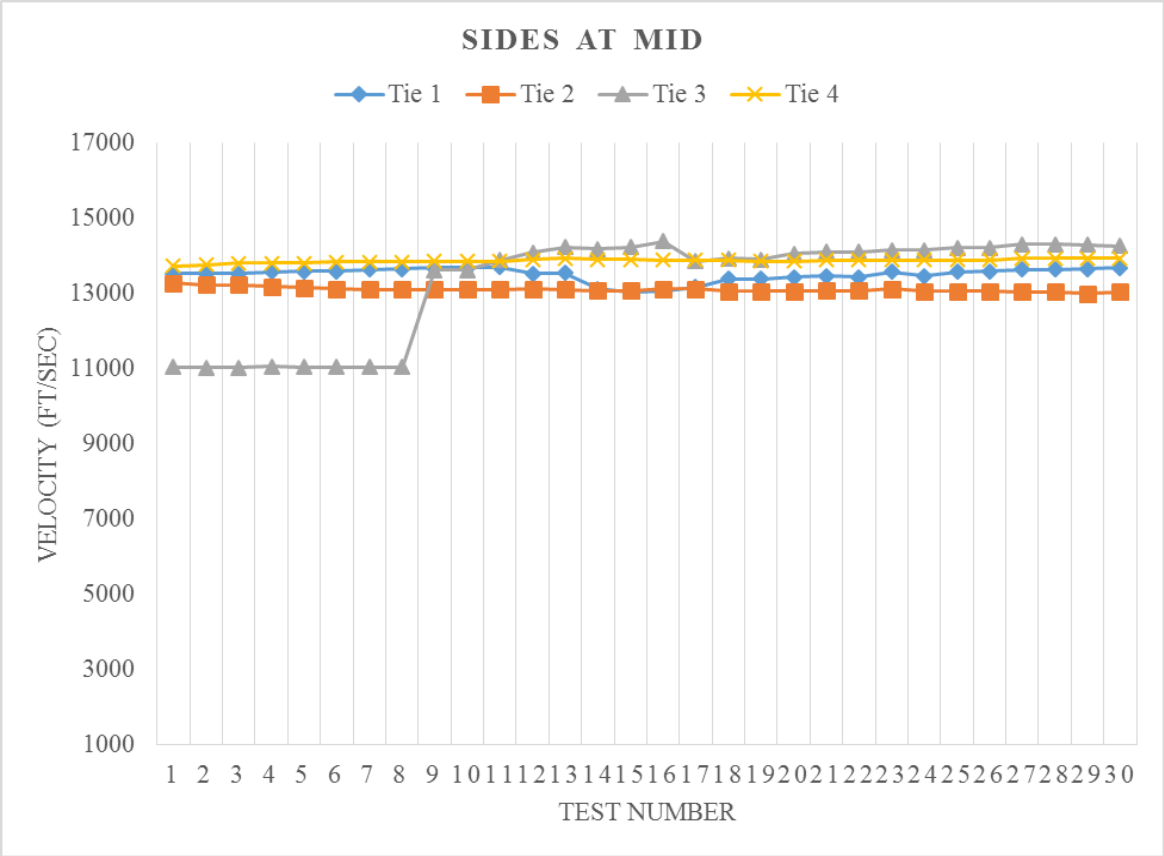

Figure 142. UPV result for mid position of transducers on tie

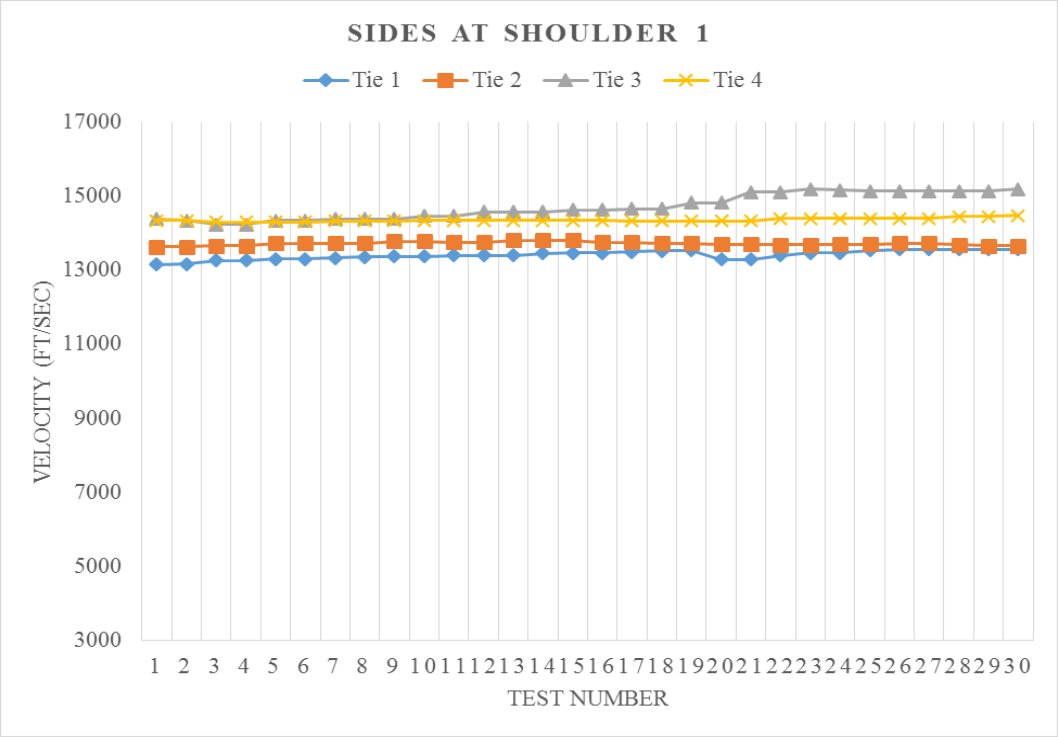

Figure 143. UPV result for side positon of transducers on right shoulder of tie

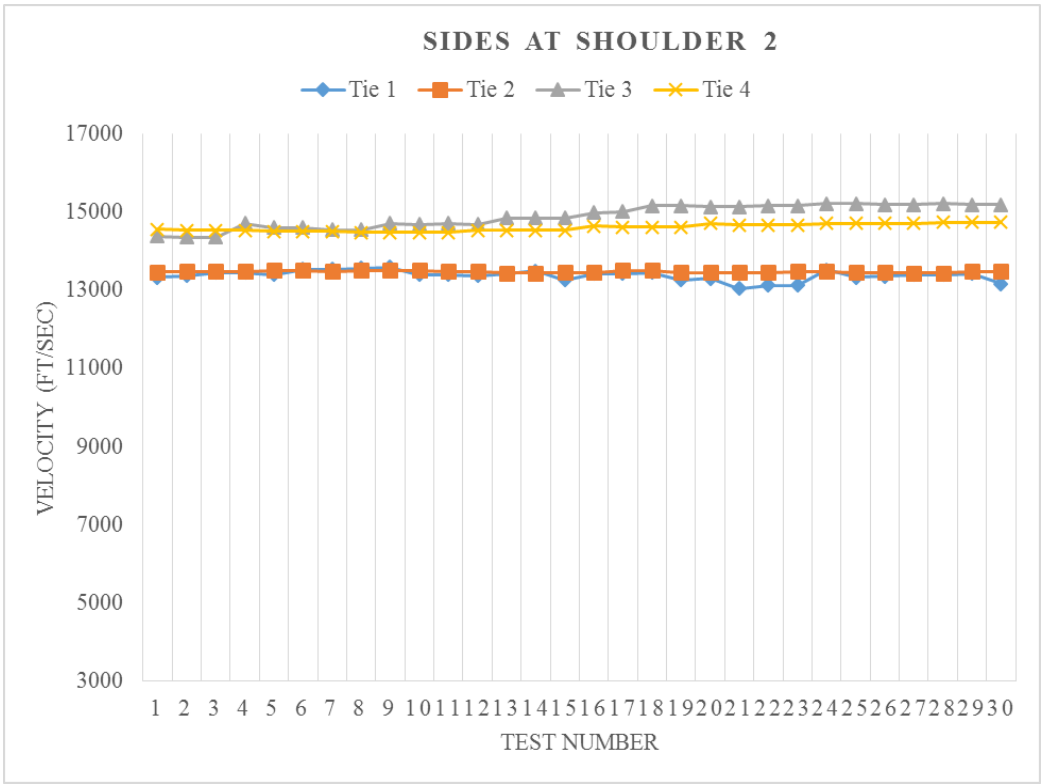

Figure 144. UPV result for side positon of transducers on left shoulder of tie

Table 18. Variability of UPV test results

Position of UPV	Sides at Shoulder 1	Sides at Shoulder 2	Sides at Mid	Shoulder to Shoulder	Shoulder to Mid	End to End
Avg. of St dev	138.24	133.24	414.03	1877.22	909.32	511.04
Coeff. of variation (%)	0.97	0.93	3.11	19.81	7.33	3.51

6.2 Impact Echo (IE)

Impact echo was invented as an acoustic method by the U.S. National Bureau of Standard (NBS) and developed from 1987 -1997 [152]. In this technique transient stress pulses made by impact return when they meet voids and cracks in concrete. When the traveled length of waves is monitored, flaws in the interior of the concrete can be diagnosed. There are two ways recommended by ASTM C1383 in which either travel time of wave passing through known distance or plate thickness of certain part can be calculated. If the variability of impact echo is small, the test method could potentially be used to detect cases of concrete bottom tie abrasion in track.

According to ASTM C 1383-15 the thickness measured by IE can be used to evaluate the presence of cracks and defects in concrete. When the wave released by impactor faces a crack, the p-waves will be reflected and received by transducer. The apparent speed and frequency of P-waves give the thickness of plate (t=V/2f)

This test was conducted based on ASTM C1383. First, the impact echo device was setup and depth of concrete tie at the location of testing was measured and input into the impact echo program. IE was run for additional 30 tests at the same location on the concrete tie. The above procedure was similarly done for three locations for each concrete ties: between the two rail-seats and the middle of concrete tie.

Figure 145. IE device on the middle of one of the uncracked ties

IE was performed on four ties and compared to actual thickness of concrete ties to evaluate the accuracy and variability of test data. Obtained results shown in Figure 146 to Figure 148 indicate low variability in IE results. All obtained thickness values by IE are less than actual thickness and only one testing condition, which is inside first clip of tie 3, gives a large deviation. However, there are a few points departed from mean which are possibly caused by operational error. Although lower thickness obtained by IE in cracked ties are expected due to cracks and

damage, the small thickness of tie 1 in Figure 147 can be explained through inherent defect of tie in construction. Like UPV, damage of concrete railroad ties did not influence the variability of IE values.

There are some errors in determining IE result including systematic error, operational error and errors by nature of concrete plate. Inherent systematic error occurs due to digital nature of waves ($e_p=\delta t/\Delta t$ and $e_f=\Delta f/2f$). Correct contact between IE apparatus and concrete surface should be established by operator. This test is based on the assumption that P-wave speed throughout concert plate is constant [148, 153]. All ties in this report have longitudinal tie bar which affects the wave pulses increasing the error. The results acquired by IE are influenced by those errors which may indicate unsuitability of this test in concrete railroad ties. Table 19 and

Table 20 indicates average of standard deviation of all ties for each position to have a better perspective on the effect of testing condition on variability of UPV and IE results.

Table 20 exhibits more variation in average of IE results comparing to UPV. On the other hand, observed trend of IE values presents consistency in majority of results which means, to better understanding of final values of IE, egregious errors made by either environmental condition or operator should be eliminated from data interpretation.

Table 19. IE thickness results

Tie #		Tie 1	Tie 2	Tie 3	Tie 4
Inside right rail-seat	Actual Thickness (in)	9.5	9.5	8	8
	Average (in)	6.66	7.81	5.78	5.64
	Standard Deviation	0	0.56	1.04	0.26
Middle of tie	Actual Thickness (in)	6.6	7	6.5	6
	Average (in)	1.96	6.62	5.52	5.41
	Standard Deviation	1.04	0	0	0.04
Inside left rail-seat	Actual Thickness (in)	9.5	9.5	8	8
	Average (in)	7.71	6.86	5.56	6.19
	Standard Deviation	0.02	0.4	0.37	0.39

Table 20. Variability of IE test results

Location of IE	Inside right clip	Middle	Inside left Clip
Average of Standard Deviation	0.46	0.27	0.29
Coeff. of Variation (%)	7.43	13.35	4.74

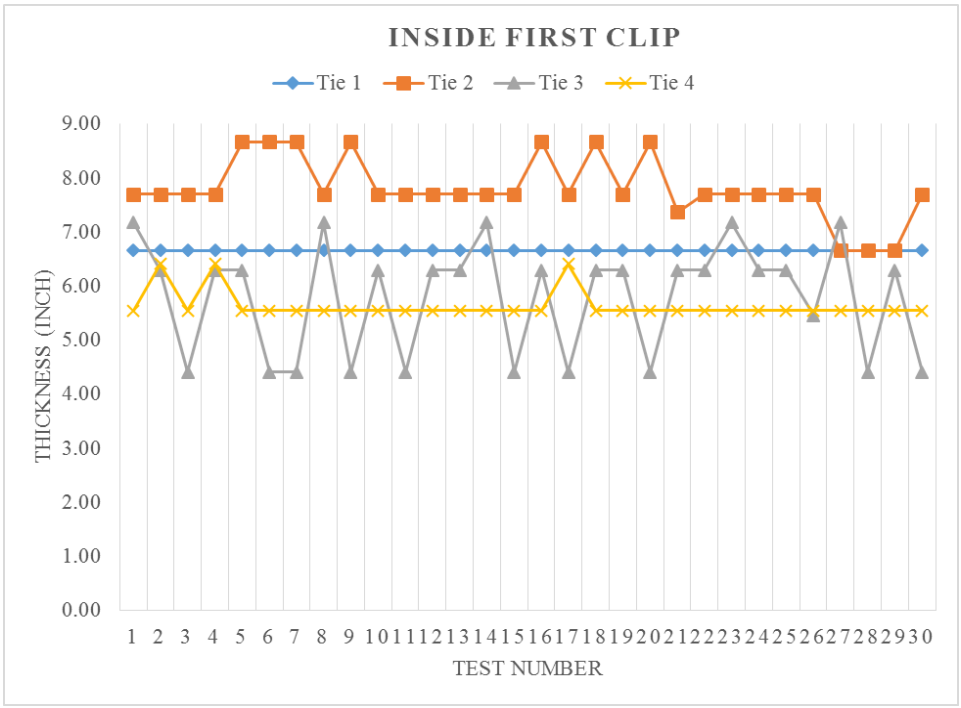

Figure 146. IE thickness results inside right rail-seat

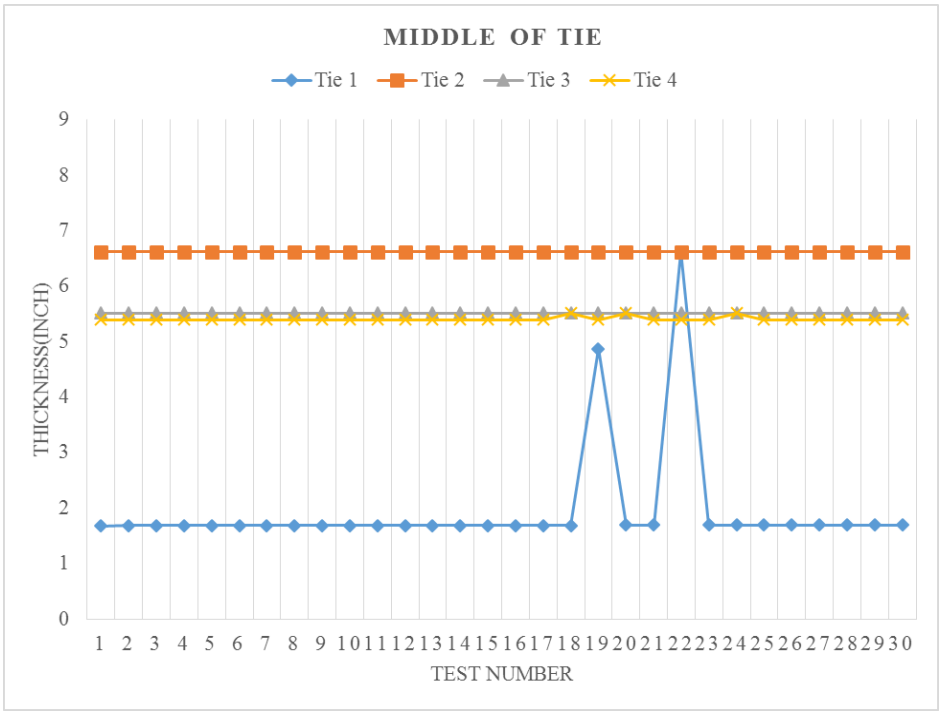

Figure 147. IE thickness results on the middle of tie

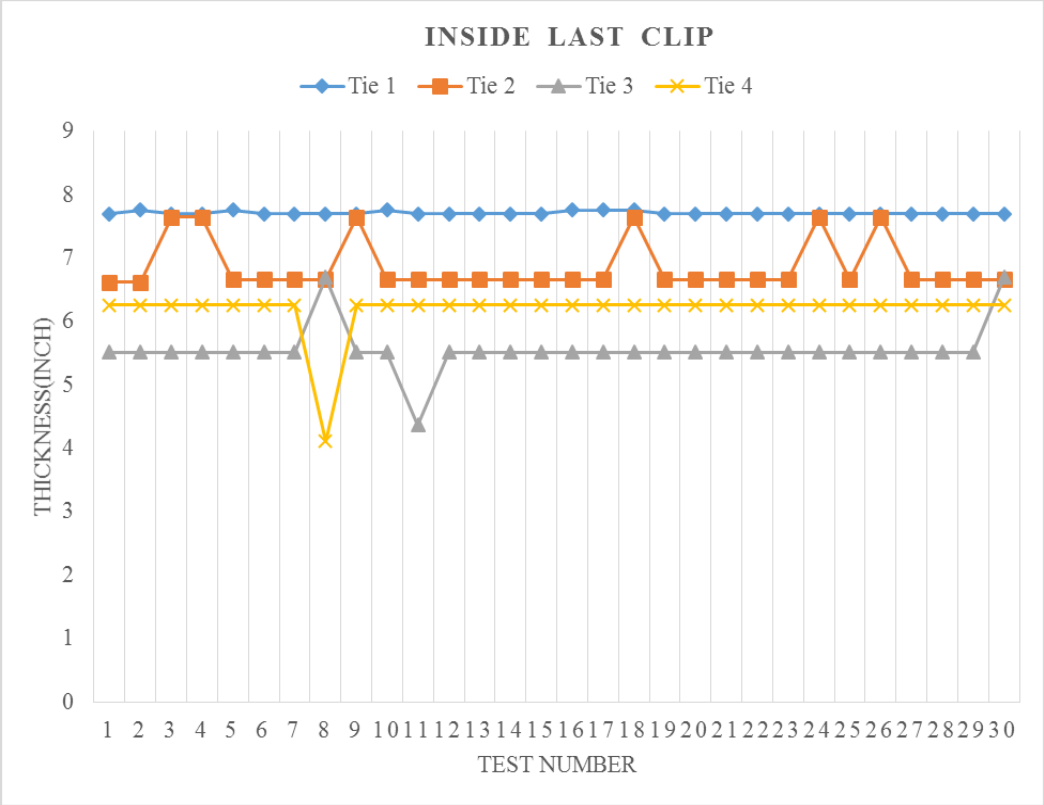

Figure 148. IE thickness results inside left rail-seat

6.3 Conclusion

As mentioned earlier, variability of two types of non-destructive tests on concrete railroad ties were assessed, obtaining standard deviation and coefficient of variation of tests results. UPV in shoulder-to-shoulder and shoulder-to-tie middle location exhibit the most variation which is 19.81% and 7.33% respectively. It may be attributed to the wave propagation direction which is horizontally and vertically through concrete ties. Moreover, it can be concluded that the more distance traveled by pulses, the more variation is observed. Based on the obtained results from UPV, the better results were given for positions in which transducers are directly opposite of each other such as sides and end-to-end state.

In the field condition where only top of ties are visible and accessible shoulder-to-mid state may give acceptable results. However, in end-to-end situation, despite longer distance, the UPV variability decreased, probably because the waves traveled through the prestressing steel. The effect of steel on pulse speed means that measurements taken in the end-to-end configuration could give higher than expected results.

Overall, it is important how to interpret given values by IE and UPV tests on railroad concrete ties. However, UPV and IE can be used as promising means to assess concrete ties with respect to concrete properties and tie structural design although further discussion is needed regarding applicability of these tests on concrete railroad ties. Impact echo measurements showed low variability in thickness values, but notably lower than measured actual thickness. Field thickness calibrations should be considered for impact echo measurements.

7. Summary and Conclusion

7.1 Conclusions

This report was conducted to find the key factors of concrete composition affecting splitting-cracks in prestressed concrete railroad ties. In order to evaluate mixture performance, a fracture behavior, fracture mechanics approach was employed. Then, actual prestressed concrete prisms with identical material were made and tested to verify and assess the results obtained from fracture mechanics test. According to results of this study, angularity, coarseness of aggregate and water-to-cementitious ratio were observed to be significant in both fracture toughness test results and prestressed prisms. Although there is a high variability in fracture toughness test results, the average results are well correlated with prestressed concrete prism performance in terms of splitting-crack length. Despite the variability of fracture mechanics test results in concrete, average of fracture-mechanics test results may still be utilized to rank mix performance for use in concrete ties. The test procedure may follow testing recommendations stated in this report or in other previous research.

It was also found that using transverse reinforcement such as internal polymer fibers or stirrups in prestressed prims may be sufficient to arrests crack growth when poor-quality coarse aggregate is used. Also, in order to minimize end-splitting-cracks growth, only the end part of prestressed prisms (6 in. from end) may need reinforcement. Moreover, a “super mix” design consisting of a high volume of well-angular coarse aggregate with low water-to-cementitious ratio performed remarkably well (no cracks) even with very low concrete edge distance of (0.625 in.).

Considering the analyzed data from this report, it can be concluded that when other effective factors such as edge distance, wire indentation and prestressing force are restricted to any changes, improving the fracture toughness of concrete by increasing release strength, coarse aggregate fraction, percentage of crushed aggregate, and decreasing water-to-cementitious ratio, may serve to reduce splitting-cracks.

The result of this research may contribute to a better understanding of the effect of concrete composition on splitting-crack performance. Statistical models were developed based on concrete elements predicting behavior of splitting-cracks regardless of wire type and reinforcement. Due to the variability of test data, further investigation would need to be conducted, and more data utilized to attain a more reliable and robust model predicting splitting-crack behavior.

7.2 Recommendation

According to findings of this report, it is recommended that concrete mixture should be taken into consideration, especially when enhancing edge distance and wire characteristics are restricted. Moreover, the optimal mix design should include a high percentage of well-distributed and well-angular coarse aggregate with a low water-to-cementitious ratio. Transverse reinforcements such as polymer fibers or stirrups are recommended when concrete design suffers from a shortage of quality aggregates. A use of polymer fiber in the 6 in. end region only could be used in order to reduce material costs.

8. References

[1] Janssen, M., Zuidema, J., and Wanhill, R., 2006, "Fracture Mechanics VSSD," .

[2] Holste, J. R., Haynes, M., Peterman, R. J., 2014, "Tensioned Pullout Test used to Investigate Wire Splitting Propensity in Concrete Railroad Ties," Proceedings of the 2014 Joint Rail Conference, JRC2014-3799 April, Anonymous pp. 2-4.

[3] Irwin, G. R., 1997, "Analysis of Stresses and Strains Near the End of a Crack Traversing a Plate," SPIE MILESTONE SERIES MS, 137pp. 167-170.

[4] Westergaard, H., 1939, "Bearing Pressures and Cra; C];< Si," Journal of Applied Mechanics,

[5] Zampini, D., Jennings, H., and Shah, S., 1995, "Characterization of the Paste-Aggregate Interfacial Transition Zone Surface Roughness and its Relationship to the Fracture Toughness of Concrete," Journal of Materials Science, 30(12) pp. 3149-3154.

[6] Elfgren, L., and International Union of Testing and Research Laboratories for Materials and Structures Technical Committee 90-FMA--Fracture Mechanics,to Concrete, 1989, "Fracture mechanics of concrete structures : from theory to applications : report of the Technical Committee 90-FMA Fracture Mechanics to Concrete - Applications, RILEM (the International Union of Testing and Research Laboratories for Materials and Structures)," London ; New York : Chapman and Hall, London ; New York, .

[7] Carpinteri, A., and Ingraffea, A.R., 1984, "Fracture mechanics of concrete : material characterization and testing," The Hague ; Boston : M. Nijhoff, The Hague ; Boston, .

[8] Sih, G., 1976, "Fracture Toughness Concept," Properties Related to Fracture ToughnessASTM, Philadelphia, pp. 3-15.

[9] Hillerborg, A., Modéer, M., and Petersson, P., 1976, "Analysis of Crack Formation and Crack Growth in Concrete by Means of Fracture Mechanics and Finite Elements," Cement and Concrete Research, 6(6) pp. 773-781.

[10] Hillerborg, A., Modéer, M., and Petersson, P. -., 1976, "Analysis of Crack Formation and Crack Growth in Concrete by Means of Fracture Mechanics and Finite Elements," Cement and Concrete Research, 6(6) pp. 773-781.

[11] Petersson, P., 1981, "Crack Growth and Development of Fracture Zones in Plain Concrete and Similar Materials," .

[12] Bazant, Z.P., and Planas, J., 1997, "Fracture and size effect in concrete and other quasibrittle materials," CRC press, .

[13] Bažant, Z. P., 2002, "Concrete Fracture Models: Testing and Practice," Engineering Fracture Mechanics, 69(2) pp. 165-205.

[14] Bazant, Z. P., and Pfeiffer, P. A., 1987, "Determination of Fracture Energy from Size Effect and Brittleness Number," ACI Materials Journal, 84(6) .

[15] Karihaloo, B., and Nallathambi, P., 1989, "An Improved Effective Crack Model for the Determination of Fracture Toughness of Concrete," Cement and Concrete Research, 19(4) pp. 603-610.

[16] Jenq, Y., and Shah, S. P., 1985, "Two Parameter Fracture Model for Concrete," Journal of Engineering Mechanics, 111(10) pp. 1227-1241.

[17] Tang, T., Shah, S. P., and Ouyang, C., 1992, "Fracture Mechanics and Size Effect of Concrete in Tension," Journal of Structural Engineering, 118(11) pp. 3169-3185.

[18] Bažant, Z., Gettu, R., and Kazemi, M., 1991, "Identification of nonlinear fracture properties from size effect tests and structural analysis based on geometry-dependent R-curves," International journal of rock mechanics and mining sciences & geomechanics abstracts, Anonymous Elsevier, 28, pp. 43-51.

[19] Aliha, M., Heidari-Rarani, M., Shokrieh, M., 2012, "Experimental Determination of Tensile Strength and K (IC) of Polymer Concretes using Semi-Circular Bend(SCB) Specimens," Structural Engineering and Mechanics, 43(6) pp. 823-833.

[20] Mirsayar, M., Shi, X., and Zollinger, D., 2017, "Evaluation of Interfacial Bond Strength between Portland Cement Concrete and Asphalt Concrete Layers using Bi-Material SCB Test Specimen," Engineering Solid Mechanics, 5(4) pp. 293-306.

[21] Aliha, M., Sarbijan, M., and Bahmani, A., 2017, "Fracture Toughness Determination of Modified HMA Mixtures with Two Novel Disc Shape Configurations," Construction and Building Materials, 155pp. 789-799.

[22] Brühwiler, E., and Wittmann, F., 1990, "The Wedge Splitting Test, a New Method of Performing Stable Fracture Mechanics Tests," Engineering Fracture Mechanics, 35(1) pp. 117-125.

[23] Gerstle, W., 2010, "Progress in developing a standard fracture toughness test for concrete," Structures Congress 2010, Anonymous pp. 1915-1926.

[24] ACI Committee 446 on Fracture Mechanics, 1992, "Fracture mechanics of concrete: concepts, models and determination of material properties," Anonymous American Concrete Institute, .

[25] Shah, S.P.(., Carpinteri, A., and RILEM Committee 89-FMT Fracture Mechanics,of Concrete, 1991, "Fracture mechanics test methods for concrete : report of Technical Committee 89-FMT Fracture Mechanics of Concrete, Test Methods, RILEM (the International Union of Testing and Research Laboratories for Materials and Structures)," London ; New York : Chapman and Hall, London ; New York, .

[26] Bordelon, A. C., 2007, Fracture Behavior of Concrete Materials for Rigid Pavement Systems, .

[27] Kitagawa, H., and Takahashi, S., 1976, "Applicability of fracture mechanics to very small cracks or the cracks in the early stage," Second International Conference on Mechanical Behavior of Materials. ASM, Metals Park, Ohio. 1976, 627-631, Anonymous .

[28] Baluch, M., Qureshy, A., and Azad, A., 1989, "Fracture of Concrete and Rock,"Springer, pp. 80-87.

[29] Bazant, Z. P., and Xu, K., 1991, "Size Effect in Fatigue Fracture of Concrete," ACI Materials Journal, 88(4) .

[30] Shah, S. G., and Chandra Kishen, J. M., 2012, "Use of Acoustic Emissions in Flexural Fatigue Crack Growth Studies on Concrete," Engineering Fracture Mechanics, 87pp. 36-47.

[31] Kolluru, S. V., O'Neil, E. F., Popovics, J. S., 2000, "Crack Propagation in Flexural Fatigue of Concrete," Journal of Engineering Mechanics, .

[32] McEvily, A. J., 1988, "On Crack Closure in Fatigue Crack Growth," Mechanics of Fatigue Crack Closure, 982pp. 35-43.

[33] Perdikaris, P. C., Calomino, A. M., and Chudnovsky, A., 1986, "Effect of Fatigue on Fracture Toughness of Concrete," Journal of Engineering Mechanics, 112(8) pp. 776-791.

[34] Kim, J., and Kim, Y., 1999, "Fatigue Crack Growth of High-Strength Concrete in Wedge-Splitting Test," Cement and Concrete Research, 29(5) pp. 705-712.

[35] Lou, J., Bhalerao, K., Soboyejo, A., 2006, "An Investigation of the Effects of Mix Strength on the Fracture and Fatigue Behavior of Concrete Mortar," Journal of Materials Science, 41(21) pp. 6973-6977.

[36] Holmen, J. O., 1982, "Fatigue of Concrete by Constant and Variable Amplitude Loading," ACI Special Publication, 75.

[37] Hilsdorf, H. K., and Kesler, C. E., 1966, "Fatigue strength of concrete under varying flexural stresses," ACI Journal Proceedings, Anonymous ACI, 63, .

[38] Brake, N. A., and Chatti, K., 2013, "Prediction of Size Effect and Non-Linear Crack Growth in Plain Concrete Under Fatigue Loading," Engineering Fracture Mechanics, 109pp. 169-185.

[39] Zhang, X., and Xu, S., 2011, "A Comparative Study on Five Approaches to Evaluate Double-K Fracture Toughness Parameters of Concrete and Size Effect Analysis," Engineering Fracture Mechanics, 78(10) pp. 2115-2138.

[40] Carpinteri, A., and Spagnoli, A., 2004, "A Fractal Analysis of Size Effect on Fatigue Crack Growth," International Journal of Fatigue, 26(2) pp. 125-133.

[41] Ray, S., and Chandra Kishen, J. M., 2011, "Fatigue Crack Propagation Model and Size Effect in Concrete using Dimensional Analysis," Mechanics of Materials, 43(2) pp. 75-86.

[42] Ziegeldorf, S., Müller, H., and Hilsdorf, H., 1980, "A Model Law for the Notch Sensitivity of Brittle Materials," Cement and Concrete Research, 10(5) pp. 589-599.

[43] Carpinteri, A., 1981, "Static and Energetic Fracture Parameters for Rocks and Concretes," Matériaux Et Construction, 14(3) pp. 151-162.

[44] Nallathambi, P., Karihaloo, B., and Heaton, B., 1984, "Effect of Specimen and Crack Sizes, Water/Cement Ratio and Coarse Aggregate Texture upon Fracture Toughness of Concrete," Magazine of Concrete Research, 36(129) pp. 227-236.

[45] Zhang, X. X., Ruiz, G., Yu, R. C., 2009, "Fracture Behaviour of High-Strength Concrete at a Wide Range of Loading Rates," International Journal of Impact Engineering, 36(10–11) pp. 1204-1209.

[46] Awad, M. E., 1971, Strength and Deformation Characteristics of Plain Concrete Subjected to High Repeated and Sustained Loads, .

[47] Sparks, P. R., and Menzies, J., 1973, "The Effect of Rate of Loading upon the Static and Fatigue Strengths of Plain Concrete in Compression*," Magazine of Concrete Research, 25(83) pp. 73-80.

[48] Kesler, C. E., 1953, "Effect of speed of testing on flexural fatigue strength of plain concrete," Highway Research Board Proceedings, Anonymous 32, .

[49] Raithby, K., and Galloway, J., 1974, "Effects of Moisture Condition Age, and Rate of Loading on Fatigue of Plain Concrete," ACI Special Publication, 41.

[50] RAY, S., and CHANDRA KISHEN,J., 2012, "Fatigue Crack Growth due to Overloads in Plain Concrete using Scaling Laws," Sadhana; Academy Proceedings in Engineering Sciences, 37(1) pp. 107-124.

[51] Watanabe, K., Bangi, M. R., and Horiguchi, T., 2013, "The Effect of Testing Conditions (Hot and Residual) on Fracture Toughness of Fiber Reinforced High-Strength Concrete Subjected to High Temperatures," Cement and Concrete Research, 51pp. 6-13.

[52] Abdel-Fattah, H., and Hamoush, S. A., 1997, "Variation of the Fracture Toughness of Concrete with Temperature," Construction and Building Materials, 11(2) pp. 105-108.

[53] Zhang, B., and Bicanic, N., 2002, "Residual Fracture Toughness of Normal-and High-Strength Gravel Concrete After Heating to 600 C," Materials Journal, 99(3) pp. 217-226.

[54] Prokopski, G., 1995, "Fracture Toughness of Concretes at High Temperature," Journal of Materials Science, 30(6) pp. 1609-1612.

[55] Bazant, Z. P., and Prat, P. C., 1988, "Effect of Temperature and Humidity on Fracture Energy of Concrete," ACI Materials Journal, 85(4) .

[56] Ohlsson, U., Daerga, P. A., and Elfgren, L., 1990, "Fracture Energy and Fatigue Strength of Unreinforced Concrete Beams at Normal and Low Temperatures," Engineering Fracture Mechanics, 35(1) pp. 195-203.

[57] Nordby, G. M., 1958, "Fatigue of Concrete-A Review of Research*," ACI Journal Proceedings, Anonymous ACI, 55, .

[58] Zollinger, D., Tang, T., and Yoo, R., 1993, "Fracture Toughness of Concrete at Early Ages," ACI Materials Journal, 90(5) .

[59] Galloway, J., Harding, H., and Raithby, K., 1979, Effects of Moisture Changes on Flexural and Fatigue Strength of Concrete, .

[60] Tepfers, R., and Kutti, T., 1979, "Fatigue strength of plain, ordinary, and lightweight concrete," ACI Journal Proceedings, Anonymous ACI, 76, .

[61] Klaiber, F., Thomas, T., and Lee, D., 1979, Fatigue Behavior of Air-Entrained Concrete: Phase II, .

[62] Zhou, J. H., Cheng, L., and Dong, W., 2013, "Waste Fiber Recycled Concrete Performance Based on Fracture Mechanics Research," Applied Mechanics and Materials, Anonymous Trans Tech Publ, 387, pp. 105-109.

[63] Guo, Y. C., Zhang, J. H., Chen, G., 2014, "Fracture Behaviors of a New Steel Fiber Reinforced Recycled Aggregate Concrete with Crumb Rubber," Construction and Building Materials, 53pp. 32-39.

[64] Piva, A., and Viola, E., 1980, "Biaxial Load Effects on a Crack between Dissimilar Media," Engineering Fracture Mechanics, 13(1) pp. 143-174.

[65] Mahaboonpachai, T., Matsumoto, T., and Inaba, Y., 2010, "Investigation of Interfacial Fracture Toughness between Concrete and Adhesive Mortar in an External Wall Tile Structure," International Journal of Adhesion and Adhesives, 30(1) pp. 1-9.

[66] Wang, X., Yang, Z., Yates, J., 2015, "Monte Carlo Simulations of Mesoscale Fracture Modelling of Concrete with Random Aggregates and Pores," Construction and Building Materials, 75pp. 35-45.

[67] Brown, J., and Pomeroy, C., 1973, "Fracture Toughness of Cement Paste and Mortars," Cement and Concrete Research, 3(4) pp. 475-480.

[68] Isu, N., Teramura, S., Ishida, H., 1995, "Influence of Quartz Particle Size on the Chemical and Mechanical Properties of Autoclaved Aerated Concrete (II) Fracture Toughness, Strength and Micropore," Cement and Concrete Research, 25(2) pp. 249-254.

[69] Dittmer, T., and Beushausen, H., 2014, "The Effect of Coarse Aggregate Content and Size on the Age at Cracking of Bonded Concrete Overlays Subjected to Restrained Deformation," Construction and Building Materials, 69pp. 73-82.

[70] Li, O., Deng, Z., and Fu, H., 2004, "Effect of Aggregate Type on Mechanical Behavior Of," ACI Materials Journal, .

[71] Karamloo, M., Mazloom, M., and Payganeh, G., 2016, "Effects of Maximum Aggregate Size on Fracture Behaviors of Self-Compacting Lightweight Concrete," Construction and Building Materials, 123pp. 508-515.

[72] Nikbin, I., Beygi, M., Kazemi, M., 2014, "Effect of Coarse Aggregate Volume on Fracture Behavior of Self Compacting Concrete," Construction and Building Materials, 52pp. 137-145.

[73] Feng, N., Ji, X., Zhuang, Q., 1995, "Effect of Concrete Materials on Fracture Performance," Fracture Mechanics of Concrete Structures.Proceedings of the FRAMCOS-2, Aedificatio Publishers, D-79104, Freiburg, pp. 119-124.

[74] Siregar, A., Rafiq, M. I., and Mulheron, M., 2017, "Experimental Investigation of the Effects of Aggregate Size Distribution on the Fracture Behaviour of High Strength Concrete," Construction and Building Materials, 150pp. 252-259.

[75] Siregar, A. P., 2016, The Effect of Aggregate Size Distribution on Fracture Mechanic of Concrete., .

[76] Şahin, Y., and Köksal, F., 2011, "The Influences of Matrix and Steel Fibre Tensile Strengths on the Fracture Energy of High-Strength Concrete," Construction and Building Materials, 25(4) pp. 1801-1806.

[77] Prokopski, G., and Langier, B., 2000, "Effect of Water/Cement Ratio and Silica Fume Addition on the Fracture Toughness and Morphology of Fractured Surfaces of Gravel Concretes," Cement and Concrete Research, 30(9) pp. 1427-1433.

[78] Bharatkumar, B., Raghuprasad, B., Ramachandramurthy, D., 2005, "Effect of Fly Ash and Slag on the Fracture Characteristics of High Performance Concrete," Materials and Structures, 38(1) pp. 63-72.

[79] Sadrmomtazi, A., Tahmouresi, B., and Kohani Khoshkbijari, R., 2017, "Effect of Fly Ash and Silica Fume on Transition Zone, Pore Structure and Permeability of Concrete," Magazine of Concrete Research, 70(10) pp. 519-532.

[80] Zhang, P., Li, Q., and Zhang, H., 2012, "Fracture Properties of High-Performance Concrete Containing Fly Ash," Proceedings of the Institution of Mechanical Engineers, Part L: Journal of Materials Design and Applications, pp. 1464420711435759.

[81] Golewski, G. L., and Sadowski, T., 2016, "Macroscopic Evaluation of Fracture Processes in Fly Ash Concrete," Solid State Phenomena, 254pp. 188.

[82] Brown, J., 1972, "Measuring the Fracture Toughness of Cement Paste and Mortar," Magazine of Concrete Research, 24(81) pp. 185-196.

[83] Rozière, E., Granger, S., Turcry, P., 2007, "Influence of Paste Volume on Shrinkage Cracking and Fracture Properties of Self-Compacting Concrete," Cement and Concrete Composites, 29(8) pp. 626-636.

[84] Chen, B., and Liu, J., 2004, "Effect of Aggregate on the Fracture Behavior of High Strength Concrete," Construction and Building Materials, 18(8) pp. 585-590.

[85] Song, Y., Das, A., Lange, D. A., 2018, "A Performance-Based Approach to Concrete Freeze-Thaw Durability," 2018 Joint Rail Conference, Anonymous American Society of Mechanical Engineers, pp. V001T01A010-V001T01A010.

[86] Arabali, P., and Shekarchi, M., 2015, "Durability of jointed reinforced concrete pavements under sever exposure conditions: a case study in IRAN," XIII International Conference on Durability of Building Materials and Components, Anonymous .

[87] Aliha, M., Fazaeli, H., Aghajani, S., 2015, "Effect of Temperature and Air Void on Mixed Mode Fracture Toughness of Modified Asphalt Mixtures," Construction and Building Materials, 95pp. 545-555.

[88] Vejmelková, E., Keppert, M., Rovnaníková, P., 2012, "Properties of High Performance Concrete Containing Fine-Ground Ceramics as Supplementary Cementitious Material," Cement and Concrete Composites, 34(1) pp. 55-61.

[89] Auskern, A., and Horn, W., 1974, "Fracture Energy and Strength of Polymer Impregnated Cement," Cement and Concrete Research, 4(5) pp. 785-795.

[90] Banthia, N., and Sheng, J., 1996, "Fracture Toughness of Micro-Fiber Reinforced Cement Composites," Cement and Concrete Composites, 18(4) pp. 251-269.

[91] Matsumoto, T., and Li, V. C., 1999, "Fatigue Life Analysis of Fiber Reinforced Concrete with a Fracture Mechanics Based Model," Cement and Concrete Composites, 21(4) pp. 249-261.

[92] ASTM, 2012, "ASTM C150/C150M-12: Standard Specification for Portland Cement," .

[93] Amparano, F. E., Xi, Y., and Roh, Y., 2000, "Experimental Study on the Effect of Aggregate Content on Fracture Behavior of Concrete," Engineering Fracture Mechanics, 67(1) pp. 65-84.

[94] Živica, V., 2009, "Effects of the very Low Water/Cement Ratio," Construction and Building Materials, 23(12) pp. 3579-3582.

[95] Sadrmomtazi, A., Tajasosi, S., and Tahmouresi, B., 2018, "Effect of Materials Proportion on Rheology and Mechanical Strength and Microstructure of Ultra-High Performance Concrete (UHPC)," Construction and Building Materials, 187pp. 1103-1112.

[96] Bilodeau, A., and Malhotra, V. M., 2000, "High-Volume Fly Ash System: Concrete Solution for Sustainable Development," ACI Materials Journal, 97(1) pp. 41-48.

[97] Helmuth, R., 1987, "Fly ash in cement and concrete," .

[98] Siddique, R., 2004, "Performance Characteristics of High-Volume Class F Fly Ash Concrete," Cement and Concrete Research, 34(3) pp. 487-493.

[99] Hoff, G. C., 1972, "Porosity-Strength Considerations for Cellular Concrete," Cement and Concrete Research, 2(1) pp. 91-100.

[100] Kumar, R., and Bhattacharjee, B., 2003, "Porosity, Pore Size Distribution and in Situ Strength of Concrete," Cement and Concrete Research, 33(1) pp. 155-164.

[101] Chen, X., Wu, S., and Zhou, J., 2013, "Influence of Porosity on Compressive and Tensile Strength of Cement Mortar," Construction and Building Materials, 40(Supplement C) pp. 869-874.

[102] Wee, T., Daneti, S. B., and Tamilselvan, T., 2011, "Effect of W/C Ratio on Air-Void System of Foamed Concrete and their Influence on Mechanical Properties," Magazine of Concrete Research, 63(8) pp. 583-595.

[103] Kirane, K., and Bažant, Z. P., 2015, "Microplane Damage Model for Fatigue of Quasibrittle Materials: Sub-Critical Crack Growth, Lifetime and Residual Strength," International Journal of Fatigue, 70pp. 93-105.

[104] Kirane, K., and Bažant, Z. P., 2015, "Size Effect in Paris Law for Quasibrittle Materials Analyzed by the Microplane Constitutive Model M7," Mechanics Research Communications, 68pp. 60-64.

[105] Kirane, K., and Bažant, Z. P., 2016, "Size Effect in Paris Law and Fatigue Lifetimes for Quasibrittle Materials: Modified Theory, Experiments and Micro-Modeling," International Journal of Fatigue, 83pp. 209-220.

[106] Savic, A., Robertson, A. A., and Peterman, R. J., 2019, "THE INFLUENCE OF CONCRETE COVER, COMPRESSIVE STRENGTH, THE TYPE OF WIRE INDENTATION AND CONCRETE MIX ON BOND AMONG STEEL AND CONCRETE IN PRISMATIC PRESTRESSED CONCRETE MEMEBRS," 2019 Joint Rail Conference, Anonymous ASME, .

[107] Beck, B. T., Robertson, A. A., Peterman, R. J., 2019, "A High Resolution AUTOMATED PRESTRESSING WIREINDENT PROFILING SYSTEM FOR VERIFICATION OF WIRE-CONCRETE MIX COMPATIBILITY," 2019 Joint Rail Conference, Anonymous ASME, .

[108] Savic, A., Beck, B. T., Robertson, A. A., 2018, "Effects of Cover, Compressive Strength, and Wire Type on Bond Performance in Prismatic Prestressed Concrete Members," 2018 Joint Rail Conference, Anonymous American Society of Mechanical Engineers, pp. V001T01A007-V001T01A007.

[109] Savic, A., Beck, B. T., Shafiei Dastgerdi, A., 2019, "The effect of wire type on cracking propensity in prestressed concrete prisms," 2019 ASME Joint Rail Conference, Anonymous ASME, .

[110] Krishnamurthy, D., 1972, "Relationship between Transmission Length and Diameter of Prestressing Tendons," Journal of the Institution of Engineers.Civil Engineering Division, 52pp. 243-247.

[111] Kaar, P. H., and Hanson, N. W., 1975, "Bond Fatigue Test of Beams Simulating Pretensioned Concrete Crossties," .

[112] Momeni, A. F., Peterman, R. J., Beck, B. T., 2015, "Effect of Concrete Release Strength on the Development Length and Flexural Capacity of Members Made with Different Prestressing Wires Commonly Used in Pretensioned Concrete Railroad Ties," 2015 Joint Rail Conference, Anonymous American Society of Mechanical Engineers, pp. V001T01A025-V001T01A025.

[113] Martí-Vargas, J. R., Serna, P., Navarro-Gregori, J., 2012, "Effects of Concrete Composition on Transmission Length of Prestressing Strands," Construction and Building Materials, 27(1) pp. 350-356.

[114] Bodapati, N., Peterman, R. J., Zhao, W., 2013, "Transfer-length measurements on concrete railroad ties fabricated with 15 different prestressing reinforcements," 2013 PCI Convention and National Bridge Conference, September, Anonymous pp. 21-24.

[115] Riding, K. A., Ferraro, C. C., Almarshoud, M., 2018, "Durability Evaluation of Ternary Mix Designs for Extremely Aggressive Exposures," .

[116] Riding, K. A., Peterman, R. J., Guthrie, S., 2018, "Environmental and Track Factors That Contribute to Abrasion Damage," 2018 Joint Rail Conference, Anonymous American Society of Mechanical Engineers, pp. V001T01A009-V001T01A009.

[117] Arabali, P., and Shekarchi, M., 2015, "Durability of jointed reinforced concrete pavements under sever exposure conditions: a case study in IRAN," XIII International Conference on Durability of Building Materials and Components, Anonymous .

[118] Bodapati, N. N. B., Zhao, W., Peterman, R. J., 2013, "Influence of Indented Wire Geometry and Concrete Parameters on the Transfer Length in Prestressed Concrete Crossties," 2013 Joint Rail Conference, Anonymous American Society of Mechanical Engineers, pp. V001T01A010-V001T01A010.

[119] Haynes, M., Wu, J. C., Beck, B. T., 2012, "Non-Contact Measurement of Wire Indent Profiles on Prestressing Reinforcement Steel," Proceedings of the 2012 AREMA Conference, Anonymous .

[120] Haynes, M., Wu, C. J., Beck, B. T., 2013, "3D non-contact profilometry for reinforcement steel quality control," IIE Annual Conference. Proceedings, Anonymous Institute of Industrial and Systems Engineers (IISE), pp. 3421.

[121] Dastgerdi, A. S., Savic, A., Peterman, R. J., 2019, "Evaluation of Splitting Crack Propagation in Pre-Stressed Concrete Ties Made With Different Types of Coarse Aggregate," 2019 Joint Rail Conference, Anonymous American Society of Mechanical Engineers, pp. V001T01A015-V001T01A015.

[122] Haynes, M. D., 2015, Quality by Design: Improving Pre-Stressed Reinforcement for Concrete Railroad Ties Via Geometrical Dimensioning and Tolerancing, .

[123] Golewski, G. L., 2018, "Effect of Curing Time on the Fracture Toughness of Fly Ash Concrete Composites," Composite Structures, 185pp. 105-112.

[124] Oluokun, F. A., Burdette, E. G., and Deatherage, J. H., 1991, "Splitting Tensile Strength and Compressive Strength Relationships at Early Ages," Materials Journal, 88(2) pp. 115-121.

[125] Oluokun, F., 1991, "Prediction of Concrete Tensile Strength from its Compressive Strength: An Evaluation of Existing Relations for Normal Weight Concrete," Materials Journal, 88(3) pp. 302-309.

[126] Zain, M. F. M., Mahmud, H. B., Ilham, A., 2002, "Prediction of Splitting Tensile Strength of High-Performance Concrete," Cement and Concrete Research, 32(8) pp. 1251-1258.

[127] Özturan, T., and Çeçen, C., 1997, "Effect of Coarse Aggregate Type on Mechanical Properties of Concretes with Different Strengths," Cement and Concrete Research, 27(2) pp. 165-170.

[128] Bartlett, F. M., and MacGregor, J. G., 1994, "Effect of Core Diameter on Concrete Core Strengths," Materials Journal, 91(5) pp. 460-470.

[129] Arıoglu, N., Girgin, Z. C., and Arıoglu, E., 2006, "Evaluation of Ratio between Splitting Tensile Strength and Compressive Strength for Concretes Up to 120 MPa and its Application in Strength Criterion," ACI Materials Journal, 103(1) pp. 18-24.

[130] Zeman, J. C., Edwards, J. R., Barkan, C. P., 2009, "Failure mode and effect analysis of concrete ties in North America," Proc. of the 9th International Heavy Haul Conference, Anonymous pp. 270-278.

[131] Du, L., and Folliard, K. J., 2005, "Mechanisms of Air Entrainment in Concrete," Cement and Concrete Research, 35(8) pp. 1463-1471.

[132] Mehta, P. K., and Monteiro, P., 1993, "Concrete: Structure, Properties and Materials," Unpublished Manuscript for Revision of Mehta, PK and Monteiro, PJM Concrete: Structure, Properties, and Materials, .

[133] Mindess, S., and Young, J. F., 1981, "Concrete Prentice-Hall," Englewood Cliffs, NJ, 481.

[134] McCurrich, L., 1987, "PERMEABILITY TESTING OF SITE CONCRETE. A REVIEW OF METHODS AND EXPERIENCE," Concrete Society Technical Report, (31) .

[135] Bakharev, T., and Struble, L., 1997, "Microstructural Features of Railseat Deterioration in Concrete Ties," Journal of Materials in Civil Engineering, 9(3) pp. 146-153.

[136] Liu, T. C., 1981, "Abrasion resistance of concrete," Journal Proceedings, Anonymous 78, pp. 341-350.

[137] Vassou, V., Short, N., and Kettle, R., 2008, "Microstructural Investigations into the Abrasion Resistance of Fiber-Reinforced Concrete Floors," Journal of Materials in Civil Engineering, 20(2) pp. 157-168.

[138] Sadegzadeh, M., Page, C., and Kettle, R., 1987, "Surface Microstructure and Abrasion Resistance of Concrete," Cement and Concrete Research, 17(4) pp. 581-590.

[139] Van Dam, E., 2014, "Abrasion Resistance of Concrete and the use of High Performance Concrete for Concrete Railway Crossties," .

[140] Powers, L., and Shrimer, F., 2009, "Quantification of ASR in concrete: An introduction to the Damage Rating Index," ICMA conference. International Cement Microscopy Association/Society of Concrete Petrographers joint meeting, Quebec City, Canada, Anonymous .

[141] Rivard, P., and Ballivy, G., 2005, "Assessment of the Expansion Related to Alkali-Silica Reaction by the Damage Rating Index Method," Construction and Building Materials, 19(2) pp. 83-90.

[142] Sanchez, L., Fournier, B., Jolin, M., 2016, "Use of Damage Rating Index to Quantify Alkali-Silica Reaction Damage in Concrete: Fine Versus Coarse Aggregate." ACI Materials Journal, 113(4) .

[143] Carino, N. J., 2001, "The impact-echo method: an overview," Proceedings of the 2001 Structures Congress & Exposition, Anonymous pp. 21-23.

[144] Tomsett, H. N., 1980, "The Practical use of Ultrasonic Pulse Velocity Measurements in the Assessment of Concrete Quality," Magazine of Concrete Research, 32(110) pp. 7-16.

[145] Komloš, K., Popovics, S., Nürnbergerová, T., 1996, "Ultrasonic Pulse Velocity Test of Concrete Properties as Specified in various Standards," Cement and Concrete Composites, 18(5) pp. 357-364.

[146] Trtnik, G., Kavčič, F., and Turk, G., 2009, "Prediction of Concrete Strength using Ultrasonic Pulse Velocity and Artificial Neural Networks," Ultrasonics, 49(1) pp. 53-60.

[147] Neville, A.M., 2011, "Properties of concrete," Harlow, England ; New York : Pearson, Harlow, England ; New York, .

[148] ASTM, A., 2009, "C597–standard Test Method for Pulse Velocity through Concrete," ASTM International, West Conshohocken, PA, .

[149] Jones, R., 1962, "Non-destructive testing of concrete," Cambridge Eng. : University Press, Cambridge Eng.], .

[150] Jones, R., and Fącąoaru, I., 1969, "Recommendations for Testing Concrete by the Ultrasonic Pulse Method," Materials and Structures, 2(4) pp. 275-284.

[151] Kaplan, M., 1958, "Compressive strength and ultrasonic pulse velocity relationships for concrete in columns," ACI Journal Proceedings, Anonymous ACI, 54, .

[152] Sansalone, M. J., and Streett, W. B., 1997, "Impact-Echo. Nondestructive Evaluation of Concrete and Masonry," .

[153] ASTM C1383-04, 2010, "Standard Test Method for Measuring the P-Wave Speed and the Thickness of Concrete Plates using the Impact-Echo Method," .

Appendix A.
Fracture Toughness Calculation

For a set of data including crack opening mouth displacement (COMD) and load tabulated in Table 21 , fracture toughness can be calculated as shown in following.

Table 21. Raw data obtained from fracture toughness test

Time	Force	Stroke	COMD
sec	lbf	in	in
3.8	0.8349A4B4:B40	0	0
4.35	26.4771	0.000354	5.80E-06
5.55	86.8946	1.14E-03	4.67E-05
8.4	101.6476	1.26E-03	5.26E-05
17.05	97.0812	0.000984	8.18E-05
36.25	104.809	0.001417	7.59E-05
41.2	116.0495	0.001535	8.18E-05
42	117.8058	0.001575	9.35E-05
53.95	143.7993	0.00189	9.35E-05
57.9	152.2297	0.002008	1.05E-04
73.75	183.4922	0.002402	1.17E-04
92.6	234.0742	0.00315	1.34E-04
94.8	240.0457	0.003228	1.64E-04
104.7	275.1721	0.00374	1.75E-04
128.2	353.8553	0.005	2.40E-04
130.75	362.9881	0.005118	2.45E-04
148.1	421.6492	0.006024	3.27E-04
175.8	520.7057	0.00748	4.09E-04
183.2	549.1581	0.007874	0.00045
206.95	639.433	0.009134	4.73E-04
226.5	718.1161	0.010157	5.38E-04
250.75	815.7676	0.011417	6.19E-04
285.2	961.893	0.013228	7.95E-04

293.95	1001.938	0.013701	8.47E-04
294.6	1003.343	0.013701	8.41E-04
301.4	1033.2	0.014094	8.88E-04
312.05	1077.459	0.014646	9.93E-04
327.5	1131.203	0.015433	1.23E-03
338.5	1165.275	0.016024	1.45E-03
342.6	1179.677	0.01622	1.54E-03
345.7	1180.38	0.016417	1.68E-03
348	1161.06	0.015866	1.97E-03
348.4	1052.52	0.015197	1.83E-03
348.75	962.245	0.014606	0.001718
349.3	832.6282	0.013701	1.59E-03
349.65	755.7014	0.01311	1.47E-03
350.1	661.2114	0.012362	1.35E-03
351.35	423.4056	0.010276	1.01E-03
352.2	279.036	0.008858	8.12E-04
352.55	224.5901	0.008268	7.19E-04
353.1	141.6917	0.007362	6.25E-04
353.65	68.9801	0.006457	0.000538
353.95	37.3663	0.005945	4.67E-04
354.25	3.9962	0.005433	4.62E-04
436.05	0.8349	0.005315	3.33E-04

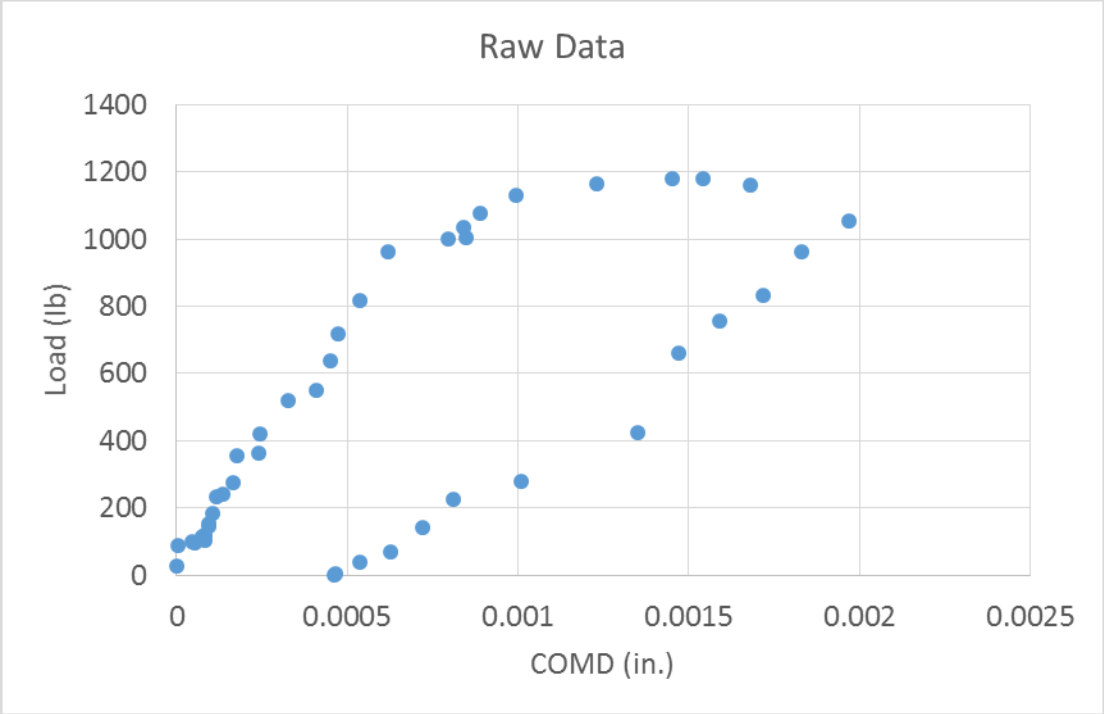

Figure 149. Load- COMD curve for data set in Table 21

Before running the test, it is required to measure dimensions shown in Figure 16 and initial length of notch.

Initial length of notch = a_0 = 1.583 in

Prism width = B = 3 in

Prism depth = W= 6 in

Loading span = S = 18 in

H_0 = 0.08 in.

8.1.1 Step 1: Calculation of loading and unloading compliance

Loading compliance, *Ci* in range of 10% to 50% of maximum load should represent linear elastic behavior of concrete before hardening point which is shown in Figure 150.

Maximum load in given data (P_{max})= 1180.38 Ib

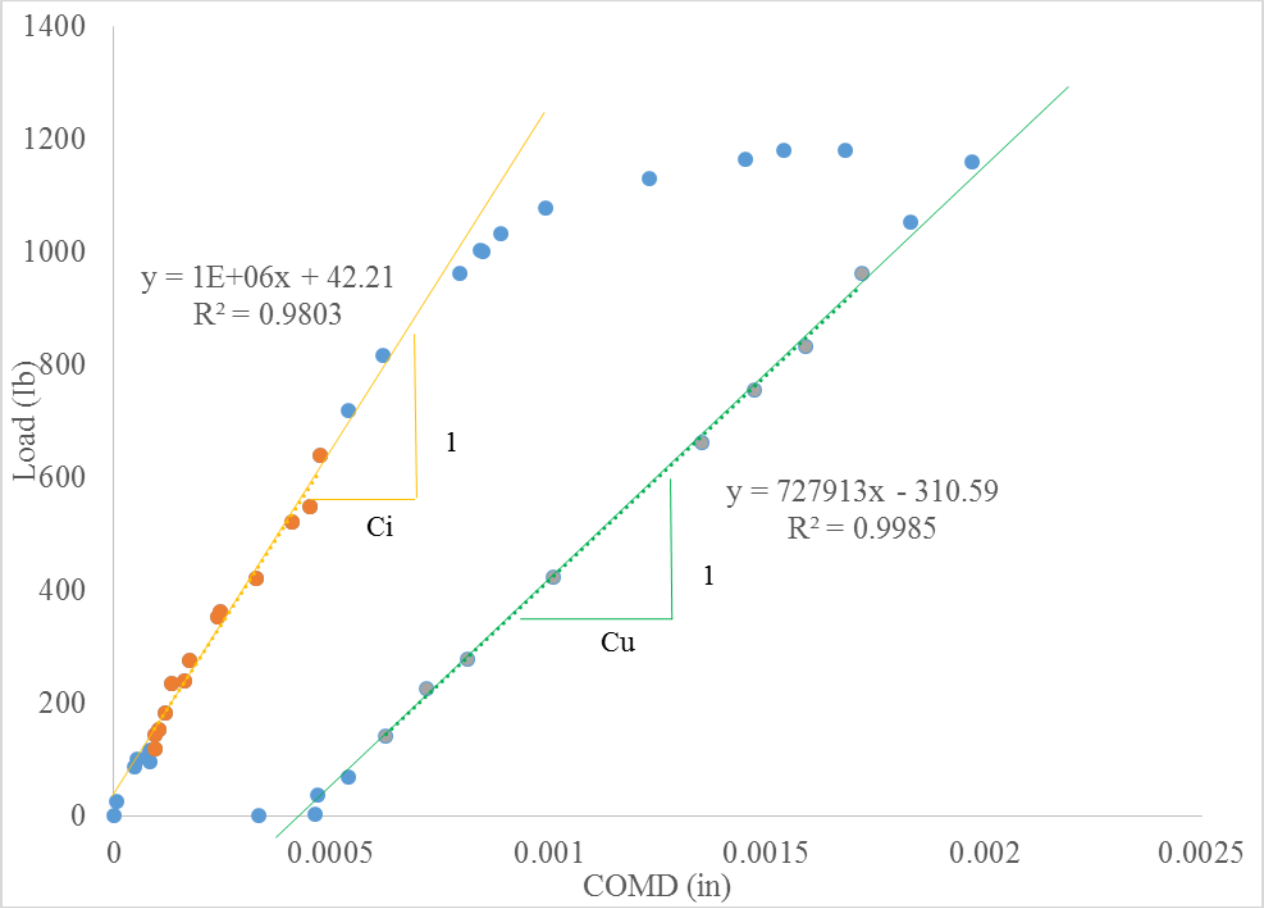

Figure 150. Loading and unloading compliance calculation

Ci = 1/ 1204810 = 8.30006E-07 (in/lb)

Unloading compliance (*Cu*) is calculated based on unloading data in the range of 10%-80% of maximum load.

Cu = 1/ 727913.2987 = 1.37379E-06 (in/lb)

8.1.2 Step 2: Calculation of Young modulus (E)

The Young modulus is calculated from the obtained initial compliance (*Ci*):

$$E = \frac{6Sa_0\,V_1(\alpha)}{C_i W^2 B} = \frac{6 \times 18\ in. \times 1.583\ in. \times 1.63}{8.30006E-07\left(\frac{in}{lb}\right) \times (6\ in.)^2 \times 3\ in.} = 3117711\ Psi$$

$$V_1(\alpha) = 0.7 - 2.28\alpha + 3.87\alpha^2 - 2.04\alpha^3 + \frac{0.66}{(1-\alpha)^2}$$

$$= 0.7 - 2.28 \times 0.27 + 3.87 \times 0.27^2 - 2.04 \times 0.27^3 + \frac{0.66}{(1-0.27)^2} = 1.63$$

$$\alpha = \frac{a_0 + H_0}{W + H_0} = \frac{1.583\ in. + 0.08\ in.}{6\ in. + 0.08\ in.} = 0.27$$

8.1.3 Step 3: Calculation of effective crack length (a_e)

The effective crack length which is the sum of initial crack length (a_0) and stable crack growth at peak load can be calculated by substituting *Cu* with *Ci* and a_0 with a_e in Step 2 and solving:

$$E = \frac{6Sa_e V_1(\alpha)}{C_u W^2 B} = \frac{6 \times 18\ in. \times a_e \times V_1(\alpha)}{1.37379E-06\ \left(\frac{in}{lb}\right) \times (6\ in)^2 \times 3\ in} = 3117711\ Psi$$

$$\alpha = \frac{a_e + H_0}{W + H_0} = \frac{a_e + 0.08\ in}{6\ in + 0.08\ in}$$

$$V_1(\alpha) = 0.7 - 2.28\alpha + 3.87\alpha^2 - 2.04\alpha^3 + \frac{0.66}{(1-\alpha)^2}$$

By solving above equation:

a_e = 2.62 in

8.1.4 Step 4: Calculation of fracture toughness (K_{IC})

The critical intensity factor or fracture toughness then can be calculated:

$$K_{IC} = \frac{3SP_{max}}{2BW^2}\sqrt{\pi a_e} F(\alpha) =$$
$$\frac{3 \times 18\ in \times 1180.3\ \text{lb}}{2 \times 3\ in \times (6\ in)^2}\sqrt{\pi \times 2.62\ in} \times 1.25 = 1059.4\ Psi\sqrt{in}$$

$$F(\alpha) = \frac{1}{\sqrt{\pi}} \frac{1.99 - \alpha(1-\alpha)(2.15 - 3.93\alpha + 2.7\alpha^2)}{(1+2\alpha)(1-\alpha)^{\frac{3}{2}}}$$
$$= \frac{1}{\sqrt{\pi}} \frac{1.99 - 0.43(1-0.43)(2.15 - 3.93 \times 0.43 + 2.7 \times 0.43^2)}{(1+2\times 0.43)(1-0.43)^{\frac{3}{2}}} = 1.25$$

$$\alpha = \frac{a_e}{W} = \frac{2.62\ in}{6\ in} = 0.43$$

Appendix B.
Picture of prisms

In this section, photos of prisms tested in this study are documented.

- Photos from B114

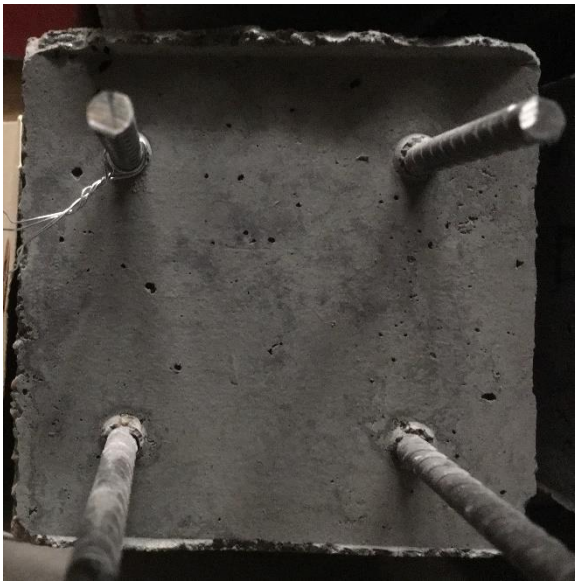

Live End (0.750 edge distance)

Dead End (0.750 edge distance)

Live End (0.625 edge distance)

Dead End (0.625 edge distance)

Live End (0.500 edge distance)

Dead End (0.500 edge distance)

Photos from B121

Live End (0.750 edge distance)

Dead End (0.750 edge distance)

Live End (0.625 edge distance)

Dead End (0.625 edge distance)

Live End (0.500 edge distance)

Dead End (0.500 edge distance)

Photos from B131

Live End (0.750 edge distance)

Dead End (0.750 edge distance)

Live End (0.625 edge distance)

Dead End (0.625 edge distance)

Live End (0.500 edge distance)

Dead End (0.500 edge distance)

- Photos from B141

Live End (0.750 edge distance)

Dead End (0.750 edge distance)

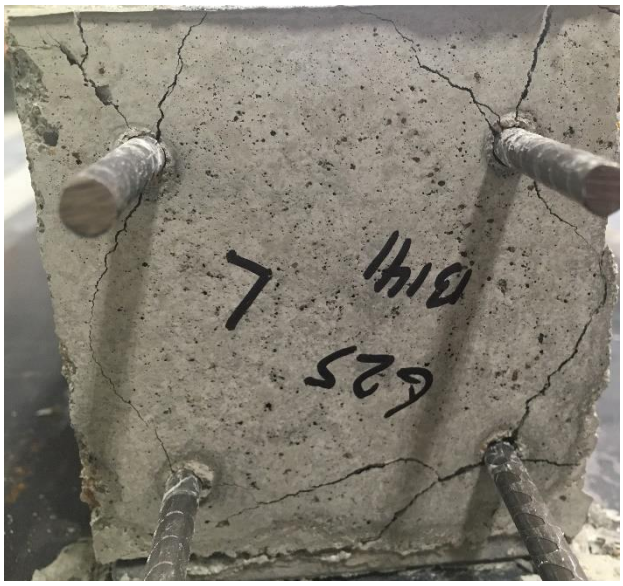

Live End (0.625 edge distance)

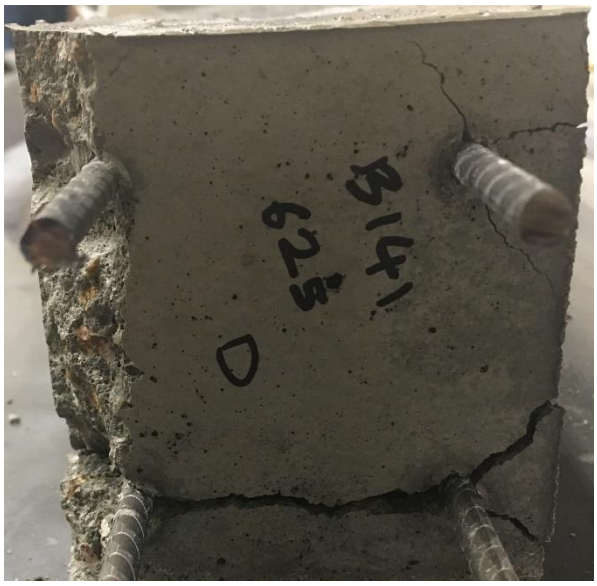

Dead End (0.625 edge distance)

Live End (0.500 edge distance)

Dead End (0.500 edge distance)

-Photos from B151

Live End (0.750 edge distance)

Dead End (0.750 edge distance)

Live End (0.625 edge distance)

Dead End (0.625 edge distance)

Live End (0.500 edge distance)

Dead End (0.500 edge distance)

- Photos from B161

Live End (0.750 edge distance)

Dead End (0.750 edge distance)

Live End (0.625 edge distance)

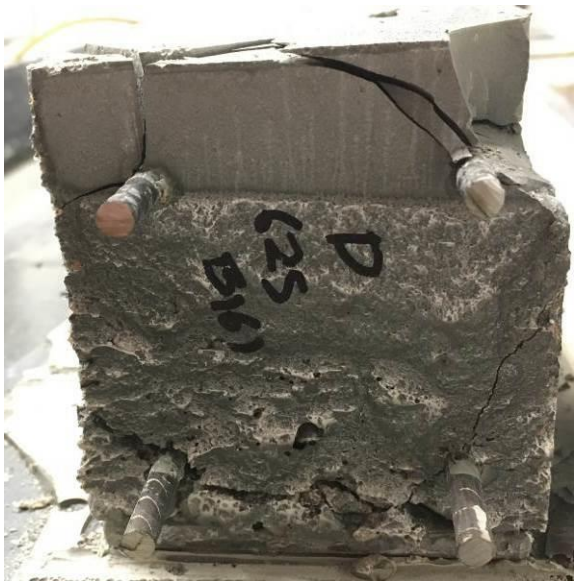

Dead End (0.625 edge distance)

Live End (0.500 edge distance)

Dead End (0.500 edge distance)

- Photos from B171

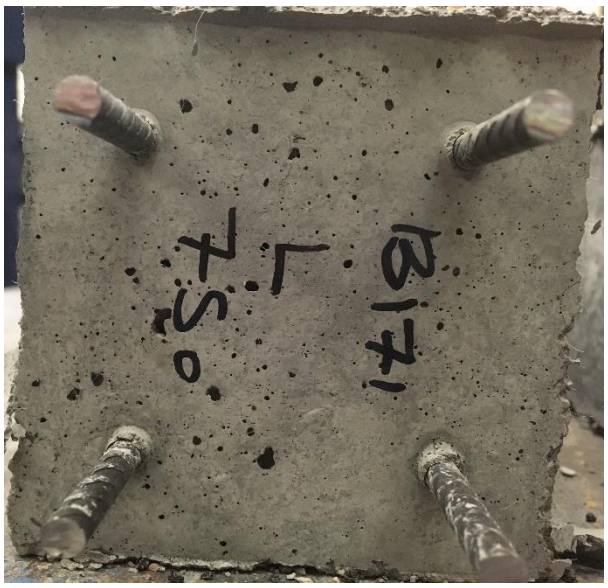

Live End (0.750 edge distance)

Dead End (0.750 edge distance)

Live End (0.625 edge distance)

Dead End (0.625 edge distance)

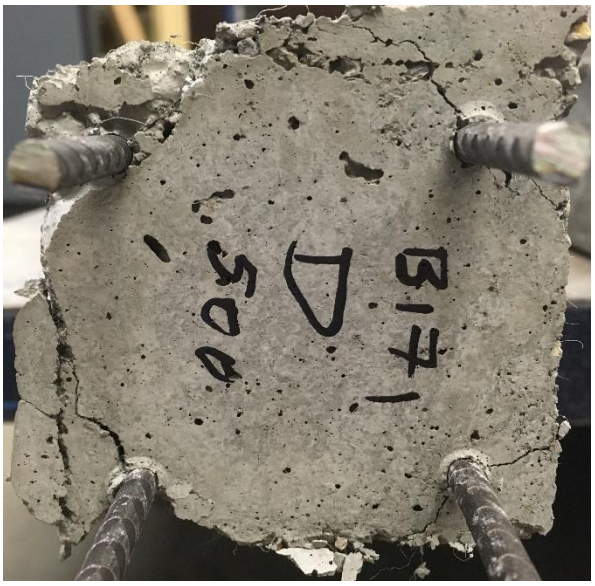

Live End (0.500 edge distance)

Dead End (0.500 edge distance)

- Photos from B181

Live End (0.750 edge distance)

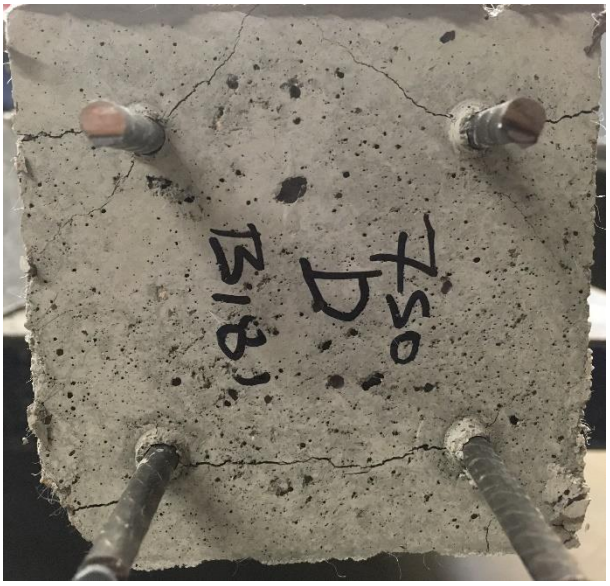

Dead End (0.750 edge distance)

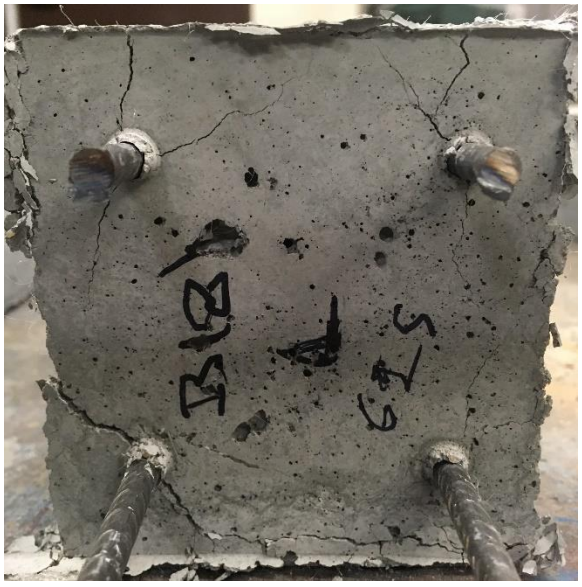

Live End (0.625 edge distance)

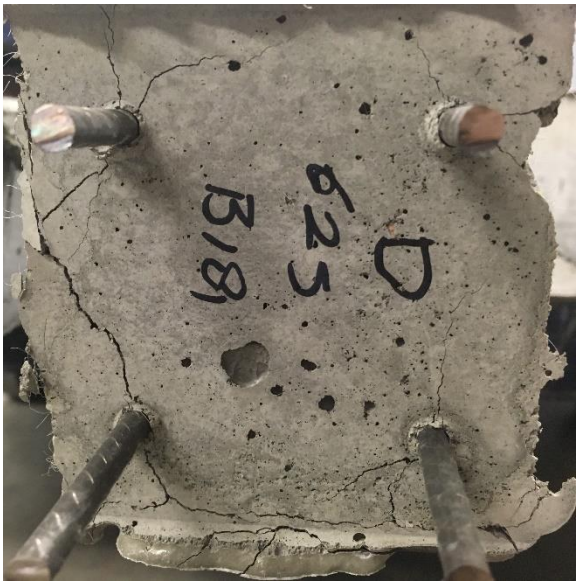

Dead End (0.625 edge distance)

Live End (0.500 edge distance)

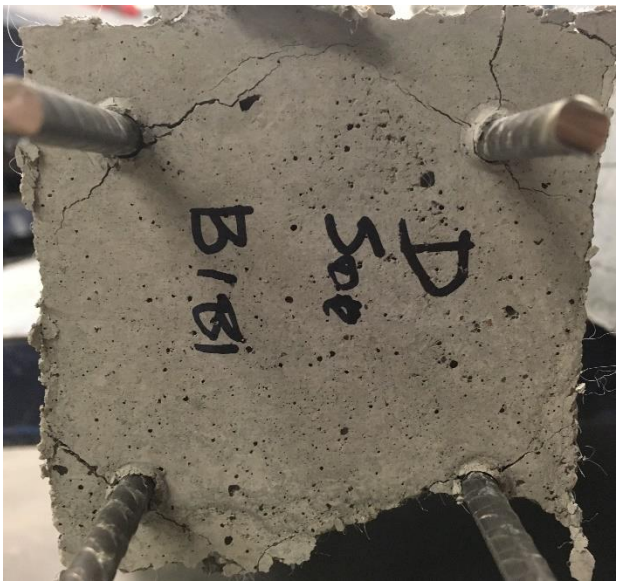

Dead End (0.500 edge distance)

- Photos from B191

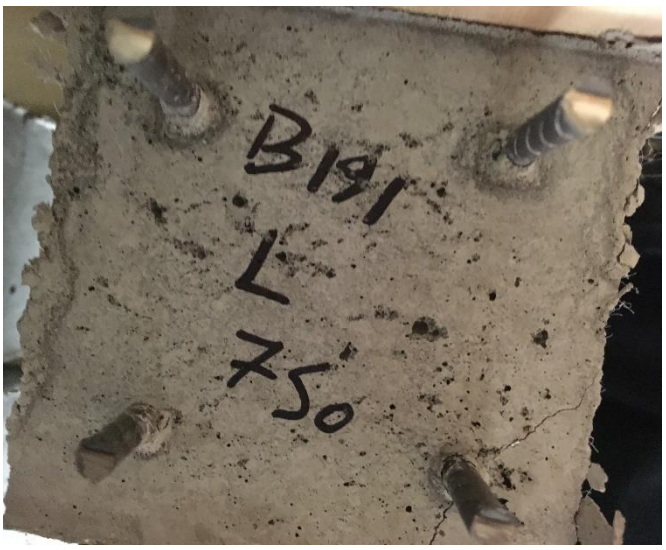

Live End (0.750 edge distance)

Dead End (0.750 edge distance)

Live End (0.625 edge distance)

Dead End (0.625 edge distance)

Live End (0.500 edge distance)

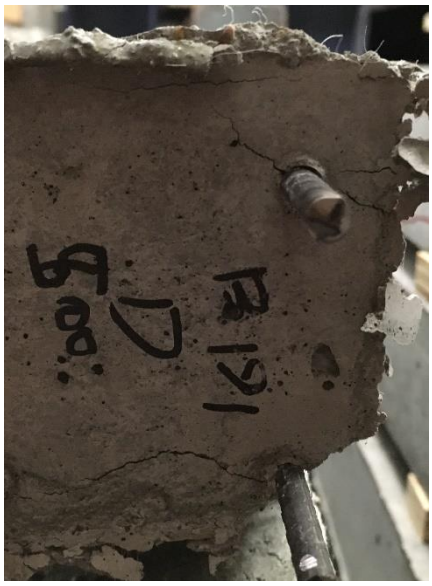

Dead End (0.500 edge distance)

- Photos from B201

Live End (0.750 edge distance)

Dead End (0.750 edge distance)

Live End (0.625 edge distance)

Dead End (0.625 edge distance)

Live End (0.500 edge distance)

Dead End (0.500 edge distance)

8.1.5 - Photos from B211

Live End (0.750 edge distance)

Dead End (0.750 edge distance)

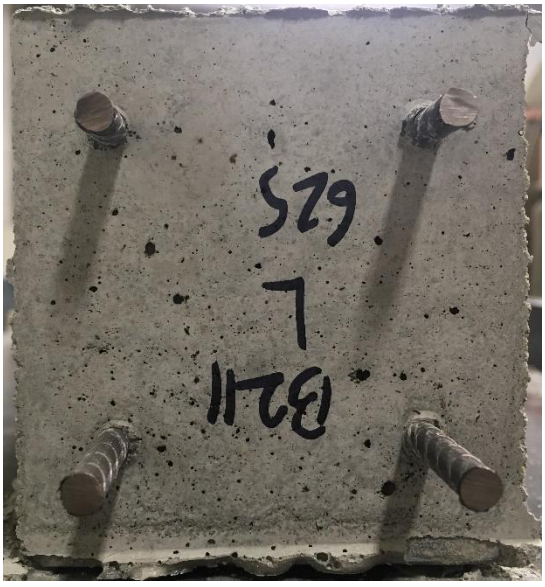

Live End (0.625 edge distance)

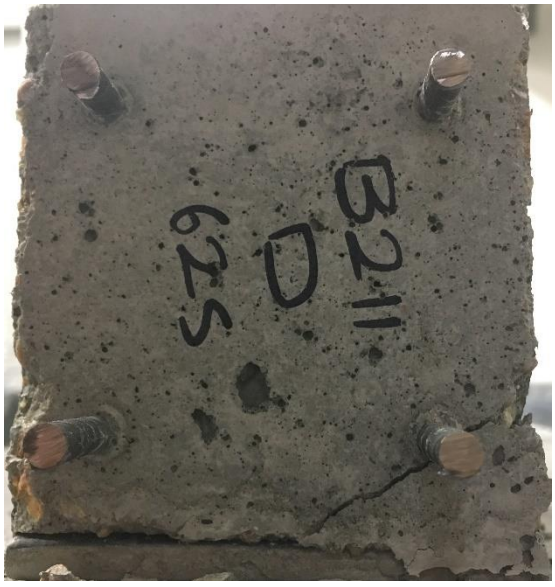

Dead End (0.625 edge distance)

Live End (0.500 edge distance)

Dead End (0.500 edge distance)

Abbreviations and Acronyms (sample)

BLE	Brotherhood of Locomotive Engineers
CFR	Code of Federal Regulations
FMVSS	Federal Motor Vehicle Safety Standards
MBTA	Massachusetts Bay Transit Authority
OSHA	Occupational Safety and Health Administration
UTU	United Transportation Union